PRODUCTION, MICROSTRUCTURE AND TENSILE PROPERTIES OF MECHANICALLY MILLED TITANIUM-BORON ALLOYS.

A THESIS SUBMITTED FOR THE
DEGREE OF DOCTOR OF PHILOSOPHY
OF THE UNIVERSITY OF LONDON.

BY
TANYA MICHELLE TERESA GODFREY
MEng. (Hons)

DEPARTMENT OF MATERIALS
IMPERIAL COLLEGE OF SCIENCE, TECHNOLOGY AND MEDICINE
LONDON SW7 2BP

JULY 2001

ACKNOWLEDGEMENTS

I would like to thank QinetiQ for supporting me during this project.

My supervisors, Prof. Harvey Flower and Prof. Malcolm Ward-Close for their support over the past four years and for proof reading my reports and papers. I would like to thank all those people in QinetiQ who helped me during the course of this thesis, especially: Andy Wisbey, Paul Goodwin, Jeff Brooks, Chandra, Singh Uhbi, Alastair Godfrey, Ian Wallis, Rob Savage, Paul Blackwell, Wendy Westby, Sharon Goodwin, and Phil Holdway. Thanks also to ex-colleagues David Wilkes and Simon Howard.

Thanks to Andy Tarrant from AMC for his useful discussions and to Chris Hammond and Andy Brown from The University of Leeds for their useful discussions, in particular relating to superplastic forming.

A special mention goes to my family for their support over the years and their continued interest in my studies.

Finally I would like to thank Stuart for his moral encouragement, technical support and outstanding domestic abilities without which I would have had great difficulty in completing this thesis.

ABSTRACT

Titanium is gaining popularity in a wide range of applications. Future applications require titanium alloys with improved mechanical properties, wear resistance and formability. This study aimed to improve the room temperature mechanical properties of titanium; in particular its stiffness by producing a titanium particulate metal matrix composite (MMC) based on the titanium boron system. Additionally the potential to improve the superplastic performance of titanium by utilising titanium boron alloys was assessed.

The titanium boron alloys were produced by mechanical milling powders and hot isostatic pressing to produce solid billets. Mechanical milling is a powder metallurgy technique used to disperse ceramic particles within metal powders. The effect of milling time, titanium powder characteristic (size, morphology and alloy) and boron concentration on the microstructure, room temperature properties and superplastic properties was assessed.

Mechanical milling produced a fine dispersion of boron or titanium boride within the deformed titanium powders with a nanometer grain size, however difficult was found in achieving an even distribution of boron even after long milling times. During hot isostatic pressing the boron or TiB_2, which was incorporated during mechanical milling, formed TiB, although remnants of TiB_2 were still observed. Subsequent high temperature heat treatments resulted in full reaction of boron and TiB_2 to TiB. Mechanical milling was not detrimental to the room temperature mechanical properties of titanium. The addition of TiB was found to significantly improve the stiffness of titanium, however a reduction in ductility was reported. The addition of boron was found to improve the high strain rate superplasticity of Ti-6Al-4V by pinning the grain boundaries.

CONTENTS

1. INTRODUCTION 13

2. REVIEW OF MECHANICAL ALLOYING 15

2.1 MECHANICAL ALLOYING OF TITANIUM 16

3. REVIEW OF TITANIUM PARTICULATE METAL MATRIX COMPOSITES – PRODUCTION AND MECHANICAL PROPERTIES 19

3.1 INTRODUCTION 19
3.2 REINFORCEMENT SELECTION 20
3.3 PRODUCTION ROUTES 21
3.3.1 Vacuum arc melting 21
3.3.2 Rapid solidification 21
3.3.3 Gas atomisation 21
3.3.4 Powder blending 22
3.3.5 Compaction 22
3.3.6 Secondary forming 23
3.4. MECHANICAL PROPERTIES 23
3.4.1 Room temperature tensile properties 23
3.4.2 High temperature tensile 24
3.4.3 Fatigue 24
3.4.4 Creep 25
3.4.5 Wear resistance 25
3.5 SUMMARY 26

4. REVIEW OF THE TITANIUM-BORON SYSTEM 30

4.1 FORMATION OF TiB 30
4.2 THE EFFECT OF TiB ON THE β TRANSUS 31

5. REVIEW OF SUPERPLASTICITY 34

5.1 SUPERPLASTICITY IN TITANIUM ALLOYS 35
5.1.1 Grain size effect 36
5.1.2 Grain size distribution effects 36
5.1.3 Texture 36
5.1.4 Phase ratio effects 37
5.2 HIGH STRAIN RATE SUPERPLASTICITY 37

6 EXPERIMENTAL METHOD 43

6.1 MATERIAL PRODUCTION 43
6.1.1 Powder blending 43
6.1.2 Mechanical milling 43
6.1.3 Mechanical alloying with hydrogen 44
6.2 POWDER CONSOLIDATION 44
6.3 ANALYSIS OF POWDERS 45
6.3.1 Metallography 45
6.3.2 X-ray diffraction and crystallite size measurement 45
6.3.3 Chemical analysis 46

6.3.4 Sieve analysis 46
6.4 ANALYSIS OF CONSOLIDATED SAMPLES 47
6.4.1 Metallography 47
6.4.2 β transus approach 47
6.4.3 Grain size analysis 47
6.4.4 Heat treatments 48
6.4.5 Argon analysis 48
6.5 MECHANICAL TESTING 48
6.5.1 Room temperature tensile testing 48
6.5.2 Elevated temperature sample design and testing 48

7. ASSESSMENT OF AS RECEIVED AND MILLED POWDERS 54

7.1 RESULTS 54
7.1.1 As received powders 54
7.1.2 Characterisation of the milled powders. 54
7.1.3 Oxygen, nitrogen, iron and hydrogen analysis 55
7.1.4 Powder particle size 55
7.2 DISCUSSION 56
7.2.1 Interstitial contamination 57
7.2.2 The effect of milling on powder size and morphology 58
7.2.3 Distribution of TiB in the titanium powders 60
7.2.4 Crystallite size 61
7.3 SUMMARY 61

8 MICROSTRUCTURAL CHARACTERISATION OF HIPED POWDERS 71

8.1 RESULTS 71
8.1.1 Microstructure of as received HIPed powders 71
8.1.2 Microstructure of milled Ti-6Al-4V 71
8.1.3 Microstructure of blended powders 72
8.1.4 Microstructure of milled titanium and boron powders 73
8.1.5 Effect of milling time on distribution of the TiB 74
8.1.6 Effect of heat treatment on the milled and HIPed powders 75
8.2 DISCUSSION 76
8.2.1 The development of the matrix microstructure 76
8.2.2 The influence of TiB on the microstructure of the titanium alloy matrix 79
8.2.3 Heat treatment 83
8.3 SUMMARY 85

9 ROOM TEMPERATURE TENSILE PROPERTIES OF THE HIPED BILLETS 110

9.1 RESULTS 110
9.1.1 Consolidated as received powder properties 110
9.1.2 Consolidated mechanically milled Ti-6Al-4V 110
9.1.3 Consolidated titanium (alloy) powders blended with either boron or TiB_2. 112
9.1.4 The tensile properties of milled and HIPed Ti-6Al-4V+0.5B 112
9.1.5 The tensile properties of consolidated and milled Ti-6Al-4V+2B and Ti-6Al-4V+6.4TiB_2 113
9.1.6 The tensile properties of consolidated and milled Ti+2B and Ti+6.4TiB_2 113
9.1.7 The effect of the hydrogen on milling of titanium 114
9.1.8 The effect of boron on the stiffness of titanium 114
9.2 DISCUSSION 114
9.2.1 Quality of the matrices and the effect of HIPing temperature 114
9.2.2 The effect of boron or TiB_2 on the blended titanium HIPed powders 115
9.2.3 The effect of milling on the mechanical properties of the consolidated titanium boron alloys .. 115
9.3 SUMMARY 119

10 HOT TENSILE PROPERTIES OF MECHANICAL MILLED Ti-6Al-4V AND Ti-6Al-4V+0.5B BILLETS IN COMPARISON WITH CONVENTIONAL Ti-6Al-4V.....134

10.1 RESULTS.....134
10.2 DISCUSSION.....136
10.2.1 Microstructural morphology.....136
10.2.2 Grain size.....137
10.2.3 Grain size distribution.....138
10.2.4 Volume fraction of β.....139
10.2.5 Argon entrapment and consolidation defects.....139
10.2.6 The effect of TiB on the superplastic properties.....140
10.2.7 The effect of TiB as a grain pinner on the superplastic properties.....141
10.2.8 Effect of fine grain size on forming temperature.....143
10.2.9 TiB as an internal marker for superplastic flow in Ti-6Al-4V.....143
10.3 SUMMARY.....145

11. CONCLUSIONS.....154

12. FUTURE WORK.....156

13. REFERENCES.....158

APPENDIX A.....168

APPENDIX B.....170

LIST OF TABLES

Table		Page
1-1	A comparison of the properties of difference engineering materials and the ceramic TiB.	13
3-1	A comparison of the physical properties of titanium and potential ceramic reinforcing phases (Saito (1995), Clyne and Withers (1993)).	27
5-1	Superplastic properties of some α/β titanium alloys (Nieh et al. (1997)).	40
6-1	A list of the powder blends produced and the HIPing conditions are given.	50
6-2	Summary of the milling combinations used with gas atomised titanium powders.	50
6-3	A summary of the combinations when milling with either hydrogen or using TiH_2.	51
7-1	The crystallite size measurements of Ti-6Al-4V powders milled with boron for 60T seconds	62
7-2	Shows the oxygen, nitrogen and iron concentrations of milled powders compared with the gas atomised powders.	62
7-3	Showing the powder particle size and hydrogen content of the milled powders.	63
8-1	The interstitial contamination of HIPed powders.	87
8-2	Volume fraction of transformed β (%) of Ti-6Al-4V milled for 60 T seconds, HIPed and heat-treated samples at 900°C.	87
9-1	The tensile mechanical properties of the gas atomised Ti-6Al-4V, Ti, HDH Ti-15-3-3-3 and Ti_{sf}.	120
9-2	The mechanical properties of Ti-6Al-4V that was milled for 12 T seconds and HIPed at 900°C for 2 hours at 150 MPa.	120
9-3	The mechanical properties of Ti-6Al-4V milled for 60 T seconds and HIPed at various temperatures for 2 hours at 150 MPa.	120
9-4	The tensile mechanical properties of the blended titanium with boron or titanium boride	121
9-5	The mechanical properties of Ti-6Al-4V + 0.5%B milled for 60 T seconds and HIPed at various temperatures for 2 hours at 150 MPa.	121
9-6	The tensile mechanical properties of Ti-6Al-4V with boron and titanium boride HIPed at 500 °C for 2 hours at 150 MPa followed by 900°C for 2 hours at 150 MPa.	122
9-7	The tensile mechanical properties of the Ti-6Al-4V milled with either boron or titanium diboride HIPed at 500°C for 2 hours at 150 MPa followed by 900°C for 2 hours at 150 MPa and heat treatment at 1300°C for 8 hours in argon.	122
9-8	The tensile mechanical properties of Ti with boron and titanium boride HIPed at 500 °C for 2 hours at 150 MPa followed by 900°C for 2 hours at 150 MPa.	123
9-9	The tensile mechanical properties of the Ti milled with either boron or titanium diboride HIPed at 500°C for 2 hours at 150 MPa followed by 900°C for 2 hours at 150MPa and heat treatment at 1300°C for 8 hours in argon.	123
9-10	Tensile properties of $Ti+6.4TiB_2$ milled with a hydrogen atmosphere.	124

LIST OF FIGURES

Figure		Page
2-1	A schematic of the mechanical alloying process. Elements A and B are milled. Layering of the powders occurs and milling is continued until a homogeneous distribution of the elements is achieved giving the alloy C (Gardiner *et al.* (1996))	18
2-2	A comparison of powder particle size when milling copper powder with and without a process control agent (Harris *et al.* (1993))	18
3-1	A comparison of (a) the coarsening behaviour of TiB and TiC particles in Ti-4.3Fe-7Mo-1.4Al-1.4V based MMCs at 1300°C and (b) the difference in the length and width of TiB particles at 1300°C (Saito *et al.* (1995a)).	27
3-2	The effect of TiB volume fraction on the Young's moduli of various titanium alloys.	28
3-3	The effect of TiB volume fraction on the 0.2% proof stress of titanium MMC's	28
3-4	The effect of TiB on the ultimate tensile strength of titanium MMC's. The graph shows the increase in the ultimate tensile strength with the addition of TiB_x	29
3-5	The effect of TiB on the ductility of titanium MMC's.	29
4-1	The titanium boron phase diagram (Murray (1987)).	33
4-2	A schematic illustration of the atomic packing in TiB. a) The TiB unit cell (B27); b) the basic triangular prismatic arrangement of titanium atoms around each boron atom; c) the arrangement of the basic triangular prisms to form the TiB structure. (Fan (1993)).	33
5-1	The effect of average grain size on the flow stress and strain rate sensitivity (m) for Ti-6Al-4V at 927°C (Ghosh and Hamilton (1979)).	40
5-2	The effect of grain size distribution on the flow stress of Ti-6Al-4V at 927°C (Paton and Hamilton (1979))	41
5-3	Predictions of flow stress for various grain size distributions (Ghosh and Raj (1981)).	41
5-4	(a) strain rate sensitivity and (b) elevated temperature ductility as a function of β phase of several titanium alloys (Hamilton (1984)).	42
5-5	Grain size dependence of superplastic strain rate in aluminium based materials (Higashi and Mabuchi (1997)).	42
6-1	A schematic of the material production method.	52
6-2	A schematic of the HIPing cycle of 500°C for 2 hours followed by 900°C for 2 hours at 150 MPa.	52
6-3	1/4 BSF tensile test piece dimensions.	53
6-4	The test piece dimensions for elevated temperature tensile testing with a square neck design.	53
7-1	SEM micrographs of the as received powders.	64
7-2	Optical micrographs of the cross sections of the gas atomised powders.	64
7-3	X-ray diffraction of gas atomised Ti-6Al-4V powder indicating detection of the α phase only.	65
7-4	An optical micrograph of Ti-6Al-4V+0.5B after milling for 60T seconds.	65

7-5	X-ray diffraction of gas atomised Ti-6Al-4V powder after milling for 60T seconds and indicate the presence of the α phase only.	66
7-6	SEM micrograph of the Ti-6Al-4V+0.5B milled for 60T seconds.	66
7-7	The effect of boron or TiB_2, which is expressed in terms of predicted volume fraction TiB if the boron/TiB_2 fully reacts on (a) oxygen and (b) nitrogen concentration.	67
7-8	Powder particle analysis showing the effect of milling time on particles size with a) Ti and b) Ti-6Al-4V with boron or TiB_2 and the effect of boron or TiB_2 on particle size of c) Ti and d) Ti-6Al-4V.	68
7-9	Micrographs of Ti-6Al-4V+6.4%TiB_2 after 18T seconds milling at different sieve fractions.	69
7-10	SEM micrographs of Ti-6Al-4V+6.4%TiB_2 powder after milling for 18T seconds.	70
7-11	Shows the increasing deformation observed in Ti-8Al-4V + 6.4%TiB_2 after milling from 18T seconds.	70
8-1	An optical micrograph of (a) gas atomised Ti-6Al-4V with a lamellar microstructure, where the arrows indicate a powder particle, (b) gas atomised Ti with an equiaxed microstructure.	88
8-2	An optical micrograph of Ti-6Al-4V milled for 60T seconds HIPed at 900°C for 2 hours at 150 MPa (a) shows the equiaxed α phase and (b) lamellar α microstructure from a powder particle that has not been moved.	88
8-3	A backscattered FEG-SEM micrograph of Ti-6Al-4V milled for 60T seconds and (a) HIPed at 800°C and (b) HIPed at 900°C for 2 hours at 150 MPa.	89
8-4	A backscattered FEG-SEM micrograph of Ti-6Al-4V milled for 60T seconds and (a) HIPed at 800°C and heat treated for 20 hours at 800°C and (b) HIPed at 900°C and heat-treated for 20 hours at 900°C.	89
8-5	The β transus approach curve for Ti-6Al-4V milled for 60T seconds and HIPed at either 900°C for 2 hours at 150 MPa or 800°C for 2 hours at 150 MPa and at 800°C for 96 hours compared with the β transus predicted for Ti-6Al-4V and Ti-6Al-4V+2B using JMatPro.	89
8-6	The relative concentrations of (a) Al and (b) V in α and β titanium and liquid phases between 600°C and 1800°C predicted using JMatPro and compared with data from Brown *et al.* (1999a) and Sastry *et al.* (1980).	90
8-7	Optical micrographs of (a) Ti-6Al-4V + 2B and (b) Ti-6Al-4V + 6.4 TiB_2, blended and HIPed at 500°C for 2 hours at 150 MPa, followed by 900°C for 2 hours at 150 MPa.	91
8-8	Backscattered electron micrographs of (a) Ti-6Al-4V + 2B showing TiB at prior powder particle boundaries and (b) Ti-6Al-4V + 6.4TiB_2, showing TiB needles growing from the TiB_2 particles located at prior powder particle boundaries, after blending and HIPing.	91
8-9	XRD of (a) blended Ti + 2B and (b) Ti + 6.4TiB_2. Both samples were HIPed at 500°C for 2 hours at 150 MPa followed by 900°C for 2 hours at 150 MPa.	92
8-10	Optical micrographs of (a) the HDH Ti-15-3-3-3 + 6.4TiB_2 and (b) Ti_{sf} + 6.4TiB_2 blended and HIPed at 900°C for 2 hours at 150 MPa.	93
8-11	Backscattered electron micrographs of (a) blended Ti-6Al-4V + 2B and (b) blended Ti-6Al-4V + 6.4TiB_2. HIPed at 500°C for 2 hours at 150 MPa followed by 900°C for 2 hours at 150 MPa and heat treated at 1300°C for 8 hours in vacuum.	93
8-12	Micrographs of Ti-6Al-4V + 0.5B milled for 60T seconds HIPed billets.	94

8-13	The effect of heat treatment on the average grain size of samples milled for 60T seconds, HIPed and heat-treated at (a) 800°C and (b) 900°C.	95
8-14	The grain size distribution of the Ti-6Al-4V and Ti-6Al-4V+0.5B after milling for 60T seconds, HIPed at 800°C and heat-treated at 800°C.	96
8-15	The grain size distribution of the Ti-6Al-4V and Ti-6Al-4V+0.5B after milling for 60T seconds, HIPed at 900°C and heat-treated at 900°C.	97
8-16	The area distribution of grain size of the Ti-6Al-4V and Ti-6Al-4V+0.5B after milling for 60T seconds, HIPed at 800°C and heat-treated at 800°C.	98
8-17	The area distribution of grain size of the Ti-6Al-4V and Ti-6Al-4V+0.5B after milling for 60T seconds, HIPed at 900°C and heat-treated at 900°C.	99
8-18	Optical micrographs of Ti-6Al-4V + 2B milled for (a) 0, (b) 3T, (c) 6T, (d) 12T and (e) 18T seconds. Samples were HIPed at 500°C for 2 hours at 150 MPa followed by 900°C for 2 hours at 150 MPa.	100
8-19	Optical micrographs of Ti-6Al-4V + 6.4TiB_2 milled for (a) 0, (b) 3T, (c) 6T, (d) 12T and (e) 18T seconds. Samples were HIPed at 500°C for 2 hours at 150 MPa followed by 900°C for 2 hours at 150 MPa.	100
8-20	Optical micrographs of Ti + 2B milled for (a) 0, (b) 3T, (c) 6T and (d) 12T seconds. Samples were HIPed at 500°C for 2 hours at 150 MPa followed by 900°C for 2 hours at 150 MPa.	101
8-21	Optical micrographs of Ti + 6.4TiB_2 milled for (a) 0, (b) 3T and (c) 6T seconds. Samples were HIPed at 500°C for 2 hours at 150 MPa followed by 900°C for 2 hours at 150 MPa.	101
8-22	XRD of (a) Ti + 2B milled for 12T seconds and (b) Ti + 6.4TiB_2 6T seconds. Both samples were HIPed at 500°C for 2 hours at 150 MPa followed by 900°C for 2 hours at 150 MPa.	102
8-23	A backscattered FEG-SEM micrograph showing (a) Ti-6Al-4V+2B and (b) Ti-6Al-4V+6.4TiB_2. The samples were milled for 18T seconds and HIPed at 500°C for 2 hours at 150 MPa followed by 900°C for 2 hours at 150 MPa.	103
8-24	Optical micrographs of Ti+6.4TiB_2 with (a) 180 ppm and milled for 6T seconds (1 purge for 10 minutes), (b) 220 ppm and milled for 6T seconds (2 purges each 30 minutes), (c) 770 ppm and milled for 6T seconds (6 purges each 10 minutes) (d) 630 ppm and milled for 9T seconds (9 purges each 10 minutes) (e,f) TiH_2+6.4TiB_2 (21000 ppm hydrogen) milled for 18T seconds.	103
8-25	SEM images of TiB needles in Ti-6Al-4V + TiB_2 after milling for 18T seconds HIPed at 500°C for 2 hours at 150 MPa followed by 900°C for 2 hours at 150 MPa and heat treated at 1300°C for 8 hours.	104
8-26	XRD of (a) Ti + 2B milled for 12T seconds and (b) Ti + 6.4TiB_2 milled for 6T seconds. Both samples were HIPed at 500°C for 2 hours at 150 MPa followed by 900°C for 2 hours at 150 MPa and heat treated at 1300°C for 8 hours.	105
8-27	Backscattered FEG-SEM micrographs of the increase in TiB needle size with heat treatment temperature in Ti+6.4TiB_2 milled for 6T seconds and HIPed at 500°C for 2 hours at 150MPa followed by 2 hours at 900°C and 150 MPa and heat treated at 1300°C for (a) 8 hours, (b) 20 hours and (c) 100 hours.	106
8-28	A backscattered FEG-SEM micrograph showing (a) Ti-6Al-4V+2B milled for 18T seconds, (b) Ti-6Al-4V+6.4TiB_2 milled for 18T seconds, (c) Ti+2B milled for 12T seconds and (d) Ti+6.4TiB_2 milled for 6T seconds. All samples were HIPed at 500°C for 2 hours followed by 2 hours at 900°C and 150 MPa and heat-treated at 1300°C for 8 hours.	106
8-29	An optical micrograph of Ti-6Al-4V+6.4TiB_2 milled for 18T seconds HIPed and heat-treated at 1300°C	107
8-30	Diffusivity of Ti-6Al-4V (a) shows a comparison between predicted values for lattice, pipe and grain boundary diffusion, (b) shows pipe diffusion and (c)	107

shows lattice diffusion.

8-31 The growth of the reaction layer of TiB between TiB_2 and Ti at 900°C and at 1300°C (Reeves (1992)). 108

8-32 A schematic of the growth of TiB from TiB_2 particles in titanium. After Reeves (1992). 108

8-33 The effect of particle size on the grain size of a material given (a) randomly oriented particles and (b) particles located at grain boundaries. 109

9-1 Fractographs of the gas atomised a) Ti-6Al-4V and b) Ti after HIPing at 500°C for 2 hours at 150MPa, followed by 900°C for 2 hours at 150 MPa. 125

9-2 Fractography shows (a) ductile failure of the milled Ti-6Al-4V 60T seconds and HIPed at 900°C for 2 hours at 150 MPa and (b) prior powder particle powder boundary failure after HIPing at 700°C for 2 hours at 150 MPa. 125

9-3 Shows the effect of grain size on the yield strength of Ti-6Al-4V milled for 60T seconds. 125

9-4 ~~Shows the effect of grain size on the yield strength of Ti-6Al-4V milled for 60T seconds.~~ The difference in the mechanical properties of the blended powders compared to the matrix after HIPing. 126

9-5 Fractographs of the a) the gas atomised Ti-6Al-4V + B blend and (b) Ti + 2B. 126

9-6 The tensile properties of Ti-6Al-4V+0.5B milled for 60T seconds and HIPed at temperatures between 600°C and 900°C. 127

9-7 (a) shows prior powder particle boundary failure (b) shows brittle fracture. ~~The tensile properties of Ti-6Al-4V+0.5B milled for 60T seconds and HIPed at temperatures between 600°C and 900°C.~~ 127

9-8 The difference in mechanical properties between (a) the Ti-6Al-4V + B milled for various times and (b) the Ti-6Al-4V + TiB_2 milled for various times with Ti-6Al-4V milled for 12T seconds. 128

9-9 An optical micrograph of Ti-6Al-4V+2B showing failure of the sample through regions that are heavily reinforced with TiB. 128

9-10 A scanning electron micrograph of Ti-6Al-4V + 6.4TiB_2 milled for 12 T seconds and HIPed. The fracture surface shows evidence of failure along prior powder particle boundaries. 129

9-11 The difference in room temperature tensile properties between milled Ti-6Al-4V and the (a) Ti-6Al-4V + 2B and (b) Ti-6Al-4V + 6.4 TiB_2 HIPed and heat treated at 1300°C. 129

9-12 An optical micrograph shows the early stages of fracture in Ti-6Al-4V + 6.4TiB_2 that was heat treated at 1300°C for 8 hours prior to tensile testing. 130

9-13 Scanning electron micrograph of Ti-6Al-4V + 2B after heat treating at 1300°C for 8 hours. TiB needles can be seen on the surface of the fracture along with ductile areas. 130

9-14 The difference in mechanical properties of gas atomised Ti and Ti+B after milling at different times can be seen. 130

9-15 The difference in mechanical properties of the gas atomised Ti and Ti+TiB_2 after various milling times can be seen. 131

9-16 Prior powder particle boundary failure are observed in Ti+2B when milled 3 T seconds. 131

9-17 The fracture surface of the Ti+2B when milled for 12T seconds is much flatter. 131

9-18 The tensile mechanical properties of the (a) Ti+2B and (b) Ti+6.4TiB_2 compared with the gas atomised Ti can be seen in comparison with the samples heat treated at 1300°C for 8 hours. 132

9-19	The stiffness of Ti, Ti_{sf}, Ti-6Al-4V and Ti-15-3-3-3 can be seen to increase with increasing volume fraction of TiB.	133
9-20	The time for a 1 μm boron particle to react fully to form TiB. Data calculated using data from Reeves (1992) detailed in §8.2.2.1	133
10-1	Graphs showing the superplastic properties of conventional Ti-6Al-4V shows the effect of (a) temperature at a strain rate of $6x10^{-4}s^{-1}$ and (b) strain rate on the elongation to failure of conventional Ti-6Al-4V	146
10-2	Graphs showing the superplastic properties of gas atomised Ti-6Al-4V and milled Ti-6Al-4V tested at their HIPing temperatures at a strain rate of $6x10^{-4}s^{-1}$ and compared with conventional Ti-6Al-4V tested at a range of temperatures.	147
10-3	Graphs showing the flow stress of gas atomised Ti-6Al-4V compared with conventional Ti-6Al-4V tested at a strain rate of $6x10^{-4}s^{-1}$ at (a) 800°C and (b) 900°C.	147
10-4	A SEM micrograph showing a cross section of the gas atomised sample HIPed 900°C and tested at 900°C at a strain rate of $6x10^{-4}s^{-1}$. Cavitation can be seen in the cross section.	148
10-5	Graphs showing the superplastic properties of milled Ti-6Al-4V HIPed at a range of temperatures and tested at 900°C and tested at a strain rate of $6x10^{-4}s^{-1}$, where (a) shows the tensile elongation and (b) shows the flow stress.	148
10-6	A graph showing the tensile elongation of milled Ti-6Al-4V HIPed at a range of temperatures and tested at their HIPing temperatures at a strain rate of $6x10^{-4}s^{-1}$.	149
10-7	Graphs showing the superplastic properties of milled Ti-6Al-4V HIPed at various temperatures and tested at 900°C at different strain rates, where (a) shows the elongation and (b) the flow stress in comparison with conventional Ti-6Al-4V.	149
10-8	Micrographs of superplastic formed milled Ti-6Al-4V are shown where, (a) shows cavitation in gauge length of the HIPed and formed at 900°C at a strain rate of $6x10^{-4}s^{-1}$, (b) shows no cavitation in the head of the sample HIPed and formed at 900°C at a strain rate of $6x10^{-4}s^{-1}$, (c) shows cavitation in the gauge length of sample HIPed at 800°C, tested at 900°C at a stain rate of $6x10^{-4}s^{-1}$ and (d) shows grows cavitation in the sample HIPed at 700°C, tested at 900°C at a strain rate of $6x10^{-4}s^{-1}$.	150
10-9	Graphs shows the superplastic properties of Ti-6Al-4V+0.5B milled showing (a) the tensile elongation of samples tested at their HIPing temperature at a strain rate of $6x10^{-4}s^{-1}$ and (b) the flow stresses.	151
10-10	Graphs show the superplastic properties of Ti-6Al-4V+0.5B milled and HIPed at various temperatures showing the (a) tensile elongation with increasing strain rate and (b) the flow stresses.	152
10-11	SEM images showing the Ti-6Al-4V+0.5B HIPed at 900°C and tested at 900°C at a strain rate of $6x10^{-4}s^{-1}$ where (a) shows the TiB particles aligned in the tensile direction and (b) shows the 'i' particles which bend around α grains, 'ii' particles that normal to the tensile direction and 'iii' shows a grain which has been sheared along a TiB needle.	153
B-1	Grain growth of Ti-6Al-4V produced by mechanical milling for 60T seconds and hot isostatic pressing for 2 hours at 150 MPa.	171
B-2	The reduction in dislocation density with increasing temperature. Given a dislocation density of 10^{12} (mm^{-2}) at room temperature in mechanically alloy powders and an annealed structure (with a dislocation density of 10^{5} mm^{-2}) at 600°C.	171

1. INTRODUCTION

Titanium and its alloys are relatively new engineering materials and have been in structural use since 1952. Despite being new, titanium is used widely for aerospace, defence, chemical, food and medical applications because of its high strength to weight ratio, high temperature capability, low density, excellent corrosion resistance and biocompatability. Ti-6Al-4V (wt. %) is the most common titanium alloy, accounting for approximately 50 % of world sales (Smith (1993)). The properties of titanium in comparison with other engineering alloys and TiB are shown in Table 1-1.

Material	Young's Modulus (GPa)	Tensile Strength (MPa)	Density (gcm^{-3})	Reference
α-Ti	105	340-620	4.5	Smithells (1983) Donachie (1988)
Ti-6Al-4V	110	1040	4.4	Smithells (1983) Donachie (1988)
TiB†	480-550	3500	5.0	Saito (1995) Dubey *et al.* (1997)
Steel	210	200-2500	7.9	Smith (1993)
Nickel superalloys	250-300	580-900	8.3	Smith (1993)

Table 1-1. A comparison of the properties of difference engineering materials and the ceramic TiB.
† Estimated values of the properties of TiB

Titanium is limited in its application as a result of its low stiffness and difficult formability particularly in comparison to steels. Improvements in strength, stiffness and formability are required if titanium is going to satisfy the future requirements of the aerospace industry, both for engine and structural components.

The stiffness of titanium can be improved by producing a titanium metal matrix composite (MMC). MMC's combine the high strength, stiffness and wear resistance of a ceramic reinforcement with the toughness and damage tolerance provided by a metal matrix. In this study TiB was chosen as the ceramic to reinforce either Ti, Ti-6Al-4V or Ti-15-3-3-3 alloy matrices.

Superplasticity is a novel forming method suited to Ti-6Al-4V, which utilises gas pressure to form sheet material into a die. Producing components using superplastic forming technology requires high temperatures (900°C) and long forming times. It is

therefore commercially attractive to increase the strain rate and/or decrease the processing temperature at which superplastic forming can occur.

The aim of this study is to produce titanium boron alloys with a uniform distribution of TiB within titanium. Based on industrial experience in developing aluminium MMC's, mechanical milling, in which the powders are 'kneaded' together to achieve a uniform dispersion of the ceramic phase, was selected for this study as the most promising route for producing the titanium boron alloys. Titanium and boride powder selection and process conditions relating to mechanical milling were assessed during this study. Their effect on the microstructure and the room temperature tensile properties was assessed. Additionally the effect of grain refinement, as a result of heavy deformation during mechanical milling, on the superplastic properties of Ti-6Al-4V was assessed.

2. REVIEW OF MECHANICAL ALLOYING

Mechanical alloying or milling was initially developed for oxide dispersion strengthening (ODS) of nickel based superalloys with yttria as the dispersed phase in the late 1960's (Benjamin (1970)). The aim was to produce a superalloy with oxides that would not coarsen during processing or in-service. This material could not be produced by conventional melting technology and so yttria, which was chosen as the stable oxide, was incorporated using the solid state mechanical alloying technique. Since this initial development, mechanical alloying has been used to produce novel alloys that cannot be made using conventional techniques (Ward-Close *et al.* (1995)), metastable phases (Shultz (1988)) and nanocrystalline microstructures (Fecht *et al.* (1989)). The milling has also been used in the production of aluminium metal matrix composites, where SiC is distributed evenly in an aluminium alloy matrix. This distribution, and hence mechanical properties, are superior ~~than~~ to those achieved by casting (Tarrant (1998)).

Mechanical alloying is defined as a high energy mixing process, where alloying is achieved by deformation, fracture and cold welding of ductile powders. This results in a layering of the elemental powder giving a lamellar type microstructure (Shultz (1988), Bormann (1993)) as shown in Figure 2-1. The layering continues refining the powders until a homogeneous distribution of the two elements is achieved. Milling of brittle powders consists only of welding and fracture and so layering does not occur. In mixed systems the brittle powder fractures into small particles and becomes engulfed in the ductile powder and this is the principle of the ODS alloys.

For successful mechanical alloying to occur there needs to be a balance between the cold welding and fracturing process. However, with ductile powders, that readily cold weld, the balance between cold welding and fracture is difficult to achieve and cold welding can dominate. Where welding dominates a rapid increase in powder particle size occurs as well as an increase in the build-up of powder within the mill and hence powder yields are reduced. Process control agents (PCA) (Harris *et al.* (1993)) and cryogenic milling have been explored to encourage the fracture of ductile powders (Lu and Lai (1998)).

For a process control agent to work effectively it should not react chemically with the powder being milled and should decompose at relatively low temperatures during post milling processing. PCAs are typically organic compounds such as stearic acid, heptane or polyethylene glycol, which act as surfactants and reduce the cold welding and are effective at controlling the particle size of powders during milling. Work by Harris *et al.* (1993) clearly shows a reduction in the average particle size when milling copper powder with the PCA dodecane (Figure 2-2).

Cryogenic milling is used to enable milling of materials below their ductile to brittle transition temperatures however it may be problematic and uneconomic for commercial milling operations. Cryogenic milling is unlikely to be suitable for milling titanium and its alloys because it remains ductile to very low temperatures.

2.1 Mechanical alloying of titanium

Mechanical milling of titanium alloys has concentrated on a number of areas:

- Titanium aluminides have been milled to reduce the grain size with the aim of increasing their ductility (Oehring and Bormann (1991), Oehring *et al.* (1995), Goodwin and Ward-Close (1993)).
- Titanium has been milled under atmospheres of hydrogen to form titanium hydride for application as a hydrogen storage material (Small *et al.* (1999), MacKay (1999)).
- Ultra lightweight titanium has been produced consisting of an alloy of titanium and magnesium, which cannot be formed by conventional processing (Ward-Close *et al.* (1995)).
- Titanium metal matrix composites have been produced to increase the stiffness of titanium alloys (Goodwin *et al.* (1995)).

Mechanical milling of titanium and titanium aluminide powders has resulted in the progressive refinement of the grain size within the powders to a nanocrystalline level. In the case of titanium aluminides, a metastable hexagonal close packed microstructure is produced. Initially it was thought that face centred cubic and amorphous phases could be produced by milling titanium and its alloys, however more recent work has concluded that these effects are the result of contamination of the titanium powders during milling. The process of mechanical alloying, as previously discussed, involves the deformation, welding and fracture of powder particles. These processes involve the

formation of new surfaces that react with the surrounding atmosphere. A number of authors (Goodwin and Ward-Close (1993), Ohering and Bormann (1993), Lauer *et al.* (1997)) concluded that the formation of amorphous or face centred cubic phases is related to contamination by oxygen and nitrogen, which form titanium nitride and oxynitride.

Critical to success in milling titanium and its alloys is control of the atmosphere. This can be most readily achieved by placing the mills within a glovebox that contains a purified argon atmosphere (Goodwin *et al.* (1997), Liu *et al.* (1998)). By milling under these carefully controlled conditions the hexagonal close packed titanium phase was retained (Goodwin *et al.* (1997), Liu *et al.* (1998)).

Process control agents are commonly used to enhance the welding and fracture behaviour of the titanium during milling thus inhibiting a build up in the powder particle size. However, titanium is susceptible to interstitial contamination and can accommodate up to 24 at. % oxygen, 23 at. % nitrogen and 1.6 at. % carbon in solid solution within the α Ti phase (Massalski *et al.* (1986)). This highly reactive nature of titanium prohibits the use of organic process control agents because they result in unacceptable levels of interstitial contamination (Goodwin and Ward-Close (1993)).

For titanium and its alloys, the benefits of high purity mechanical milling are clear. The production of nanocrystalline grains in titanium aluminides has enabled them to be consolidated at much lower temperatures than those prepared by conventional powder metallurgy techniques. The mechanical milling has also enabled the incorporation of yttria into titanium aluminides enabling further control of the grain size during heat treatment (Bormann (1993)).

For this study mechanical milling was used to produce a fine grain material. The milling also distributed boron or TiB_2 into either titanium or Ti-6Al-4V. The aim was to study the effect of boron on the room temperature properties of titanium and Ti-6Al-4V and the effect of boron on superplastic properties of Ti-6Al-4V.

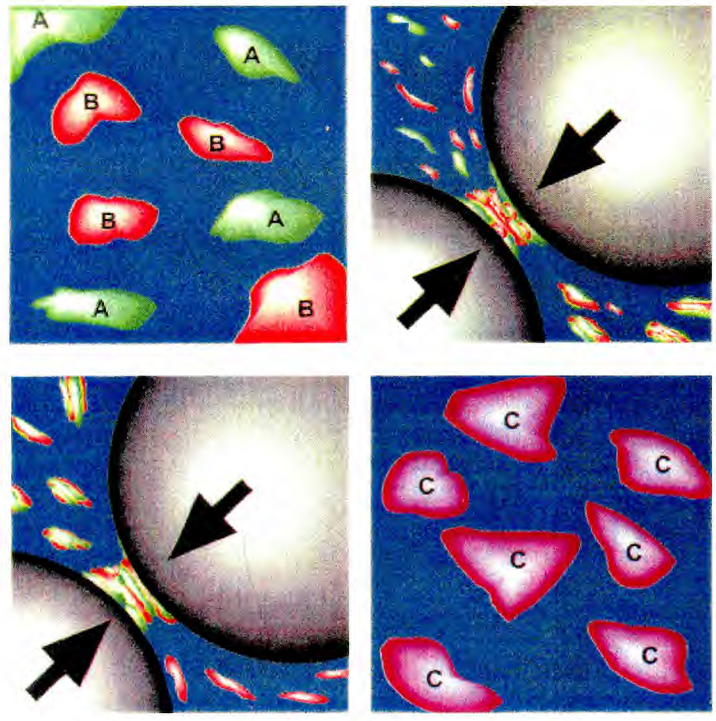


Figure 2-1 A schematic of the mechanical alloying process. Elements A and B are milled. Layering of the powders occurs and milling is continued until a homogeneous distribution of the elements is achieved giving the alloy C (Gardiner *et al.* (1996))

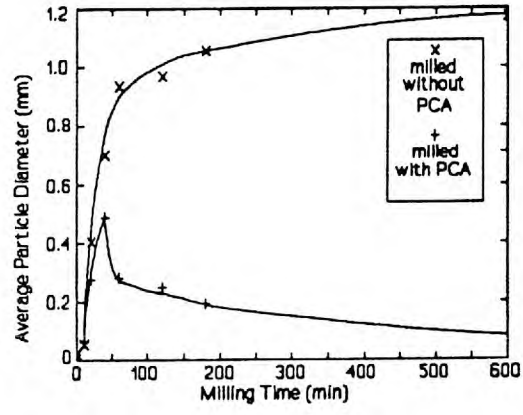


Figure 2-2 A comparison of powder particle size when milling copper powder with and without a process control agent (Harris *et al.* (1993))

3. REVIEW OF TITANIUM PARTICULATE METAL MATRIX COMPOSITES – PRODUCTION AND MECHANICAL PROPERTIES.

3.1 Introduction

Metal matrix composites (MMC's) are a class of materials that seek to combine the high strength and stiffness of a ceramic with the damage tolerance and toughness provided by a metal matrix. Additional improvements such as enhanced wear resistance and improved high temperature capability may also be obtained. MMC's were first produced for aerospace applications, where a high cost of manufacture could be justified. However, advances in MMC manufacturing have led to their being considered for applications in the automotive industry and other industrial applications where high strength and stiffness combined with low density and good wear resistance are required.

The MMC reinforcement can be a particulate, short fibres or continuous fibres. A particulate can have either a spherical, cubic, platelet or random morphology, with a particle size of approximately 1-100 μm. However, particulate reinforced MMC's also have the advantage of being isotropic, can be cheaper to manufacture and amenable to subsequent processing or component forming operations compared with fibre reinforced MMC's.

Aluminium particulate MMCs are far in advance of their titanium counterpart, with many examples of commercial motor sport, sporting goods and aerospace applications (Tarrant (1998)). Successful production routes have included mechanical alloying and melt stirring, where melt stirring is cheaper but inferior compared to the mechanically alloyed product. Greater difficulty has been found in producing a particulate MMC from titanium alloys due to the highly reactive nature of titanium with both the atmosphere and the proposed reinforcing phases.

Methods for the production of particulate MMC's include arc melting, rapid solidification, gas atomisation, powder blending and mechanical milling. This review assesses the selection of a suitable reinforcement and compares the manufacturing process and mechanical properties of titanium TiB reinforced composites.

3.2 Reinforcement selection

A number of different particulates have been selected to reinforce titanium alloys and these include TiB_2, TiN, B_4C, ZrC (Simmons *et al.* (1997)), SiC (Tong *et al.* (1995)), (Hu and Loretto (1994a)), TiB, TiC (Saito *et al.* (1995a)), and Al_2O_3. The relative properties of some of these reinforcements are shown in Table 3-1. TiB, TiB_2, B_4C and TiC all have a high modulus and are therefore attractive as a reinforcement. B_4C, SiC and Si_3N_4 offer the potential for a reduction in density of the composite. However, density and modulus are not the only criteria that need be considered. Both TiB and Al_2O_3 have similar coefficients of thermal expansion to titanium and hence there is no problem associated with the formation of residual stresses during processing. Another consideration is the stability of the reinforcement phase in the titanium matrix. Problems associated with the formation of embrittling reaction zones, because of the highly reactive nature of titanium, during the production of the MMC also need to be addressed. In the case of SiC reinforcements, Tong *et al.* (1995), Jong *et al.* (1992) and Hu *et al.* (Hu and Loretto (1994a), Hu and Loretto (1994b), Hu *et al.* (1995a)) have commented on large reaction zones of TiC and Ti_5Si_3 around SiC particles. Work on the production of long fibre Ti-SiC composites has centred on the development of coatings (~ 5 μm thick) to reduce reaction rates and these coatings include carbon and TiB_2 (Upadhyaya *et al.* (1994)). This approach is not practical or economic for the development of a particulate reinforced composite. Work at DERA has found that Al_2O_3 has resulted in the formation of $TiAl_3$. Saito *et al.* (1995b) have shown that TiC particles coarsened rapidly during processing (Figure 3-1). However, the TiB particles did not coarsen significantly after 100 hours at the sintering temperature resulting in a needle size of approximately 3 x 8 μm (Saito *et al.* (1995a)). This resistance to coarsening of TiB particles in Ti has also been observed by Hu *et al.* (1995b) and is likely to result from the low solid solubility of the boron in titanium (<0.001 at. %) compared with 1.6 at. % for carbon and 23 at. % for nitrogen (Saito *et al.* (1995b), Massalski *et al.* (1986)).

In summary, previous work suggests for the formation of a particulate reinforced MMC it is essential that reinforcing phase does not react with the matrix and does not coarsen at the processing temperature. TiB, although offering no density advantage, is attractive as a reinforcement, due to its stability of size in the matrix, the similarity of thermal

expansion coefficient with titanium and its high Young's modulus. This review will concentrate on the production and mechanical properties of titanium/TiB MMC's.

3.3 Production routes

Methods for the production of a titanium MMC have included conventional ingot melting, (Brown *et al.* (1961), Dubey *et al.* (1997), Philliber *et al.* (1995)), rapid solidification (Fan *et al.* (1997)), direct powder atomisation (Yolton and Moll (1995)), powder blending (Saito *et al.* (1995b), Saito (1995)) and mechanical milling (Goodwin *et al.* (1995)). Where powders are produced, compaction methods also need to be considered as well as secondary forming. Compaction methods for powders include cold compaction and sintering, hot isostatic pressing and powder extrusion. Secondary forming techniques include forging, rolling, swaging and extrusion.

3.3.1 Vacuum arc melting

Vacuum arc remelting and induction skull melting are attractive as production methods for MMC's because they offer the potential of a relatively cheap product (Brown *et al.* (1961), Dubey *et al.* (1997), Philliber *et al.* (1995)). The TiB forms as both primary and eutectic needles (§ 4, Figure 4-1). The formation of large primary TiB particulates (100-200 μm) can be detrimental to the subsequent working and cold deformation because particle cracking can occur (Simmons *et al.* (1997)).

3.3.2 Rapid solidification

Rapid solidification (RS) has been used by Fan *et al.* (Fan and Miodownik (1995), Fan *et al.* (1995)) to produce melt spun ribbon and by Sastry *et al.* (1984) and Soboyejo *et al.* (1994) for the production of powder. Rapid solidification of ribbon has been found to give a metastable product of supersaturated boron in α Ti solid solution. The TiB particles were produced by precipitation from the boron in supersaturated solid solution. Fan *et al.* (1995) found that by undertaking a low temperature (<700°C) heat treatment prior to consolidation, equiaxed TiB particles can be produced and this is discussed in greater detail in § 4.1.

3.3.3 Gas atomisation

Inert gas atomisation, which is often considered as a rapid solidification technique, has been used to produce Ti-6Al-4V-TiB composites (Hu *et al.* (1995b), Yolton and Moll

(1995)) and these powders generally have a particle size < 250 μm. The titanium which is atomised with boron produces TiB needles within a dendritic matrix. A small number of relatively coarse TiB particles were also seen and these were approximately 25 μm in length. Atomised powders, due to their spherical nature, have a good packing density and flowability making them amenable to conventional powder processing.

3.3.4 Powder blending

Powder blending has also been used for the production of Ti-TiB composites. The titanium powders can be produced by a number of methods, including hydride dehydride, gas atomisation, sponge fines and plasma rotating electrode process. These powders have been blended with boron or boride powders to produce a titanium MMC after subsequent consolidation. Both prealloyed titanium powders, such as Ti-6Al-4V, or titanium powders with the addition of a master alloy have been used to give alloy matrices (Saito *et al.* (1995a)). The particle size and morphology of the powders is an important factor to achieving a good distribution of the TiB. Saito *et al.* (1995a) have assessed sponge fines with a particle size of approximately 100 μm and an open structure. Therefore on blending the TiB_2 can penetrate this open structure and a better distribution can be achieved (Fan *et al.* (1997), Saito *et al.* (1995c)). Sponge powders have poor flowability and a low packing density, however this can be improved by short mechanical attrition of the powders (Fan *et al.* (1997)). Hydride-dehydride or hydrided powders have also been used for powder blending and with a particle size of approximately 45 μm a good distribution of TiB can be achieved (Saito *et al.* (1995b), Furuta *et al.* (1999)). Where sponge fines have been used, titanium alloys have been produced by blending in master alloy powder. A homogenising high temperature heat treatment is used to produce the alloy. Where titanium hydride is used the hydrogen can be removed during subsequent degassing or vacuum sintering.

A progression from the powder blending process is mechanical milling. The difficulties of milling titanium have been discussed in §2.1. The aim of milling, as opposed to blending alone, is to improve the distribution of the reinforcement.

3.3.5 Compaction

With all powder processing routes consolidation needs to be considered and techniques include cold pressing and sintering, hot isostatic pressing or direct powder extrusion.

Cold pressing and sintering have been used (Saito *et al.* (1995b)) as a cost effective consolidation technique. Hot isostatic pressing produces a solid with much lower porosity and, although more expensive, it becomes more efficient with larger batch sizes. Direct powder extrusion has also been used (Yolton and Moll (1995)) however this results in the alignment of the TiB needles. Another benefit of titanium MMC's produced by powder metallurgy is the potential to exploit net and near net shape forming techniques which require no secondary forming and reduce both machining and waste material.

3.3.6 Secondary forming

Secondary forming techniques have been used successfully on titanium particulate MMC's and include swaging, rolling and extrusion. These techniques all result in the alignment of the TiB needles and the titanium MMC is no longer isotropic but resembles a whisker reinforced MMC. This loss of the isotropic nature may not be a problem depending on the potential application.

3.4. Mechanical properties

Particulate MMC's offer many potential advantages compared with conventional titanium alloys including increased stiffness, good creep performance, fatigue resistance and wear resistance. Much of the work on mechanical properties has concentrated on the tensile performance and some of this data are presented in this summary. Other properties such as fatigue, creep and wear resistance have been mentioned briefly as they represent a lower proportion of the data available.

3.4.1 Room temperature tensile properties

Figure 3-2 shows experimental results of Young's modulus compared with theoretical predictions. It can be seen that the Young's modulus increases with the volume fraction of reinforcing phase. There is variability in the results, especially where the volume fraction additions are low. The variability may relate to particle size, particle orientation and experimental testing techniques used. The Eshelby approach (Clyne and Withers (1993)) using an aspect ratio of one, fits the data from MMC's produced by powder metallurgy where the TiB has a random orientation. The rule of mixtures approach fits work by Brown *et al.* (1961) where large needles (~7.6-12.5 μm long) were found oriented in the tensile direction.

Figure 3-3 and Figure 3-4 show the effect of TiB on 0.2 % proof stress and ultimate tensile strength. In general, the addition of TiB appears to give a strength increase. However, care needs to be taken when assessing the data because variations in oxygen and nitrogen concentration, the size of the TiB and other processing defects, such as pores, all affect the MMC's strength and may also relate to very limited ductility and brittle fracture.

Figure 3-5 gives the reported ductility of some of the titanium MMC's. The results indicated a ductility of approximately 5-7 % for 10 volume % TiB and 3% for 20 volume % TiB (Saito *et al.* (1995b)). Again the oxygen and nitrogen strongly affect the ductility as do the particle distribution and size. Much of the material produced with a ductility greater than 5% has been subjected to secondary forming processes such as forging, rolling or extrusion. During these processes the TiB needles grow and align in the working direction, often resulting in the formation of essentially a whisker reinforced composite. Failure of these composites tends to occur by cracking of the TiB whiskers and these cracks then link up to cause final failure (Tsang *et al.* (1997)).

3.4.2 High temperature tensile

A few studies have assessed the high temperature tensile properties of particulate Ti MMCs, however initial results by Yolton and Moll (1995) indicate strength and modulus improvements were retained up to temperatures of 540°C. Soboyejo et al (1994) with a Ti-6Al-4V + 0.5% B composite and Ranganath and Mishira (1996) with a composite containing particles of both TiB and TiC, both showed that the composites have higher yield strengths than monolithic materials up to 500°C. Soboyejo compares the MMC material with conventional mill annealed Ti-6Al-4V, with the MMC showing better high temperature performance.

3.4.3 Fatigue

A number of authors have studied the fatigue behaviour of particulate Ti MMC's and the results are encouraging. Saito *et al.* (1995c) report an increasing fatigue strength with increasing TiB content. Greater than 10^7 cycles at 600 MPa peak load and an r ratio of 0.1, was achieved for a Ti-6Al-4V + 10 volume % TiB MMC (Saito (1995)). This was better than their Ti-6Al-4V alloy produced by the blended elemental powder route, however no comparison was given with conventional Ti-6Al-4V. Crack initiation

occurred from the pores within the material, unrelated to TiB particles or its interface with the matrix. The fatigue cracks tended to avoid TiB particles, if the crack encountered a particle it was first trapped, then cut through the particle. This indicates the good interfacial bond between the TiB and the matrix. Srivatsan *et al.* also tested Ti-6Al-4V/TiB composites (Srivatsan *et al.* (1995)) where the TiB needles were perpendicular to the crack growth direction. In all conditions, the material was either as good as, or better than the mill annealed Ti-6Al-4V. Improvements in fatigue crack growth rate were associated with the increased whisker length, which was shown to promote crack-tip shielding and a tortuous crack path.

3.4.4 Creep

Tsang *et al.* (1997) found that for a Ti/TiB composite the steady state creep rates were between 1 and 3 orders of magnitude lower than the base alloys tested at 550°C and higher threshold stresses were also seen. This creep strengthening increases with increasing volume fraction of reinforcing phase. This is unlike aluminium MMC's where creep life tends to be reduced by the presence of SiC particles, due to decohesion and void initiation at the particle matrix interfaces (El-Nasr *et al.* (1996)). The interfacial bond strength in the titanium MMC's reinforced with TiB appears to be high and so represents a much more favourable case. It is also encouraging that Saito (1995) showed that their titanium MMC had ~~far~~ superior ~~properties~~ properties ~~than~~ to the conventional titanium alloys at temperatures above 627°C. However conventional titanium alloy matrices are unlikely to be used above 600°C due to their poor oxidation resistance above that temperature.

3.4.5 Wear resistance

Wear resistance is an important property consideration for engineering materials. Traditionally titanium is considered poor in terms of wear, prompting work on titanium nitride coatings for enhanced wear resistance. Wear testing can be complicated and it is essential to choose a test that uses the wear regime seen in service. However, initial work by Saito (1995) indicates that the wear resistance of Ti-6Al-4V + 10 volume % TiB MMC in pin on a medium carbon steel disk was similar to that of Stellite 6, a typical wear resistant material.

3.5 Summary

- TiB has been chosen for the production of particulate and whisker reinforced titanium MMC's due to its high modulus, good stability, low solid solubility and similar coefficient of thermal expansion to titanium.
- A successful composite material is one which is commercially viable, in terms of both cost and production capability. Methods such as rapid solidification (melt spun ribbon) are costly and difficult to establish on a commercial scale.
- To date, mechanical properties of titanium TiB composites are encouraging, indicating increases in strength, stiffness, wear resistance, fatigue and creep resistance with increasing TiB concentration, whilst retaining some ductility.
- For this study mechanical milling was chosen to distribute the titanium boride precursor within the titanium (alloy) matrices.

	Young's Modulus (GPa)	Density ($g\ cm^{-3}$)	CTE ($x\ 10^{-6}\ K^{-1}$)
α–Ti	105	4.5	8.8
Ti-6Al-4V	115	4.4	8.8
TiB	480 - 550	5.0	8.6
TiC	460	4.9	7.4
TiN	250	5.2	9.3
SiC	420	3.2	4.3
Si_3N_4	320	3.1	3.2
TiB_2	529	4.5	6.4
B_4C	449	2.5	4.5
Al_2O_3	350	3.8	8.1

Table 3-1. A comparison of the physical properties of titanium and potential ceramic reinforcing phases (Saito (1995), Clyne and Withers (1993)).

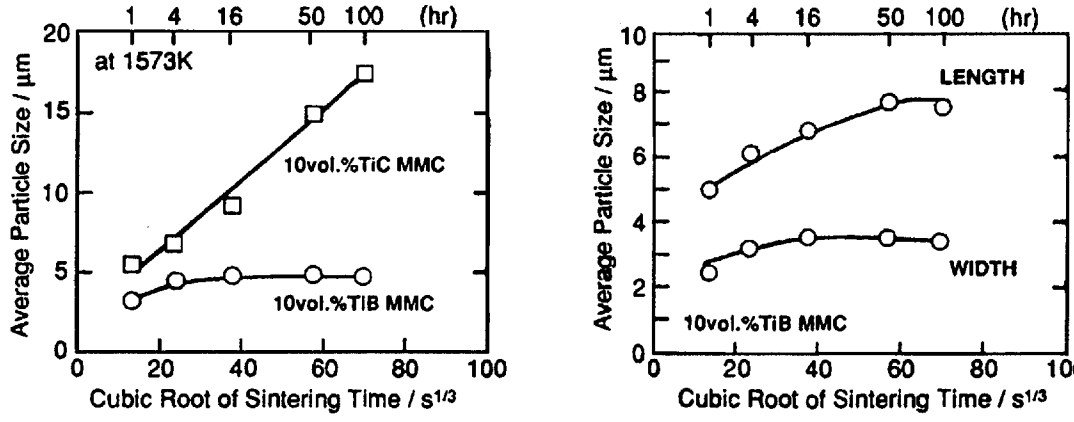


Figure 3-1 A comparison of (a) the coarsening behaviour of TiB and TiC particles in Ti-4.3Fe-7Mo-1.4Al-1.4V based MMCs at 1300°C and (b) the difference in the length and width of TiB particles at 1300°C (Saito *et al.* (1995a)).

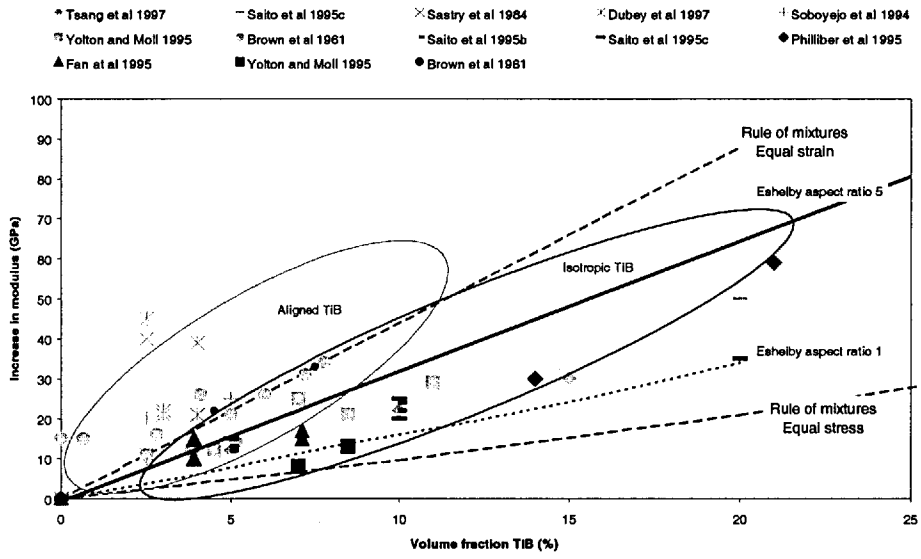


Figure 3-2 The effect of TiB volume fraction on the Young's moduli of various titanium alloys. The graph shows the increase in the modulus with the addition of TiB. The modulus of the monolithic matrix used has been subtracted from the modulus of the composite. The black symbols indicate material where the TiB needles have a random orientation and the grey symbols indicate material where the TiB needles are aligned.

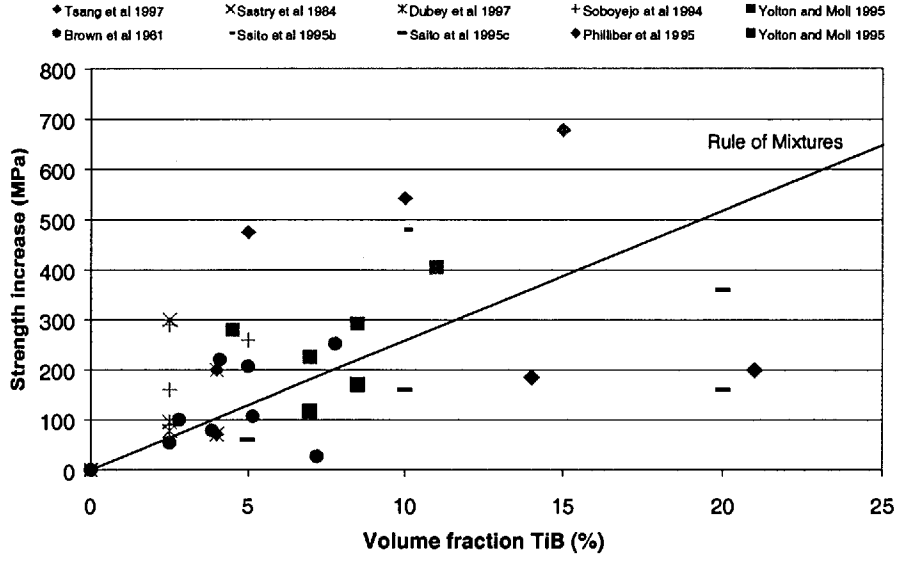


Figure 3-3 The effect of TiB volume fraction on the 0.2% proof stress of titanium MMC's The graph shows the increase in the 0.2 % proof strength with the addition of TiB. The 0.2% proof strength of the monolithic matrix used has been subtracted from the 0.2 % proof strength of the composite. The black symbols indicate material where the TiB needles have a random orientation and the grey symbols indicate material where the TiB needles are aligned.

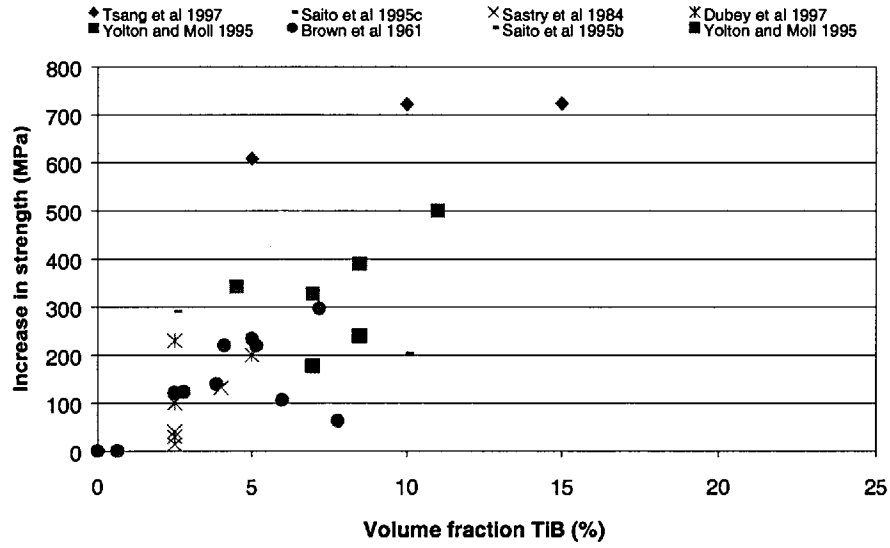


Figure 3-4 The effect of TiB on the ultimate tensile strength of titanium MMC's. The graph shows the increase in the ultimate tensile strength with the addition of TiB. The ultimate tensile strength of the monolithic matrix used has been subtracted from the ultimate tensile strength of the composite. The black symbols indicate material where the TiB needles have a random orientation and the grey symbols indicate material where the TiB needles are aligned.

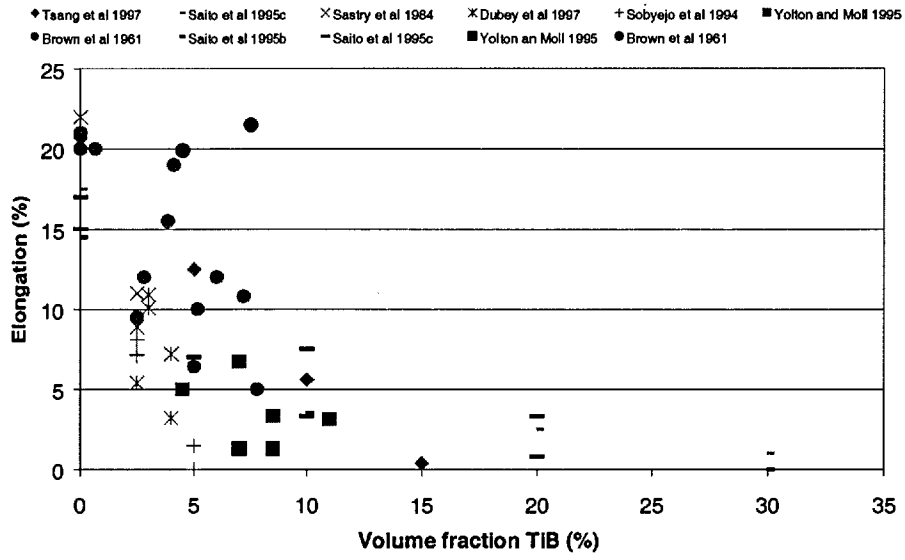


Figure 3-5 The effect of TiB on the ductility of titanium MMC's. The black symbols indicate material where the TiB needles have a random orientation and the grey symbols indicate material where the TiB needles are aligned.

4. REVIEW OF THE TITANIUM-BORON SYSTEM

The titanium-boron phase diagram is shown in Figure 4-1. Boron has less that 1 at. % solubility in both α and β-Ti at all temperatures, up to the melting point. There are three intermetallic compounds, TiB, Ti_3B_4, and TiB_2 (Murray (1987)). TiB and TiB_2 are almost stoichiometric, the range being 1-2 at. %B. TiB is the most stable phase within titanium and has a B27 crystal structure as shown in Figure 4-2.

To distribute the TiB within titanium a number of methods have been considered and assessed as discussed in §3.3 and these methods include molten and solid state techniques. The formation of TiB during solid state processing will be discussed as this relates to the powder techniques used in the current study.

4.1 Formation of TiB

Work by Brandstotter and Lengauer (1997) on pack-boriding titanium at 1300°C for 3 hours indicated that two boride layers were formed. The TiB_2 was on the outside (8 μm thick), titanium monoboride was the next layer (20 μm thick) and α Ti on the inside; the Ti_3B_4 phase was not observed. Equally, work by Jong *et al.* (1992) and Reeves (1992) assessed the reaction of TiB_2 that was blended with titanium powder and compacted, either by HIPing at 900°C (Jong *et al.* (1992)) or extruded at 950°C (Reeves (1992)). In neither study was the Ti_3B_4 phase observed in α titanium boron alloys. Reeves (1992) suggests the boron initially diffused into the unsaturated matrix resulting in the transformation of the diboride into the monoboride (an inwards moving reaction front). This reaction zone was approximately 1 μm in an 8 μm particle after heat treatment for 80 minutes at 950°C. Following saturation of the matrix, monoboride needles nucleated at the original particle/matrix interface. Rapid diffusion of the boron along the faulted needles enabled an inward moving diboride to monoboride transformation to continue.

Both Jong *et al.* (1992) and Reeves (1992) observe the formation of TiB needles emanating from the TiB_2 particles. The B27 structure of TiB is characterised by zigzag chains of boron atoms parallel to the 'b' direction (Figure 4-2a). Each boron atom lies at the centre of a triangular prism of six titanium atoms (Figure 4-2b). These triangular

are stacked in columnar arrays as shown in Figure 4-2c. The prisms are connected at edges forming boron free pipes. Growth normal to the planes containing metal and boron atoms, in the same stoichometry as the crystal, should be faster than growth involving alternate planes of boron and titanium. It is also argued that strong bond directions tend to grow at a faster rate (B-B > B-M > M-M). Based on these arguments the 'b' direction will grow fastest.

However Fan *et al.* (1995) assessed the formation of TiB in rapidly solidified Ti-6Al-4V + *X*B alloys, where equiaxed TiB particles were observed as a result of low temperature heat treatment. Rapid solidification results in fibres of supersaturated solid solution of boron in α and β solid solutions. Fan *et al.* (1995) found heat treatment of the ribbons below 800°C prior to compaction resulted in the formation of an "equiaxed" TiB structure. The equiaxed particles of TiB were approximately 100 nm in diameter.

Fan *et al.* (1995) have found the morphology of the TiB particles was dependent on the thermal condition in which the TiB phase nucleates and grows. Experimental results indicate that high temperature annealing resulted in the formation of needle shaped TiB, whereas annealing below 800°C the TiB formed in a nearly equiaxed morphology with a small population of needle shaped particles. It was suggested that if precipitation occurred at a lower temperature, the diffusion of boron became rate controlling and therefore the morphology depended on the supply of boron. The supersaturated solid solution of boron allowed the formation of a large number of nuclei. When the amount of boron in solid solution reached equilibrium, growth of the TiB became difficult and the difference in growth rates along the crystallographic directions was reduced, therefore nearly equiaxed particles were produced. However, at higher temperatures the diffusion of the boron was thought to be higher and so needles were formed and the dominating growth direction was in the plane containing both boron and metal atoms.

4.2 The effect of TiB on the β transus

Sobeyejo *et al.* (1994) has noted an increase in the β transus, by as much as 300°C, in a titanium-TiB particulate composite and this could not be attributed to high oxygen and nitrogen concentrations. The solubility of boron in titanium is low at all temperatures and would be expected to have minimal effect. This is supported by Fan *et al.* (1995) and Sysoeva *et al.* (1996) who found that boron had no effect on the β transus temperature

due to its low solubility in both the α and β phases. The phase diagram assessed by Murray (1987) indicates a peritectoid for the $\beta + TiB \rightarrow \alpha$. Therefore within the limits of solid solubility the boron could increase the β transus temperature from that seen for Ti. The increase in β transus in Murray's assessment is from 882.5°C to 884°C. Variations of this amount were unlikely to be observed in the experimental work of the aforementioned authors and does not explain the observations of Soboyejo *et al.* Further work is required to clarify the effect of boron on microstructure of titanium and Ti-6Al-4V matrix with varying heat treatment conditions.

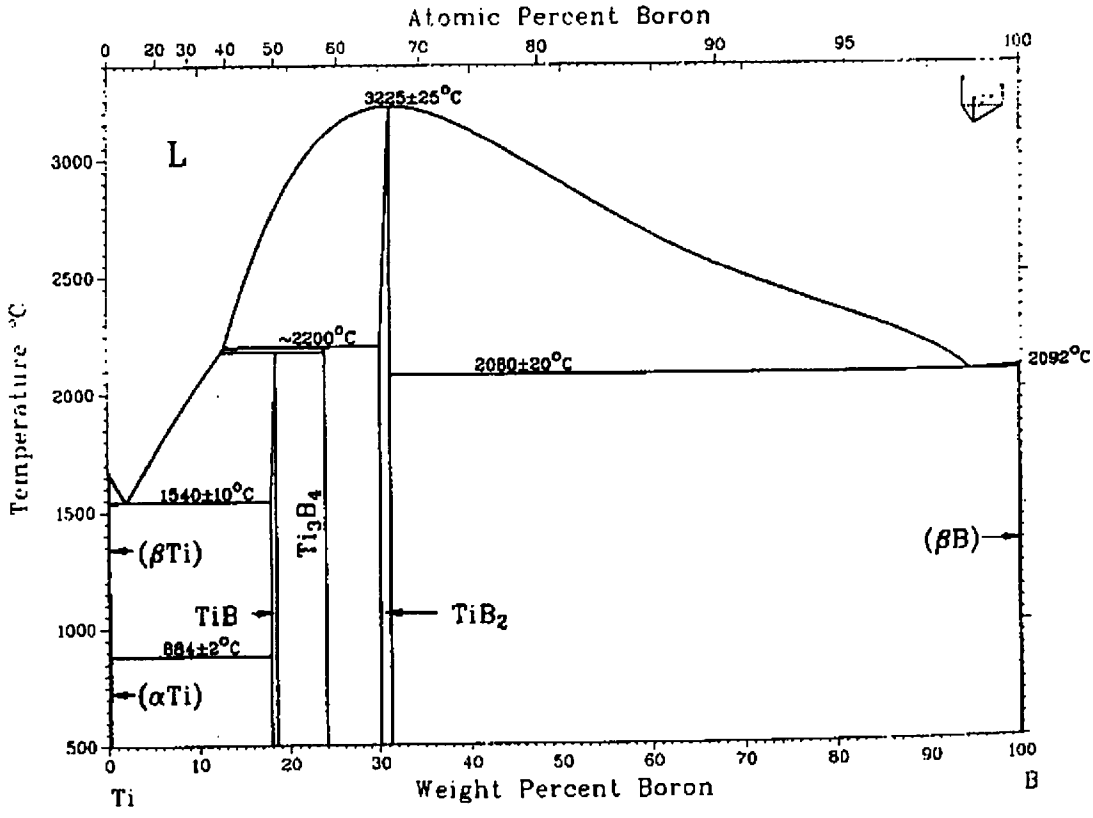


Figure 4-1 The titanium boron phase diagram (Murray (1987)).

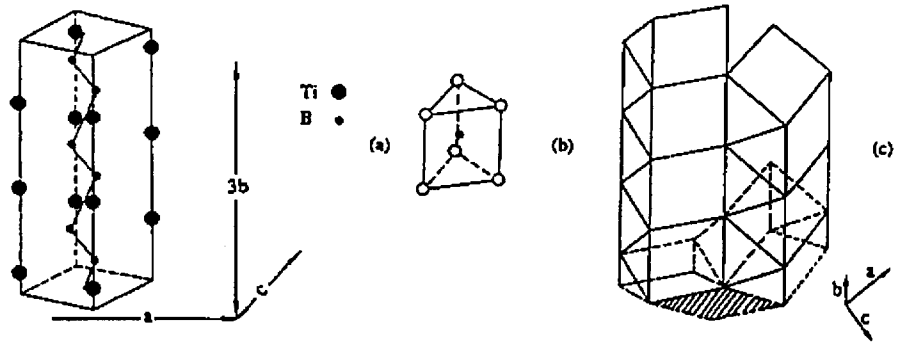


Figure 4-2 A schematic illustration of the atomic packing in TiB. a) The TiB unit cell (B27); b) the basic triangular prismatic arrangement of titanium atoms around each boron atom; c) the arrangement of the basic triangular prisms to form the TiB structure. (Fan (1993)).

5. REVIEW OF SUPERPLASTICITY

Superplasticity is the ability of a polycrystalline material to exhibit, in a generally isotropic manner, very high tensile elongations to failure. Superplastic materials exhibit high values of the strain rate sensitivity exponent, *m*, during deformation according to the following equation:

$$\sigma = \dot{\varepsilon}^m \varepsilon^n \exp^{-(Q/RT)}$$

Equation 5-1

where σ is flow stress, Q is activation energy, R is the gas constant, T is absolute temperature, ε is strain, $\dot{\varepsilon}$ is strain rate and n is a strain hardening exponent,

When considering superplasticity at a constant temperature, when the temperature is such that strain hardening does not occur (i.e. the mobile dislocation density is constant), then n = 0 and the basic equation is:

$$\sigma = k\dot{\varepsilon}^m$$

Equation 5-2

where k is a constant dependant on material condition. m = 1 represents ideal Newtonian viscous flow, for example hot glass, and typical values for hot metal, m=0.25.

Superplastic materials are generally considered to have a strain rate sensitivity (m) between 0.3 and 0.9 in the temperature range between 0.6 and 0.8 of the absolute melting point of the material. Superplastic deformation occurs at low flow stresses, usually below 20 MPa (Pearce (1987)). The low flow stresses are important for the practical application of superplasticity where gas pressure is used to form sheet material.

The large tensile elongation that is observed during superplasticity requires a mechanism by which the strain can be accommodated to avoid the formation of voids or cracks particularly at grain boundary triple points. Many theories debate the mechanism for the accommodation of the large tensile strains indicative of superplastic forming. It has generally been accepted that superplastic flow occurs by grain boundary sliding which is accommodated by a variety of processes including; diffusion, dislocation climb, recrystallisation, grain boundary migration and slip (Arieli and Mukherjee (1980), Gifkin (1976), Gittus, (1977)).

Attempts have been made to model superplastic flow and to compare these models with experimental results (Arieli and Mukherjee (1980), Gifkin (1976), Gittus (1977)).

These models fall into two forms; the accommodation of grain boundary sliding by either diffusion or dislocation climb and these are outlined below;

for diffusion accommodated grain boundary sliding:

$$\dot{\varepsilon} = \frac{A\sigma\Omega D_{eff}}{kTd^{a}} \qquad where \quad D_{eff} = D_{v}\left(1 + \frac{\Pi\delta D_{b}}{LD_{V}}\right)$$

Equation 5-3

for dislocation climb accommodated grain boundary sliding

$$\dot{\varepsilon} = \frac{A'Gb^{3}D_{B}}{kTd^{2}}\left(\frac{\sigma}{G}\right)^{2}$$

Equation 5-4

where, A and A' are constants, σ is stress, Ω is the atomic volume, D_v is the bulk self diffusivity, D_B is the boundary self diffusivity, d is the grain size, a is the grain size exponent (~2), δ is the grain boundary width, G is the shear modulus, b is Burger's vector and T is the temperature. In reality, it is unlikely that accommodation of superplastic deformation occurs by any single mechanism and will be highly dependant on the material being studied.

5.1 Superplasticity in titanium alloys

Superplasticity of titanium alloys has been widely studied (Hamilton (1984), Mahoney (1994), Paton and Hamilton (1979)) and the general properties of superplastic titanium alloys are summarised in Table 5-1. Ti-6Al-4V, which accounts for approximately half of the commercial titanium sales, is widely used for commercial superplastic forming, where the sheet needs no special processing. Titanium alloys, and Ti-6Al-4V in particular, can be superplastically formed enabling the production of complex shapes from sheet and also the production of structurally efficient components when used in conjunction with diffusion bonding e.g. honeycomb structures. Superplastic forming and diffusion bonding of Ti-6Al-4V has led to applications such as the Rolls Royce wide chord fan blade, the foreplane in the Eurofigher Typhoon and Rolls Laval heat exchangers.

The following review attempts to explain the effect of microstructure on the superplastic properties of Ti-6Al-4V, which was the alloy chosen for modification in this study. Variables that have been shown to affect superplasticity of titanium alloys are (Hamilton (1984)):

- grain size,
- grain size distribution

- grain size aspect ratio
- grain growth kinetics
- texture
- phase ratio (α/β)

5.1.1 Grain size effect

Grain size is known to strongly affect superplasticity and generally the optimum strain rate for superplastic forming materials is considered to be proportional to the inverse square of the grain size as shown in Equation 5-3 and Equation 5-4. The dependence of superplastic properties on grain size has been demonstrated by Ghosh and Hamilton (1979). They showed that an increase in grain size led to a higher flow stress and reduced the strain rate at which maximum strain rate sensitivity was achieved (Figure 5-1). The dependence of grain size on the flow stress was however found to reduce at higher strain rates between 10^{-3} and 10^{-2} s^{-1}. It was suggested that this change in dependence on the grain size was related to a change in deformation mechanism from grain boundary sliding accommodated by diffusion to power law creep.

5.1.2 Grain size distribution effects

In addition to grain size, the grain size distribution has also been shown to affect the superplastic properties. Paton and Hamilton (1979) showed a wider grain size distribution resulted in higher flow stresses and a lower maximum strain rate sensitivity (0.65 compared to 0.9 in Ti-6Al-4V), even though the two samples had an average grain size of approximately 4 μm (Figure 5-2). Strain rate sensitivity is difficult to measure experimentally and a value of 0.9 is exceptionally high, however, the study by Paton and Hamilton does indicate the detrimental effect of a wide grain size distribution on the superplastic properties. This experimental evidence has been supported by Ghosh and Raj (1981) who used an Ashby and Verrall model to assess the effect of grain size distribution. This work suggested that relatively small additions of large grain sizes could have a large effect on the flow stress of Ti-6Al-4V (Figure 5-3).

5.1.3 Texture

Studies have been undertaken to assess the effect of texture on superplasticity in titanium and these studies have been contradictory. Hamilton (1984) suggests that texture has little effect on the superplastic behaviour of titanium alloys. By contrast, Kaibyshev *et al.* (1981) found large variations in elongation to failure between the rolling direction and 45°, but not at 90° to the rolling direction. Rolling can lead to the formation of contiguous α and work by McDarmaid *et al.* (1985) has shown that it is

this and not the texture that affects superplasticity. Contiguous α hinders superplasticity by reducing the ability for grain boundary sliding

5.1.4 Phase ratio effects

The combination of α and β phases is thought to be the reason for the excellent superplastic behaviour of Ti-6Al-4V. The β phase has approximately two orders of magnitude greater self-diffusivity than that of the α phase. The high self-diffusivity of the β phase enables good accommodation of grain boundary sliding. A consequence of the high self-diffusivity is rapid grain growth in the β phase. The retention of the α phase is beneficial in that it restricts β grain growth. Therefore the optimum temperature for superplastic forming is where there is a balance between the α and β phases. Work by Hamilton (1984) suggest a maximum elongation is observed when the β content is between 20 and 40 % and a maximum in strain rate sensitivity occurs between 40 and 60 % β (see Figure 5-4 a and b respectively). The difference between the optimum volume fraction of β phase ~~between~~ to achieve a maximum elongation to failure ~~and~~ or maximum strain rate sensitivity is thought to relate to grain growth during testing. Stepped strain rate tests used to determine strain rate sensitivity take a short time to perform, however grain growth can occur when taking a sample to failure, especially at low strain rates.

5.2 High strain rate superplasticity

Superplastic forming of Ti-6Al-4V usually occurs at a strain rate between 10^{-4} to 10^{-3} s^{-1}. These strain rates are much lower than those used in conventional forming techniques, where typical strain rates are between 10^{-1} to 10^{2} s^{-1}, and account in part for the long production times associated with component manufacture. For superplastic forming of titanium, the following improvements are required to make the process viable for a wider range of applications:

1. reducing the cost of titanium
2. reducing the temperature for forming
3. increasing the strain rate at which titanium can be formed

For this study, the prime objective was to assess material suitable for higher strain rate forming and in addition to investigate whether a reduction in forming temperature was feasible.

Equation 5-3 and Equation 5-4 show that a reduction in grain size can improve the rate at which a material can be formed. This effect, in aluminium alloys and aluminium metal matrix composites, has been demonstrated and summarised by Hagashi *et al.* (1997) who has shown the inverse of the grain size was approximately proportional to the strain rate (Figure 5-5). The beneficial effect of a reduction in grain size has also

been reported in titanium alloys by Ghosh and Hamilton (1979). Therefore, to achieve high strain rate superplasticity ($\geq 10^{-2}$ s^{-1}) in titanium alloys fine grain sizes are required.

A number of authors have produced fine grain Ti-6Al-4V (Inagaki (1995), Warren *et al.* (1995)). Inagaki (1995) modified the processing technique for Ti-6Al-4V by heat treating sheet at 1050°C and warm rolling at 750°C. The resulting material had 2100% elongation at 850°C at a strain rate of 10^{-2} s^{-1} and this is two orders of magnitude faster than conventional Ti-6Al-4V sheet. The exact grain size was not measured, however it appeared to be less than 1 μm.

A novel technique was chosen by Warren *et al.* (1995), who produced Ti-6Al-4V by physical vapour deposition with a grain size of 30-100 nm. Heat treatment between 760 and 900°C for 3 hours resulted in a grain size of between 1.2 and 2 μm. In-spite of this grain growth, the authors suggested that enhanced superplastic behaviour was observed when testing between 760 to 900°C, although neither elongation to failure nor strain rate sensitivity values were reported.

In an attempt to produce fine stable grain sizes a number of authors have attempted to exploit boundary pinning with either ceramic or intermetallic particles (Frommeyer and Von Czarnowski (1990), Liu *et al.* (1995), Korzh *et al.* (1997)). Lui *et al.* (1995) report superplasticity in fine grained (~0.5 μm) Ti-12Co-5Al and Ti-6Co-6Ni-5Al alloys (wt%). In these two alloys approximately 27% V_f of intermetallic particles Ti_2Co and Ti_2Ni was present to refine grains and inhibit grain coarsening during superplastic flow. An elongation of over 2000% was observed at a strain rate as high as $3x10^{-2}s^{-1}$ and at a temperature as low as 700°C. These test conditions are at significantly higher rates and lower temperatures than used for Ti-6Al-4V sheet.

Korzh *et al.* (1997) used physical vapour deposition in an attempt to form a fine dispersion of ZrB_2 in Ti-6Al-4V matrix. The initial grain size was between 0.27 and 0.6 μm, however, significant α grain growth occurred during superplastic testing at 600°C. TiB acicular particles, 6-8 nm thick and 20-60 nm long, were formed. The tensile elongation at 500°C was greater than 100% and at 600°C the average elongation was 550 %. At 800°C failure occurs without a neck with a total elongation to failure of 320%, m=0.45 at $\dot{\varepsilon} = 8 \times 10^{-2}$ sec^{-1} and at lower strain rates greater elongation were seen.

Lederich *et al.* (1984) also commented on improved formability of Ti-6Al-4V because of the grain pinning effects of yttria and erbium oxides produced by adding yttrium or erbium to titanium through conventional processing. Agrawal *et al.* (1980) have also reported on the peak strain rate sensitivity value at higher strain rates small additions of yttria ~ 0.028 wt % Y_2O_3.

Work on enhanced superplasticity of titanium alloys differs from much of the work on high strain rate superplasticity of aluminium alloys and MMCs, where it has been suggested that liquid phases at the grain boundaries may accommodate grain boundary sliding. These liquid phases relax the stress concentrations at triple points and around the hard particles. In aluminium alloys the longest elongation to failure were often achieved at temperatures close to the incipient melting point of the alloy. When considering high strain rate superplasticity in titanium alloys a liquid phase at grain boundaries has not been considered because the testing temperatures are far below the solidus.

The work noted above shows encouraging properties and high elongation to failure at high strain rates, as well as superplasticity at lower temperatures. Once a suitable production method has been achieved a full picture of high strain rate superplastic forming, the mechanism by which it occurs and the effect of particulate dispersions can be better understood. This study aimed to produce a fine grain size in Ti-6Al-4V by mechanical milling and to distribute a fine particulate within the powders to pin these grains during subsequent processing and superplastic forming. The aim was to retain a fine, stable grain size enabling high strain rate superplasticity and possibly superplasticity at lower temperature.

Alloy	Temperature °C	Strain rate s^{-1}	*m*	Elongation %
Ti-6Al-4V	840-870	1.3×10^{-3} to 1.3×10^{-4}	0.75	750-1170
Ti-6Al-5V	850	8×10^{-4}	0.70	700-1100
Ti-6Al-2Sn-4Zr-2Mo	900	2×10^{-4}	0.67	538
Ti-4.5Al-5Mo-1.5Cr	871	2×10^{-4}	0.63-0.81	>510
Ti-6Al-4V-2Ni	815	2×10^{-4}	0.85	720
Ti-6Al-4V-2Co	815	2×10^{-4}	0.53	670
Ti-6Al-4V-2Fe	815	2×10^{-4}	0.54	650
Ti-5Al-2.5Sn	1000	2×10^{-4}	0.49	420

Table 5-1 Superplastic properties of some α/β titanium alloys (Nieh *et al.* (1997)).

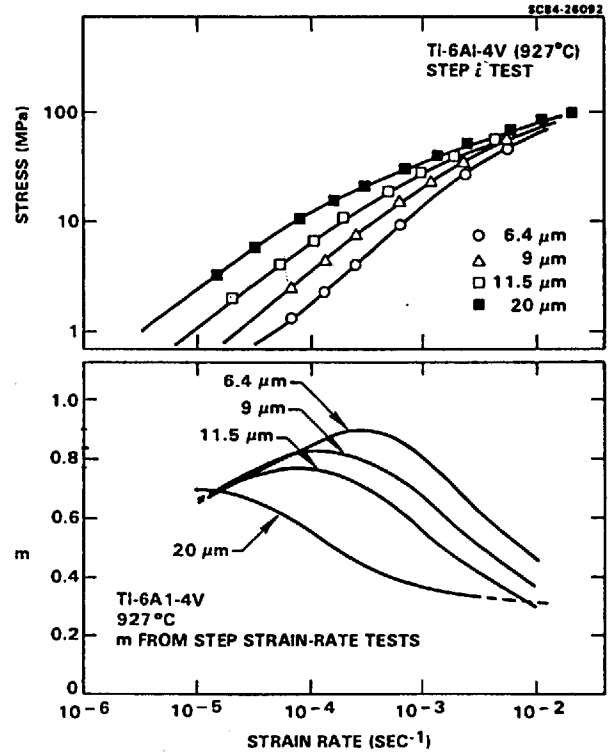


Figure 5-1 The effect of average grain size on the flow stress and strain rate sensitivity (m) for Ti-6Al-4V at 927°C (Ghosh and Hamilton (1979)).

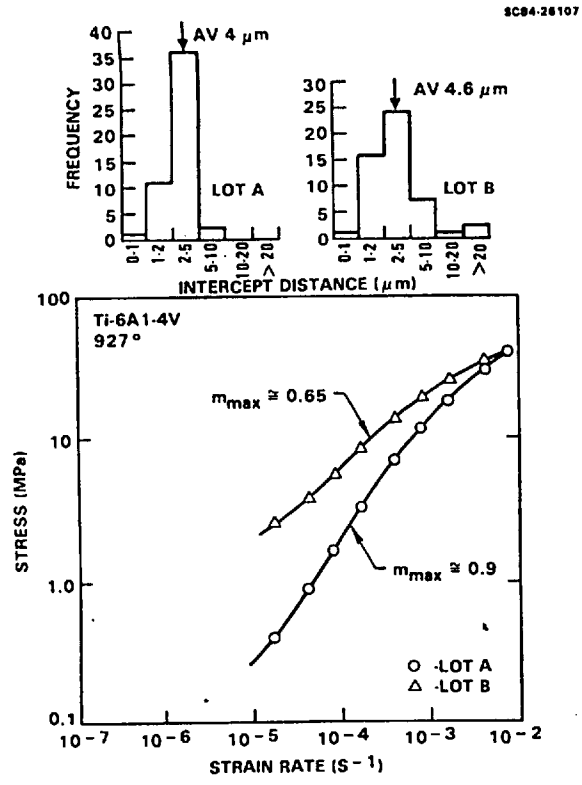


Figure 5-2 The effect of grain size distribution on the flow stress of Ti-6Al-4V at 927°C (Paton and Hamilton (1979)).

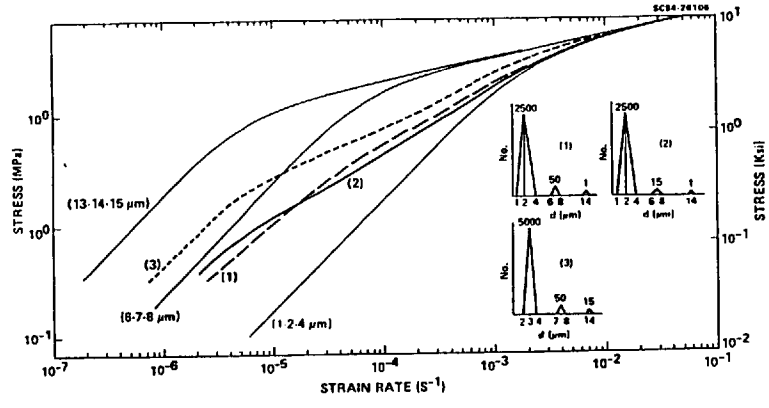


Figure 5-3 Predictions of flow stress for various grain size distributions (Ghosh and Raj (1981)).

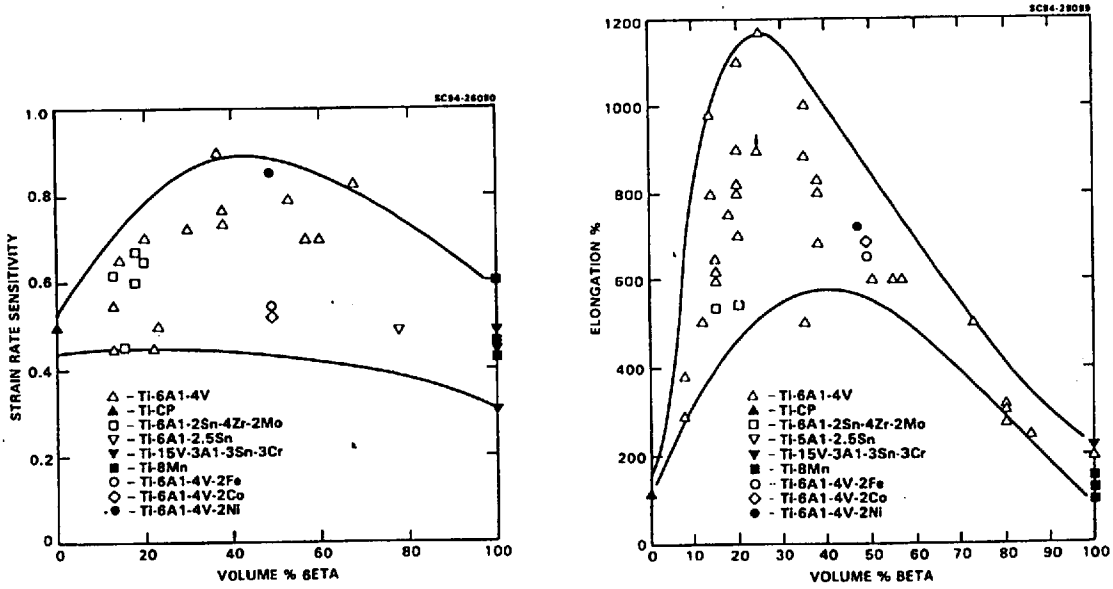


Figure 5-4 (a) strain rate sensitivity and (b) elevated temperature ductility as a function of β phase of several titanium alloys (Hamilton (1984)).

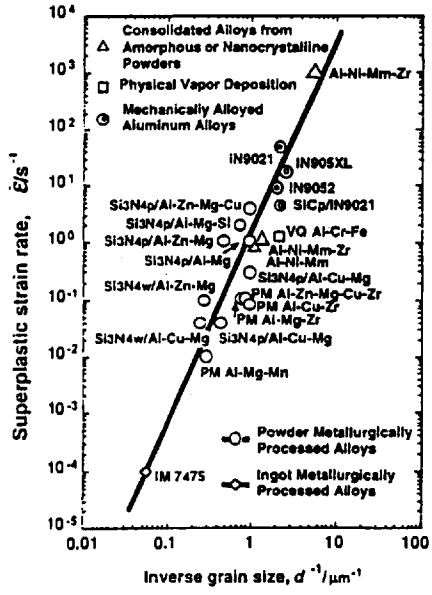


Figure 5-5 Grain size dependence of superplastic strain rate in aluminium based materials (Higashi and Mabuchi (1997)).

6 EXPERIMENTAL METHOD

6.1 Material Production

The aim of this study was to (a) produce titanium with a homogeneous distribution of TiB; (b) use a low volume fraction of TiB (0.5 and 2.5 vol. % TiB) to assess the effect of TiB as a grain boundary pinning agent and the effect of grain size on superplastic properties of Ti-6Al-4V and (c) use high volume fractions (10 and 20 vol.% TiB) to assess the effect of TiB on the room temperature mechanical properties.

The titanium boron alloys were produced using powder blending, mechanical milling and mechanical alloy with hydrogen. In all cases either boron or TiB_2 was incorporated with the either titanium or titanium alloy powder. During subsequent hot isostatic pressing this boron or TiB_2 reacted with the titanium or titanium alloy powder to form TiB.

6.1.1 Powder blending

The effect of different titanium powders on blending with boron and TiB_2 was assessed. These powders were produced by gas atomisation, hydride dehydride processing and sponge fines. Information detailing each of the powders used in this study is given in Appendix A. The different powder blends produced are shown in Table 6-1. Each powder mixture was blended for 20 minutes in a Turbula T2C mixer, prior to canning for hot isostatic pressing.

6.1.2 Mechanical milling

Mechanical milling was chosen to improve the distribution of TiB within titanium. A schematic of the material production process is given in Figure 6-1. Mechanical milling was undertaken in a purified argon atmosphere in the proprietary DERA ultra clean mills located at Aerospace Metal Composites Ltd. (AMC). Powder combinations were blended as described in §6.1.1 above and then milled. The milling times used in this process remain proprietary information. Therefore, the shortest milling time used has been denoted as T and all other times are expressed as multiples of T. Table 6-2 gives a summary of the milling combinations used.

6.1.3 Mechanical alloying with hydrogen

As a further development to the milling process, detailed in Table 6-2 and §6.1.2, a hydrogen atmosphere was used to mill the Ti + 6.4 wt. % TiB_2 powder blends. The mills, which are located in argon gloveboxes, had pipe work attached to enable a mixture of Ar with 5%H_2 gas to be passed directly into the mill bowl. Once the purging was completed the gas was switched off and the powder was milled. This purging and milling cycle was repeated and is detailed in Table 6-3. In addition to milling gas atomised Ti + 6.4 wt. % TiB_2 with hydrogen a sample of TiH_2 + 6.4 wt % TiB_2 was milled without any hydrogen in the atmosphere.

6.2 Powder consolidation

Powder samples were canned in either 316L stainless steel or mild steel cans (100 mm high x 50 mm diameter). Mild steel cans were used after the stainless steel cans became embrittled during extended degassing and cracked during subsequent HIPing. The cans were degassed using a diffusion pump at either 300°C or 700°C until a suitable leak-up rate was achieved and then back filled with argon (Price and Kohler (1984)). These cans were removed from the de-gassing unit and placed in an electron beam welder, where they were finally degassed and electron beam welded. The cans were consolidated using hot isostatic pressing (HIPing). The degassing and HIPing parameters for each of the powders are given in Table 6-1 to Table 6-3.

To retain fine grain sizes a range of HIPing temperatures between 600°C to 900°C was used. Other powders were HIPed at 500°C for 2 hours at 150 MPa, followed by 900°C for 2 hours at 150 MPa (Figure 6-2). This two stage HIP cycle was adopted following work by Fan *et al* (1995) and previous work (Godfrey *et al.* (2000)) which suggested that a low temperature dwell prior to consolidation would promote the formation of equiaxed TiB particles. The cooling rate from the HIPing temperature was approximately 33°C per minute (Figure 6-2).

In addition to the large powder cans, samples from Ti-6Al-4V + 6.4 wt. % TiB_2 which had been milled for 6T seconds, were canned in Ti-6Al-4V cans that were 20 mm in diameter by 100 mm high. These cans were degassed at 300°C in the electron beam welder and electron beam sealed. The cans were then HIPed at 900°C for 2 hours at 150 MPa.

6.3 Analysis of powders

6.3.1 Metallography

Samples for optical and scanning electron microscopy (SEM) were prepared by mounting the powders in conducting Bakelite. Powder samples were prepared by mixing them with conducting bakelite powder. Samples were ground to 2400 grit on SiC paper and finished with colloidal silica. All samples were etched with Kroll's reagent. Powder samples were mounted on carbon DAG and observed using a SEM. Optical microscopy was undertaken using a Nikon inverted microscope and SEM was undertaken using Cambridge S100 and JEOL 840 microscope.

6.3.2 X-ray diffraction and crystallite size measurement

Gas atomised Ti-6Al-4V and milled Ti-6Al-4V powders were examined in a Philips PW 1825 X-ray diffractometer. Each sample was mounted in a specimen holder using 2 % nitric cellulose in amyl acetate. The samples were scanned using Cu K_α radiation produced by a 40 kV electron beam at 40 mA over the range 30-145 degrees 2θ using a step size of 0.02 degrees and a count time of 12 seconds per step.

Crystallite size measurements were undertaken on the milled Ti-6Al-4V + 0, 0.1 and 0.5 % B powder after milling at 1T second intervals. Data from two peaks were collected, the first being (102) over the range 51.2 - 55.5 degrees 2θ using the step size of 0.01 degrees and a count time of 100 seconds and the second being (104) over the range 91-96 degrees 2θ, also using the step size of 0.01 degrees and a count time of 150 seconds.

A standard sample was obtained by taking measurements from gas atomised powder which was vacuum heat treated at 700°C for 15 minutes and was assumed to be free from the effects of strain. For line profile analysis the difference between the standard sample and the milled sample was used to obtain the results. Philips APD1700 software was used to calculate the crystallite size using the approximate and single line methods on the two peaks separately. Two values for crystallite size and lattice strain were calculated by the software, the first being size and strain, which assumes that the line broadening is due to both effects, and the second being size or strain, which assumes that the line broadening is due to one effect or the other. Due to the mechanical action of

milling it is likely that both the crystallite size and lattice strain will give rise to line broadening and therefore the values given by size and strain are more representative.

Further HIPed samples were scanned using Cu K_α radiation produced by a 40 kV electron beam at 40 mA over the range 20-90 degrees 2θ using the step size of 0.02 degrees and a count time per step of 15 secs. The data was analysed using a Philips APD1700 and Bruker/axs Diffrac AT software and the ICDD powder database.

All XRD characterisation was undertaken by P. Holdway and S. Goodwin of the Microstructural Analysis Group, DERA Farnborough.

6.3.3 Chemical analysis

Oxygen, nitrogen and iron analysis of powder samples both before and after milling were undertaken at DERA by W. Westby and Timet UK, Witton, Birmingham using a Leco model TC436 analyser. The analyser was calibrated prior to use with a titanium standard with a known oxygen and nitrogen concentration. Additionally some of the HIPed powders were analysed for their oxygen and nitrogen concentrations. In addition, samples that were milled in the presence of hydrogen were analysed for hydrogen using a Leco model RH402 analyser at DERA.

6.3.4 Sieve analysis

Sieve analysis was undertaken on all the powders that were milled to assess the effect of milling time, hydrogen and boron or TiB_2 on the powder particle size. Approximately 10 grams of each powder was sieved through the following mesh sizes: 10, 20, 40, 60, 80 and 100, which equate to mesh openings of 1700, 850, 425, 250, 180, 150 μm. The stack of sieves were vibrated on an Octagon test sieve shaker at setting 5 for 15 minutes. Each sieve was weighed before and after the sieving and the weight of powder in each sieve and the base was noted. The sieves were cleaned in between sieving each of the powders. The cumulative distribution of the volume of powder (in percent) was plotted versus the powder particle size (which was taken as nominally the sieve size and the base as nominally 100 μm). From these plots the median powder size was taken as 50% by volume. Where the majority of the powder was finer that 150 μm the distribution curves were extrapolated to give the median particle size.

A larger volume of Ti-6Al-4V + 6.4TiB_2, powder that was milled for 18T seconds, was sieved and HIPed (as detailed in §6.2) as individual compacts.

6.4 Analysis of consolidated samples

6.4.1 Metallography

Consolidated powders for optical and SEM were prepared by mounting in conducting Bakelite. Samples were ground to 2400 grit on SiC paper and finished with colloidal silica. All samples were etched with Kroll's reagent. Samples for backscattered electron imaging (BEI) analysis on a CamScan field emission gun (FEG) SEM were etched and repolished on colloidal silica to remove any surface deformed layer, which was found to impair the image.

6.4.2 β transus approach

To establish the β transus of the milled Ti-6Al-4V, samples were encapsulated in silica glass under a partial pressure of argon. The samples were heat treated for 1 hour, with a calibrated thermocouple placed on the sample, then the sample was air-cooled. The volume fraction of transformed β was taken from four optical micrographs and calculated using a non-random point counting method.

6.4.3 Grain size analysis

Grain size analysis was undertaken on samples where the aim was to retain a fine grain size and to assess the grain size stability. Therefore the milled Ti-6Al-4V, Ti-6Al-4V + 0.1B and Ti-6Al-4V +0.5B were heat treated in air at their HIPing temperatures for 20 and 96 hours, followed by an air cool. Micrographs were taken on the CamScan FEG SEM in BEI mode for measuring the α grain size. At least 5 random micrographs were taken from each sample at a magnification that enabled the grains to be easily measured. Where varying grain sizes were observed two different magnifications were used. The α grain size was measured along a linear intercept of the micrograph. Approximately 190 grains per sample were measured with a correction factor of 1.776 used to allow for the partial sectioning of a grain. This factor is derived from a single phase material with a tetrakaidecahedron grain shape.

6.4.4 Heat treatments

The stability of the TiB particles, which formed during HIPing, was assessed by heat treatment of selected HIPed samples. Heat treatment of the blended powders was carried out at 1300°C for 8 hours in vacuum. Further heat treatments were carried out using either an argon furnace with a ramp up and cool down rate of 600°C per hour or by using glass encapsulation with a back pressure of argon and in this case the samples were placed directly into a hot furnace. Further samples were heat treated at 1300°C for 8 hours in the argon furnace for production into tensile test pieces.

6.4.5 Argon analysis

Argon analysis was undertaken by Bodycote Powdermet AB, Sweden, using a gas chromatography technique (ELTRA_WERF Ar2) with graphite crucibles.

6.5 Mechanical testing

6.5.1 Room temperature tensile testing

Standard 1/4" BSF tensile samples (Figure 6-3) were produced from all the HIPed samples, these were tested on a servo screw Zwick 1474 in accordance with BS EN 1002-1 for proportional test pieces, using a 10 mm extensometer at 3 x $10^{-4}s^{-1}$ to yielding. The extensometer was then removed and the test piece was extended at $10^{-3}s^{-1}$. Fractography was undertaken on either a Cambridge S100 or a JEOL 840 SEM.

6.5.2 Elevated temperature sample design and testing

Test piece design is an important issue because incorrectly designed samples can result in material flowing from the neck to the gauge length during the test, thus producing artificially high maximum elongation values. A square necked test piece as shown in Figure 6-4 was chosen as the best test piece design (Godfrey *et al.* (1999)). The superplastic properties of conventional Ti-6Al-4V sheet were established to provide a baseline for comparison with the powder metallurgy samples.

Testing was carried out at varying temperatures and strain rates to compare maximum elongations to failure. The tensile machine was a Zwick 1484 machine operating in displacement control with a three zone furnace for temperature stability. The test pieces were protected from oxidation with an argon shield. Water cooling of the furnace provides cooling to the pull bars. It was assumed that all the crosshead displacement

occurred in the gauge length of the sample. To facilitate nominal constant strain rate deformation to failure, at strain rates at 6 x $10^{-3}s^{-1}$ and 6 x $10^{-4}s^{-1}$, the cross head displacement was recalculated for every 20% elongation and after 400% the cross head displacement was recalculated for every 50% elongation until failure. For samples tested at a strain rate of 6 x $10^{-2}s^{-1}$ the cross head displacement was recalculated every 100% elongation.

The test pieces were produced from the powder billets by slicing 2 mm sheets using electrodischarge wire machining (EDWM). One test was undertaken to establish the effect of the 'recast' layer produced by EDWM. A sample with the recast layer removed by pickling was tested and compared with a sample in the EDWM condition. No difference was found in the total elongation to failure, therefore further tests were undertaken in the as-EDWM condition.

Powder	Reinforcement	HIPing conditions
Ti-6Al-4V (GA)	None	500°C for 2 hours at 150 MPa followed by 900°C for 2 hours at 150 MPa
Ti-6Al-4V (GA)	2 wt. % B	
Ti-6Al-4V (GA)	6.4 wt. %TiB_2	
Ti (GA)	None	500°C for 2 hours at 150 MPa followed by 900°C for 2 hours at 150 MPa
Ti (GA)	2 wt%B	
Ti (GA)	6.4 wt. %TiB_2	
HDH Ti-15-3-3-3	None	Degassed at 700°C
HDH Ti-15-3-3-3	6.4 wt. %TiB_2	HIPed at 900°C for 2 hours at 150 MPa
Ti_{sf}	None	HIPed at 900°C for 2 hours at 150 MPa
Ti_{sf}	6.4 wt. %TiB_2	

Table 6-1 A list of the powder blends produced and the HIPing conditions are given. The powders were blended for 20 minutes in a Turbula T2C mixer. The powders were degassed at 300°C, unless otherwise stated.

Key : GA – gas atomised powder
HDH – hydride dehydride powder
Ti_{sf} – sponge fines produced by the Kroll process

Matrix	Reinforcement	Milling time (seconds)					
		0	3T	6T	12T	18T	60T
Ti-6Al-4V	None	✓	✓		✓		✓
Ti-6Al-4V	0.1 wt. % B						✓
Ti-6Al-4V	0.5 wt. % B						✓
Ti-6Al-4V	2 wt. % B	✓	✓	✓	✓	✓	
Ti-6Al-4V	4 wt. % B				✓		
Ti-6Al-4V	6.4 wt. % TiB_2	✓	✓	✓	✓	✓	
Ti-6Al-4V	12.8 wt. % TiB_2				✓		
Ti	None	✓	✓				
Ti	2 wt. % B	✓	✓	✓	✓		
Ti	4 wt. % B				✓		
Ti	6 wt. % B				✓		
Ti	6.4 wt. % TiB_2	✓	✓	✓			
Ti	12.8 wt. % TiB_2			✓	✓		
Ti	19.2 wt. % TiB_2				✓		

Table 6-2. Summary of the milling combinations used with gas atomised titanium powders. These powders were degassed at 300°C and HIPed at 500°C for 2 hours and 900°C for 2 hours at 150 MPa.

	Purge length (minutes)	Milling time (seconds)	Number of purge/ milling cycles	Total milling time (seconds)
Ti + 6.4 wt. % TiB_2	10	6T	1	6T
Ti + 6.4 wt. % TiB_2 ‡	30	6T	2	12T
Ti + 6.4 wt. % TiB_2 ‡	10	1T	6	6T
Ti + 6.4 wt. % TiB_2 ‡	10	1T	9	9T
TiH_2 + 6.4 wt. TiB_2 ‡	No hydrogen atmosphere used			18T

Table 6-3 A summary of the combinations when milling with either hydrogen or using TiH_2. These powders were degassed at 700°C to remove the hydrogen. The powders were then HIPed at 900°C for 2 hours at 150MPa. The cans of the samples marked with a '‡' failed during the HIPing cycle. The material was removed from the cans, re-canned, degassed and HIPed again at 900°C for 2 hours at 150 MPa.

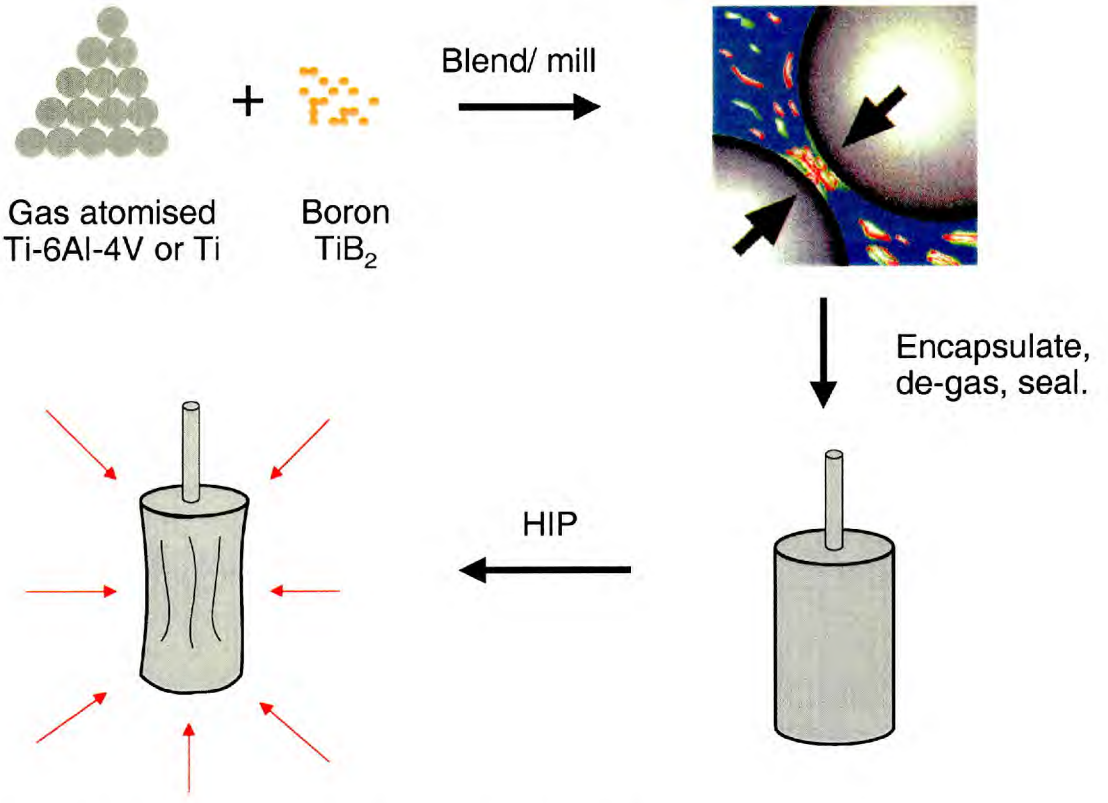


Figure 6-1 A schematic of the material production method.

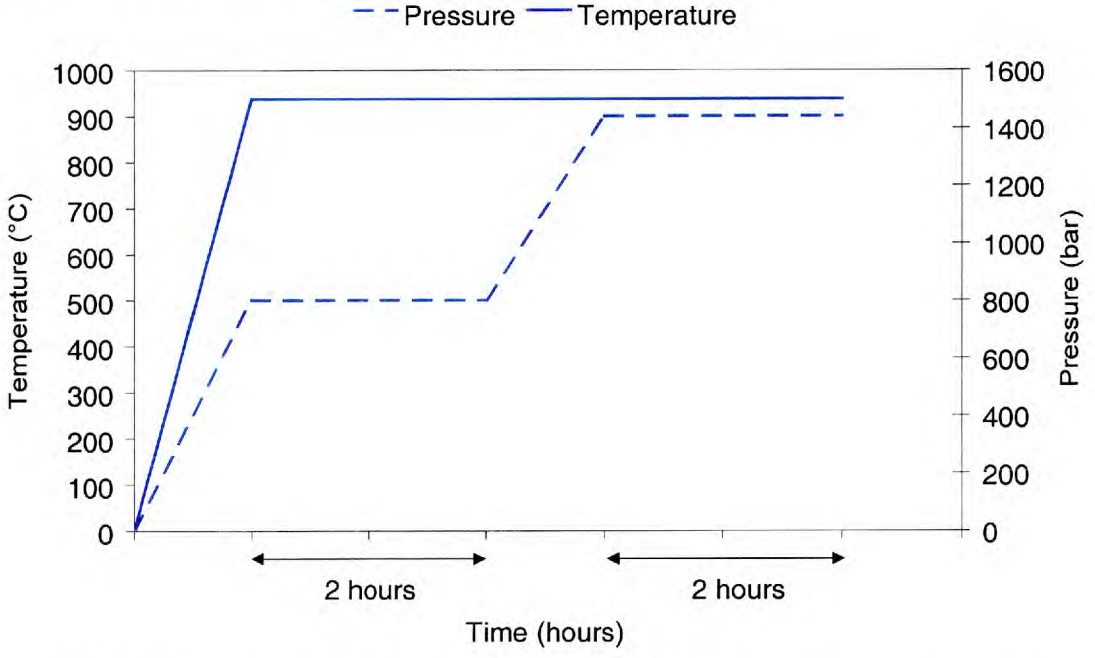


Figure 6-2 A schematic of the HIPing cycle of 500°C for 2 hours followed by 900°C for 2 hours at 150 MPa.

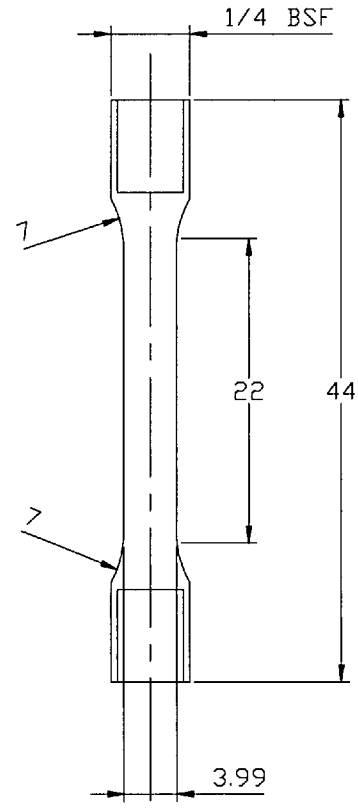


Figure 6-3. 1/4 BSF tensile test piece dimensions. All dimensions in millimetres unless other wise stated.

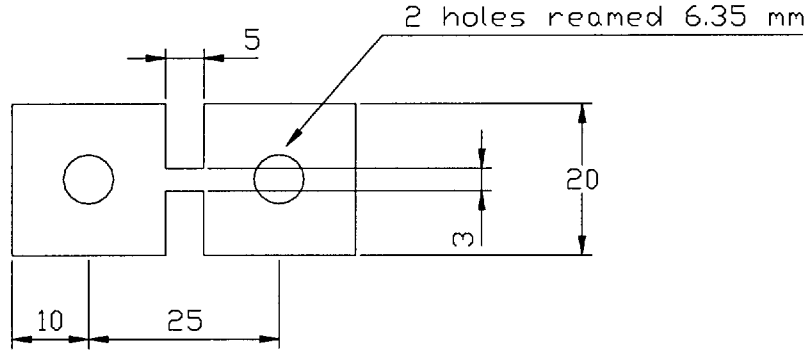


Figure 6-4. The test piece dimensions for elevated temperature tensile testing with a square neck design (all dimensions in mm unless otherwise stated).

7. ASSESSMENT OF AS RECEIVED AND MILLED POWDERS

7.1 Results

7.1.1 As received powders

The as received gas atomised Ti-6Al-4V powder was less than 250 μm in diameter and spherical. The powders were decorated with small powder satellites, as shown in Figure 7-1a. The gas atomised Ti powder was similar to the Ti-6Al-4V powder. Figure 7-1b shows that the HDH Ti-15-3-3-3 powder, which had a particle size less than 45 μm, was angular in nature. Figure 7-1c shows the Ti_{sf}, which was approximately 100 μm in diameter, and has an open form.

Figure 7-2s a and b show the microstructure of the gas atomised Ti-6Al-4V and Figure 7-2c shows the microstructure of the Ti. Both powders have an acicular microstructure, which is α martensitic within equiaxed prior β grains. The α' is formed as a result of the fast cooling rates involved during gas atomisation. Gas porosity can also be seen internally in many of the powders (Figure 7-2b). X-ray diffraction of the gas atomised Ti-6Al-4V powder, shown in Figure 7-3, indicates the presence of only α phase.

7.1.2 Characterisation of the milled powders.

Figure 7-4 shows a section of Ti-6Al-4V + 0.5B powder that has been milled for 60T seconds. Isolated areas can be seen which contain very little boron, indicated by 'i' in Figure 7-4. Layering of the boron and titanium powders can also be seen and is indicated by 'ii' in Figure 7-4.

X-ray diffraction of the Ti-6Al-4V powders after 60T seconds milling, shown in Figure 7-5, indicated that only an α phase could be detected; some broadening of the peaks had occurred (compared with Figure 7-3 for the gas atomised Ti-6Al-4V). Crystallite size measurements calculated from the peak broadening were also undertaken and these results are shown in Table 7-1. To obtain a good approximation of crystallite size the standard sample should be the same as the milled material, but without any strain, i.e. annealed. There were, however, a number of differences between the standard and the milled sample. The difference in particle size between the gas atomised powder (which was annealed for the standard) and the milled powder can be seen by comparing Figure 7-1 and Figure 7-6). Also, because of the large milled powder sizes (~ 1 mm), it was almost impossible to get a flat surface. This leads to peak broadening because the data

are collected from the sample at different heights across its surface. The microstructure of the milled powder is probably deformed α', however, the standard which was an annealed α' may consist of both α and β phases. The combination of these effects may lead to inaccurate absolute values of crystallite size. The data given can be used for comparison between the crystallite sizes measured. There does, however, appear to be little effect of the milling time and/ or boron on the crystallite size. Crystallite size measurements do however suggest the powders have a grain size in the region of 20-50 nm.

7.1.3 Oxygen, nitrogen, iron and hydrogen analysis

Table 7-2 shows an increase in the oxygen and nitrogen concentration of both the Ti-6Al-4V and Ti with milling. There was a maximum pick up of 65 ppm for nitrogen and 50 ppm for oxygen when milling all the gas atomised powders in a purified argon atmosphere up to 60T seconds milling. A limited amount of iron pick up was also observed. In some cases, there was an apparent reduction in oxygen concentration with milling, however, it is suggested that this relates to experimental error in the measurement technique. Errors are likely to relate to differences between test machines and weighing of small quantities of powders. There was, however, a substantial increase in the oxygen and nitrogen with the addition of boron and TiB_2 (Figure 7-7). The increase in the interstitial contamination was higher when using boron than when using TiB_2 as a precursor to TiB.

Table 7-3 lists the oxygen, nitrogen and hydrogen analysis of the powders milled under a hydrogen atmosphere. Hydrogen was absorbed during the milling process. An increase in the frequency of the purging and milling enabled more hydrogen to be absorbed. Milling with hydrogen also resulted in a higher oxygen and nitrogen concentration in the powders, between 150-250 ppm oxygen and 120-160 ppm nitrogen. The TiH_2+6.4TiB_2 that was milled under argon had a high hydrogen concentration and very high oxygen and nitrogen concentrations.

7.1.4 Powder particle size

Milling of either Ti-6Al-4V or Ti with the addition of either boron or TiB_2 showed differences in the milling behaviour and this was particularly evident when comparing the powder particle size (Figure 7-8). The powders produced by milling Ti-6Al-4V with either boron or TiB_2, up to a total of 18T seconds, have a relatively stable median

powder particle size in the region of 100-300 μm. Even after relatively long milling times of 60T seconds the Ti-6Al-4V + 0.5B has a median particle size of approximately 280 μm and this was not dissimilar to the Ti-6Al-4V milled with higher concentrations of boron or TiB_2 shown in Figure 7-8(b,d). However, when Ti, with no additions, was milled for longer than 6T seconds the "powder" was equivalent in size to that of a golf ball, approximately 30 mm in diameter (and a median particle size of 13 mm). The boron and to a lesser extent TiB_2 reduce the powder particle size of the milled powders as shown in Figure 7-8(c,d) and this effect was greater with the Ti powders.

Ti-6Al-4V + 6.4TiB_2 that was milled for 18T seconds was sieved to give sufficient quantity of powder to consolidate the various size fractions to enable evaluation of the various size fractions. Figure 7-9a shows the powder size fraction greater than 1700 μm. It is clear that some of these powders are agglomerates of powders that have undergone very little deformation. In other areas the powders are clearly layered with well distributed borides. Large agglomerates of these gas atomised deformed powders, can be seen in Figure 7-10(i) and is an example of the areas seen in Figure 7-9a(i). In addition, large featureless powders can also be seen (Figure 7-10(ii)) and these are thought to relate to the areas in Figure 7-9a (ii) where deformation and layering can be seen. The compacts with powders that are greater than 250 μm all contain a mixture of layered and deformed gas atomised powders (Figure 7-9a-d). However, where the compact contains powders with a particle size less than 250 μm diameter there is qualitatively a higher volume fraction of unreinforced powders. These powders are more spherical in shape indicating they have had very little deformation (Figure 7-9e,f). The sample, which contains powders less than 150μm in diameter, qualitatively has a higher number of TiB_2 particles at the powder boundaries (Figure 7-9f(iii)).

Figure 7-11 identifies the various features observed in the milled powders. These features include powders that have experienced very little deformation (Figure 7-11a), agglomerated powders and increased layering (Figure 7-11b,c) and finally areas where the TiB is well distributed (Figure 7-11d).

7.2 Discussion

There are a number of factors to assess when trying to produce a commercially viable titanium boron alloy using the mechanical milling route. These factors include low

interstitial contamination, the powder particle size, grain size and the distribution of the reinforcement and each of these areas is discussed.

7.2.1 Interstitial contamination

The initial oxygen and nitrogen concentrations in the gas atomised powders were 1050 ppm oxygen and 120 ppm nitrogen in the Ti-6Al-4V powder and 1130 ppm oxygen and 120 ppm nitrogen in the Ti powder. Additional contamination as a result of the milling process was limited to a maximum of 65 ppm nitrogen and 50 ppm oxygen with milling times up to 60T seconds (Table 7-2).

Any increases in oxygen and nitrogen levels during milling were the result of the deformation and fracturing of powder particles exposing clean surfaces which react with adsorbed moisture and residual impurities in the protective argon atmosphere. In other earlier studies high levels of contamination (8000 ppm oxygen and 15200 ppm nitrogen) have been observed (Goodwin *et al.* (1997)). In this study control over interstitial contamination was achieved by milling in an argon filled glovebox where residual oxygen and moisture was gettered. The argon was continually circulated through these getters maintaining the extremely low levels of moisture and oxygen (< 10 ppm). The effect of using unpurified gas can be seen when milling with hydrogen, where, higher values of interstitial contamination were observed. This was likely to be a result of purging the mills with the argon-hydrogen mixture directly from the gas bottle.

Close control of oxygen and nitrogen in titanium alloys is critical because of the occupancy of interstitial sites in the titanium lattice and the strong strengthening/ embrittling response of relatively low oxygen and nitrogen concentrations (Fujii *et al.* (1995)). Commercial compositions usually specify a maximum combined oxygen and nitrogen concentration of 2500 ppm for Ti-6Al-4V (BSI2TA10 (1974)) and the powders milled using the DERA ultra clean milling process remain well within these values. High levels of oxygen and nitrogen were noted in the milled TiH_2+6.4TiB_2. These high concentrations were not produced as a result of the milling process and were present in the original TiH_2 powders. The powders were known to be high in oxygen and nitrogen and this was likely to be a result of contamination during hydriding, the fine powder size and the old age of the powder stock. The powders were used for this study to assess the effect of powder size and the ability to mill the hydrided powders with a view to using TiH_2 with lower interstitial contamination in future studies.

To produce the desired TiB particulate reinforcement or grain pinning phase, additions of either boron or TiB_2 are made. Figure 7-7 shows an increase in oxygen and nitrogen concentration with the addition of either boron or TiB_2. The addition of boron leads to a greater increase in oxygen compared to the addition of TiB_2. It is thought that the TiB_2 powder has a lower initial impurity level compared with the boron powder and this is confirmed in Annex A, which shows typical impurity levels in boron and TiB_2 powders. Therefore, TiB_2 is a more suitable addition to the titanium powder than boron. Figure 7-7 shows that for a 10 vol. % TiB reinforced MMC, the total interstitial content remains below 2500 ppm. However, the addition of 4 wt. % boron to titanium powder which produced 20 vol. % TiB, takes the interstitial content outside specification. It is very important that this level be kept as low as possible because it determines the properties of the matrix and therefore affects the overall performance of the MMC.

A small increase in the iron concentration was observed in all the milled Ti and Ti-6Al-4V powders, including those powders with additions of boron or TiB_2 (Table 7-2). The iron was introduced from the mill, however, this iron was not thought to be detrimental to the properties of the material because no isolated areas of iron contamination were observed. It is suggested that any iron was homogeneously dispersed within the titanium by the milling process.

7.2.2 The effect of milling on powder size and morphology

Powder particle sizes and morphology are important when considering subsequent processing. High powder packing densities are desirable to minimise shrinkage and to avoid can failure during HIPing because of excessive strains on the can.

The size and morphology of the powder produced by milling depends on a number of factors, which include alloy deformability, milling time, reinforcement type and impurity level of the powder being milled. The gas atomised powders of Ti-6Al-4V and Ti were spherical in nature with all particles less than 250 μm in diameter. Figure 7-8 shows the effect of milling on the median powder particle size for the various powder blends and, in general, an increase in powder particle size was seen with increasing milling. The milling of ductile materials is well understood (Harris *et al.* (1993)) and has been shown to result in an increase in powder particle size with milling time. This is consistent with the work shown in this study where the increase in particle size is much greater in the more ductile Ti powder than the Ti-6Al-4V alloy (Figure 7-8). Previous

work at DERA on milling Ti powder with an oxygen content of 2100 ppm showed a particle size of the order of 1 mm, after milling for 60T seconds (Godfrey (1996)). In the present case, however, Ti powder with an oxygen content of 1130 ppm produced very large particles, one of which was approximately 30 mm in diameter after a short milling time of 6T seconds. It is therefore clear that the oxygen concentration, and hence the strength and ductility, of the powder has a strong effect on the particle size produced. These observations suggest that with the high purity Ti powder little or no fracturing occurred. It is thought that because of the greater deformability of the Ti powder a greater surface area of the powders was created per collision; therefore more free surface areas contacted each other and greater amounts of cold welding occurred and so large particles formed quickly.

In previous work (Harris *et al.* (1993)), where cold welding dominates, process control agents (PCAs) are used to enhance milling (§ 2). However, due to the highly reactive nature of titanium, the use of PCAs results in unacceptable increases in oxygen, nitrogen and carbon concentrations and therefore cannot be considered.

The addition of boron or TiB_2 in the present work results in a reduction in the particle size produced by milling (Figure 7-8 c and d). The median particle size decreases from 280 μm for Ti-6Al-4V to 160 μm when 2 wt. % B was added and from 1300 μm to 560 μm for Ti milled with either boron or TiB_2, where the volume fraction is 10 vol. % TiB. The addition of boron or TiB_2, as the precursor to the TiB reinforcement, had the additional benefit of modifying the milling behaviour and acting as a form of PCA. The boron and TiB_2 affect the milling behaviour by coating the titanium powders and reducing the strength of the cold welds that form. The use of boron had a greater effect in reducing the powder particle size compared with the TiB_2. For a given 100 g mill load there would be either 2 g of boron or 6.4 g of TiB_2 present. However, given the respective powder particle sizes, the number of particles per load was approximately 2.3×10^{12} and 2.7×10^{9} for boron and TiB_2 respectively. Hence the greater number of boron particles was thought to have a greater effect on the cold welding of the titanium powder. From this it is suggested that the addition of boron or finer TiB_2 would be better than the addition of TiB_2 in improving the milling performance of the titanium powder. However, with regard to oxygen and nitrogen contamination TiB_2 is the better addition. The boron powder was also agglomerated and was difficult to disperse throughout the titanium powder.

To enable more efficient milling of the titanium powders hydrogen was incorporated during the milling process. Hydrogen was milled into titanium with the aim of forming TiH_2. The formation of TiH_2 has been reported by Small *et al.* (1999) when milling titanium powder in the presence of hydrogen. Table 7-3 shows the particle size of the powders milled in the presence of hydrogen in comparison to the powders milled under argon alone. It can be seen that milling with hydrogen results in a finer median powder particle size. It is thought that the brittle nature of the TiH_2, which is probably located within the titanium powders, enables more fracturing to occur (compared to milling in the absence of hydrogen) and hence results in a finer median powder particle size (from 560 μm to 100 μm). In this respect hydrogen can be used as a PCA during the milling of titanium. The hydrogen can subsequently to removed from titanium during degassing of the titanium powders at 700°C prior to HIPing.

7.2.3 Distribution of TiB in the titanium powders

The Ti-6Al-4V + 6.4TiB_2 (Figure 7-9) powder milled for the longest time (18T seconds) was sieved into the various size fractions to establish whether there was a difference in the homogeneity of the different size fractions. In the largest size fraction, where the powder particle size was greater than 1700 μm, there were two types of microstructure. The first type was powders that had been heavily milled and show some layering and the second type were agglomerates of the powders that had not been heavily milled. Examples of these two types of powders were observed in all the sieve sections. The reason for the different microstructures was thought to relate to the amount of milling the individual powders experienced. Figure 7-11 shows examples of the different stages of milling taken from the micrographs in Figure 7-9. Figure 7-11a shows powders which are less than 150 μm. Although these powders have been milled for 18T seconds many are still spherical in nature and have probably experienced very little milling. Figure 7-11b shows some powders from the greater that 1700 μm sieve fraction. These powders are agglomerated and have experienced some deformation because they are no longer spherical in shape. Ti-6Al-4V milled with the TiB_2 can be seen at the powder boundaries and has been indicated by 'i'. As the milling proceeds further deformation and welding occurs and this can be seen in Figure 7-11c and Figure 7-4, where the Ti-6Al-4V powders are elongated and layering can be seen. As the milling continues, the refinement proceeds until a homogeneous distribution is observed (Figure 7-11d(i)).

Longer milling times would enable more complete distribution of the boron or TiB_2 within the titanium powders, however this was not undertaken for the 10-20 vol% TiB additions. Long milling times are undesirable for the production of a commercially viable titanium MMC. Other titanium powders are available, such as, hydride, hydrided dehydride and sponge fines (Figure 7-1). These powders have a finer initial size and a more open structure that may take less time for full milling to occur, because less time is required for the TiB_2 or boron to fully penetrate the finer titanium powder.

7.2.4 Crystallite size

The milling, in addition to distributing the boron or TiB_2, can be used to refine the grain size. Crystallite size measurements indicated a fine crystallite size of approximately 50 nm (Table 7-1). This has been confirmed by Brown *et al.* (1999a) who have assessed the same material. Using transmission electron microscopy (TEM) they have observed crystallite sizes in the region of 5 –40 nm. These powders, which have been milled for 60T seconds, have no resemblance to the gas atomised powders. The acicular α', present in the gas atomised powders (Figure 7-2), was heavily deformed during the milling process (Figure 7-4) until the α' lamellae were broken up and equiaxed crystallites were observed. This occurs by the consecutive deformation and welding of the powders which introduces a high incidence of dislocations and point defects into the microstructure, indicated by peak broadening in the X-ray diffraction analysis (Figure 7-5). XRD indicated the crystallites in the milled powders were hcp (Figure 7-5). Previous work on the milling of titanium alloys has suggested that milling results in the formation fcc and amorphous structures (Suryanarayana *et al.* (1990), Abe and Johnson (1992)). These structures have largely been discounted and are thought to relate to contamination during the milling process (Goodwin *et al.* (1997), Ohering and Bormann (1993), Lauer *et al.* (1997). This study agrees with this previous work because interstitial contamination was minimised and neither fcc nor amorphous structures were observed.

7.3 Summary

Deformation, welding and fracture during the milling process were used to incorporate either boron or TiB_2 within the titanium powder particles. This milling also resulted in powders with fine crystallite sizes. Milling of the more ductile Ti powders resulted in a rapid increase in the powder particle size. However, incorporating hydrogen, either by

using a hydrogen atmosphere or TiH_2, increased the fracturing during milling and kept the powder particle size small.

Material	(102)				(104)			
	Size AND Strain		Size OR Strain		Size AND Strain		Size OR Strain	
	A	B	A	B	A	B	A	B
Ti 6Al 4V	436.1	0.489	137.7	0.621	506.8	0.202	193.4	0.274
	155.8	0.313	116.5	0.734	207.0	0.114	168.1	0.315
Ti 6Al 4V+0.1B	376.6	0.510	129.3	0.664	460.1	0.210	183.6	0.289
	177.9	0.373	117.2	0.733	232.3	0.146	166.2	0.319
Ti 6Al 4V+0.5B	409.7	0.489	136.0	0.631	489.6	0.200	193.0	0.275
	154.2	0.325	114.3	0.750	201.5	0.117	164.0	0.323

A = Crystallite size (Å), B = Lattice Strain (%)
Approximate method in normal text, Single Line method in italics.

Table 7-1 The crystallite size measurements of Ti-6Al-4V powders milled with boron for 60T seconds

Sample	Mill time (T seconds)	Oxygen (ppm)	Nitrogen (ppm)	Iron (wt%)
Ti-6Al-4V	0	1050	120	0.045
Ti-6Al-4V	60	1000	175	0.09
Ti-6Al-4V+0.1B	60	1050	105	0.12
Ti-6Al-4V+0.5B	60	1100	140	0.08
Ti-6Al-4V+2B	12	1500	200	0.05
Ti-6Al-4V+4B	12	2300	240	0.05
Ti-6Al-4V+6.4TiB_2	12	1250	320	0.06
Ti-6Al-4V+12.8TiB_2	12	1850	480	0.07
Ti	0	1130	120	0.047
Ti	12	1050	165	1.1
Ti+2B	12	1500	200	0.06
Ti+4B	12	3000	260	0.06
Ti+6.4TiB_2	6	1550	340	0.07
Ti+12.8TiB_2	6	2200	590	0.05

Table 7-2 Shows the oxygen, nitrogen and iron concentrations of milled powders compared with the gas atomised powders.

Sample	Purge Cycle	Total milling Time (T seconds)	Median particle size (μm)	Hydrogen (μg/g)	Oxygen (ppm)	Nitrogen (ppm)
Ti	--	0	125	--	--	--
Ti + 6.4 TiB_2	No H_2	3	190	--	--	--
Ti + 6.4 TiB_2	No H_2	6	560	--	1550	340
Ti + 6.4 TiB_2	(10 min purge, 1T mill) x6	6	112	770	1800	500
Ti + 6.4 TiB_2	(10 min purge, 1T mill) x9	9	137	630	1710	480
Ti + 6.4 TiB_2	10 min purge, 6T mill	6	100	180	1700	420
Ti + 6.4 TiB_2	(30 min purge, 6T mill) x2	12	120	220	1830	460
TiH_2 + 6.4 TiB_2	No H_2	18	103	21000	16500	8700

Table 7-3 showing the powder particle size and hydrogen content of the milled powders.

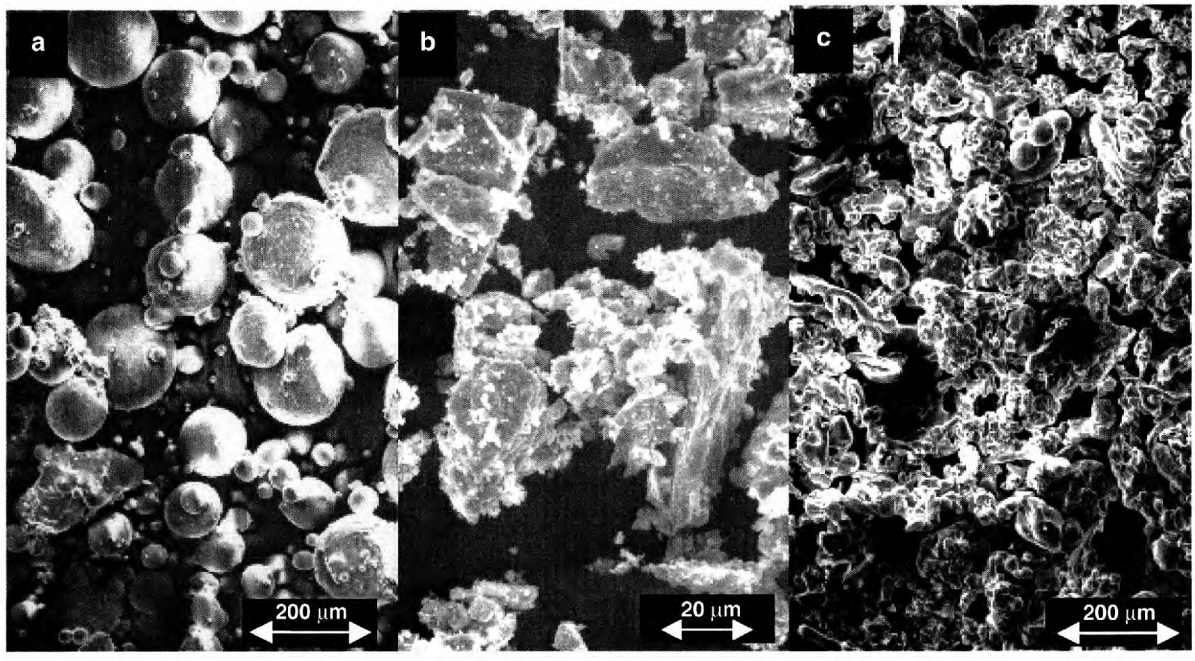


Figure 7-1 SEM micrographs of the as received powders where a) shows gas atomised Ti-6Al-4V, b) shows the hydride dehydride Ti-15-3-3-3 and c) shows the sponge titanium fines.

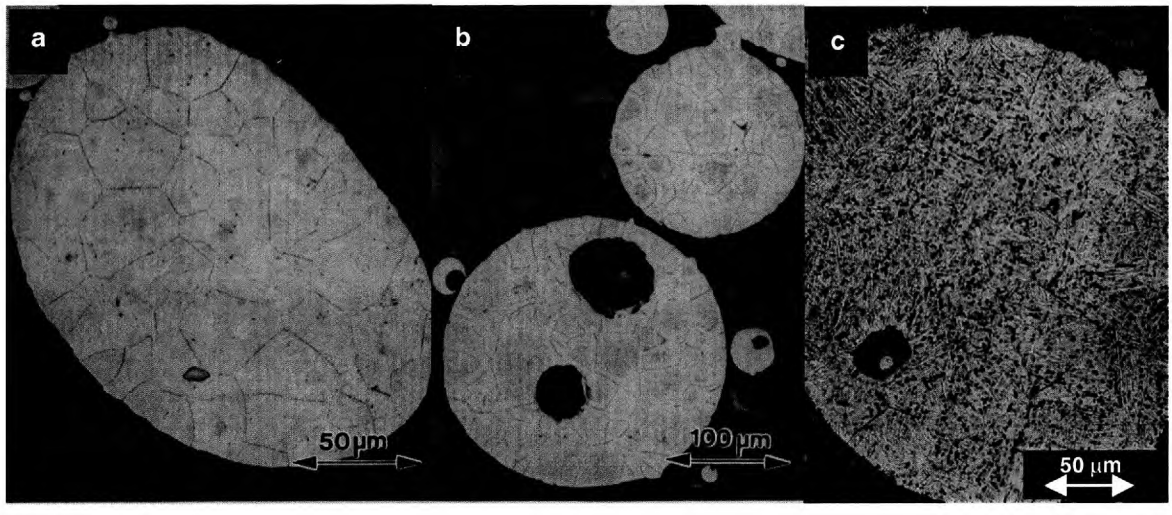


Figure 7-2 Optical micrographs of the cross sections of the gas atomised powders where a) equiaxed prior β grains with an acicular transformed β internal microstructure are observed in the gas atomised Ti-6Al-4V, b) gas porosity observed within the gas atomised Ti-6Al-4V powders and c) the gas atomised Ti has similar features compared with the Ti-6Al-4V powder.

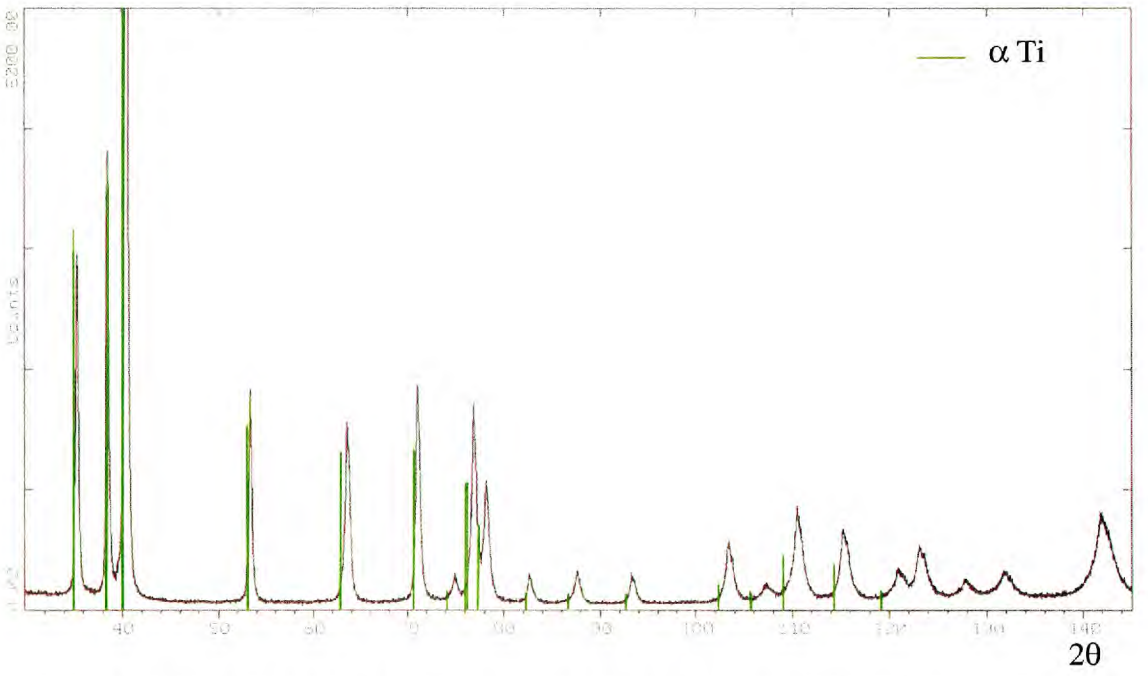


Figure 7-3 X-ray diffraction of gas atomised Ti-6Al-4V powder indicating detection of the α phase only. The vertical markers indicate the peaks usually observed for pure Ti, consequently the peaks are slightly shifted for the Ti-6Al-4V alloy because of the change in lattice parameter.



Figure 7-4 An optical micrograph of Ti-6Al-4V+0.5B after milling for 60T seconds where 'i' indicates boron free areas and 'ii' indicate where layering of the boron and titanium can be seen.

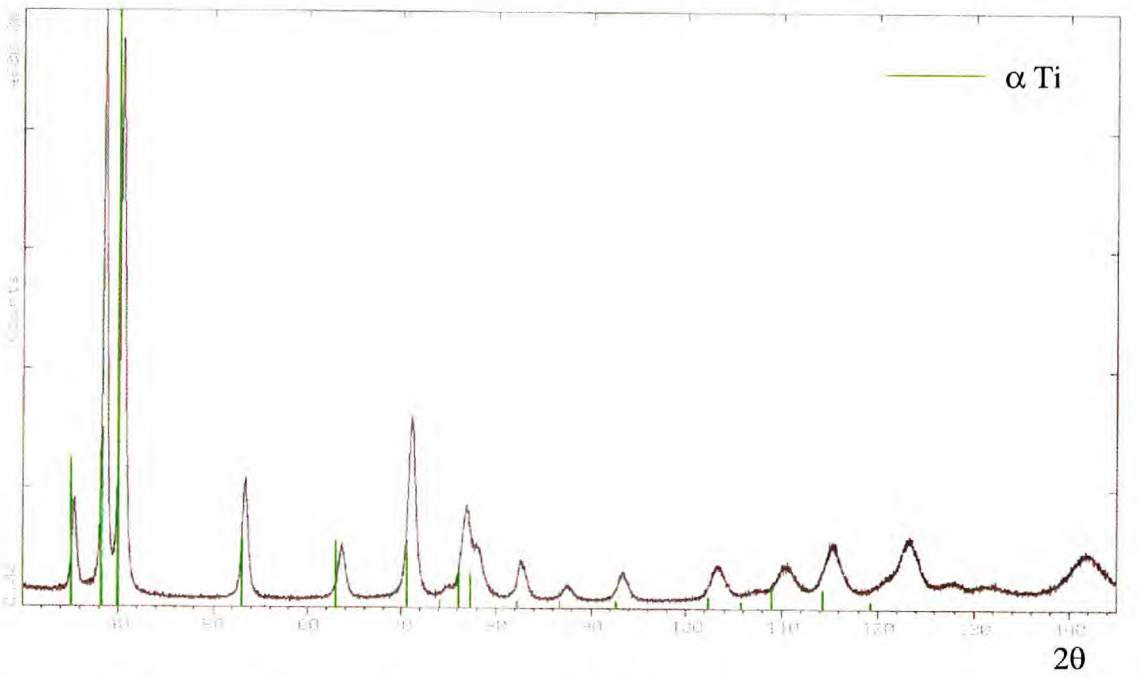


Figure 7-5 X-ray diffraction of gas atomised Ti-6Al-4V powder after milling for 60T seconds and indicate the presence of the α phase only. The vertical markers indicate the peaks usually observed for pure Ti, consequently the peaks are slightly shifted for the Ti-6Al-4V alloy because of the change in lattice parameter.

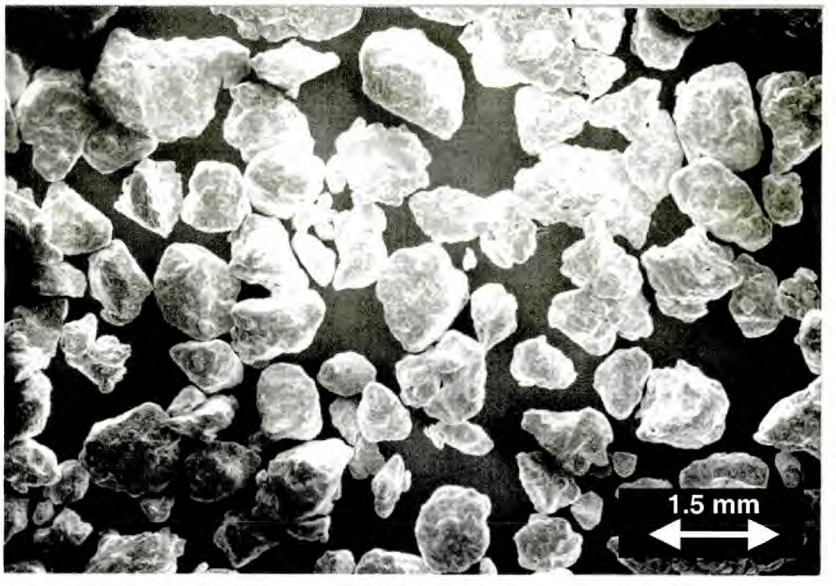


Figure 7-6 SEM micrograph of the Ti-6Al-4V+0.5B milled for 60T seconds.

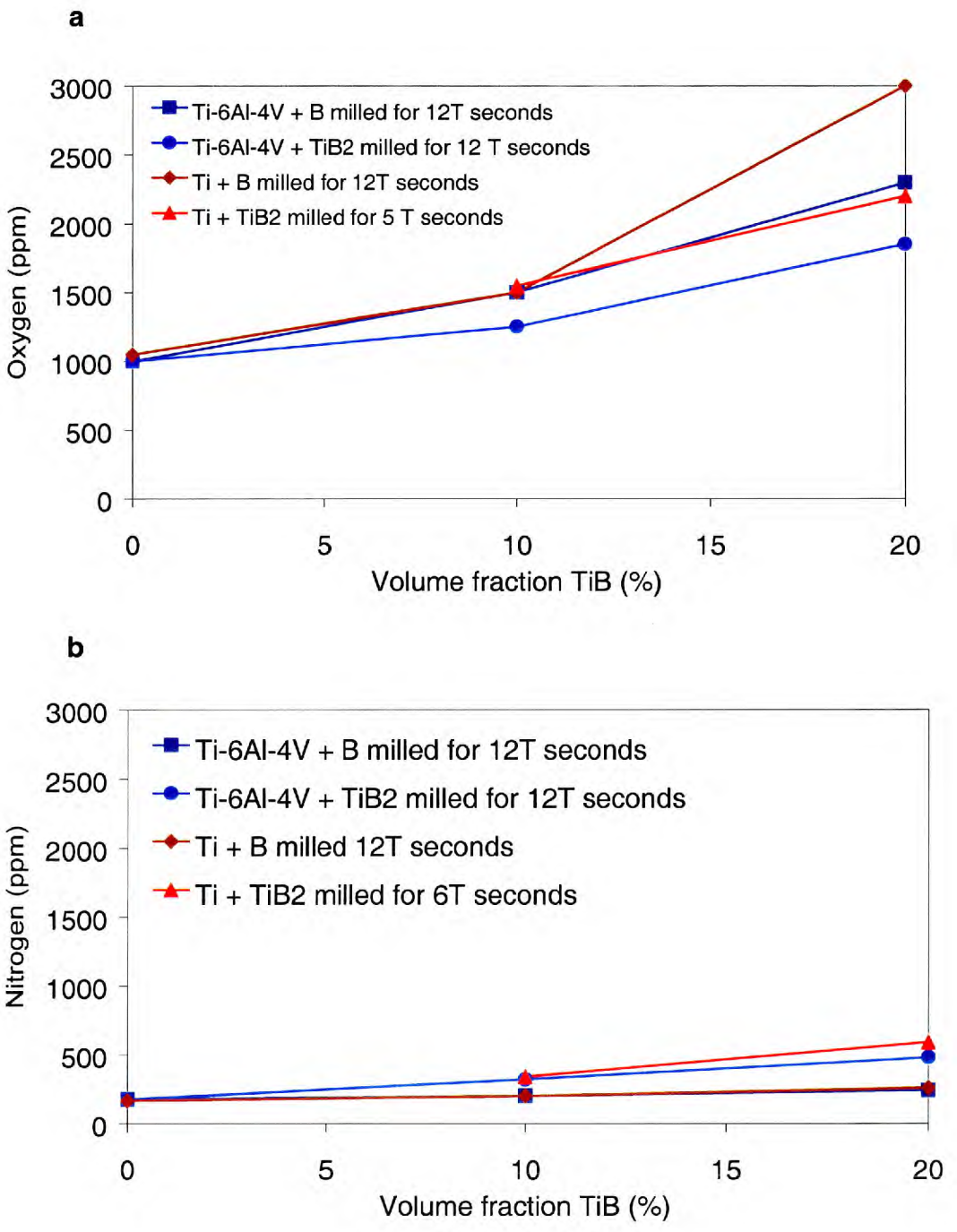


Figure 7-7 The effect of boron or TiB_2, which is expressed in terms of predicted volume fraction TiB if the boron/TiB_2 fully reacts on (a) oxygen and (b) nitrogen concentration.

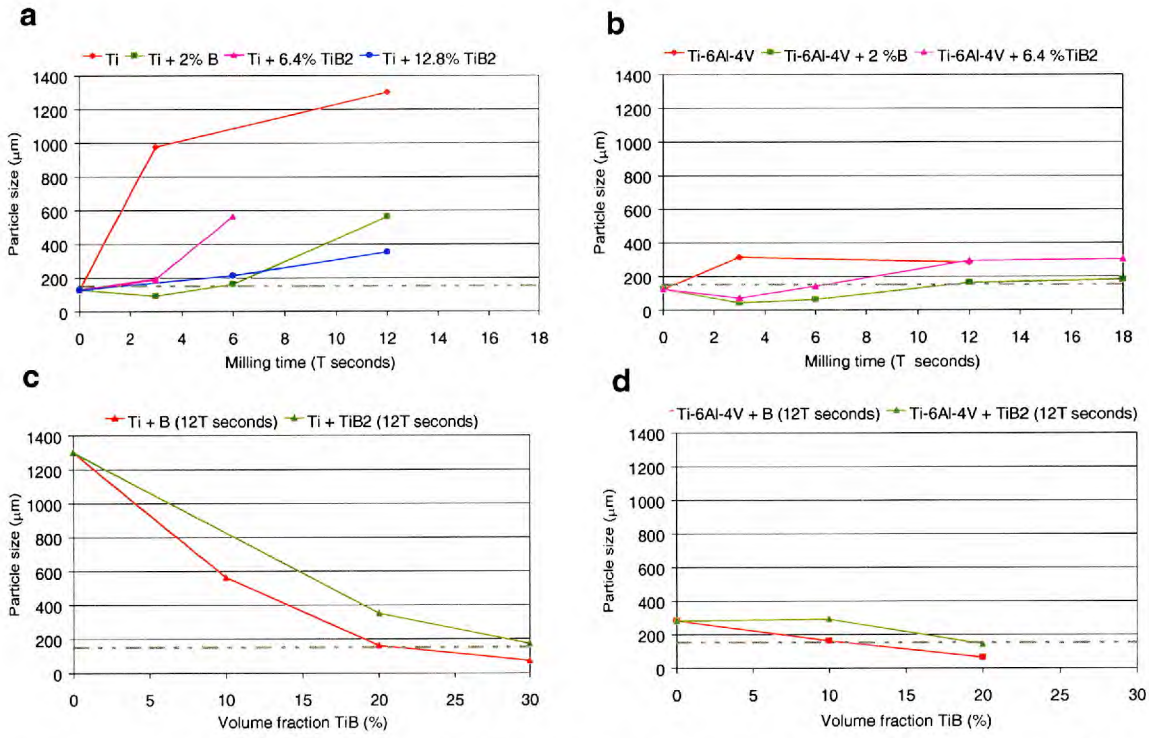


Figure 7-8 Powder particle analysis showing the effect of milling time on particles size with a) Ti and b) Ti-6Al-4V with boron or TiB_2 and the effect of boron or TiB_2 on particle size of c) Ti and d) Ti-6Al-4V. The particle size is taken as 50%. The area below the dotted grey line indicates a particle size of 150 µm or less. Values falling within this area have been calculated by extrapolating the particle size data obtained by sieve analysis.

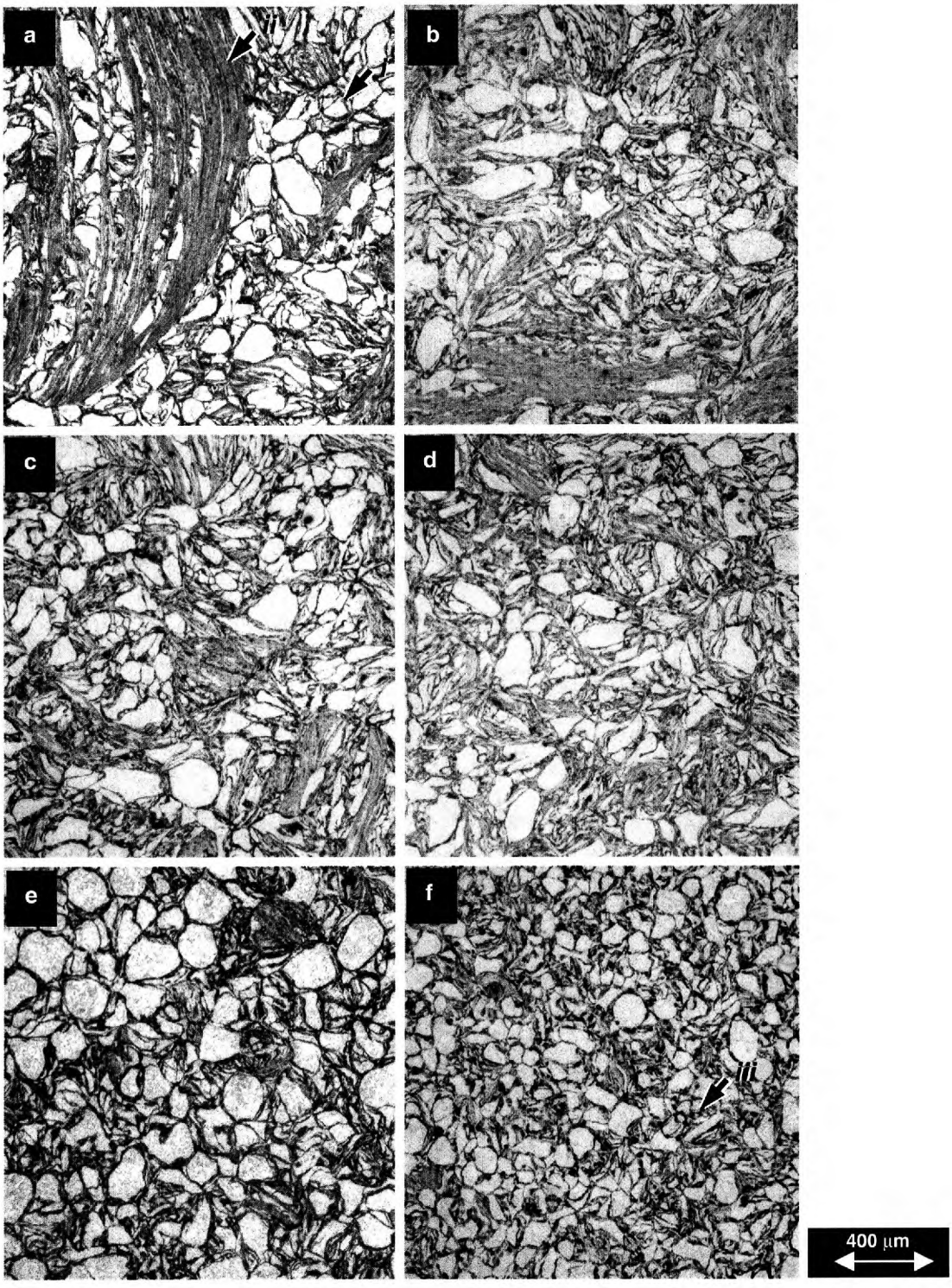


Figure 7-9 Micrographs of Ti-6Al-4V+6.4%TiB_2 after 18T seconds mi ling at different sieve fractions where (a) >1700µm, (b) 1700µm ≤ X >850µm, (c) 850µm ≤ X > 42µm, (d) 425µm ≤ X > 250µm, (e) 250µm ≤ X > 150µm and (f) 150µm < X. 'i' indicates undeformed powders, 'ii' indicates areas of heavy deformation and 'iii' indicates TiB_2 particles.

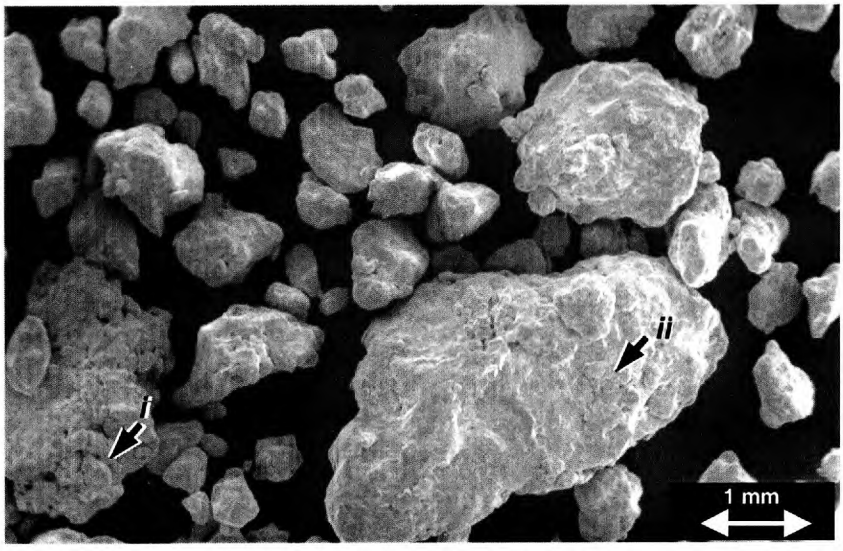


Figure 7-10 SEM micrographs of Ti-6Al-4V+6.4%TiB_2 powder after milling for 18T seconds where 'i' indicates agglomerates of gas atomised powders and 'ii' indicates the large featureless powders.

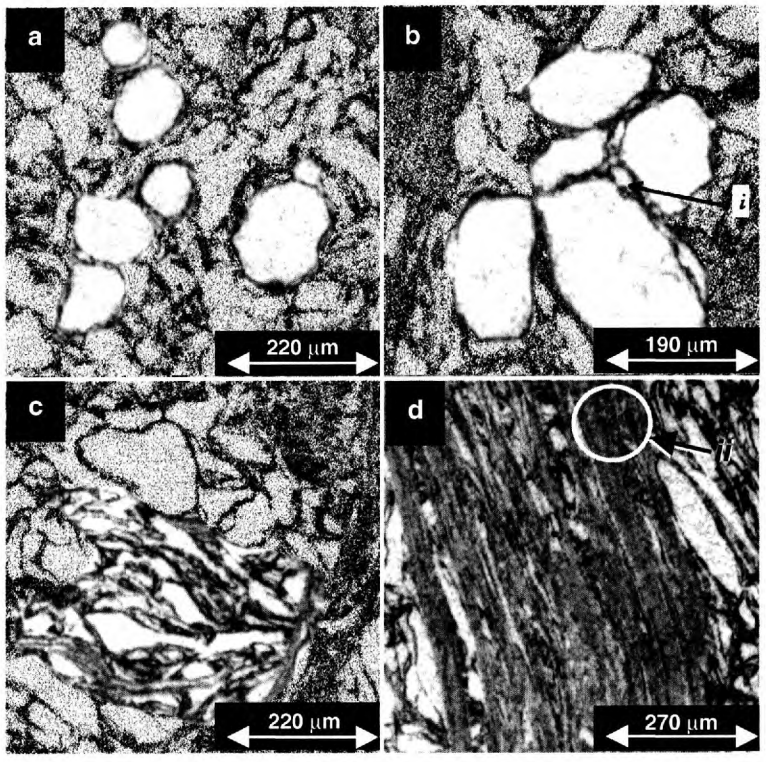


Figure 7-11 Shows the increasing deformation observed in Ti-8Al-4V + 6.4%TiB_2 after milling from 18T seconds. (a-c) have been masked using computer imaging to identify features of interest where (a) is an area from Figure 7-9e shows powders that are less than 150 μm in size and have experienced little deformation. (b-d) show areas from Figure 7-9(a) and (b) shows agglomerated areas where some deformation of the gas atomised powders has occurred, some layering can be seen as indicated by 'i'. (c) shows agglomerated powders where further deformation and welding has occurred during milling and layering can be seen and (d) 'ii' where in the final stages of a good distribution of TiB_2 within the Ti-6Al-4V can be seen.

8 MICROSTRUCTURAL CHARACTERISATION OF HIPED POWDERS

8.1 Results

Powders were consolidated at three different stages of the processing route to assess the development of microstructure with processing. The three stages were:

- prior to any processing i.e. each titanium alloy was consolidated in the as received condition

- after blending the titanium (alloy) powders with either TiB_2 or boron

- after the titanium alloy powders were milled with either TiB_2 or boron at each time interval

8.1.1 Microstructure of as received HIPed powders

Consolidation of the gas atomised Ti-6Al-4V powder using HIPing resulted in an α lamellar microstructure as shown in Figure 8-1a. The powder particles boundaries can also be observed in the HIPed Ti-6Al-4V (indicated by arrows in Figure 1a). In contrast a large equiaxed α microstructure was observed in the gas atomised Ti (Figure 8-1b), where the grain size was approximately 280 μm.

HDH and sponge fines (Ti_{sf}) powders, which had different powder sizes and morphology to the gas atomised powders, were also HIPed. These powders were chosen to assess the effect of powder particle size and morphology on the distribution of the TiB_2. The oxygen and nitrogen concentration of the HDH Ti-15-3-3-3 and Ti_{sf} consolidated powders are shown in Table 8-1. The oxygen and nitrogen concentration of the HDH powders was extremely high.

8.1.2 Microstructure of milled Ti-6Al-4V

An equiaxed α microstructure was observed in the consolidated Ti-6Al-4V after milling for both 12T and 60T seconds (Figure 8-2a). The oxygen and nitrogen concentration of the HIPed Ti-6Al-4V powder, which was milled for 60T seconds, is given in Table 8-1. Occasionally areas of lamellar α can be seen (Figure 8-2b) and these are similar in appearance to the α lamellae in the HIPed gas atomised Ti-6Al-4V powder (Figure 8-1).

A backscattered FEG scanning electron micrograph of the milled Ti-6Al-4V which was HIPed at 800°C, is shown in Figure 8-3a. The dark grains are equiaxed α and the light phase located at triple points and grain boundaries is β. Increasing either the HIPing temperature (Figure 8-3b) or time at temperature (Figure 8-4a) increases both the thickness of the grain boundary β and the equiaxed α grain size. Further heat treatment of the milled Ti-6Al-4V at 900°C for 20 hours resulted in a microstructure of equiaxed α and transformed β (Figure 8-4b).

Table 8-2 shows the relative volume fraction of transformed β after heat treating the milled Ti-6Al-4V at 900°C, after HIPing and heat-treated at either 800°C or 900°C. The β transus approach curve (Figure 8-5) for milled Ti-6Al-4V, which was HIPed at 800°C for 2 hours at 150 MPa and heat treated for 96 hours at 800°C, is compared to Ti-6Al-4V that was HIPed at 900°C for 2 hours at 150 MPa. These experimental measurements are shown in comparison with equilibrium values calculated from JMatPro[1] using the composition given in the powder release data (Appendix A) and the oxygen and nitrogen analysis given in Table 8-1. JMatPro was also used to assess the relative equilibrium concentration of each element in each phase over the temperature range 600 to 1800°C and these graphs are shown in Figure 8-6.

8.1.3 Microstructure of blended powders

The microstructure of the blended and consolidated Ti-6Al-4V+2B and Ti-6Al-4V+6.4TiB_2 are shown in Figure 8-7 (a-b) respectively. The α lamellae observed in the gas atomised Ti-6Al-4V powders is consistent with that seen when HIPing gas atomised Ti-6Al-4V in the absence of boron (compare Figure 8-1 with Figure 8-7). The boride phase was agglomerated at the circumference of the titanium powders as a result of blending the gas atomised powders with either boron or TiB_2. Porosity was observed at the titanium prior powder particle boundaries and the highest incidence of this was observed in the titanium powders that were blended with boron (Figure 8-7a 'i'). Similar observations were also noted when assessing the Ti+2B and Ti+6.4TiB_2 however, as with the HIPed Ti gas atomised powders the titanium powders contain equiaxed α grains.

---

[1] JMatPro is a Material Property Simulation Package by Thermotech Ltd © 1999-2000

The powder boundaries were assessed using backscattered imaging on a FEG SEM. The powder boundaries of the Ti-6Al-4V + 2B can be seen in Figure 8-8a. A dark phase is present at the powder boundaries and dark needles can be seen emanating from this dark region. This dark phase was titanium boride and XRD confirms the presence of both TiB_2 and TiB. Qualitatively the TiB was found to be the predominant phase (Figure 8-9a). Small needles, indicated by 'i' in Figure 8-8a, were observed close to, but not in contact with the titanium boride. Porosity was frequently observed and is shown in Figure 8-8a annotated by 'ii'.

Titanium boride particles, approximately 7 μm in diameter, were seen at the titanium powder boundaries in the blended Ti-6Al-4V+6.4TiB_2 and are indicated by 'iii' in Figure 8-8b. Needles (indicated by 'iv') were found emanating from a lighter band which surrounded the dark particles centres. XRD of Ti + 6.4TiB_2 suggests that the borides present were both TiB_2 and TiB (Figure 8-9 b) and qualitatively the majority boride phase was TiB_2.

Figure 8-10a and b show the distribution of the TiB_2 when blended with HDH Ti 15-3-3-3 and Ti_{sf} respectively. Qualitatively a better distribution of the titanium boride within the matrix was observed and fewer agglomerated boride particles were observed in comparison to the gas atomised Ti-6Al-4V+6.4TiB_2 powder blend.

Subsequent heat treatments were undertaken to assess the effect of temperature on the blended boride. The TiB needles, which were seen emanating from the boron rich areas after HIPing, grew on heat treatment at 1300°C to approximately 10-20 μm (Figure 8-11a). A region of very fine needles were also seen and are indicated by 'i'.

The dark centre and light band of the boride particles observed in the as-HIPed Ti-6Al-4V + 6.4TiB_2 blends were not observed after heat treatment at 1300°C. However, regions containing fine boride needles were observed and are indicated by 'i' in Figure 8-11b. In addition to the areas containing fine needles, coarse needles approximately 10-20 μm in length were noted.

8.1.4 Microstructure of milled titanium and boron powders

The influence of HIPing temperature and boron on the microstructure and mechanical properties of Ti-6Al-4V were assessed by comparing Ti-6Al-4V and Ti-6Al-4V+0.5B that had been mechanically milled for 60T seconds. In general the following observations were noted:

- Increasing the HIPing temperature reduced porosity. Porosity was observed when HIPing at 600°C (Figure 8-12a). At HIPing temperatures greater than 600°C porosity was no longer observed.
- Increasing the HIP temperature increased the grain size of the ~~titanium~~ Ti-6Al-4V (Figure 8-13)
- The addition of boron resulted in a finer grain size at any of the HIP temperatures compared to the boron free ~~titanium~~ Ti-6Al-4V (alloy) processed under similar conditions (Figure 8-13b)

To fully characterise the effect of boron the grain size was characterised after heat treatments at the HIP temperature for 20 and 96 hours. Grain size measurements were not undertaken on samples HIPed at 600°C and 700°C because it was difficult to resolve the grain structure using SEM. The grain size and the grain size distribution of the samples HIPed at 800°C and 900°C after heat treatment are shown in Figure 8-13 and Figure 8-17.

The grain sizes measured were skewed towards the finer sizes particularly in the samples HIPed at 800°C (Figure 8-14a and b) where the majority of the grains are between 2 and 6 μm. With prolonged time at temperature the frequency of larger grains (>10 μm) increased and this was most pronounced in the milled Ti-6Al-4V HIPed at 900°C and heat-treated at 900°C for 96 hours (Figure 8-15f). Few large grains were observed in the presence of TiB (Figure 8-14b, d, f and Figure 8-15 b, d, f). Although only few large grains may be present, these grains may contribute to a significant volume of a sample (Figure 8-16 and Figure 8-17).

8.1.5 Effect of milling time on distribution of the TiB

The effect of milling time, alloy, boron addition and quantity of boron are shown in Figure 8-12 and Figure 8-18 to Figure 8-21. When blending boron or TiB_2 with gas atomised Ti-6Al-4V or Ti porosity was observed after HIPing at 900°C. Porosity was not observed in the equivalent milled samples, except when HIPing at the lowest temperature of 600°C.

Although a homogeneous distribution of titanium boride was not observed when milling titanium with either boron addition, an improvement in the distribution was observed in comparison to the blended gas atomised samples. Even after longer milling times (60T seconds) a homogeneous distribution was not observed (Figure 8-12a). However, areas where the TiB particles were well distributed (Figure 8-12b) as well as areas of TiB clusters were observed (Figure 8-12c shows the TiB indicated by 'i').

Consistent with the observations of the powders in §7, the general features in the milled and HIPed Ti-6Al-4V or Ti with either boron or TiB_2 samples were:

- Layering of the titanium and boron/TiB_2 powders (Figure 8-18c 'i')
- Deformed gas atomised powders that are no longer spherical (Figure 8-18e 'ii')
- Unprocessed or partially processed powders had large grain sizes (Figure 8-12b) and for Ti-6Al-4V lamellar α was also present (Figure 8-19)

Qualitatively the area fraction of layered regions was found to increase and the presence of gas atomised 'spherical powders', which had not been deformed, diminished with increased milling time. The Ti powders deformed more easily than the Ti-6Al-4V (compare Figure 8-18 and Figure 8-19 with Figure 8-20 and Figure 8-21).

After milling and HIPing XRD indicated the presence of TiB in Ti+2B (Figure 8-22). The TiB produced on HIPing was primarily in the form of needles (Figure 8-23a) and these needles varied in size, from submicron up to approximately 6 μm. When milling with TiB_2 spherical remnants of these particles were still apparent and were approximately 5-7 μm in diameter (Figure 8-23b). XRD suggests both TiB and TiB_2 were present in the Ti+6.4TiB_2 billet (Figure 8-22). Qualitatively the majority boride phase after HIPing the Ti+6.4TiB_2, which had been milled for 6T seconds, was TiB.

Hydrogen was used to enhance the milling process and increasing hydrogen content and milling time improved the distribution of the TiB (Figure 8-24a-d). Milling with fine TiH_2 powders qualitatively produced the best distribution of TiB within the titanium (Figure 8-24e-f). Only a few areas free from TiB were observed and these were thought to relate to the debris remaining in the mill from milling the previous samples containing gas atomised titanium.

8.1.6 Effect of heat treatment on the milled and HIPed powders

The effect of heat treatment on TiB was assessed and growth of the TiB particles was observed. Assessment of TiB needles using deep etching showed the needles of varying length, with some as large as 100 μm long whilst the diameters ranged between 100 nm and 5 μm (Figure 8-25b). After heat treatment the TiB was found to be the only boride phase present (Figure 8-26). Interconnected needles were also observed and are annotated in Figure 8-25a by 'i'. Although the TiB needles increased in size on heat treatment, compared to the HIPed condition, assessment of polished sections

qualitatively shows the TiB particle size did not increase with increasing time between 8 and 100 hours (Figure 8-27).

The distribution of the TiB within the matrix was found to improve as a result of the heat treatment (Figure 8-28) compared with the as HIPed microstructure (Figure 8-18 and Figure 8-21), although TiB free areas were still observed. TiB needles were found to impinge on the TiB 'free' areas (Figure 8-29 'i') and further particles were observed within the 'un-reinforced area'.

8.2 Discussion

8.2.1 The development of the matrix microstructure

The microstructure of titanium and its alloys is usually developed by thermomechanical processing to produce an equiaxed α microstructure with transformed β. This equiaxed microstructure gives the best combination of mechanical properties such as tensile strength, ductility, fracture toughness, fatigue strength and creep resistance. A coarse β grain size (5 – 20 mm) and lamellar/ Widmanstätten α with interlath β is usually observed in as cast titanium billets. Faster cooling rates (such as those observed during powder gas atomisation) produce α'martensite and this was observed in the gas atomised powders (Figure 7.2). During consolidation of these powders the α' decomposes to produce lamellar α with interlath β. This is in agreement with Peters *et al.* (1983) who have also observed coarsening of an α' structure at 800°C to give a fine lamellar α with interlath β. Extending the time at temperature further coarsens this microstructure.

The powder milling process is akin to thermomechanical processing in that it destroys the acicular martensitic α' observed in the gas atomised powders. Thermomechanical processing of the titanium produces equiaxed grains through deformation, recrystallisation and globularisation. The milled titanium powders have been subject to extreme deformation and this has been confirmed by Brown *et al.* (1999b) who showed a nanocrystalline grain structure with some grains as fine as 5 nm and high defect densities within the Ti-6Al-4V powders milled for 60T seconds. HIPing of these powders results in the formation of equiaxed α and β was located at the triple points and grain boundaries (Figure 8-3), which has been confirmed by Brown *et al.* (1999b) using TEM. The grains were also found to be free from dislocations indicating either recovery

or recrystallisation had occurred by 600°C. It is difficult to ascertain which process had occurred because, although no texture measurements were made, changes in texture and grain morphology that may indicate recrystallision, were unlikely to be observed in the milled powders or the consolidated billets as a result of the random nature of the milling process.

Recrystallisation in conventional Ti-6Al-4V is usually observed during β recrystallisation after preworking in the α + β regime. Clearly the powder produced in this study has not followed a conventional processing route. Recrystallisation is dependent on the deformation conditions as well as time and temperature. A critical dislocation density is required for recrystallisation and Peters *et al.* (1983) suggest for Ti-6Al-4V the strain required to achieve this is 0.15 at room temperature and 1.2 at 1050°C, where recrystallisation was observed after heat treating at 800°C for 96 hours. During mechanical milling the powders are deformed by collisions, resulting in high dislocation densities in the powders. Although the exact temperatures at collision sites in the mechanical milling are unknown the length of any collision is very short, therefore recovery was unlikely during milling and this agrees with the fine grain sizes and high defect densities observed in the milled powders (Brown *et al.* (1999a)). As a consequence the driving force for recovery, polygonisation and/or recrystallisation is high. Peters *et al.* (1983) report recrystallisation in water quenched structures that were deformed at 800°C and annealed at 800°C for 1 hour; whereas those deformed at 950°C required 20 hours to recrystallise at 800°C. Given the high dislocation densities in the milled powders recrystallisation may have occurred at temperatures below 600°C, the lowest HIPing temperature, resulting in the equiaxed α and intergranular β microstructure observed.

The β phase morphology and volume fraction was found to vary on heat treatment. Only a few areas of lamellar α were observed (Figure 8-2b). These areas and areas of coarse grain size (Figure 8-12c) are thought to relate powders that had been missed or only partially processed during milling. No areas of transformed β were observed in the milled Ti-6Al-4V after HIPing. By heat treating the samples HIPed at 900°C the volume fraction of β increased and transformed β was seen (Figure 8-4). Furthermore, the β transus of Ti-6Al-4V is usually quoted as 995 ± 15 °C, however the β transus of the milled Ti-6Al-4V HIPed at 900°C was approximately 1027°C. Oxygen and nitrogen are known to increase the β transus of titanium alloys (McQuillan and

McQuillan (1956)). The oxygen and nitrogen values measured in this study were well within the acceptable values for Ti-6Al-4V and thermodynamic modelling predicted the β transus to be 1005°C. Long term heat treatments, however, enabled the microstructure to equilibrate and the β transus measured experimentally was 1005°C (Figure 8-5). This suggests the microstructure produced by mechanical alloying and HIPing was metastable and this is confirmed by an increasing volume fraction of transformed β with time at temperature (Figure 8-4).

The predicted equilibrium concentration of aluminium and vanadium in the α and β phase is in agreement with work by Sastry *et al.* (1980) (Figure 8-6). Measurement made on material from this study by Brown *et al.* (1999b) showed the concentration of the aluminium and vanadium in the α phase was similar to that expected under equilibrium conditions, however, the vanadium in the β phase was much higher than the equilibrium value. This is consistent with the lower volume fraction β observed. A possible reason for the metastable microstructure may relate to the high dislocation densities in the milled Ti-6Al-4V powder, the extended α solid solution and their fine grain size. It is suggested that the high dislocation densities enables pipe diffusion to dominate at lower temperatures (Figure 8-30a)[1], whereas at higher temperatures lattice diffusion is prevalent.

The diffusion distances shown in Figure 8-30b are commensurate with the fine grain size at the low temperatures (5-500 nm) indicating that rapid diffusion of the vanadium to the lower energy grain boundary areas may occur during processing at lower temperatures. The resulting β phase has a high concentration of the β stabiliser, namely vanadium. Brown *et al.* (1999b) indicate that recovery/recrystallisation of the α phase had occurred by 600°C due to the low dislocation densities observed. Further diffusion at higher temperatures is likely to be controlled by lattice diffusion. An indication of the diffusion distances is given in Figure 8-30c, where of the order of 80 hours would be required to diffuse 2.5 μm at 900°C. These observations are consistent with the metastable microstructure observed experimentally in this study.

[1] The assumptions made relating to the distribution of dislocations and grain size with temperature, that have been used to calculate the graphs in Figure 8-30, are detailed in Appendix B.

8.2.2 The influence of TiB on the microstructure of the titanium alloy matrix

The microstructure of the titanium boron alloys is discussed in terms of formation of TiB and its morphology, the distribution of TiB in the titanium matrix and the effect of TiB on the grain size of Ti-6Al-4V.

8.2.2.1 Formation of TiB.

When HIPing titanium, which has been blended with either boron or TiB_2, at 900°C both TiB and TiB_2 are formed (Figure 8-8 and Figure 8-9). It is also possible that boron was retained when HIPing the titanium that had been blended with boron, however this was not observed using XRD because of the amorphous nature of the boron used. The mechanisms for the formation of TiB have been discussed by Brandstotter and Lengauer (1997), Reeves (1992) and Jong *et al.* (1992). In essence they suggest an inward moving reaction front. In the case of blending with boron, there will be two reaction fronts, one between the boron and TiB_2 and the other between the TiB_2 and the TiB. Whereas when blending with TiB_2 only one reaction front was observed and this is shown schematically by Reeves (Figure 8-32) (Reeves, 1992). The reaction layers observed on the TiB_2 particles were approximately 1 μm thick, after HIPing for 2 hours at 900°C and this is consistent with Reeves (1992) where a similar size reaction layer was observed after heat treating for 80 minutes at 950°C. Reeves (1992) also calculated activation energies and constants for the reaction for TiB_2 to TiB. The equation and coefficients shown below were fitted separately over the α and β temperature ranges from experimental values:

	α	β
Q (kJ mol^{-1})	140.34	259.60
k_0 (x 10^{-5} m $s^{-1/2}$)	1.22	419.14

The formation of reaction layers can be described by Fick's first law of diffusion:

$$\delta = k\, t^{1/2}$$

Equation 8-1

where δ is the reaction layer thickness, k is the reaction constant at a given temperature and t is heat treatment time. The constant k can be described as a function of temperature:

$$k = k_0 \exp(-Q/2RT)$$

Equation 8-2

where k_0 is the reaction rate constant, Q is the activation energy for the reaction, R is the gas constant and T is temperature.

Given these equations and the values calculated by Reeves (1992) the time taken for a TiB_2 particle that is 7 μm in diameter to fully react to form TiB at 1300°C is approximately 6 minutes. The approximation shown in Figure 8-31 is in agreement with work by Brandstotter and Lengauer (1997) who observed a layer 20 μm when pack boriding at 1300°C for 3 hours. In this study a heat treatment at 1300°C for 8 hours was undertaken on TiB_2 particles that had average particle size of 7 μm and the agglomerated boron was less than 10 μm in thickness and it is likely full transformation of boron and TiB_2 to TiB occurred.

There are 'coarse' and 'fine' TiB needles present in the heat-treated samples (Figure 8-11). The coarse needles are likely to nucleate at the interface between the reacted TiB_2 particles (or reacted boron agglomerate) and the titanium matrix when the matrix becomes saturated in boron. The coarse needles then act as path for fast diffusion of the boron and the needles grow (Figure 8-31). The areas of fine TiB observed are likely to be a remnant of TiB_2 particles (or agglomerated boron). The TiB_2/TiB reaction front will move inward to consume the TiB_2 particles. Once fully reacted only TiB will remain and the source of boron for the growth of the coarse TiB needles will have disappeared and only competitive growth of the TiB needles will remain.

Mechanical milling breaks up the boron and TiB_2 particles and disperses them within the titanium matrix. Brown *et al.* (1999a) assessed Ti-6Al-4V milled with boron using TEM and found that the boron was either in solution in the titanium, present as TiB or as isolated areas of boron powder within the titanium. Given the reaction rates shown in Figure 8-31 a finer size and even distribution of the TiB_2 or boron particles in the titanium matrix would reduce the time for a full reaction of the particles to form TiB. This is confirmed by XRD where α Ti and TiB are the only phases present after HIPing the milled Ti+2B at 900°C (Figure 8-22a) compared with α Ti, TiB and TiB_2 in the Ti+2B blended and HIPed at 900°C (Figure 8-9).

Unlike milling with boron, when milling with TiB_2 full reaction of the TiB_2 to TiB did not occur, although qualitatively XRD suggests there was less TiB_2 in the milled sample in comparison to the blended sample (compare Figure 8-9 and Figure 8-22). There was less TiB_2 in the milled and HIPed sample because the milling process fractures and

distributes the hard TiB_2 particles into fine TiB_2 particles. The finer the TiB_2 particles, the greater the Ti-TiB_2 contact areas and so during HIPing more TiB_2 was converted to TiB. These fine TiB_2 particles reacted to form fine TiB needles during HIPing (Figure 8-23). The larger TiB_2 particles were surrounded by TiB during HIPing (Figure 8-21 and Figure 8-23) but, as with the blended samples further heat treatment of the HIPed Ti+6.4TiB_2 results in full reaction of the TiB_2 to TiB (Figure 8-26).

8.2.2.2 Morphology of TiB

The majority of the powders in this study were HIPed using a two stage treatment, first at 500°C for 2 hours and 150 MPa and then at 900°C for 2 hours at 150 MPa (Figure 6-2). The low temperature heat treatment was undertaken following work by Fan *et al.* (1995) who reported the formation of equiaxed TiB particles when using a low temperature heat treatment prior to consolidation of rapidly solidified titanium boron alloys. It is clear from Figure 8-23 and Figure 8-25 that the TiB is acicular or needle shaped and there was no evidence to suggest the formation of equiaxed TiB particles. A possible reason for the difference in this study and that of Fan *et al* was the method in which the TiB grows. In the study by Fan *et al.* (1995) the TiB was formed from boron that was in a supersaturated solid solution. At low temperatures, where diffusion of boron is thought to be the rate determining factor that restricted the growth of TiB, the difference in growth rates along the different crystallographic directions is reduced. Therefore, at lower temperatures nearly equiaxed particles were produced. Although some boron may be present in solution, in this study, the TiB is generally thought to grow from discrete particles of boron or TiB_2 dispersed by milling throughout the titanium (alloy) matrix. In this case there is a large supply of boron and therefore growth occurs in the preferential (010) direction.

8.2.2.3 Effect of milling on the distribution

Mechanical milling clearly improves the distribution of TiB within the gas atomised powders when compared to the blending alone. The TiB was observed on a fine scale and many TiB particles were less than 1 μm in size. The distribution of the TiB was not however homogeneous even after 60 T seconds and in all samples areas with fine TiB needles and areas which are free of TiB were seen (Figure 8-12).

Milling different titanium alloy powders resulted in different distributions of TiB being achieved. The effect of the different strengths of the powders was noted in § 7.2, where

the softer Ti powders were heavily deformed during the milling process whereas after milling the harder Ti-6Al-4V powders original spherical powders still remained (compare Figure 8-18 to Figure 8-21). Further improvements in the distribution of the borides within the titanium matrix may be possible by increasing the milling times (compare Figure 8-12 and Figure 8-18). However, further milling of the Ti powders was not practicable because the powders were already large in size. Increasing the milling times, where possible, may improve the distribution of boron in titanium, however, from a commercial view point the milling time should be minimised for cost effective production.

Although the initial distribution of the TiB in titanium powders was disappointing improvements in distribution were observed as a result of heat treating the material at 1300°C for 8 hours (compare Figure 8-18e, Figure 8-19e, Figure 8-20d and Figure 8-21c with Figure 8-28). It is thought that the improvement in the distribution of the TiB is a result of growth of the TiB from the heavily reinforced, boron/TiB_2 rich, areas into the un-reinforced areas (Figure 8-29 'i'). Any isolated particles seen at the centre of the unreinforced area (Figure 8-29 'ii') were likely to have emanated from the heavily reinforced boundaries in the same way in as the particle labelled 'i' in Figure 8-29.

Two alternative methods to improve the distribution of the TiB without heat treatment were assessed:

- Finer titanium powders
- Milling under a hydrogen atmosphere

Two different types of powders were compared with the gas atomised titanium powders blended with TiB_2. The TiB_2 formed an agglomerated necklace of particles around the titanium gas atomised powders (Figure 8-7), however, fewer agglomerated TiB_2 were observed within the Ti_{sf} and HDH Ti-15-3-3-3 (Figure 8-10). The improved distribution is a result of increased surface area in the finer powders (45 μm for the HDH powder and 100 μm for the Ti_{sf} compared with the 250 μm gas atomised powders) that enables a better distribution to be achieved. In addition, the Ti_{sf} powder has an open form that further increases the surface area of the powders and hence a better distribution of boride was achieved. It is suggested that both the HDH and Ti_{sf} powders would need

only short milling times to improve the distribution and remove any agglomerated TiB_2 that may act as fracture initiation sites.

Milling under a hydrogen atmosphere was found to aid the milling of the titanium both by reducing the particle size during milling (§ 7.2) and by improving the distribution of the boride within the titanium (Figure 8-24). Hydrogen forms TiH_2 during milling which is a brittle phase and as such it encourages fracture of the powders during the milling process and consequently better distributions of the boride in the titanium powders was achieved. In a similar manner milling TiH_2 with TiB_2 resulted a good distribution of the TiB_2. Very little agglomeration of these powders occurred during milling and the distribution of the TiB_2 was even. Only a few areas of unreinforced titanium were observed. These areas were thought to be unrelated to the TiH_2 powders and were remnants of gas atomised powders from the previous milling runs. TiH_2 powder was effective in controlling the fracture and welding behaviour during milling and appears to have resulted in a good distribution of the boride within the powder. Gaseous hydrogen incorporated during the milling of $Ti+6.4TiB_2$ was not enough to fully control the fracture and welding behaviour of the powder and hence a distribution such as that observed when milling the TiH_2+TiB_2 was not achieved. Further measures could be used to incorporate greater quantities of gaseous hydrogen during milling. These measures all necessitate increasing the flow and volume of hydrogen in the mills, and this is undesirable because of the high risk of explosion associated with gaseous hydrogen hence milling TiH_2 with TiB_2 gives the best opportunity for and homogeneous distribution of TiB in titanium.

8.2.3 Heat treatment

Heat treatments were undertaken to assess the stability of the TiB and the effect of the TiB on grain size stability.

8.2.3.1 Stability of the TiB particles

Qualitatively there was an initial increase in TiB particle size by heat treating samples at 1300°C, however, the particle size appears to stabilise with further time at temperature (Figure 8-27). This observation is consistent with work by Saito *et al.* (1995a) who commented on a stable TiB particle size of 5 μm wide and 8 μm even after heat treatment at 1300°C for 100 hours. It should, however, be noted that no indication of the particle size distribution was given. Assessment of particle size using deep etching

(Figure 8-25) showed that they range in size between 100 nm and 5 μm in diameter and up to approximately 100 μm long, after heat treatment at 1300°C for 8 hours. Saito *et al.* (1995a) suggest the stability of TiB is related to the low solubility of boron in titanium and the low interfacial energy TiB/Ti boundary, hence the driving force for Oswald ripening is low. This study shows little growth in the width of the particles, however growth occurs readily in the length of the particle, which is the easy growth direction for TiB. The difference between the two studies is likely to be a result of the measurement techniques. Saito *et al.* (1995a) may have taken measurements from the optical micrographs which do not give a realistic measurement of the length of the particles (compare Figure 8-25 and Figure 8-27).

8.2.3.2 The effect of TiB on the grain size stability

Mechanical milling of titanium dramatically reduces the grain size of the titanium to the order of 10-60 nm in Ti-6Al-4V and Ti-6Al-4V+0.5B after milling for 60T seconds (§ 7.2.4). However, the milled Ti-6Al-4V grain size increased to 7.7 μm after HIPing at 900°C. This is contrary to much of the published work on nanocrystalline materials where unusual thermal stability of the fine grain sizes has been observed in HIPed samples (Suryanarayana *et al.* (1990), Oehring *et al.* (1995), Abe and Johnson, (1992)). The major difference between the material with grain size stability and the material in this study is the level of contamination. Nanocrystalline material with a thermally stable grain size is usually associated with significant levels of contamination, such as oxygen and nitrogen (Suryanarayana *et al.* (1990)). Unfortunately high levels of oxygen and nitrogen in titanium alloys are harmful to the mechanical properties (McQuillan and McQuillan (1956)) and thus preclude any structural application. In this respect the material produced in this study has been successful in controlling the contamination and gives the best basis for a nanocrystalline structural material. Boron was milled with the Ti-6Al-4V and during HIPing TiB was formed and this was found to inhibit grain growth.

In areas reinforced with TiB the grain boundaries were pinned, resulting in the stabilisation of a finer grain size than milled Ti-6Al-4V even after reasonably long dwell times at temperatures. The milled Ti-6Al-4V had a grain size of 7.7 μm in the as-HIPed condition, however, after heat treatment for 96 hours the grain size increased to 14.2 μm whereas the sample that contained 0.5 B had corresponding grain sizes of 3.0 and 4.1 μm (Figure 8-14 and Figure 8-15). Previous work (Godfrey *et al.* (2000),

Goodwin *et al.* (1997)) similarly found that even after heat treatment up to 1050°C, the addition of 0.1B reduced grain growth. The use of particles to pin grain boundaries in titanium is not new and for example, Lederich *et al.* (1984) used additions of erbium and yttria and Agrawal *et al.* (1980) also added yttria to Ti-6Al-4V. Although grain refinement has been reported and this is a similar level to that produced in this study (Agrawal *et al.* reported grain sizes of the order of 5 μm), the thermal stability of these grains was not reported. It was hoped that the TiB would stabilise the very fine grain sizes produced by the milling. However, the size of the TiB was such that the grain size was stabilised in the region of 3 to 4 μm. Zener-Gladman formulated a relationship of particle size to final grain size (Porter and Easterling (1981). Two equations were developed:

$$R = 4r/3f \quad \text{for random particles}$$

Equation 8-3

$$R = 2r/(f^{1/2}) \text{ for particles located at grain boundaries}$$

Equation 8-4

where R is grain radius, r = particle radius and f = particle volume fraction. Assuming the particles are evenly distributed and a particle radius of 2 μm the measured grain sizes are similar to those predicted using the Zener-Gladman relationship for particles located randomly within the material (Figure 8-33) and clearly for finer grain sizes to be achieved finer particles would be required.

8.3 Summary

- Mechanical alloying Ti-6Al-4V results in the formation of an equiaxed α microstructure with intergranular β. This microstructure is metastable and requires extended heat treatments to equilibrate the microstructure.
- TiB was formed by HIPing titanium with either boron or TiB_2. Full reaction to TiB during HIPing occurred when titanium was milled with boron, however subsequent heat treatments were required to enable full reaction of the TiB_2 to TiB.
- The TiB was found to stabilise the grain size of Ti-6Al-4V during HIPing. The stabilised grain size was not as fine as that produced in the milled powders and the size of the grains retained was found to relate to the size of the TiB particles.

- Mechanical milling improved the distribution of the boron within the titanium powders compared with blended samples, however longer milling times were required to produce a homogeneous distribution of the boride within the titanium.
- Further improvements to the distribution of the boride in the titanium matrix were made by using finer titanium powders such as sponge fines and hydride dehydride powders or by incorporating hydrogen in the milling process. ~~Although~~ Care needs to be taken in choosing powders with interstitial contamination particularly when considering hydrided powders.
- Milling TiH_2 with TiB_2 offers the best method for the production of a homogeneous distribution of TiB_2 in titanium. Dehydriding of the powders was successfully achieved during degassing of the powders.

Sample	mill time (T seconds)	Oxygen (ppm)	Nitrogen (ppm)
HDH Ti-15-3-3-3	0	7400	410
Sponge fines	0	2050	110
Ti-6Al-4V	60	1170	120

Table 8-1 The interstitial contamination of HIPed powders.

Sample	Volume fraction % transformed β at 900°C
Ti-6Al-4V HIP 800°C and HT 20 hours at 800°C	17
Ti-6Al-4V HIP 800°C and HT 96 hours at 800°C	49
Ti-6Al-4V HIP 900°C	29
Ti-6Al-4V HIP 900°C and HT 20 hours at 900°C	50
Ti-6Al-4V HIP 900°C and HT 96 hours at 900°C	50

Table 8-2 Volume fraction of transformed β (%) of Ti-6Al-4V milled for 60 T seconds, HIPed and heat-treated samples at 900°C.

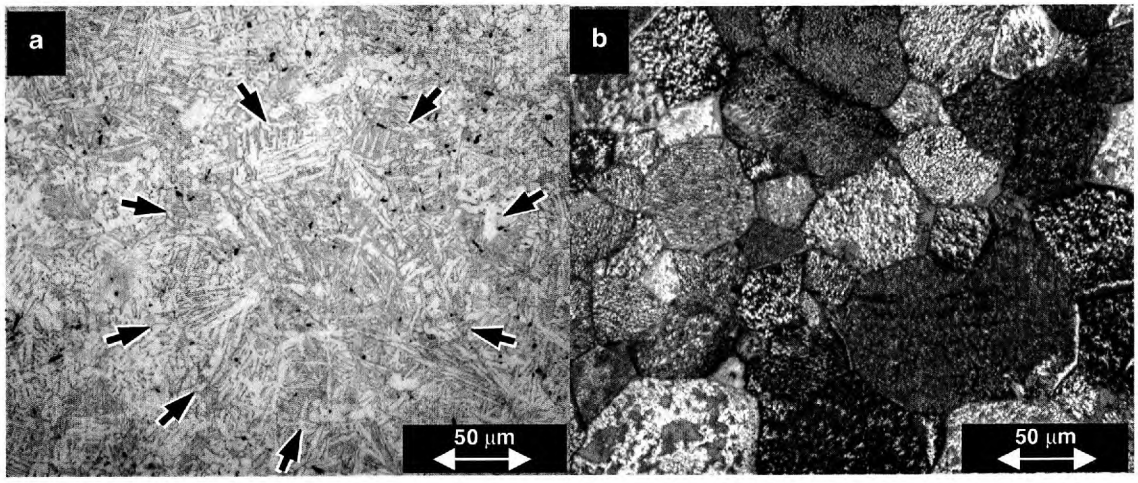


Figure 8-1 An optical micrograph of (a) gas atomised Ti-6Al-4V with a lamellar microstructure, where the arrows indicate a powder particle, (b) gas atomised Ti with an equiaxed microstructure. The powders were HIPed at 500°C for 2 hours at 150 MPa followed by 900°C for 2 hours at 150 MPa.

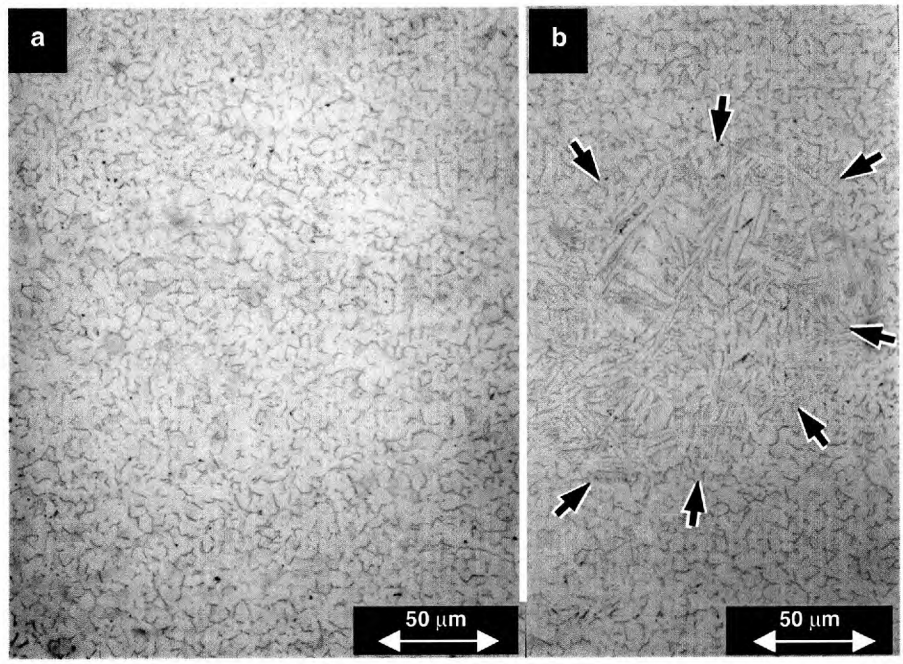


Figure 8-2 An optical micrograph of Ti-6Al-4V milled for 60T seconds HIPed at 900°C for 2 hours at 150 MPa (a) shows the equiaxed α phase and (b) lamellar α microstructure from a powder particle that has not been moved.

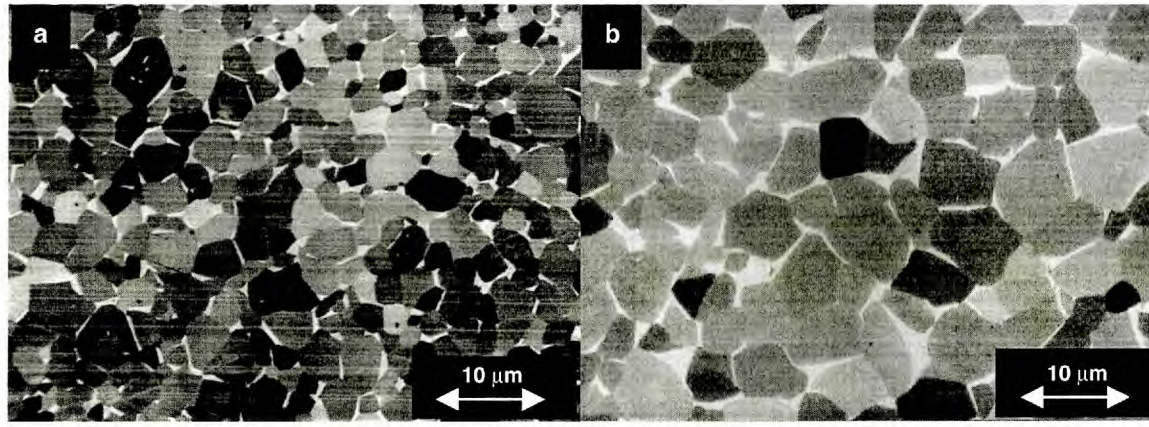


Figure 8-3 A backscattered FEG-SEM micrograph of Ti-6Al-4V milled for 60T seconds and (a) HIPed at 800°C and (b) HIPed at 900°C for 2 hours at 150 MPa.

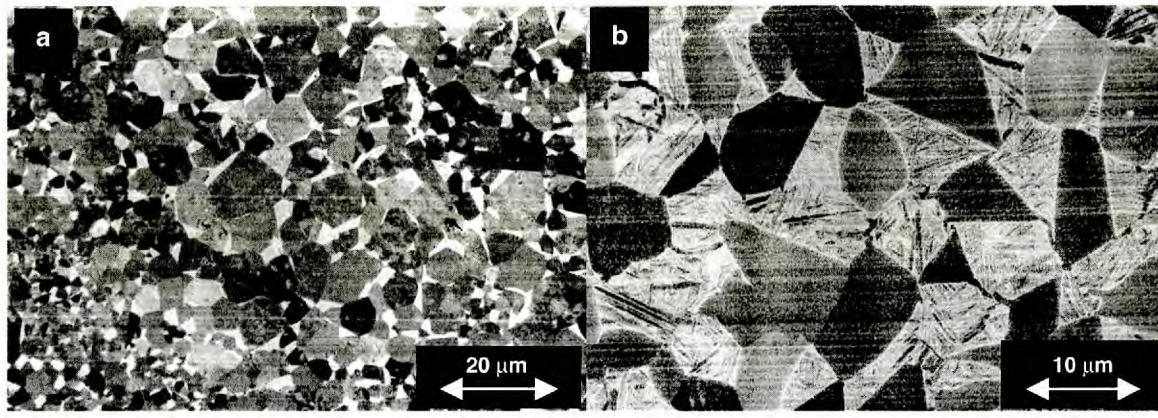


Figure 8-4 A backscattered FEG-SEM micrograph of Ti-6Al-4V milled for 60T seconds and (a) HIPed at 800°C and heat treated for 20 hours at 800°C and (b) HIPed at 900°C and heat-treated for 20 hours at 900°C.

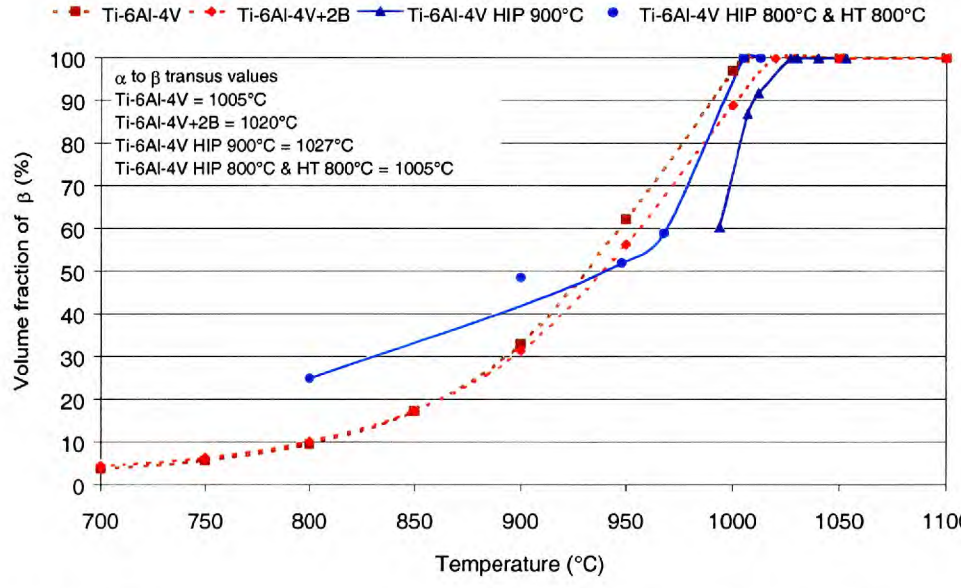


Figure 8-5 The β transus approach curve for Ti-6Al-4V milled for 60T seconds and HIPed at either 900°C for 2 hours at 150 MPa or 800°C for 2 hours at 150 MPa and at 800°C for 96 hours compared with the β transus predicted for Ti-6Al-4V and Ti-6Al-4V+2B using JMatPro.

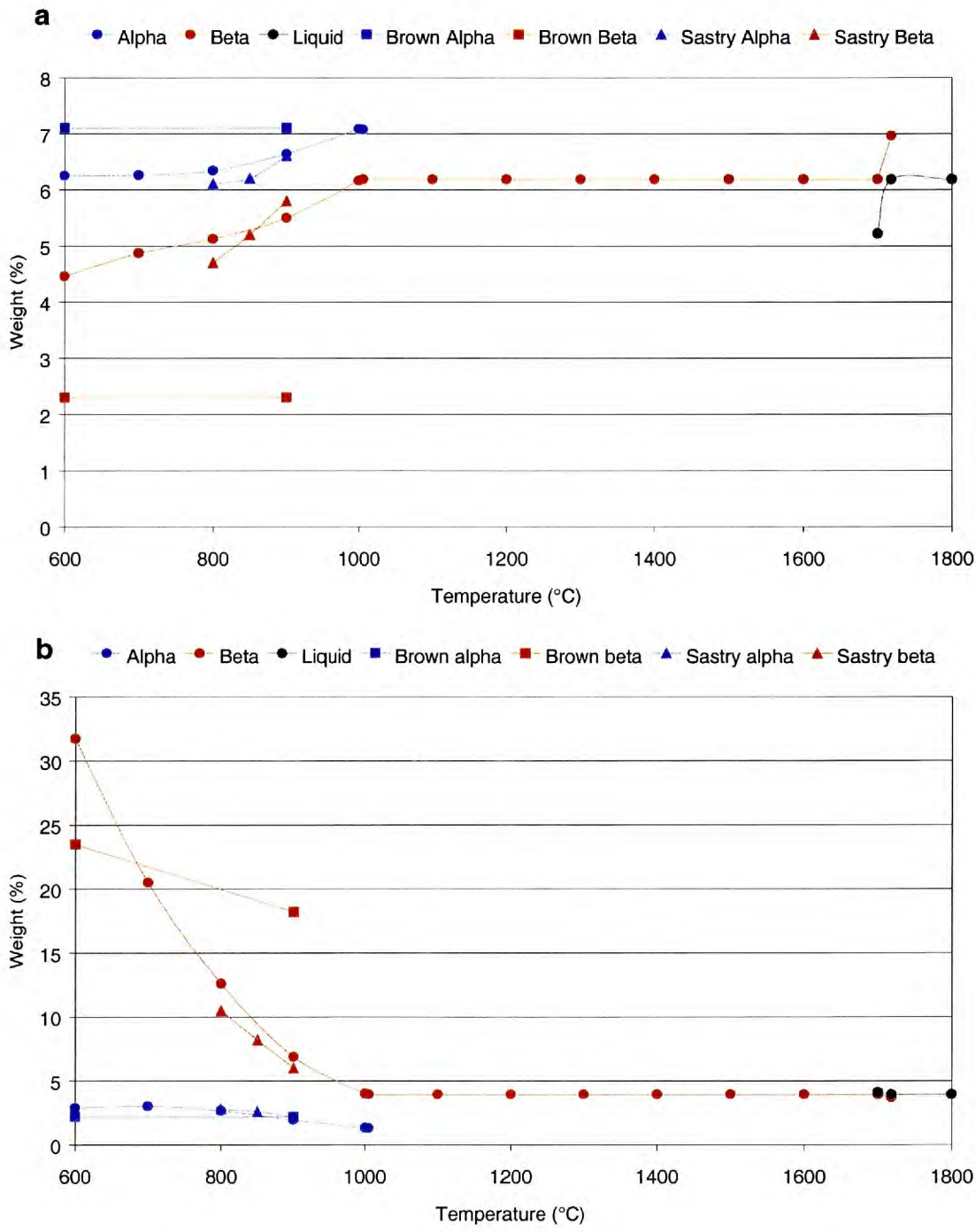


Figure 8-6 The relative concentrations of (a)Al and (b) V in α and β titanium and liquid phases between 600°C and 1800°C predicted using JMatPro and compared with data from Brown *et al.* (1999a) and Sastry *et al.* (1980).

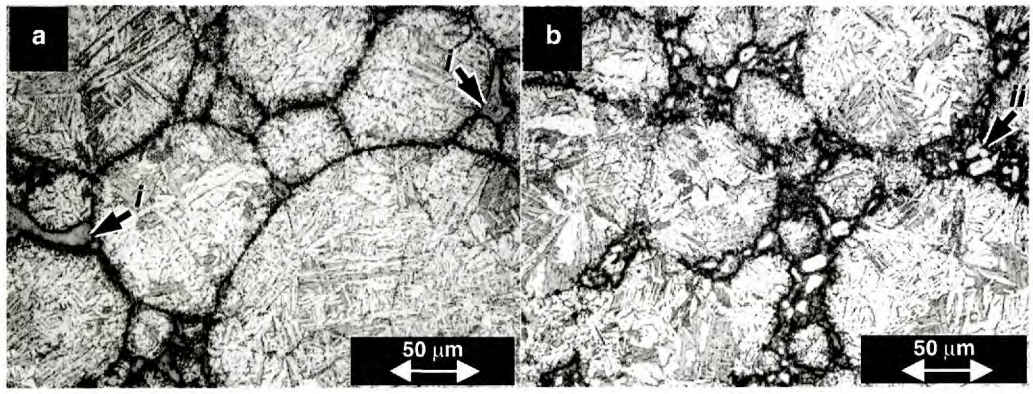


Figure 8-7 Optical micrographs of (a) Ti-6Al-4V + 2B and (b) Ti-6Al-4V + 6.4 TiB_2, blended and HIPed at 500°C for 2 hours at 150 MPa, followed by 900°C for 2 hours at 150 MPa where 'i' indicates porosity, 'ii' shows agglomerates of TiB_2.

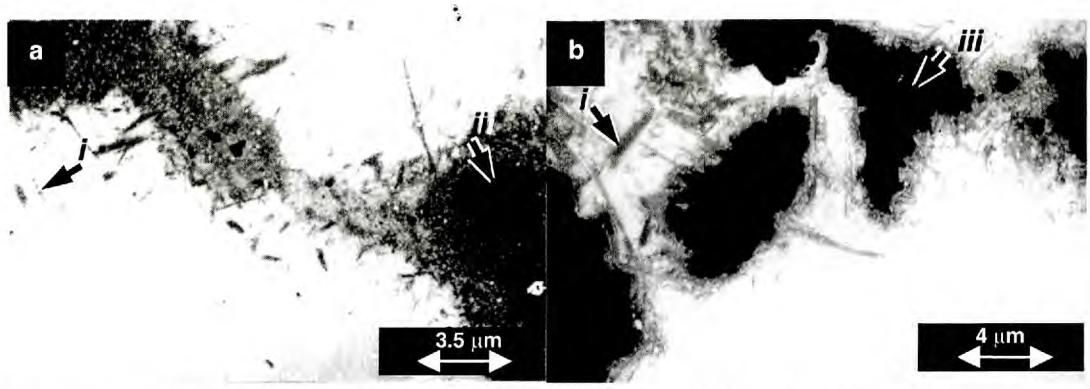


Figure 8-8 Backscattered electron micrographs of (a) Ti-6Al-4V + 2B showing TiB at prior powder particle boundaries and (b) Ti-6Al-4V + 6.4TiB_2, showing TiB needles growing from the TiB_2 particles located at prior powder particle boundaries, after blending and HIPing at 500°C for 2 hours at 150 MPa, followed by 900°C for 2 hours at 150 MPa. Where 'i' indicates an isolated TiB needle, 'ii' indicates porosity and 'iii' indicates TiB_2 particle.

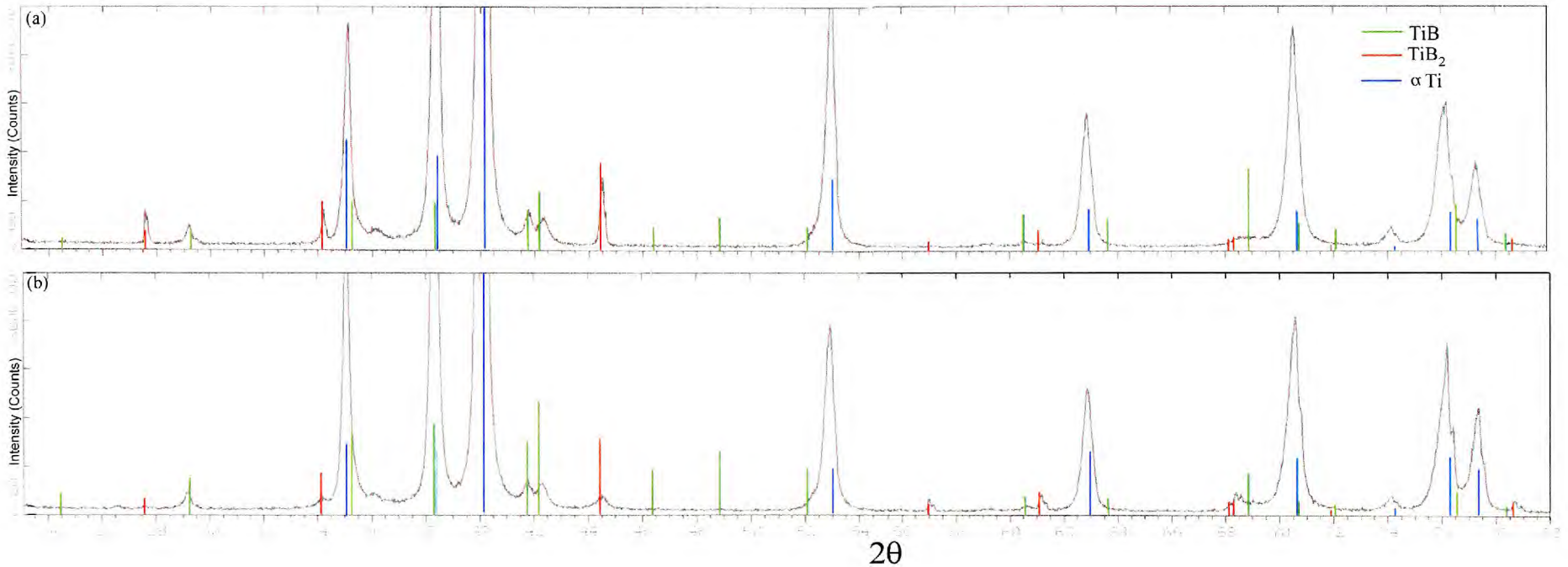


Figure 8-9 XRD of (a) blended Ti + 2B and (b) Ti + 6.4TiB_2. Both samples were HIPed at 500°C for 2 hours at 150 MPa followed by 900°C for 2 hours at 150 MPa.

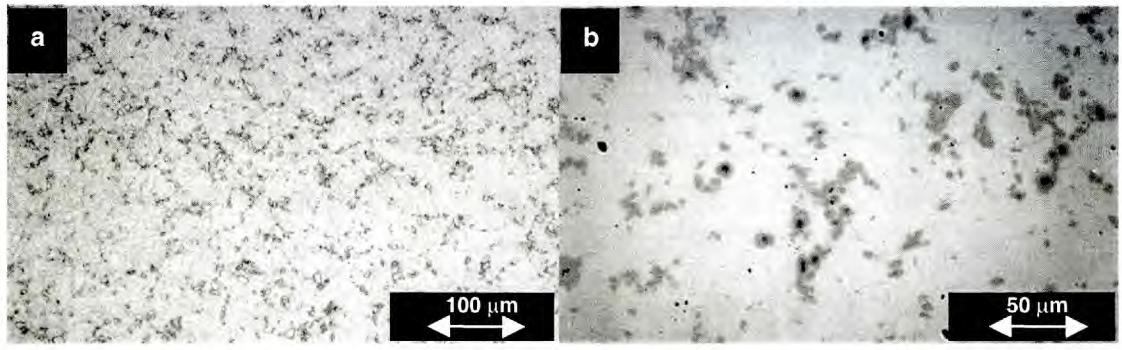


Figure 8-10 Optical micrographs of (a) the HDH Ti-15-3-3-3 + 6.4TiB_2 and (b) Ti_{sf} + 6.4TiB_2 blended and HIPed at 900°C for 2 hours at 150 MPa.

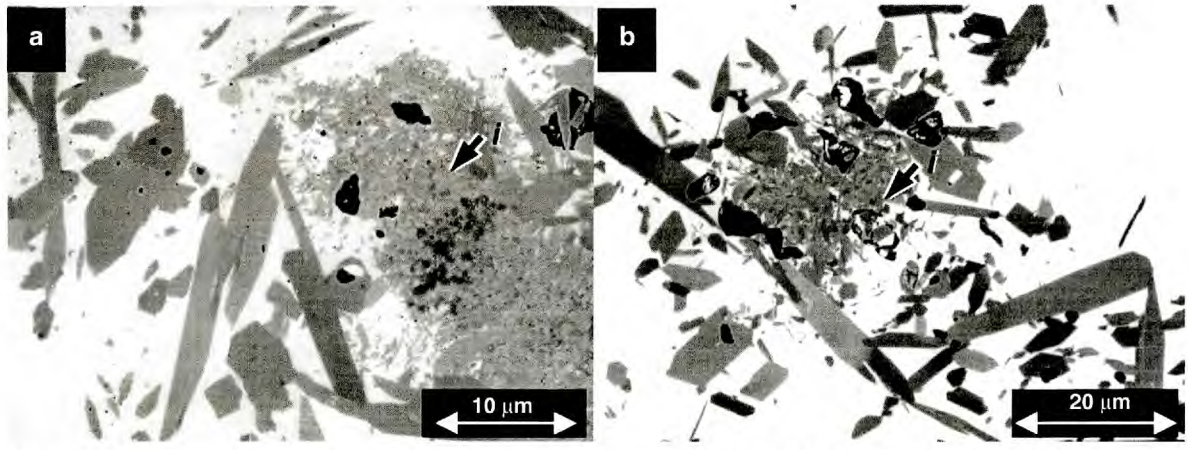


Figure 8-11 Backscattered electron micrographs of (a) blended Ti-6Al-4V + 2B and (b) blended Ti-6Al-4V + 6.4TiB_2, where 'i' indicates regions containing fine needles, HIPed at 500°C for 2 hours at 150 MPa followed by 900°C for 2 hours at 150 MPa and heat treated at 1300°C for 8 hours in vacuum.

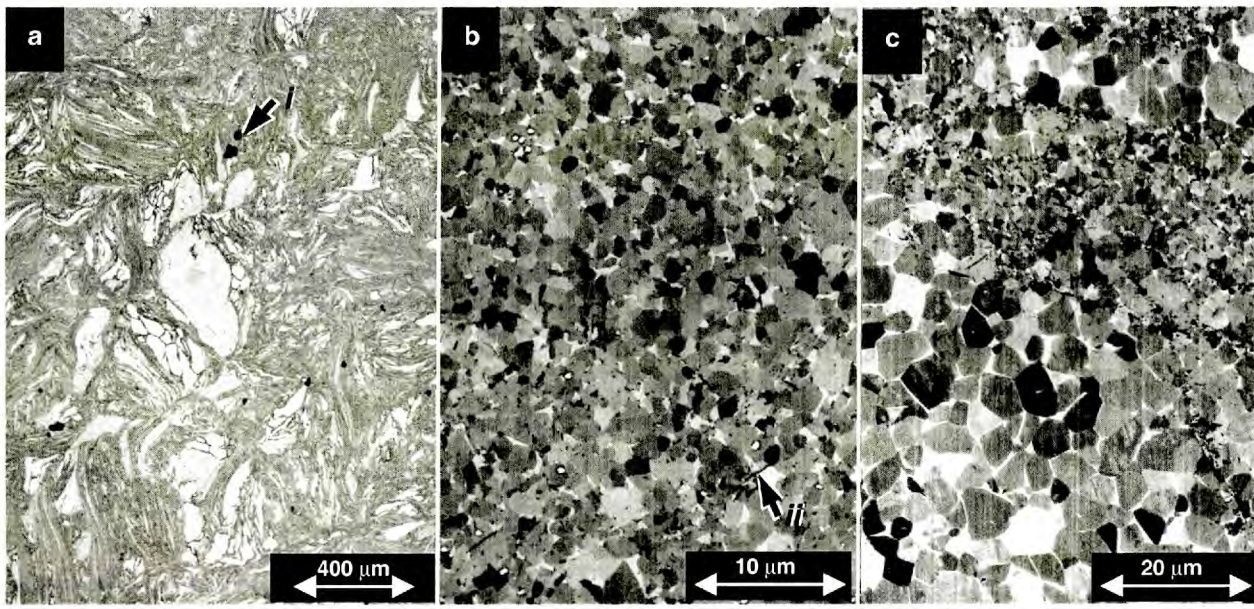


Figure 8-12 Micrographs of Ti-6Al-4V + 0.5B milled for 60T seconds, where (a) is an optical micrograph of a sample HIPed at 600°C for 2 hours at 150 MPa where 'i' indicates porosity, (b and c) are backscattered FEG-SEM images of a samples HIPed at 900°C for 2 hours at 150 MPa. An even distribution of the TiB needles can be seen in (b) and 'ii' indicates a TiB needle. Areas of high and low volume fraction TiB can be seen in (c).

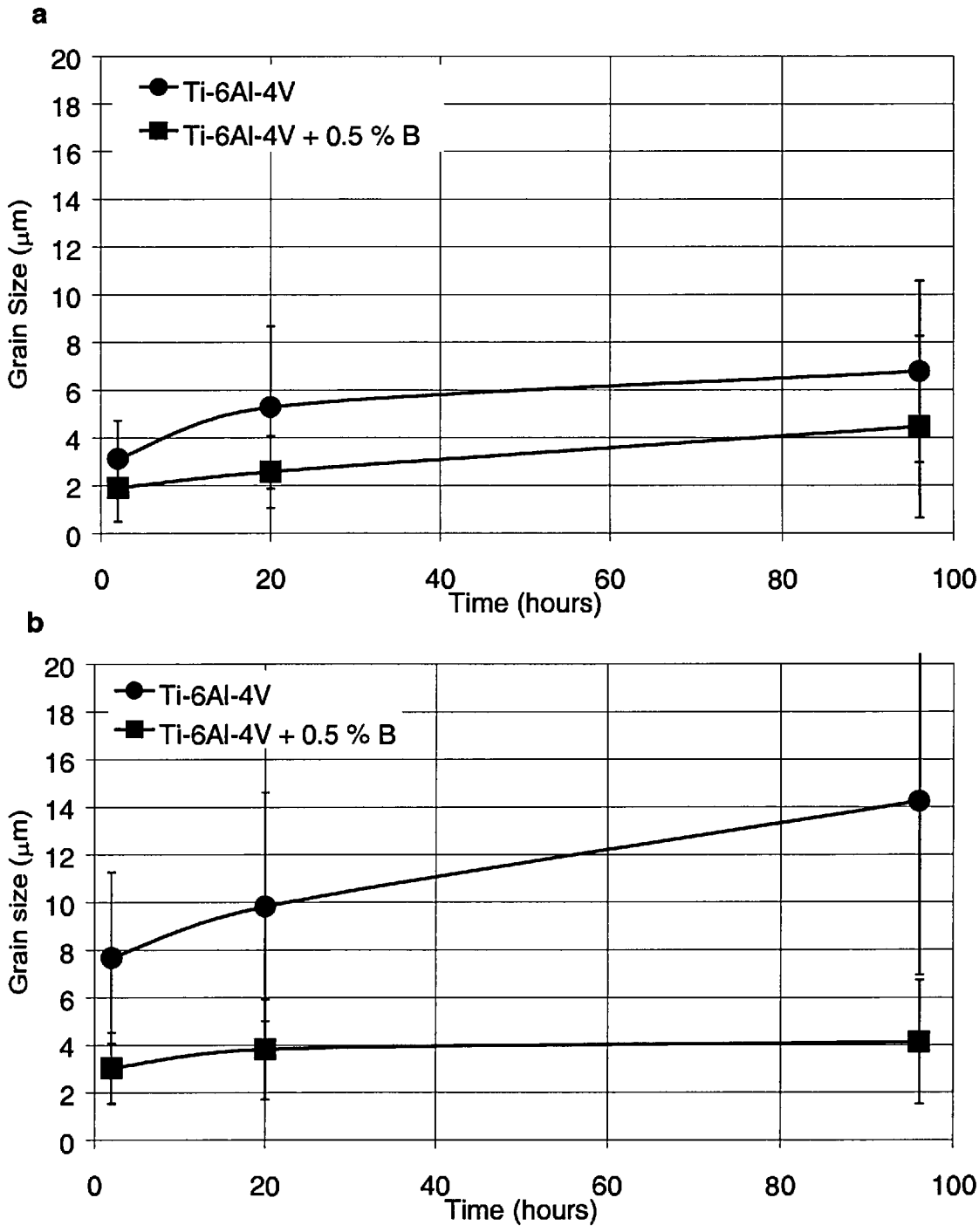


Figure 8-13 The effect of heat treatment on the average grain size of samples milled for 60T seconds, HIPed and heat-treated at (a) 800°C and (b) 900°C. Error bars indicate one standard deviation.

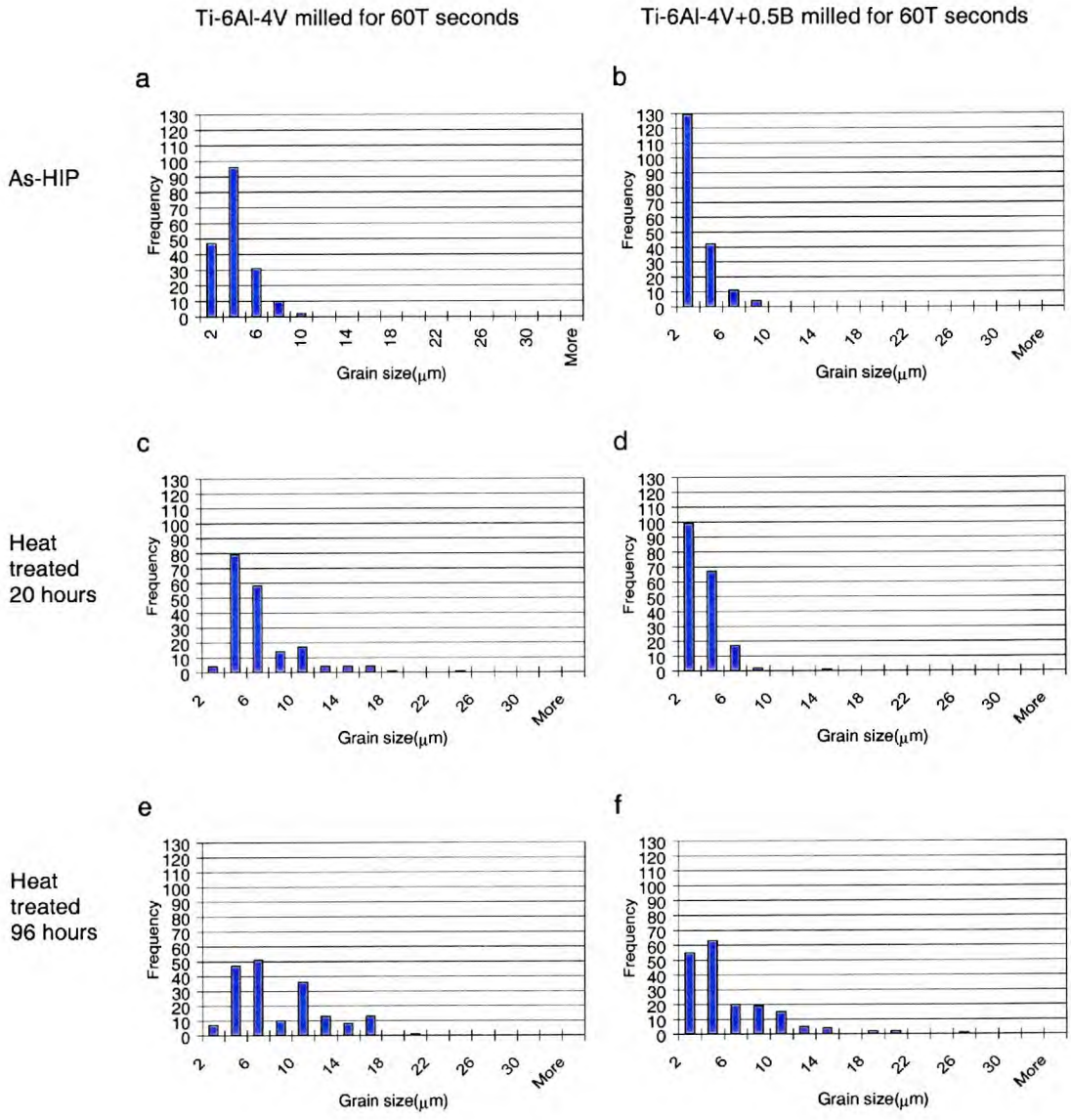


Figure 8-14 The grain size distribution of the Ti-6Al-4V and Ti-6Al-4V+0.5B after milling for 60T seconds, HIPed at 800°C and heat-treated at 800°C.

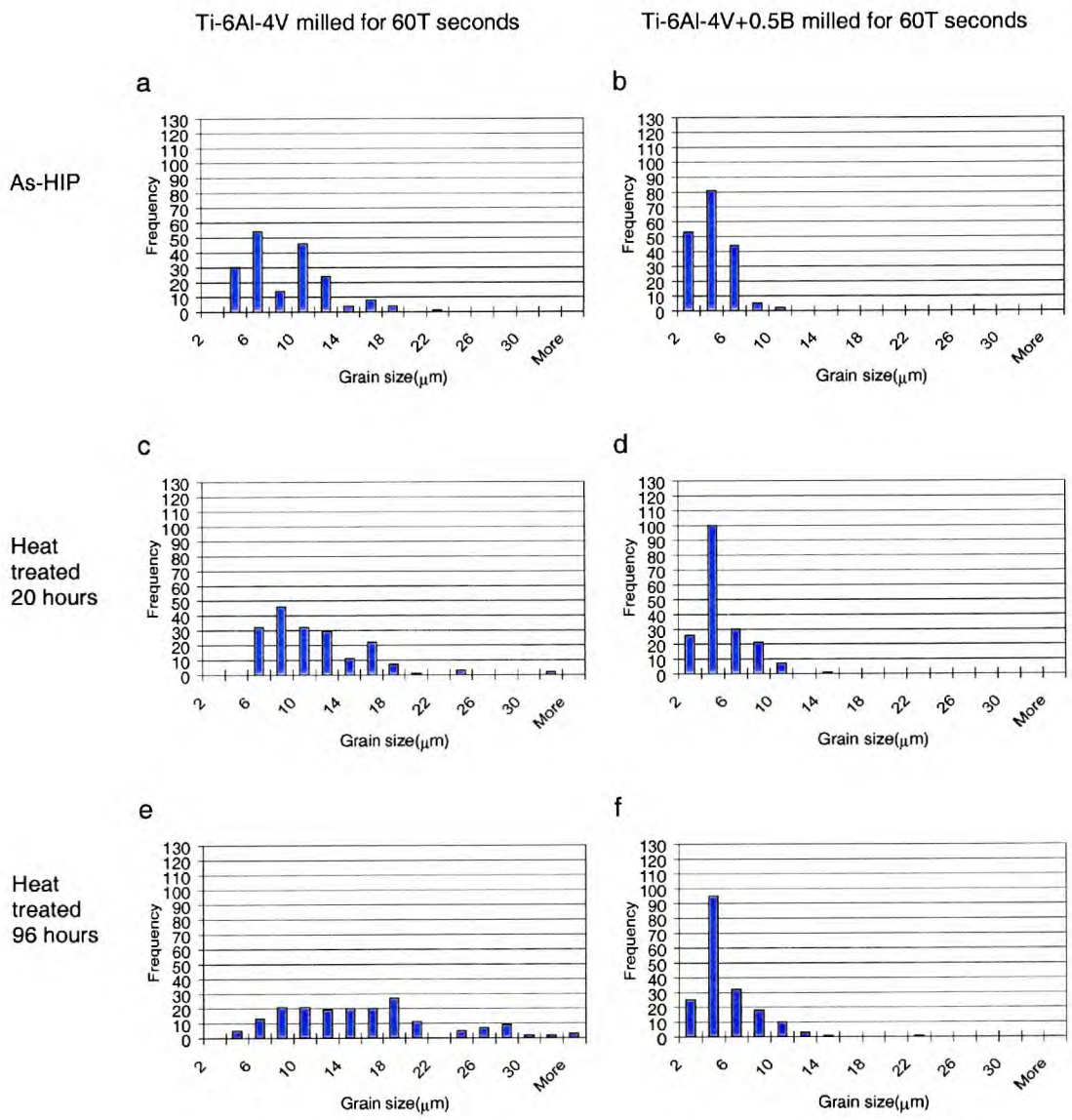


Figure 8-15 The grain size distribution of the Ti-6Al-4V and Ti-6Al-4V+0.5B after milling for 60T seconds, HIPed at 900°C and heat-treated at 900°C.

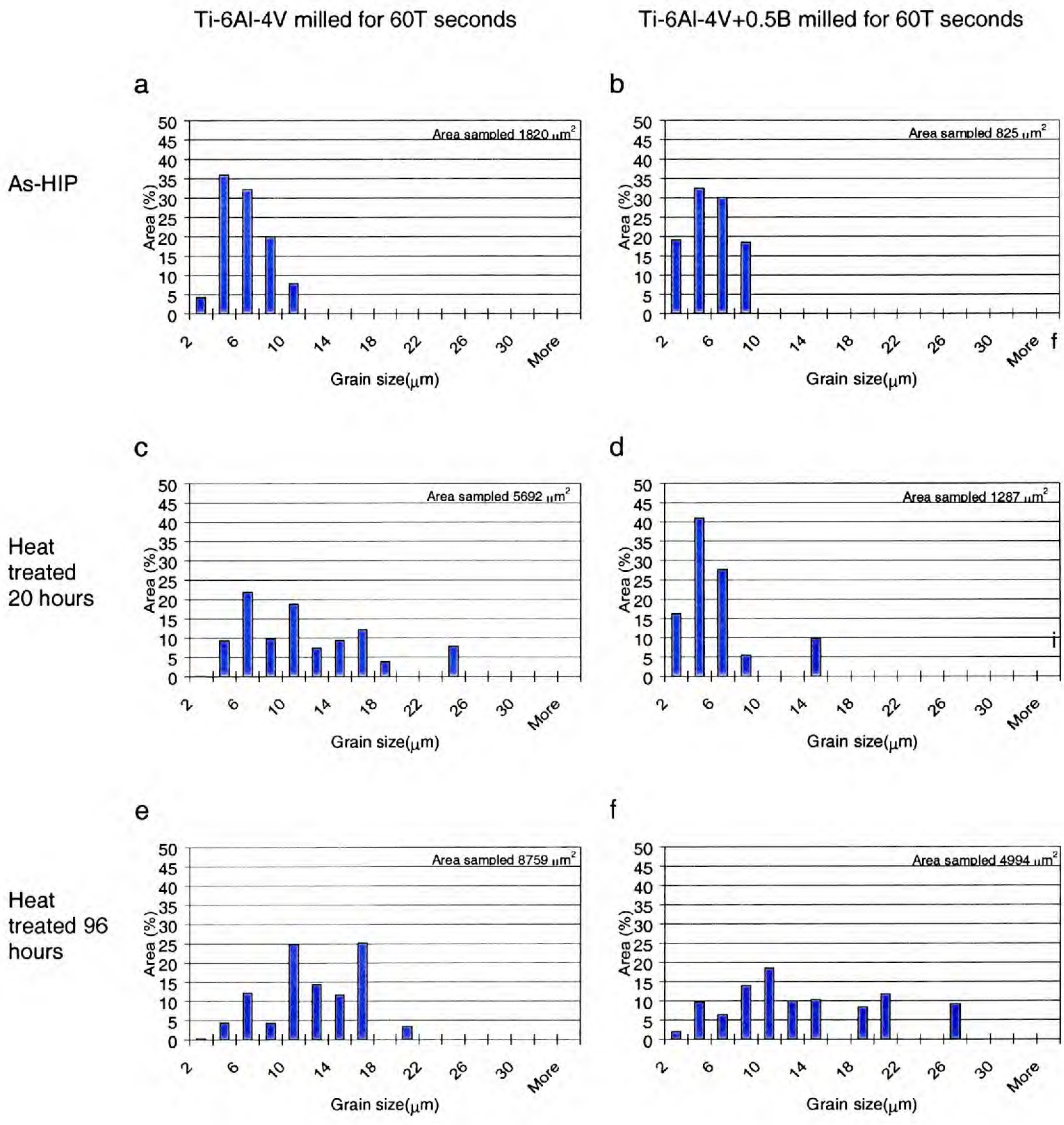


Figure 8-16 The area distribution of grain size of the Ti-6Al-4V and Ti-6Al-4V+0.5B after milling for 60T seconds, HIPed at 800°C and heat-treated at 800°C.

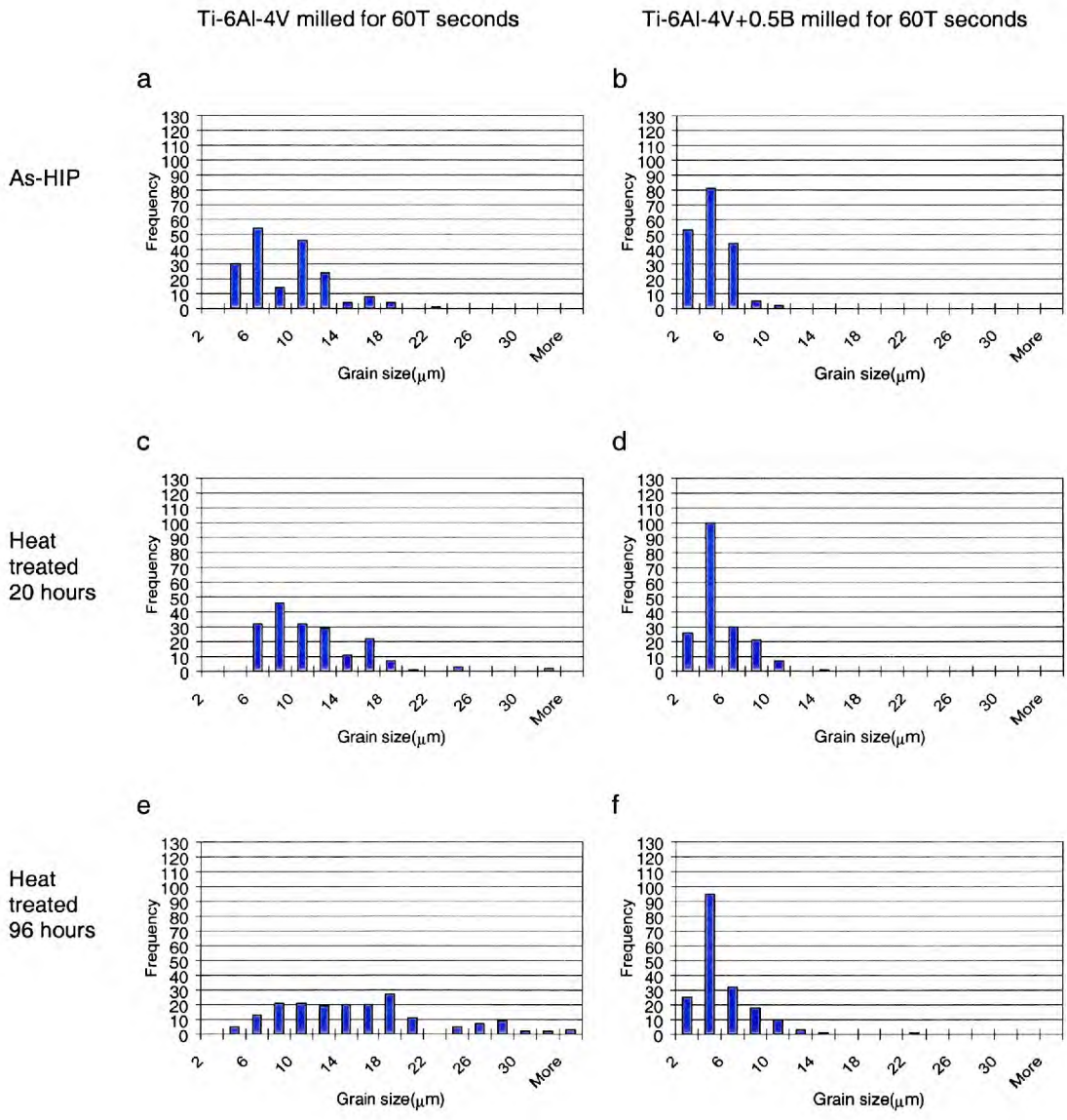


Figure 8-17 The area distribution of grain size of the Ti-6Al-4V and Ti-6Al-4V+0.5B after milling for 60T seconds, HIPed at 900°C and heat-treated at 900°C.

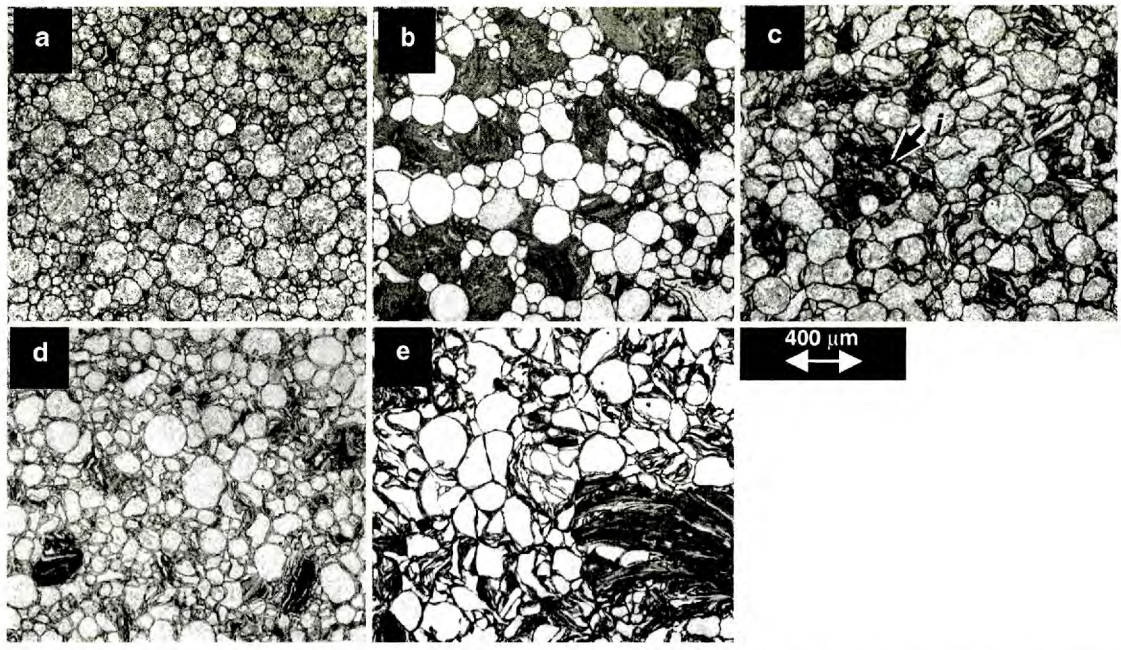


Figure 8-18 Optical micrographs of Ti-6Al-4V + 2B milled for (a) 0, (b) 3T, (c) 6T, (d) 12T and (e) 18T seconds. Samples were HIPed at 500°C for 2 hours at 150 MPa followed by 900°C for 2 hours at 150 MPa. Where 'i' indicates ~~heavily~~ a heavily deformed region.

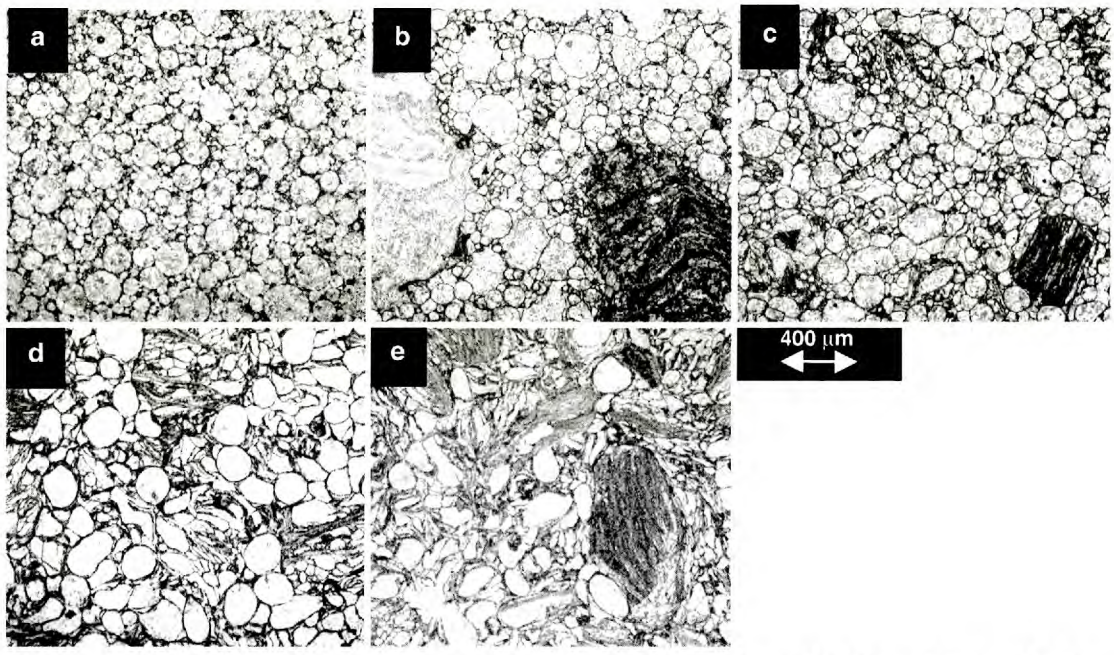


Figure 8-19 Optical micrographs of Ti-6Al-4V + 6.4TiB_2 milled for (a) 0, (b) 3T, (c) 6T, (d) 12T and (e) 18T seconds. Samples were HIPed at 500°C for 2 hours at 150 MPa followed by 900°C for 2 hours at 150 MPa.

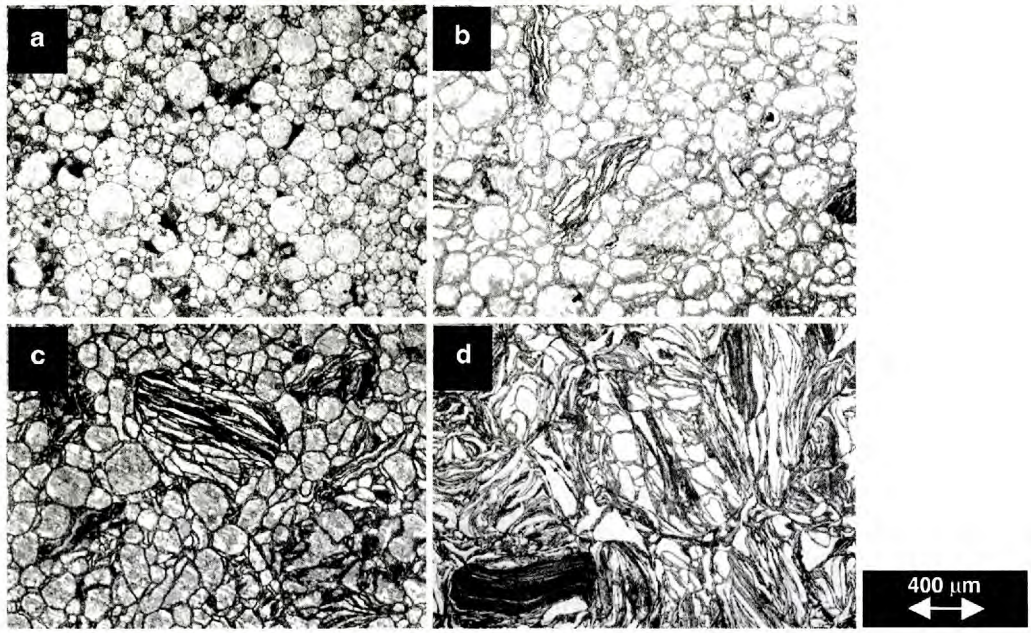


Figure 8-20 Optical micrographs of Ti + 2B milled for (a) 0, (b) 3T, (c) 6T and (d) 12T seconds. Samples were HIPed at 500°C for 2 hours at 150 MPa followed by 900°C for 2 hours at 150 MPa.

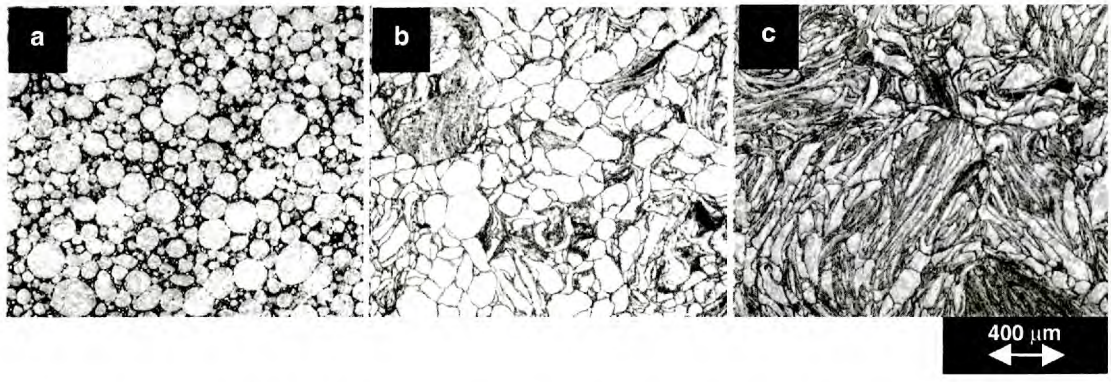


Figure 8-21 Optical micrographs of Ti + 6.4TiB_2 milled for (a) 0, (b) 3T and (c) 6T seconds. Samples were HIPed at 500°C for 2 hours at 150 MPa followed by 900°C for 2 hours at 150 MPa.

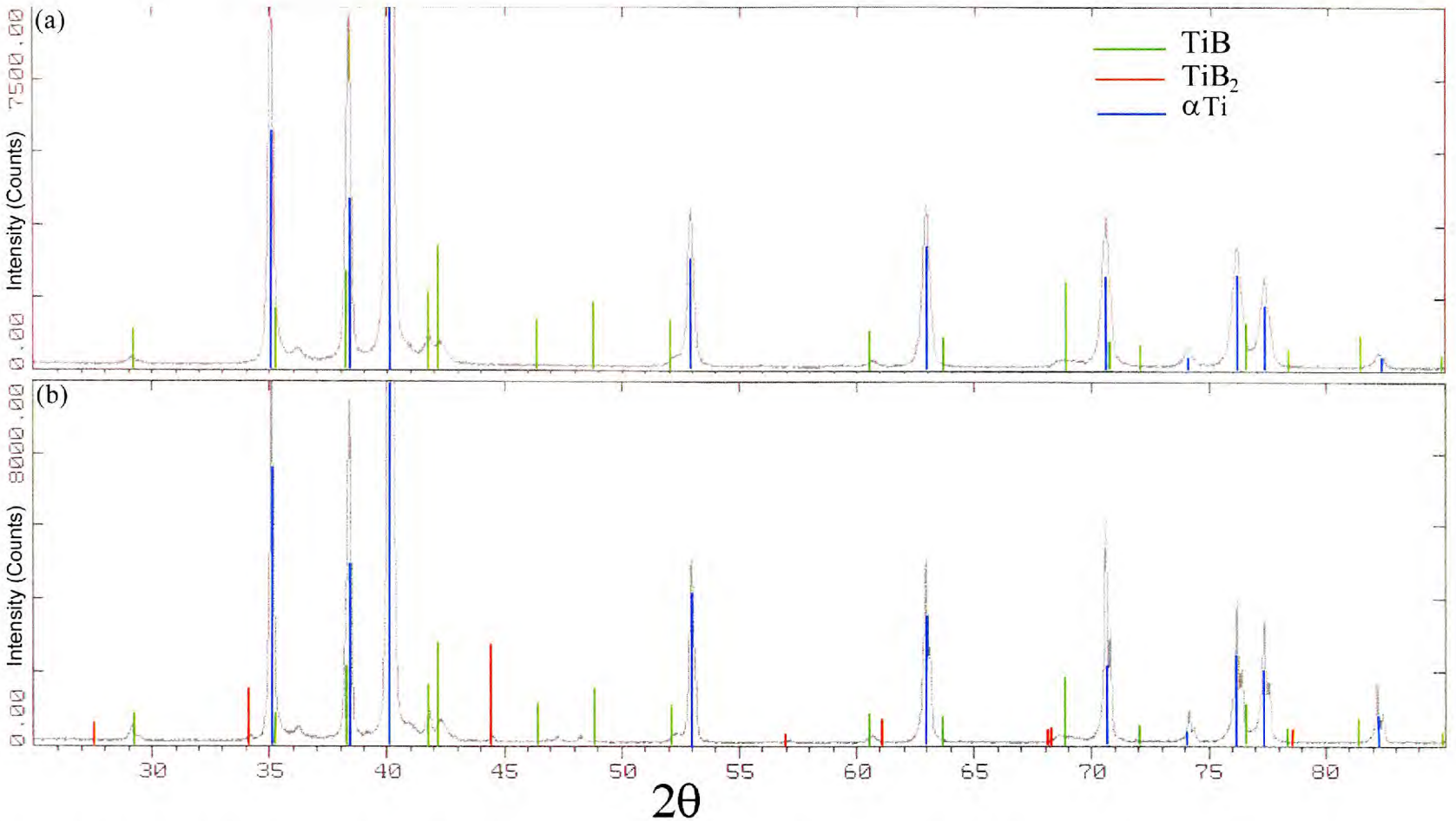


Figure 8-22 XRD of (a) Ti + 2B milled for 12T seconds and (b) Ti + 6.4TiB_2 milled for 6T seconds. Both samples were HIPed at 500°C for 2 hours at 150 MPa followed by 900°C for 2 hours at 150 MPa.

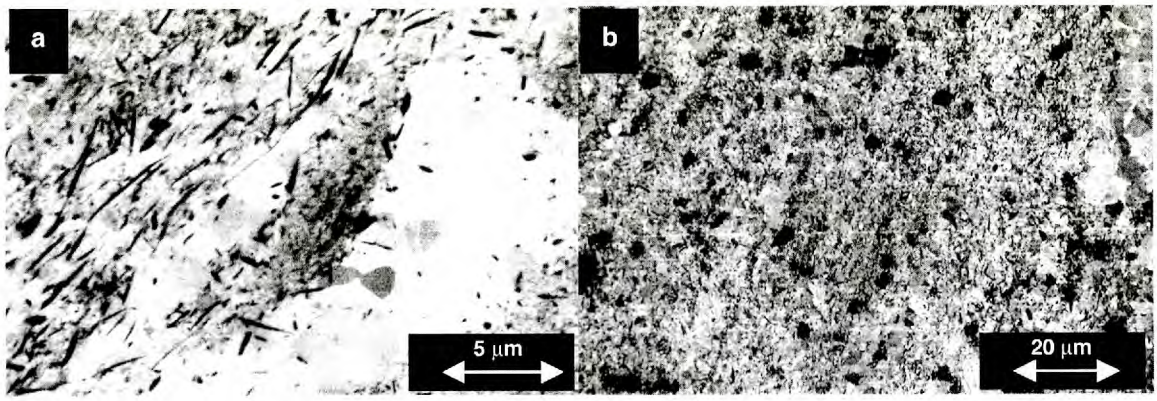


Figure 8-23 A backscattered FEG-SEM micrograph showing (a) Ti-6Al-4V+2B and (b) Ti-6Al-4V+6.4TiB_2. The samples were milled for 18T seconds and HIPed at 500°C for 2 hours at 150 MPa followed by 900°C for 2 hours at 150 MPa.

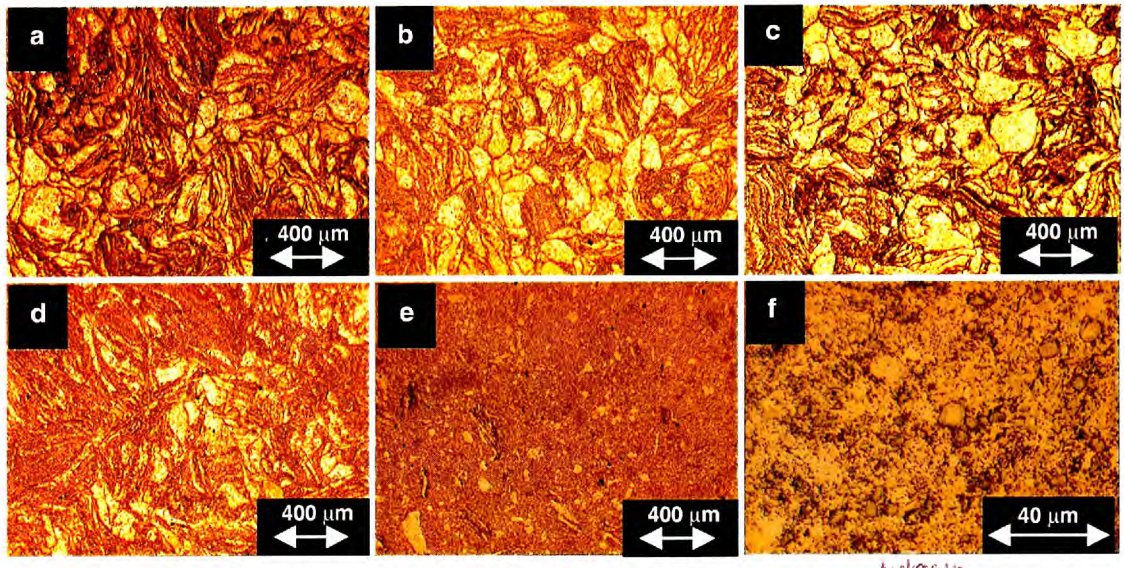


Figure 8-24 Optical micrographs of Ti+6.4TiB_2 with (a) 180 ppm hydrogen and milled for 6T seconds (1 purge for 10 minutes), (b) 220 ppm hydrogen and milled for 6T seconds (2 purges each 30 minutes), (c) 770 ppm hydrogen and milled for 6T seconds (6 purges each 10 minutes) (d) 630 ppm hydrogen and milled for 9T seconds (9 purges each 10 minutes) (e,f) TiH_2+6.4TiB_2 (21000 ppm hydrogen) milled for 18T seconds.

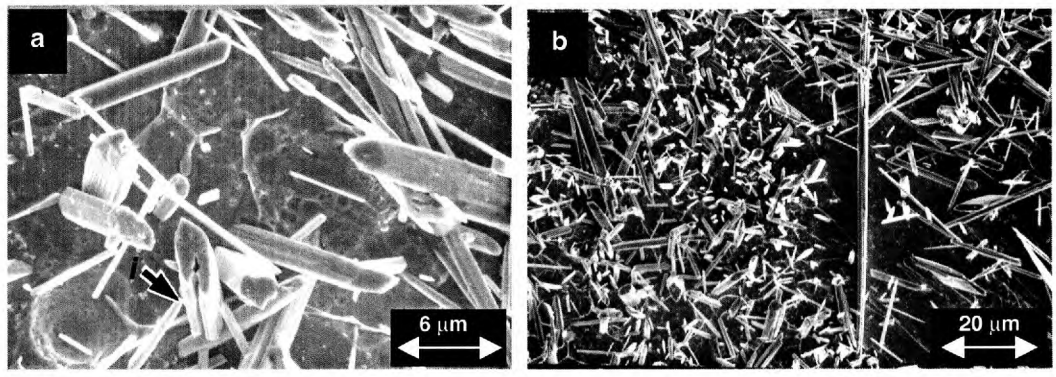


Figure 8-25 SEM images of TiB needles in Ti-6Al-4V + TiB_2 after milling for 18T seconds HIPed at 500°C for 2 hours at 150 MPa followed by 900°C for 2 hours at 150 MPa and heat treated at 1300°C for 8 hours. (a and b) show the range of needle sizes up to 100 μm long with the finest 300 nm in diameter. Where 'i' indicates interconnected TiB particles.

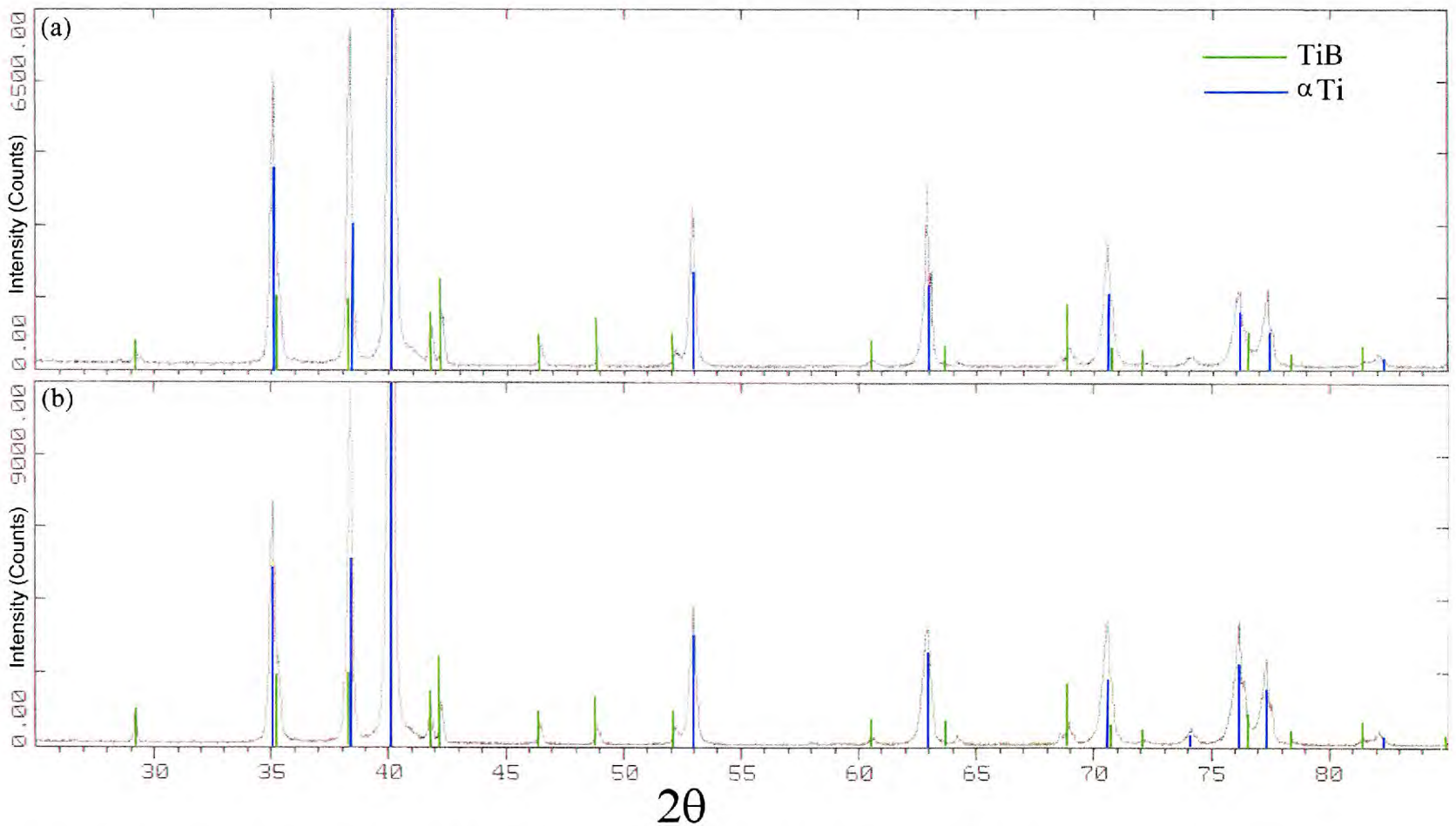


Figure 8-26 XRD of (a) Ti + 2B milled for 12T seconds and (b) Ti + 6.4TiB_2 milled for 6T seconds. Both samples were HIPed at 500°C for 2 hours at 150 MPa followed by 900°C for 2 hours at 150 MPa and heat treated at 1300°C for 8 hours.

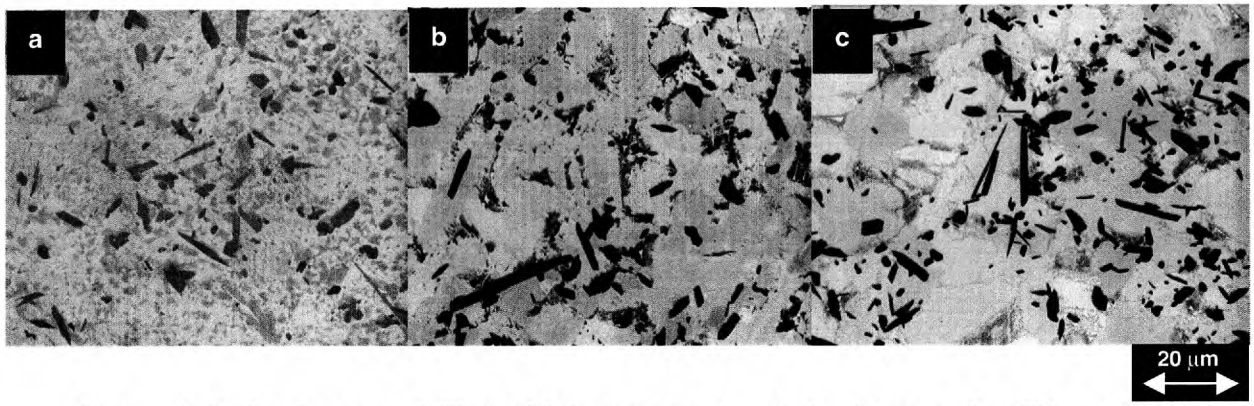


Figure 8-27 Backscattered FEG-SEM micrographs of the increase in TiB needle size with heat treatment temperature in Ti+6.4TiB_2 milled for 6T seconds and HIPed at 500°C for 2 hours at 150MPa followed by 2 hours at 900°C and 150 MPa and heat treated at 1300°C for (a) 8 hours, (b) 20 hours and (c) 100 hours.

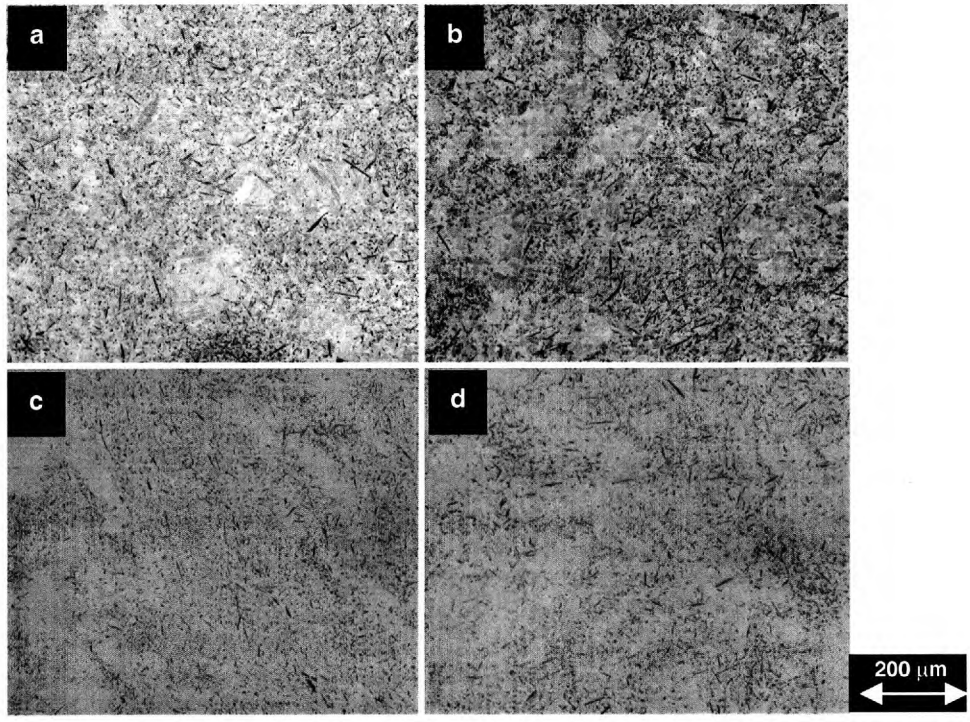


Figure 8-28 A backscattered FEG-SEM micrograph showing (a) Ti-6Al-4V+2B milled for 18T seconds, (b) Ti-6Al-4V+6.4TiB_2 milled for 18T seconds, (c) Ti+2B milled for 12T seconds and (d) Ti+6.4TiB_2 milled for 6T seconds. All samples were HIPed at 500°C for 2 hours followed by 2 hours at 900°C and 150 MPa and heat-treated at 1300°C for 8 hours.

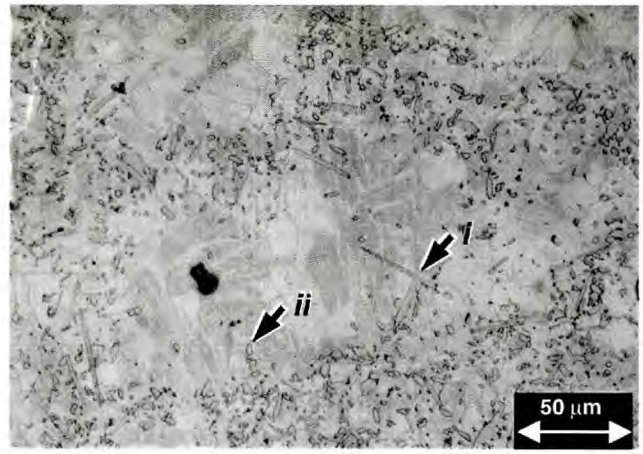


Figure 8-29 An optical micrograph of Ti-6Al-4V+6.4TiB_2 milled for 18T seconds HIPed and heat-treated at 1300°C. TiB needles can be seen penetrating a Ti-6Al-4V powder particle indicated by 'i' and 'ii' indicates particles that appear isolated from the boundary area.

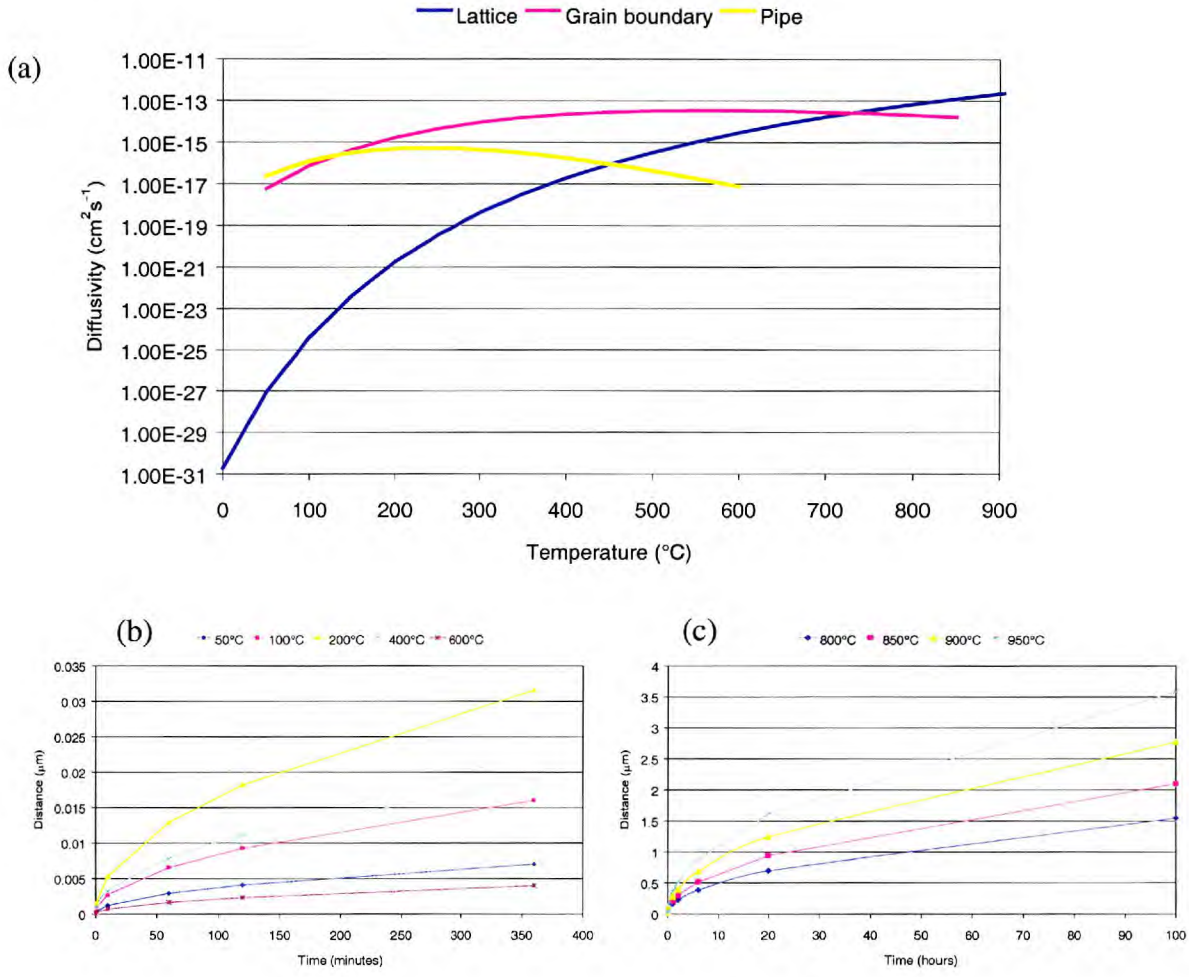


Figure 8-30 Diffusivity of Ti-6Al-4V (a) shows a comparison between predicted values for lattice, pipe and grain boundary diffusion, (b) shows pipe diffusion and (c) shows lattice diffusion.

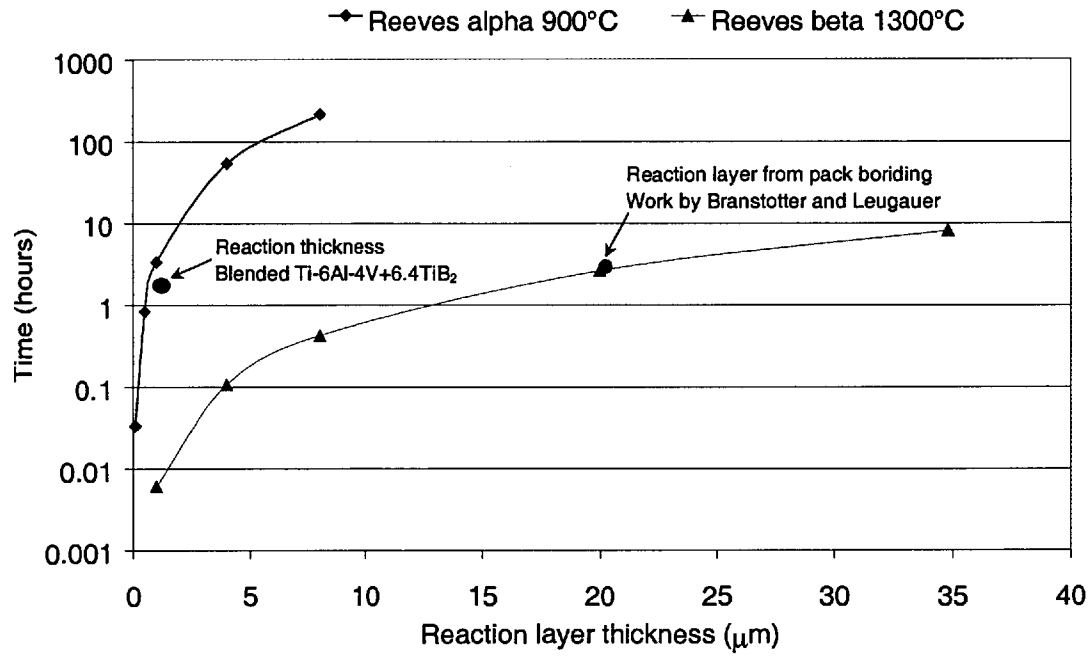


Figure 8-31 The growth of the reaction layer of TiB between TiB_2 and Ti at 900°C and at 1300°C. After Reeves (1992).

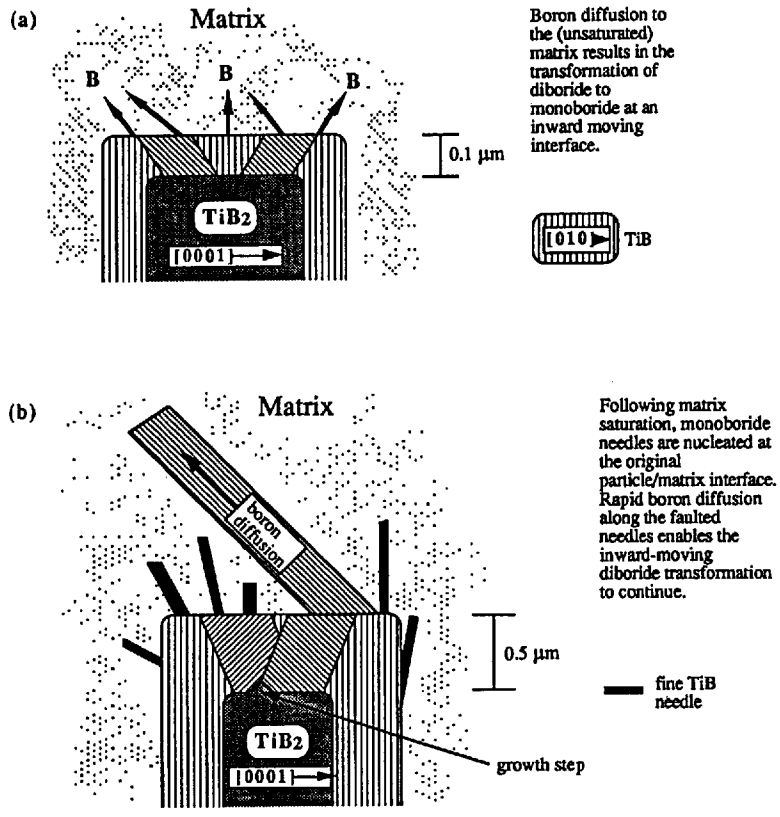


Figure 8-32 A schematic of the growth of TiB from TiB_2 particles in titanium. After Reeves (1992).

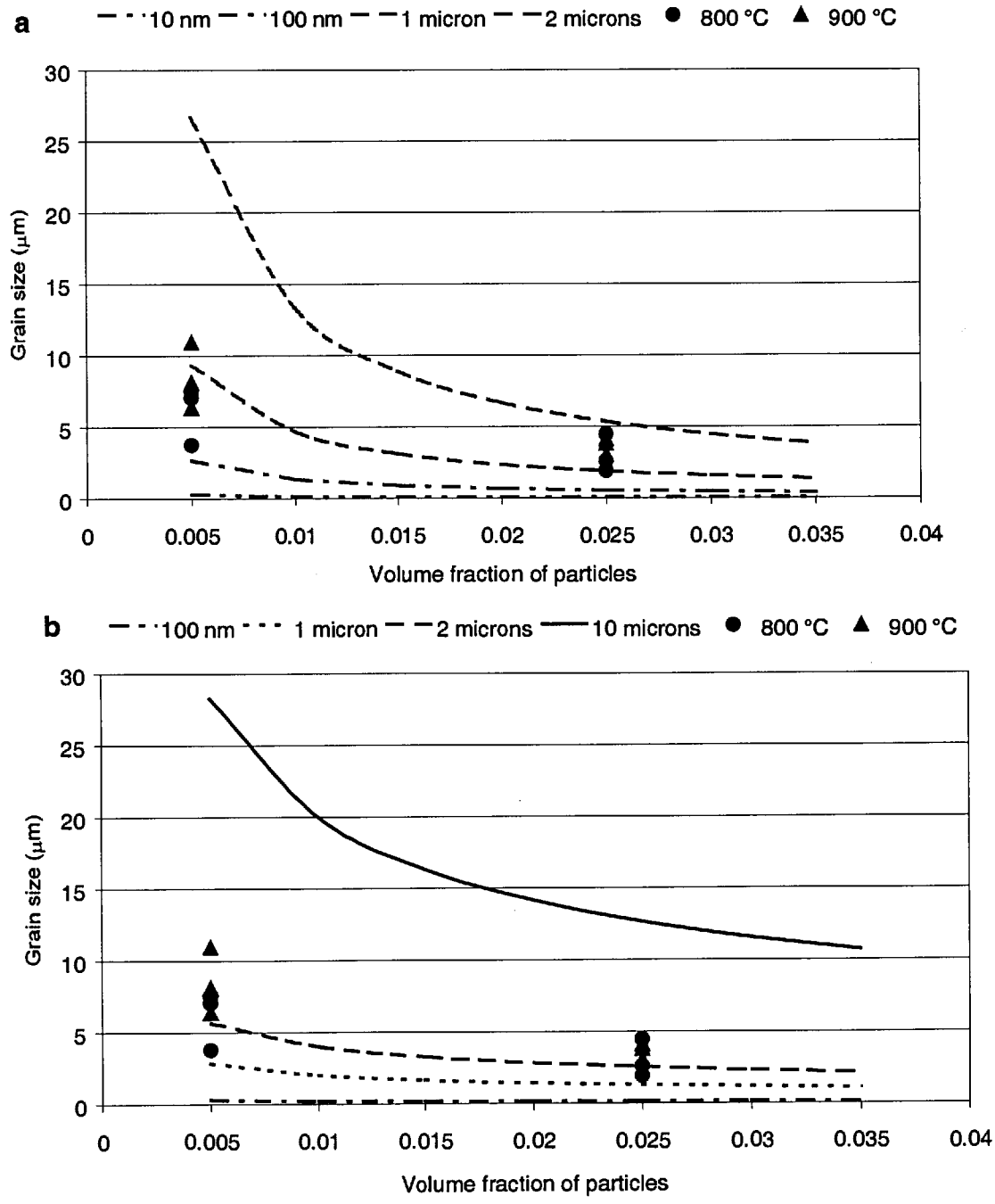


Figure 8-33 The effect of particle size on the grain size of a material given (a) randomly oriented particles and (b) particles located at grain boundaries.

9 ROOM TEMPERATURE TENSILE PROPERTIES OF THE HIPED BILLETS

9.1 Results

The mechanical properties of the as received HIPed powders were determined for comparison with the following consolidated processed powders;

a) milled boron free powders to establish the effect of milling
b) powders blended with boron or TiB_2
c) powders milled with boron or boride

9.1.1 Consolidated as received powder properties

Table 9-1 gives the average room temperature properties of the as received powders. The Ti-6Al-4V has mechanical properties within the range usual for Ti-6Al-4V (Boyer (1994)). There was a decrease in tensile strength with increasing HIPing temperature (from 800 to 900°C) and this was likely to be related to a larger grain size/ lath size associated with higher HIP temperatures. A further reduction in tensile strength was associated with the two stage HIP cycle and was thought to relate to the additional time at temperature. Fractography of the as received gas atomised HIPed Ti-6Al-4V reveals ductile failure (Figure 9-1(a)).

Two forms of titanium powders were assessed; gas atomised Ti and sponge fines (Ti_{sf}). The HIPed billets had a tensile strength of 520 MPa and 560 MPa respectively. The oxygen and nitrogen concentrations of the two powders were 1130 ppm and 120 ppm for gas atomised Ti and 2050 ppm and 110 ppm for Ti_{sf}. The higher level of interstitial contamination in the Ti_{sf} is consistent with the higher tensile strength observed. However, the tensile strength of both the Ti and Ti_{sf} billets was higher than commercial purity titanium with similar oxygen concentrations. For example, ASTM Grade 2 titanium, which has an oxygen concentration of 2500 ppm, nitrogen concentration of 300 ppm and a maximum of 0.3 wt. % Fe, has a tensile strength of 345 MPa and 20% elongation to failure (Boyer (1994)). Oxygen equivalence (Fujii *et al.* (1995)) can be used to enable comparison of titanium billets and this is expressed as:

$$[O]_{eq} = [O] + 2.77\,[N] + 0.086\,[Fe]$$

The oxygen equivalent is 3589 ppm for Grade 2 material and 1501 ppm for gas atomised Ti. Work by Fujii *et al.* (1995) on a modified Ti-Fe-O-N alloy suggests the tensile strength of the Grade 2 Ti and gas atomised Ti to be 700 MPa and 575 MPa respectively. The predicted strength of gas atomised Ti is similar to that measured, however the strength of the Grade 2 Ti is much higher than that typically reported. Clearly the higher iron and interstitial concentrations are usually related to higher strengths, however, developmental alloys such as those assessed by Fujii *et al.* (1995) and produced by powder metallurgy are likely to have different structures, such as finer grain sizes, that result in higher tensile strengths compared with conventional grades. Fractographs of the Ti and Ti_{sf} reveal ductile failure of both samples (Figure 9-1(b)).

Ti-15-3-3-3 is a β alloy and can be heat treated and aged to give a range of tensile properties. The Ti-15-3-3-3 powder in the as-HIPed condition was thought to be similar to Ti-15-3-3-3 in the annealed condition. Annealed Ti-15-3-3-3 typically has a tensile strength of 787 MPa and an elongation of 21.5%. The stiffness varies with heat treatment condition between 80 GPa after solution heat treatment and 105 GPa after ageing (Bania *et al.* (1980)). The Ti-15-3-3-3 HIPed billet had a stiffness within this range. The tensile strength of the Ti-15-3-3-3 HIPed billet was higher than that suggested by Bania *et al.* (1980). The high strength and low ductility are likely to be attributed to the high oxygen and nitrogen concentrations of 7400 ppm and 410 ppm. Typical oxygen and nitrogen concentration for wrought Ti-15-3-3-3 is 1300 ppm and 300 ppm respectively. This Ti-15-3-3-3 powder, although known to have high interstitial contamination, was chosen for its fine powder size to assess the effect of powder size on the blended microstructure.

9.1.2 Consolidated mechanically milled Ti-6Al-4V

The room temperature mechanical properties of the milled Ti-6Al-4V, which were consolidated by HIPing, were assessed to identify the effect of the milling. Unfortunately the Ti powder agglomerated heavily during milling and was therefore unsuitable for HIPing. The Ti-6Al-4V powders, which were milled for 60T seconds, were HIPed at a range of temperatures between 600 and 900°C. The tensile strength of these powders after HIPing in the range of 750°C to 900°C were typical of those observed for wrought Ti-6Al-4V (Table 9-2 and Table 9-3). The ductility was found to increase with HIPing temperature and Figure 9-2a shows ductile failure of milled Ti-6Al-4V that was HIPed at 900°C. Figure 9-3 shows the yield strength as a function

of the grain size. The strength was found to increase with reducing grain size for samples HIPed between 750 and 900°C. However, a rapid decrease in tensile strength was observed at finer grain sizes that resulted from HIPing at 600°C and 700°C. At these temperatures failure was observed along prior powder particle boundaries (Figure 9-2b).

The tensile properties of the Ti-6Al-4V milled for 12 T seconds (Table 9-2) and 60 T seconds (Table 9-3) show similar properties indicating little effect of the milling time on the tensile properties of Ti-6Al-4V. Either complete grain refinement has occurred after 12 T seconds or the subsequent HIPing cycles result in a material with a similar grain size and hence similar mechanical properties.

9.1.3 Consolidated titanium (alloy) powders blended with either boron or TiB_2.

Table 9-4 shows the tensile properties of the titanium (alloy) powders blended with either boron or TiB_2. Figure 9-4 shows the difference between the tensile properties of the titanium blended with either boron or TiB_2 compared to the as received un-reinforced matrices. An increase in stiffness was observed as a result of blending and subsequent HIPing with boron or TiB_2. A reduction in tensile strength was observed when blending Ti-6Al-4V with either boron or TiB_2 compared with gas atomised Ti-6Al-4V. A reduction in tensile strength was also observed when the Ti-15-3-3-3 was blended with TiB_2. Fractography of the blended Ti-6Al-4V or Ti-15-3-3-3 with TiB_2 powders indicated failure along the titanium powder boundaries (Figure 9-5a).

Blending TiB_2 with either Ti_{sf} or Ti powders resulted in an increase in tensile strength and Young's Modulus and a ductility of 2.5% and 1.5% respectively. Blending boron with Ti resulted in a reduction in the strength. Failure of these powders was along the titanium powder boundaries (Figure 9-5b).

9.1.4 The tensile properties of milled and HIPed Ti-6Al-4V+0.5B

The Ti-6Al-4V+0.5B milled for 60 T seconds were HIPed between 600 and 900°C and the tensile properties are shown in Table 9-5 and Figure 9-6. An increase in tensile strength of the Ti-6Al-4V+0.5B compared to the equivalent milled boron free samples when HIPed at 800°C and 900°C was observed. Prior powder particle boundary failure was observed in the test pieces that were HIPed at 600°C and 700°C (Figure 9-7a). Brittle fracture was observed in the samples HIPed at 800°C or higher (Figure 9-7b).

9.1.5 The tensile properties of consolidated and milled Ti-6Al-4V+2B and Ti-6Al-4V+6.4TiB_2

Compared with Ti-6Al-4V milled for 12T seconds, an increase in the stiffness was observed with increasing TiB addition (either when using boron or TiB_2 as a precursor). However, a reduction in the tensile strength was also observed (Figure 9-8, Table 9-6 and Table 9-7). Little or no ductility was observed in Ti-6Al-4V milled with either 2 %B or 6.4 %TiB_2. Failure occurred along prior powder particle boundaries and through the heavily milled, heavily reinforced areas (Figure 9-9). The fracture surfaces of the material shows prior powder particle boundaries on the fracture surface (Figure 9-10).

Heat treatment of consolidated Ti-6Al-4V milled with either boron or TiB_2 at 1300°C for 8 hours improved the tensile properties (Figure 9-11 a and b). A cross section of the test pieces indicated cracking of the TiB needles in the locality of the tensile failure whereas the TiB needles in the head of the test piece remained intact. Figure 9-12 shows the early stage of fracture in Ti-6Al-4V+6.4TiB_2 after heat treatment at 1300°C for 8 hours. The TiB needles that were parallel to the tensile direction were fractured into approximately 14 μm lengths. TiB needles were also observed on the fracture surface of Ti-6Al-4V+2B after heat treatment (Figure 9-13) as well as areas of ductile failure.

9.1.6 The tensile properties of consolidated and milled Ti+2B and Ti+6.4TiB_2

Milling Ti with B or TiB_2 resulted in an improvement in the tensile strength compared with gas atomised Ti powders (Table 9-8 and Figure 9-14 and Figure 9-15), with the exception of Ti+2B milled for 3T seconds. The tensile strength of consolidated Ti+6.4TiB_2 also increased with milling time. Fractography of the tensile samples milled for 3 and 6 T seconds indicated failure along prior powder particle boundaries (Figure 9-16). After longer milling times the fracture surface was less tortuous (Figure 9-17).
Heat treatment of these HIPed billets at 1300°C resulted in a further increase in tensile strength of the Ti powders milled with boron or TiB_2 (Table 9-9 and Figure 9-18). Fractography, as with the Ti-6Al-4V and B or TiB_2, shows boride needles on the fracture surface and areas of ductile failure. The ductility of these samples was approximately 2.5 %.

9.1.7 The effect of the hydrogen on milling of titanium

The milling of Ti+6.4TiB_2 results in an increase in tensile strength and Young's Modulus compared with the as received titanium powder. Increasing the hydrogen content and the milling time resulted in the highest tensile strengths and ductility.

9.1.8 The effect of boron on the stiffness of titanium

The addition of boron, present as TiB and TiB_2 increased the stiffness of titanium (Figure 9-19). In addition to the stiffness measured experimentally, the stiffness of titanium boron alloys predicted by the rule of mixtures (both equal stress and equal strain), and the Eshelby approach (Clyne and Withers (1993)) where the particles have an aspect ratio of 1 and 5 are shown. Predictions using the Eshelby approach (Clyne and Withers (1993)) with an aspect ratio of 1 gave the closest fit to the experimental data.

9.2 Discussion

9.2.1 Quality of the matrices and the effect of HIPing temperature

The strength of the milled Ti-6Al-4V samples HIPed between 750°C to 900°C agree with the Hall-Petch relationship where σ_i = 788 MPa and k = 0.43 MPa $m^{1/2}$ from the equation:

$$\sigma_y = \sigma_o + kd^{-1/2}$$

The effect of grain size on unalloyed titanium has been studied by Jones (1972) and by Wang *et al.* (1993), who have reported Hall-Petch relationships over the grain size range 0.4 to 160 μm and 10 to 50 nm respectively. Unlike the work of Jones (1972) and Wang *et al.* (1993), in this study, the Hall-Petch relationship was not followed at the finer grain sizes. It is thought the low yield strengths observed at the finer grain sizes were related to premature failure along prior powder particle boundaries, as a result of HIPing at 600°C and 700°C, rather than being an effect of the finer grain size (Figure 9-2b). Failure at prior powder particles was thought to be due to poor bonding because of the incomplete dissociation of the oxide layer (Kazakov and Kvasnitsky (1985)) during HIPing.

Limited data is available on the mechanical properties of mechanical milled titanium alloys. Much of the previous work in this area has shown poor mechanical property data due to the contamination of the titanium by oxygen and nitrogen during milling which has led to the formation of titanium-oxy nitrides (Goodwin (1995), Hinder (1995)).

This study carefully controlled the milling atmosphere and consequently interstitial contamination was minimised (§7.2.1) and subsequent mechanical properties are equivalent to those usually observed in conventional Ti-6Al-4V.

9.2.2 The effect of boron or TiB_2 on the blended titanium HIPed powders

Titanium is available in a range of powder forms including those made by plasma rotating electrode process, gas atomisation, hydride dehydride processing and sponge fines produced by the Kroll process. Powders produced by argon gas atomisation were chosen for this study because they were available with low values of interstitial contamination and therefore enabled the greatest flexibility for mechanical milling. A range of powders were blended with either boron or TiB_2 to assess the effect of titanium particle size and morphology on the distribution of the reinforcement.

The tensile strength of the consolidated gas atomised Ti-6Al-4V blended with TiB_2 or boron is reduced compared with the gas atomised Ti-6Al-4V powders (Figure 9-4). Fracture occurred along the boundary of the gas atomised powders where the TiB_2 and boron agglomerates were located. Evidence for this is the spherical nature of the powder particles seen by fractography (Figure 9-5). The greater reduction in tensile strength was observed when blending with boron. §7.2.2 postulates that for a given powder blend the number of boron particles is far higher than the equivalent number of TiB_2 particles. An almost continuous layer of TiB_x can be observed around the gas atomised titanium (Figure 8-7a) and this continuous layer may act as a site for easy crack propagation. In contrast when blending with TiB_2, agglomerated boride particles can be seen (Figure 8-7b). The titanium powders consolidated around the agglomerates. These TiB_2 agglomerates do not bond together during consolidation at 900°C and may also act as sites for initiation of crack propagation. Similar results were observed when comparing the Ti+6.4TiB_2 with Ti+2B. Tensile ductility was also observed in these samples and was likely to be a result of the softer Ti powder allowing more intimate contact and better bonding during HIPing.

9.2.3 The effect of milling on the mechanical properties of the consolidated titanium boron alloys

The poor mechanical properties of the gas atomised powder blends were not unexpected because of the large powder size and poor distribution of the boride particles. Mechanical milling was used with the aim of improving the distribution of the boride

within the titanium matrix. §7.2.3 discusses the effect of milling on the microstructure of the titanium boron alloys. An improvement in the distribution of the TiB_x was observed when milling, however areas free of boride and areas with a high volume fraction of boride were still observed.

Mechanical property data from the milled Ti-6Al-4V with boron or TiB_2 shows there is no improvement in the mechanical properties. Although there was an increase in interstitial contamination with the addition of boron or TiB_2 compared with Ti-6Al-4V (Table 7-2), the poor distribution of the TiB_x was thought to be the main contributor to the low tensile elongation observed. Interstitial contamination usually leads to increased tensile strength along with a reduction in ductility, which was not consistent with the observations in this study, furthermore failure was through heavily reinforced areas (Figure 9-9). Although, milling Ti-6Al-4V with either boron or TiB_2 results in a decrease in tensile strength compared with milled Ti-6Al-4V, the Ti-6Al-4V when milled with TiB_2 had a higher tensile strength compared to the samples milled with boron. There was no clear difference in the fracture surfaces when comparing milling with either boron or TiB_2, however, the size and distribution of the TiB particles may affect the results observed in a manner similar to the results reported when blending with boron or TiB_2 (§9.2.2).

One method to improve the distribution of TiB in titanium was to increase the milling time. Ti-6Al-4V+0.5B was milled for 60T seconds and the combination of longer milling time and lower boron addition (Ti-6Al-4V+0.5B) resulted in low tensile ductility and after HIPing at 800 and 900°C brittle failure was observed (Figure 9-7). However, unlike the samples with higher volume fractions of TiB, an increase in tensile strength was observed (Table 9-5). This strength increase was likely to be a result of the finer grain sizes (Figure 8-13) and dispersion strengthening from fine TiB particles.

Low HIPing temperatures are detrimental to the mechanical properties because of incomplete dissolution of the oxide layers and this has been discussed in §9.2.1. However, this does not account for the lower tensile strength of Ti-6Al-4V+0.5B compared with the equivalent milled Ti-6Al-4V after HIPing at 600°C and 700°C. Additionally, this is inconsistent with the higher tensile strengths observed in Ti-6Al-4V+0.5B compared with milled Ti-6Al-4V after HIPing at higher temperatures (Table 9-3 and Table 9-5). The explanation for the lower strength in the Ti-6Al-4V+0.5B at the lower HIP temperatures may be related to the reaction of the

Ti-6Al-4V+0.5B at the lower HIP temperatures may be related to the reaction of the boron during HIPing. Given that the boron particle size was 1 μm and that to form TiB, boron first reacts to give TiB_2, Figure 9-20 shows the time for a 1 μm TiB_2 particle to fully react to give TiB. Full reaction of the 1 μm particle at 600°C and 700°C would be in excess of 20 hours, whereas at 800°C and 900°C full reaction occurs during HIPing. Boron that was not reacted was probably not bonded with the titanium matrix and therefore acted as a pore. This, together with the poor bonding of the powder particles at the low HIP temperature, resulted in the lower strengths and ductility observed in the Ti-6Al-4V+0.5B compared with the milled Ti-6Al-4V. When HIPing at higher temperatures the boron was likely to be fully reacted and as a consequence the tensile strength was higher than that observed in the un-reinforced matrix. This was commensurate with the fine grain size in the Ti-6Al-4V+0.5B compared with the equivalent Ti-6Al-4V and dispersion strengthening. Dispersion strengthening is usually observed when the particle size was in the range 10-100 nm (Clyne and Withers (1993)).

Additional milling was undertaken using Ti as the matrix and boron or TiB_2 as the precursor to TiB. The Ti was chosen as a softer matrix to counteract the strengthening from fine particles and fine grain size that result from milling and are thought to 'over' strengthen the material and result in brittle fracture (Hinder (1997)). It was thought that over strengthening may be the cause of tensile strengthening and limited ductility in the milled Ti-6Al-4V+0.5B where longer milling time were used.

With the exception of the Ti+2B that was milled for 3T seconds (where poor canning and hence poor consolidation was the likely reason for the anomalous properties) the milling was found to improve the properties of Ti+2B. Yielding and tensile ductility were observed along with evidence of failure through heavily reinforced areas. Although Ti+6.4TiB_2 could not be milled for the same length of time as Ti+2B, because the Ti powders agglomerated heavily (§ 7.2.2), a tensile strength increase of 250 MPa and tensile ductility were observed.

In this study milling improved the distribution of the TiB in the titanium powders however a homogeneous distribution of the TiB was not achieved. All the milled samples, to an extent, had areas that were free of TiB and areas where the TiB was clustered. It was these heavily clustered areas which provided an easy path for crack

propagation because of the close proximity of the particles. This is agreement with work by Lewandowski *et al.* (1989) and Murphy *et al.* (1997) who found that clustered areas were preferred sites for damage initiation and damage accumulation ahead of a propagating crack in aluminium particulate MMCs.

Improvements in mechanical properties of titanium particulate MMCs were observed with the improvement in distribution either through changing the titanium particle size or use of hydrogen and heat treatment. No one mechanism was likely to give rise to the strengthening observed and is probably dependent on the particle size and the distribution in the particle size. The mechanisms involved are:

- particle strengthening (observed in both milled and blended samples with TiB_x where the particle size was >1 μm)
- dispersion strengthening (from fine TiB_x (1-100 nm) observed in all the milled samples)
- the effect of a fine grain size pinned by TiB_x

Further improvements in tensile properties may result from the balance of size of the TiB particles enabling greater load transfer to the particles. The degree of misorientation of TiB needles also affects the tensile properties. Therefore, further improvements in the mechanical properties of these materials are likely by studying the effect of mechanical work/ TiB orientation (Yolton and Moll (1995)) and the effect of heat treatment/ TiB particle size. Figure 9-12 shows the particles cracking to approximately 14 μm lengths, therefore, to minimise fracture of the needles under tensile load the optimum particle length of 14 μm should be achieved to maximise load transfer and minimise particle cracking.

An encouraging result was the improvement in Young's Modulus of the titanium, with the addition of 10 % and 20 % volume fraction TiB, by approximately 25 GPa and 40 GPa respectively. The rule of mixtures stiffness prediction is shown in Figure 9-19 and suggests a higher stiffness should be achieved. Previous work by other authors (Yolton and Moll (1995), Fan *et al.* (1997), Philliber *et al.* (1995), Saito *et al.* (1995b)) have all found that the experimentally measured stiffness values are lower than those predicted by the rule of mixtures. This is unsurprising as the rule of mixtures only works well for parallel continuous fibre reinforced composites when the test direction is parallel to the fibre array and full load transfer can apply. Other prediction methods can be used, such as the shear lag (Taya and Arsenault (1989)) and the Eshelby method

(Clyne and Withers (1993)). The shear lag method assumes fibres oriented in the axis of the applied stress, whereas in this study the needles were randomly oriented. No account is taken in the shear lag method for stress transfer at the fibre ends, therefore predictions of composites, containing fibres with low aspect ratios, as in this study can be poor.

The Eshelby model assumes an ellipsoidal shaped particle whose aspect ratio can be varied from a spherical particle to a unidirectionally reinforced whisker composite. The predictions for an aspect ratio of 1 and 5 are shown in Figure 9-19. An aspect ratio of 1 gives a good approximation for the stiffness of the composite. It is clear from Figure 9-19 however, that spherical TiB particles are not seen in this material. However using an aspect ratio of one is a reasonable first order approximation for randomly oriented fibres. When the 'ideal' distribution of the TiB has been achieved in the matrix the degree of misorientation of the TiB can be quantified and better predictive models employed.

9.3 Summary

The mechanical properties of the matrices can be summarised as follows:

- For Ti-6Al-4V gas atomised powder, HIPing temperature at or above 750°C for 2 hours at 150 MPa is sufficient to give mechanical properties within the range of that expected for Ti-6Al-4V.
- The mechanical properties of the gas atomised Ti-6Al-4V, Ti and Ti_{sf} as received powders were within the range usually expected for these alloys. The HDH Ti-15-3-3-3 has a higher tensile strength than usually expected as a result of the high interstitial contamination.
- Mechanical milling of Ti-6Al-4V for up to 60T seconds was not detrimental to the mechanical properties of Ti-6Al-4V.

The best mechanical properties, giving improved strength and stiffness compared with the un-reinforced matrix were achieved with the best distributions of TiB in the titanium matrix as a result of the following powder processing techniques:

- Using finer titanium powders
- Using hydrogen to enhance the milling process
- Using heat treatment to grow the TiB particle size and reduce the effect of TiB banded regions

Improvements are required in ductility of the titanium (alloy) MMC's and it is suggested that this will be achieved by improving the distribution of TiB within the matrix and identifying the optimum TiB particle size.

Composition	E (GPa)	0.1% PS (MPa)	0.2% PS (MPa)	0.5% PS (MPa)	TS (MPa)	Elongation (%)
Ti-6Al-4V[1]	116.5	964.5	966.0	974.1	1021.1	15.5
Ti-6Al-4V[1]	118.0	950.4	951.2	958.4	1014.8	15.0
Ti-6Al-4V[2]	116.6	912.7	920.0	929.7	994.4	16.0
Ti-6Al-4V[2]	118.3	913.2	919.6	929.3	994.4	14.5
Ti-6Al-4V[3]	117.2	878.4	881.6	888	979	10.5
Ti-15-3-3-3[2]	94	951.1	966.8	994.7	1107.5	3.5
Ti-15-3-3-3[2]	90.5	953.6	969.2	996	1110.1	4.5
Ti_{sf}[2]	100	397.3	414.6	432.2	563.3	17.5
Ti[3]	117.4	366.8	372.8	380.8	520.4	32.5
Ti[3]	109.7	362.8	370.4	381.2	521	28

Table 9-1 The tensile mechanical properties of the gas atomised Ti-6Al-4V, Ti, HDH Ti-15-3-3-3 and Ti_{sf}.

[1] HIPed at 800°C for 2 hours at 150 MPa
[2] HIPed at 900°C for 2 hours at 150 MPa
[3] HIPed at 500°C for 2 hours at 150 MPa followed by 900°C for 2 hours at 150 MPa

Composition	Milling time (T seconds)	E (GPa)	0.1% PS (MPa)	0.2% PS (MPa)	0.5% PS (MPa)	UTS (MPa)	Elongation (%)
Ti-6Al-4V	12	119.1	911.3	910.5	909.7	968.0	17

Table 9-2 The mechanical properties of Ti-6Al-4V that was milled for 12 T seconds and HIPed at 900°C for 2 hours at 150 MPa.

Composition	HIP (°C)	E (GPa)	0.1% PS (MPa)	0.2% PS (MPa)	0.5% PS (MPa)	TS (MPa)	Elongation (%)
Ti-6Al-4V	600	113.5	-	-	-	917.5	0.5
Ti-6Al-4V	600	113.8	-	-	-	1034.9	0
Ti-6Al-4V	700	114.4	1044.4	1045.2	1039.5	1103.9	2
Ti-6Al-4V	700	117.3	1029.6	-	-	1032.8	0.5
Ti-6Al-4V	750	110.2	1114.7	1120.3	1094.6	1140.7	2.5
Ti-6Al-4V	750	111.1	1103.8	1120.1	1101.9	1142.5	2.0
Ti-6Al-4V	800	114.2	1017.5	1028.6	1029.4	1042.0	6
Ti-6Al-4V	800	114.8	1015.9	1027.1	1029.5	1044.6	2.5
Ti-6Al-4V	850	109.6	1017.3	1016.8	1002.4	1053.0	1.5
Ti-6Al-4V	850	109.5	1017.4	1019.0	1003.4	1054.2	6.0
Ti-6Al-4V	900	113.8	910.7	918.7	926.7	970.6	11.5
Ti-6Al-4V	900	112.0	911.1	918.2	925.4	968.5	15.5

Table 9-3 The mechanical properties of Ti-6Al-4V milled for 60 T seconds and HIPed at various temperatures for 2 hours at 150 MPa.

Composition	E (GPa)	0.1% PS (MPa)	0.2% PS (MPa)	0.5% PS (MPa)	TS (MPa)	Elongation (%)
Ti-6Al-4V + 2B[1]	122.8	-	-	-	573.0	0
Ti-6Al-4V + $6.4TiB_2$[1]	134.3	-	-	-	790.0	0
Ti + 2B[1]	126.2	412.6	429.3	448.4	513.6	0.5
Ti + 2B[1]	120.0	415.3	430.7	451.3	513.1	1.5
Ti + $6.4TiB_2$[1]	131.8	478.7	494.6	516.7	619.1	2.5
Ti_{sf} + $6.4TiB_2$[2]	125.4	539.0	594.7	594.0	692.4	2.5
Ti_{sf} + $6.4TiB_2$[2]	128.3	558.5	577.0	604.8	693.6	2.5
Ti-15-3-3-3 + $6.4TiB_2$[2]	113.6	-	-	-	1023.5	0

Table 9-4 The tensile mechanical properties of the blended titanium and titanium alloys with boron or titanium boride

[1] HIPed at 500°C for 2 hours at 150 MPa followed by 900°C for 2 hours at 150 MPa
[2] HIPed at 900°C for 2 hours at 150 MPa

Composition	HIP (°C)	E (GPa)	0.1% PS (MPa)	0.2% PS (MPa)	0.5% PS (MPa)	UTS (MPa)	Elongation (%)
Ti-6Al-4V + 0.5B	600	119.0	-	-	-	563.3	0
Ti-6Al-4V + 0.5B	700	118.8	-	-	-	834.1	0.5
Ti-6Al-4V + 0.5B	700	118.9	-	-	-	843.7	0.5
Ti-6Al-4V + 0.5B	800	117.2	-	-	-	1034.8	0
Ti-6Al-4V + 0.5B	800	117.5	1162.1	-	-	1180.9	0.5
Ti-6Al-4V + 0.5B	900	116.2	1068.6	1084.3	1093.0	1099.3	1.0
Ti-6Al-4V + 0.5B	900	118.7	1066.3	1083.7	1094.7	1102.6	1.0

Table 9-5 The mechanical properties of Ti-6Al-4V + 0.5%B milled for 60 T seconds and HIPed at various temperatures for 2 hours at 150 MPa.

Composition	Milling time (T seconds)	E (GPa)	0.1% PS (MPa)	0.2% PS (MPa)	0.5% PS (MPa)	TS (MPa)	Elongation (%)
Ti-6Al-4V + 2B	3	134.0	-	-	-	622.3	0
Ti-6Al-4V + 2B	3	133.5	-	-	-	599.0	0
Ti-6Al-4V + 2B	6	136.8	-	-	-	675.3	0
Ti-6Al-4V + 2B	6	132.1	-	-	-	648.6	0
Ti-6Al-4V + 2B	12	132.0	-	-	-	629.6	0
Ti-6Al-4V + 2B	12	134.6	-	-	-	483.5	0.5
Ti-6Al-4V + 2B	18	136.8	-	-	-	690.7	0
Ti-6Al-4V + 2B	18	138.9	-	-	-	602.4	0
Ti-6Al-4V + 4B	12	151.2	-	-	-	433.3	0
Ti-6Al-4V + 4B	12	158.5	-	-	-	463.7	0
Ti-6Al-4V + 6.4TiB_2	3	126.4	-	-	-	793.4	0
Ti-6Al-4V + 6.4TiB_2	3	130.6	-	-	-	854.2	0
Ti-6Al-4V + 6.4TiB_2	6	135.0	-	-	-	791.0	0
Ti-6Al-4V + 6.4TiB_2	6	135.6	-	-	-	732.2	0
Ti-6Al-4V + 6.4TiB_2	12	136.4	-	-	-	778.0	0.5
Ti-6Al-4V + 6.4TiB_2	12	134.5	-	-	-	765.7	0
Ti-6Al-4V + 6.4 TiB_2	18	137.0	-	-	-	739.6	0
Ti-6Al-4V + 6.4TiB_2	18	133.7	-	-	-	799.7	0
Ti-6Al-4V +12.8TiB_2	12	150.2	-	-	-	616.6	0
Ti-6Al-4V +12.8TiB_2	12	147.7	-	-	-	685.5	0

Table 9-6 The tensile mechanical properties of Ti-6Al-4V with boron and titanium boride HIPed at 500 °C for 2 hours at 150 MPa followed by 900°C for 2 hours at 150 MPa.

Composition	Milling time (T seconds)	E (GPa)	0.1% PS (MPa)	0.2% PS (MPa)	0.5% PS (MPa)	TS (MPa)	Elongation (%)
Ti-6Al-4V + 2B	3	129.9	987.7	1023.5	-	1032.8	2
Ti-6Al-4V + 2B	3	133.8	975.7	-	-	1016.4	0.5
Ti-6Al-4V + 2B	18	134.8	969.0	1004.1	-	1047.1	0.5
Ti-6Al-4V+6.4TiB_2	3	126.8	893.9	922.9	962.8	1042.8	0.5
Ti-6Al-4V+6.4TiB_2	3	129.7	909.5	936.4	973.0	1046.0	0.5
Ti-6Al-4V+6.4TiB_2	18	132.6	960.1	996.8	1051.1	1052.1	0.5
Ti-6Al-4V+6.4TiB_2	18	134.1	964.3	1001.9	1056.0	1132.5	0.5

Table 9-7 The tensile mechanical properties of the Ti-6Al-4V milled with either boron or titanium diboride HIPed at 500°C for 2 hours at 150 MPa followed by 900°C for 2 hours at 150 MPa and heat treatment at 1300°C for 8 hours in argon.

Composition	Milling time (T seconds)	E (GPa)	0.1% PS (MPa)	0.2% PS (MPa)	0.5% PS (MPa)	TS (MPa)	Elongation (%)
Ti + 2B	3	130.8	-	-	-	272.9	0
Ti + 2B	3	127.9	-	-	-	242.5	0
Ti + 2B	6	130.2	-	-	-	586.5	0
Ti + 2B	6	131.5	-	-	-	644.5	0
Ti + 2B	12	132.0	-	-	-	611.4	0
Ti + 2B	12	131.3	-	-	-	617.8	0
Ti + 4B	12	146.9	-	-	-	537.1	0
Ti + 4B	12	144.4	-	-	-	478.1	0
Ti + 6.4 TiB_2	3	132.8	569.3	601.5	-	631.4	0.5
Ti + 6.4 TiB_2	3	131.2	598.5	629.1	674.8	675.4	2
Ti + 6.4 TiB_2	6	128.7	623.1	656.8	700.5	778.3	0.5
Ti + 6.4 TiB_2	6	132.4	621.6	654.2	698.2	798.8	1
Ti + 12.8 TiB_2	6	144.3	-	-	-	540.0	0
Ti + 12.8 TiB_2	6	149.2	-	-	-	620.3	0
Ti + 12.8 TiB_2	12	155.2	-	-	-	734.0	0
Ti + 12.8 TiB_2	12	156.0	-	-	-	705.6	0

Table 9-8 The tensile mechanical properties of Ti with boron and titanium boride HIPed at 500 °C for 2 hours at 150 MPa followed by 900°C for 2 hours at 150 MPa.

Composition	Milling time (T seconds)	E (GPa)	0.1% PS (MPa)	0.2% PS (MPa)	0.5% PS (MPa)	TS (MPa)	Elongation (%)
Ti + 2B	3	117	-	-	-	450.2	0
Ti + 2B	12	128.3	586.9	612.5	653.8	778.5	1.5
Ti + 2B	12	127.9	591.9	617.1	657.8	791.4	2
Ti + 6.4 TiB_2	3	128.8	588.9	616.1	652.0	758.9	1.5
Ti + 6.4 TiB_2	3	126.6	592.4	620.6	659.6	769.0	2
Ti + 6.4 TiB_2	6	131.4	599.6	630.1	673.2	805.6	2.5
Ti + 6.4 TiB_2	6	131.4	600.6	628.9	669.7	803.9	2.5

Table 9-9 The tensile mechanical properties of the Ti milled with either boron or titanium diboride HIPed at 500°C for 2 hours at 150 MPa followed by 900°C for 2 hours at 150MPa and heat treatment at 1300°C for 8 hours in argon.

Hydrogen (ppm)	Milling time (T seconds)	E (GPa)	0.1% PS (MPa)	0.2% PS (MPa)	0.5% PS (MPa)	UTS (MPa)	Elongation (%)
180	6	129.9	661.1	692.5	736.4	797.0	0.5
		132.4	667.9	694.2	736.4	813.0	0.5
220	12	134.6	688.7	722.3	773.0	885.2	1.0
		132.8	647.0	682.2	733.8	877.6	1.0
770	6	138.6	659.2	698.6	754.0	840.1	0.5
630	9	132.9	659.7	688.7	734.9	837.9	1.0
		137.9	655.3	686.9	733.7	783.5	0.5

Table 9-10 Tensile properties of Ti+6.4TiB_2 milled with a hydrogen atmosphere.

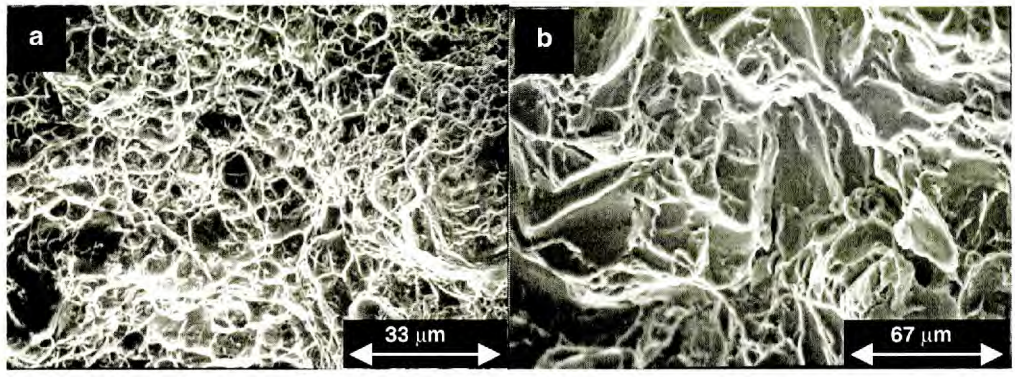


Figure 9-1 Fractographs of the gas atomised a) Ti-6Al-4V and b) Ti after HIPing at 500°C for 2 hours at 150MPa, followed by 900°C for 2 hours at 150 MPa.

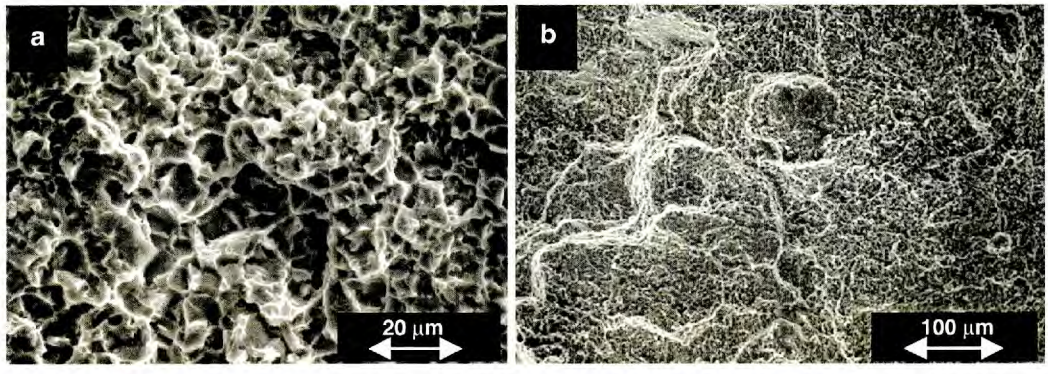


Figure 9-2 Fractography shows (a)ductile failure of the milled Ti-6Al-4V 60T seconds and HIPed at 900°C for 2 hours at 150 MPa and (b) prior powder particle powder boundary failure after HIPing at 700°C for 2 hours at 150 MPa.

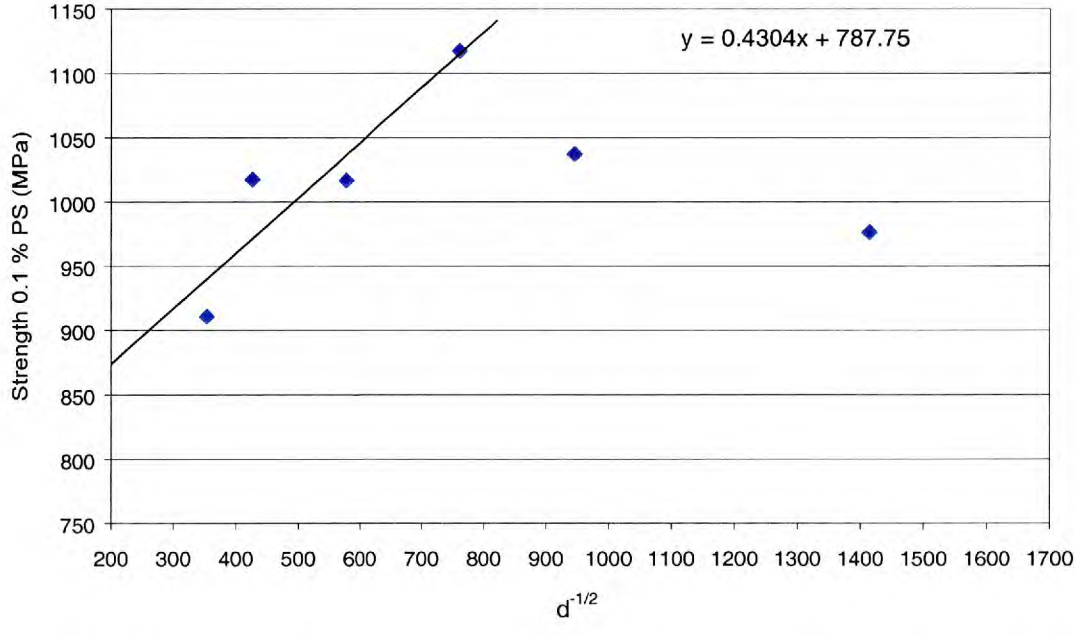


Figure 9-3 Shows the effect of grain size on the yield strength of Ti-6Al-4V milled for 60T seconds.

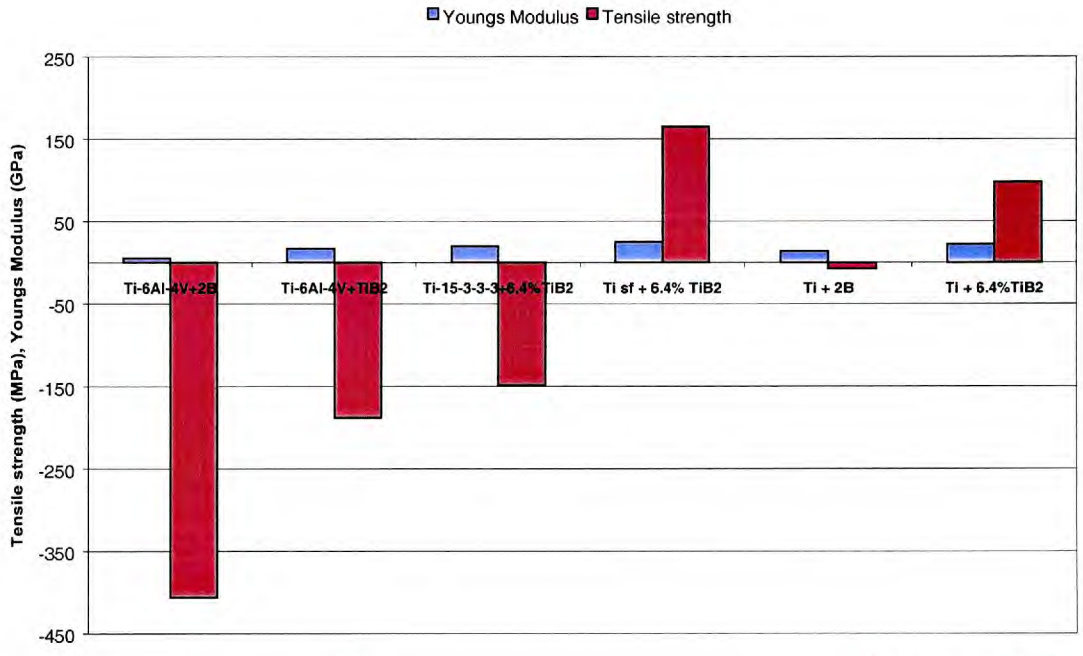


Figure 9-4 The mechanical properties of the blended powders after HIPing.

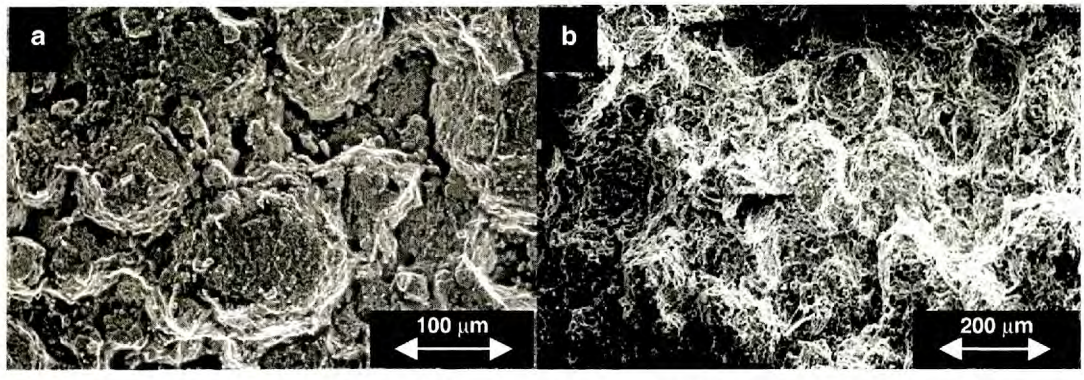


Figure 9-5 Fractographs of the a) the gas atomised Ti-6Al-4V + B blend and (b) Ti + 2B.

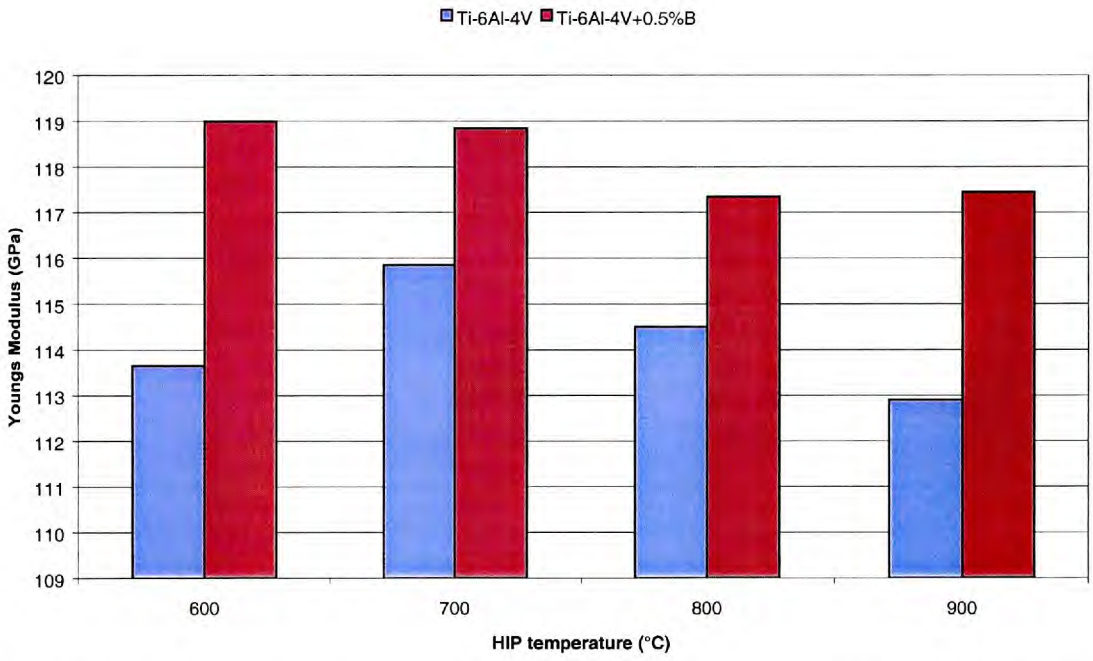


Figure 9-6 The tensile properties of Ti-6Al-4V+0.5B milled for 60T seconds and HIPed at temperatures between 600°C and 900°C.

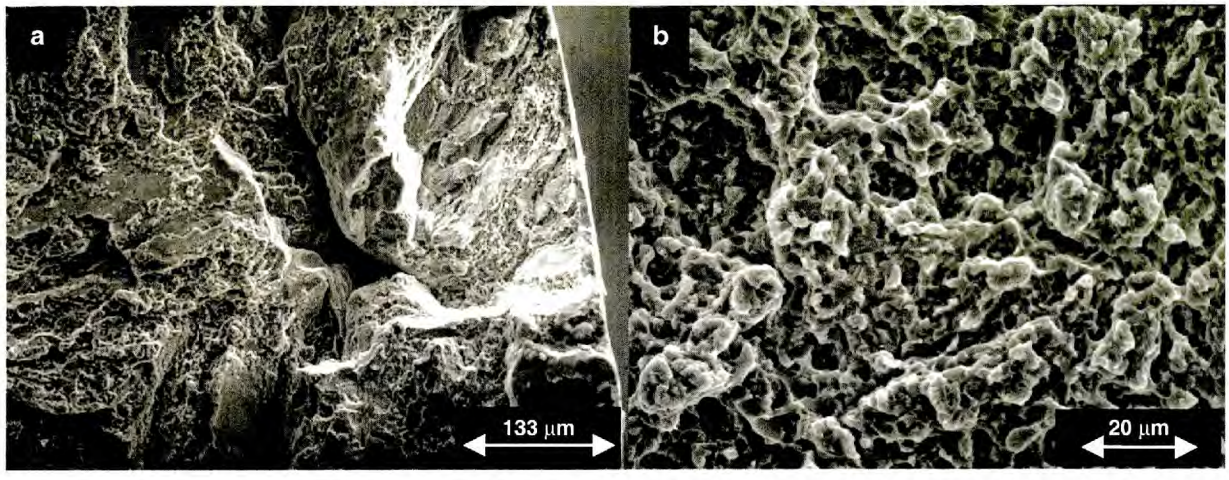


Figure 9-7 (a) shows prior powder particle boundary failure in Ti-6Al-4V+0.5B milled for 60T seconds and HIPed at 700°C and (b) shows brittle fracture in Ti-6Al-4V+0.5B HIPed at 900°C.

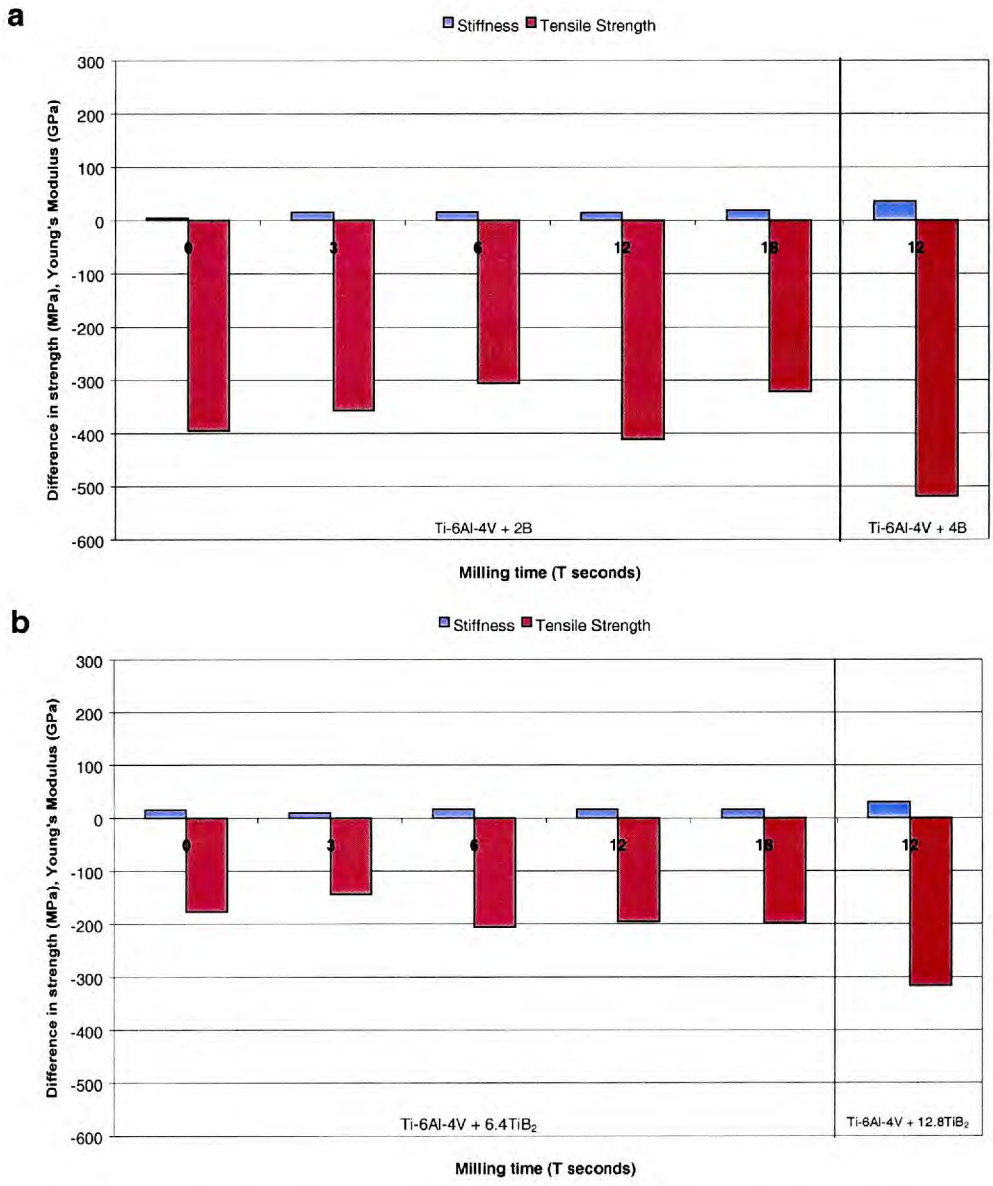


Figure 9-8 The difference in mechanical properties between (a) the Ti-6Al-4V + B milled for various times and (b) the Ti-6Al-4V + TiB_2 milled for various times with Ti-6Al-4V milled for 12T seconds.



Figure 9-9 An optical micrograph of Ti-6Al-4V+2B showing failure of the sample through regions that are heavily reinforced with TiB.

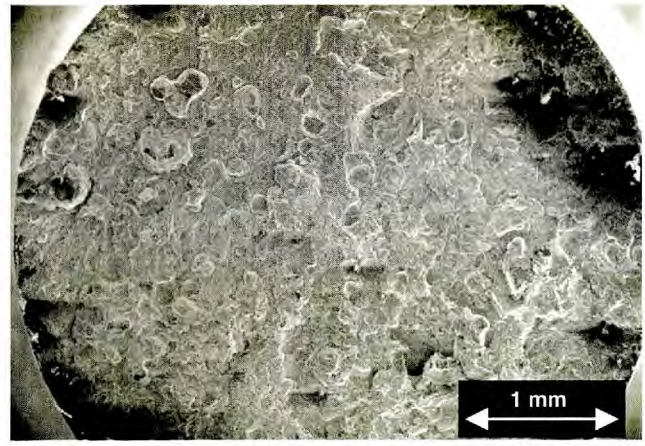


Figure 9-10 A scanning electron micrograph of Ti-6Al-4V + 6.4TiB_2 milled for 12 T seconds and HIPed. The fracture surface shows evidence of failure along prior powder particle boundaries.

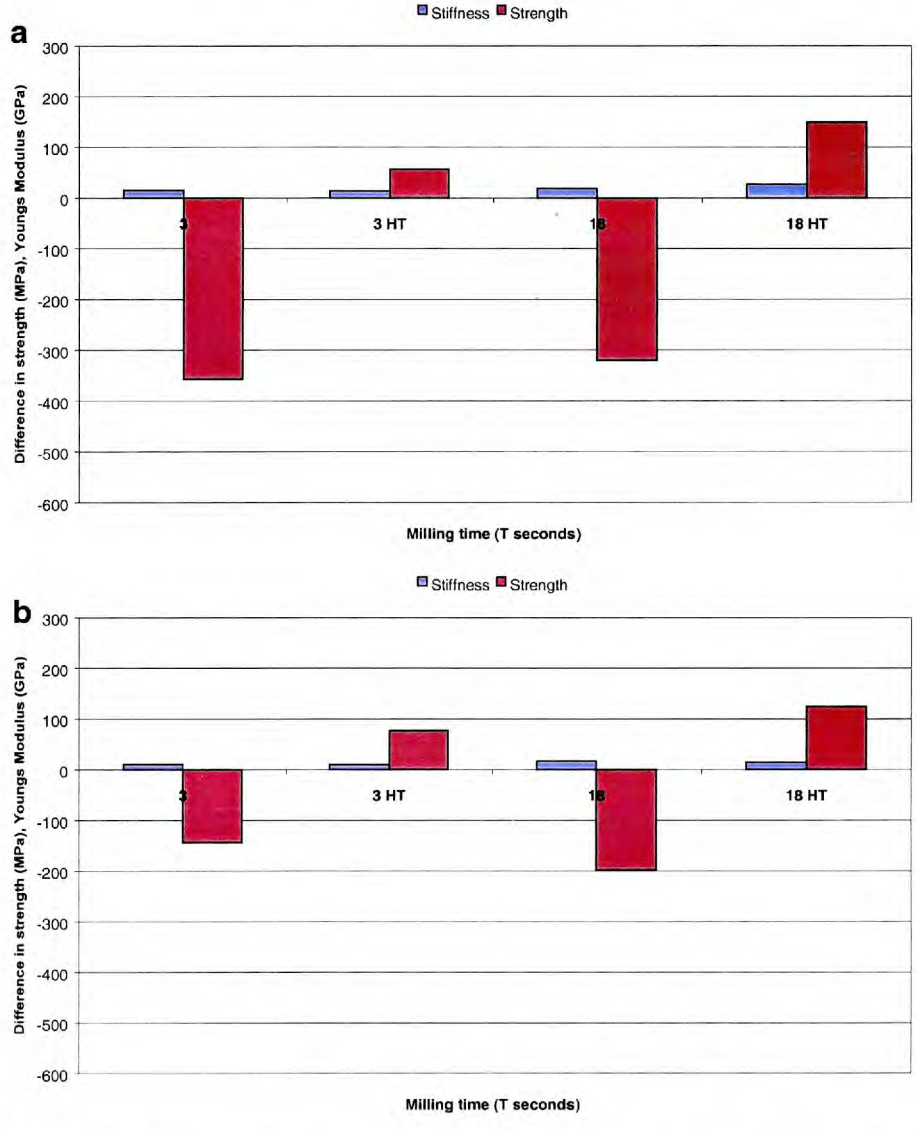


Figure 9-11 The difference in room temperature tensile properties between milled Ti-6Al-4V and the (a) Ti-6Al-4V + 2B and (b) Ti-6Al-4V + 6.4 TiB_2 HIPed and heat treated at 1300°C.

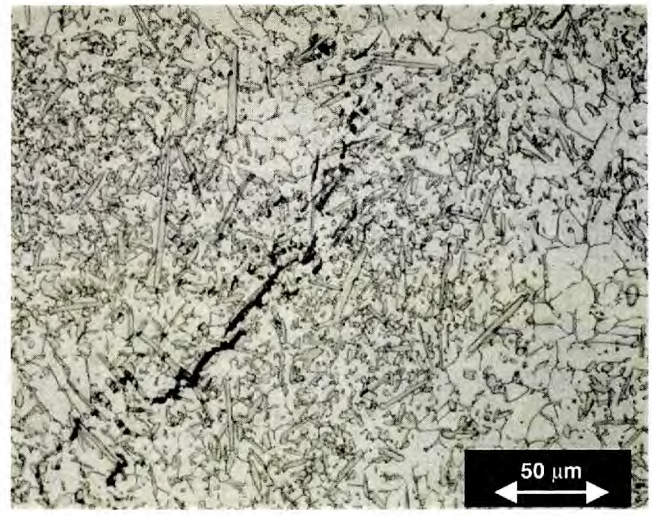


Figure 9-12 An optical micrograph shows the early stages of fracture in Ti-6Al-4V + 6.4TiB_2 that was heat treated at 1300°C for 8 hours prior to tensile testing.

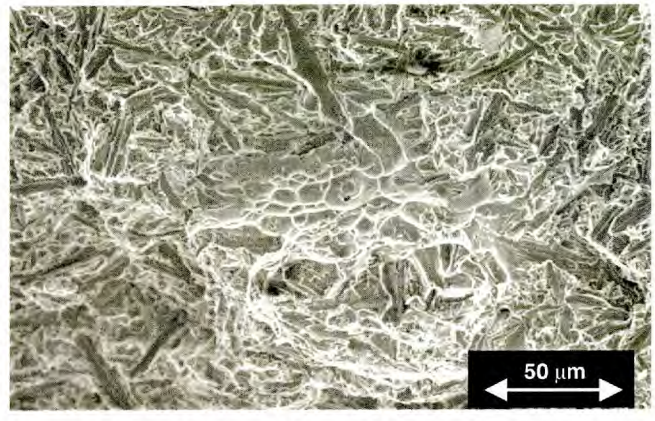


Figure 9-13 Scanning electron micrograph of Ti-6Al-4V + 2B after heat treating at 1300°C for 8 hours. TiB needles can be seen on the surface of the fracture along with ductile areas.

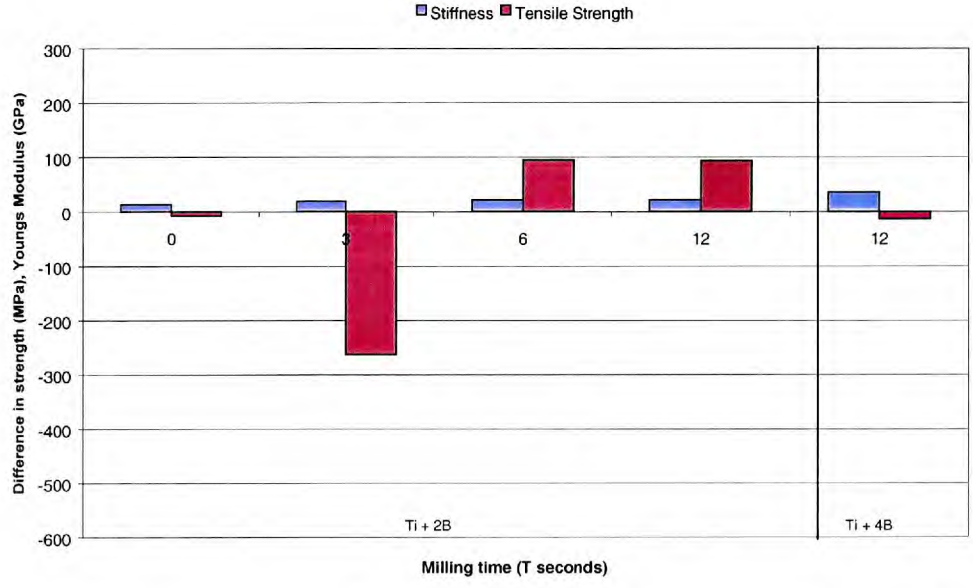


Figure 9-14 The difference in mechanical properties of gas atomised Ti and Ti+B after milling at different times can be seen.

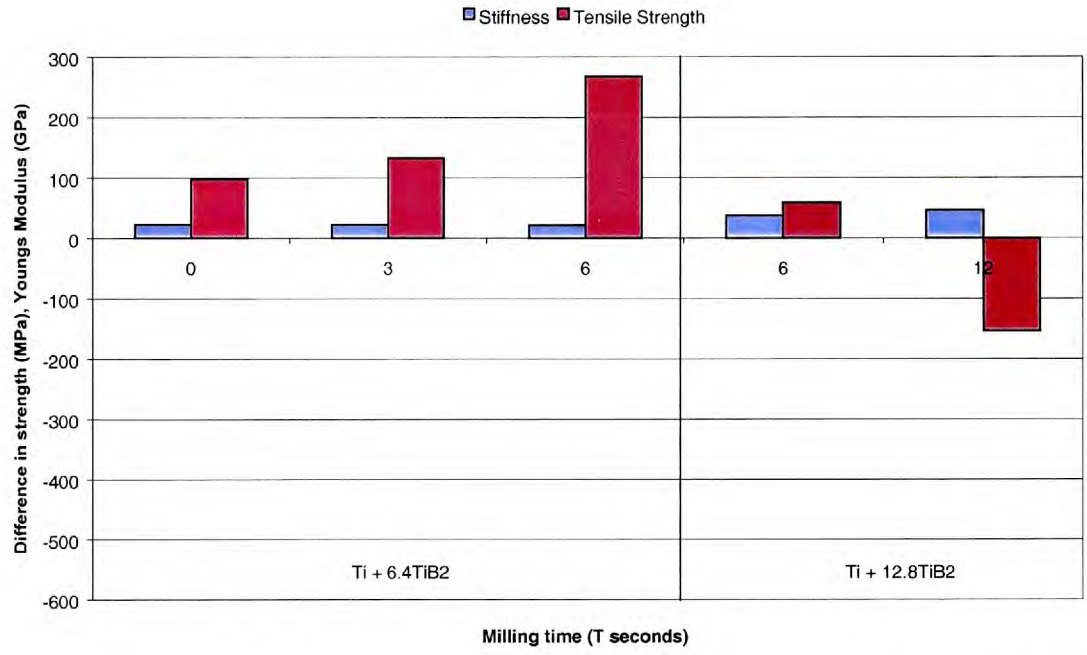


Figure 9-15 The difference in mechanical properties of the gas atomised Ti and Ti+TiB_2 after various milling times can be seen.

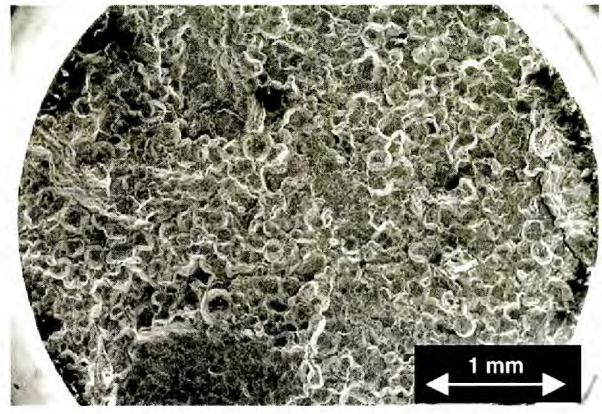


Figure 9-16 Prior powder particle boundary failure are observed in Ti+2B when milled 3 T seconds.

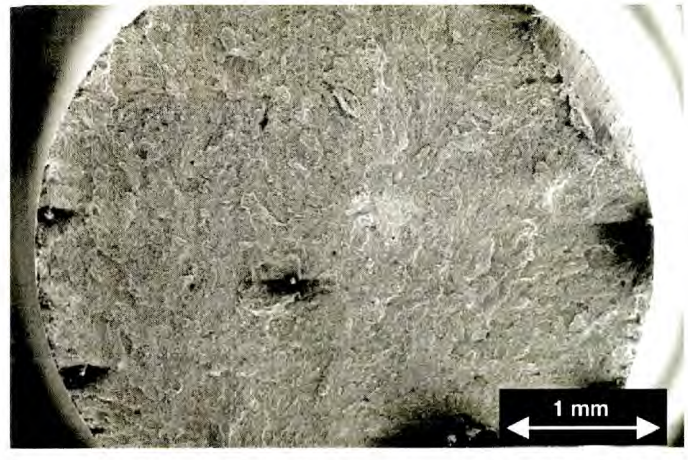


Figure 9-17 The fracture surface of the Ti+2B when milled for 12T seconds is much flatter.

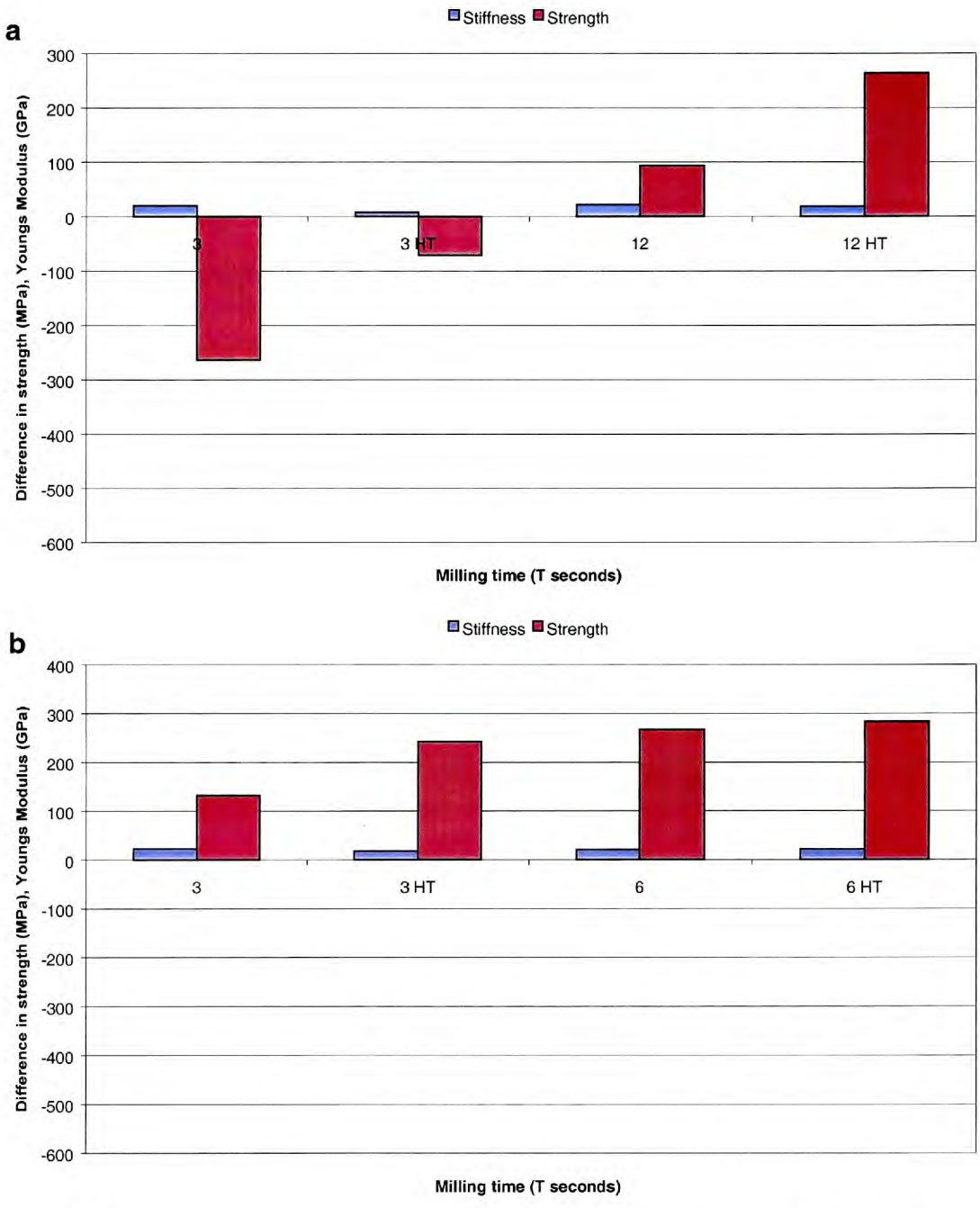


Figure 9-18 The tensile mechanical properties of the (a) Ti+2B and (b) Ti+6.4TiB_2 compared with the gas atomised Ti can be seen in comparison with the samples heat treated at 1300°C for 8 hours.

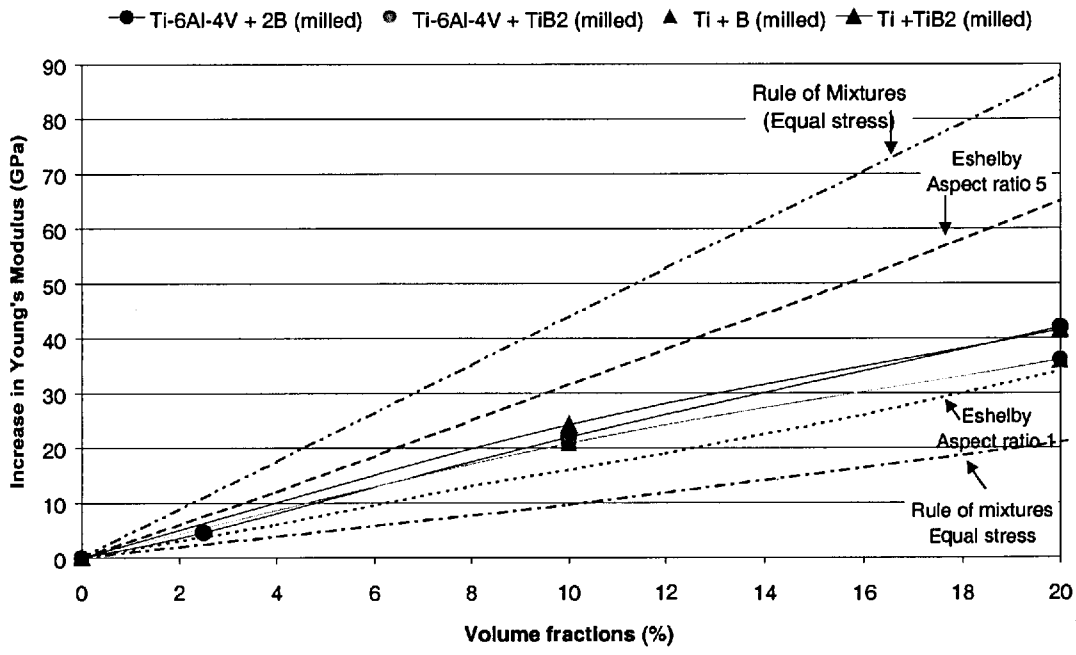


Figure 9-19 The stiffness of Ti, Ti_{sf}, Ti-6Al-4V and Ti-15-3-3-3 can be seen to increase with increasing volume fraction of TiB.

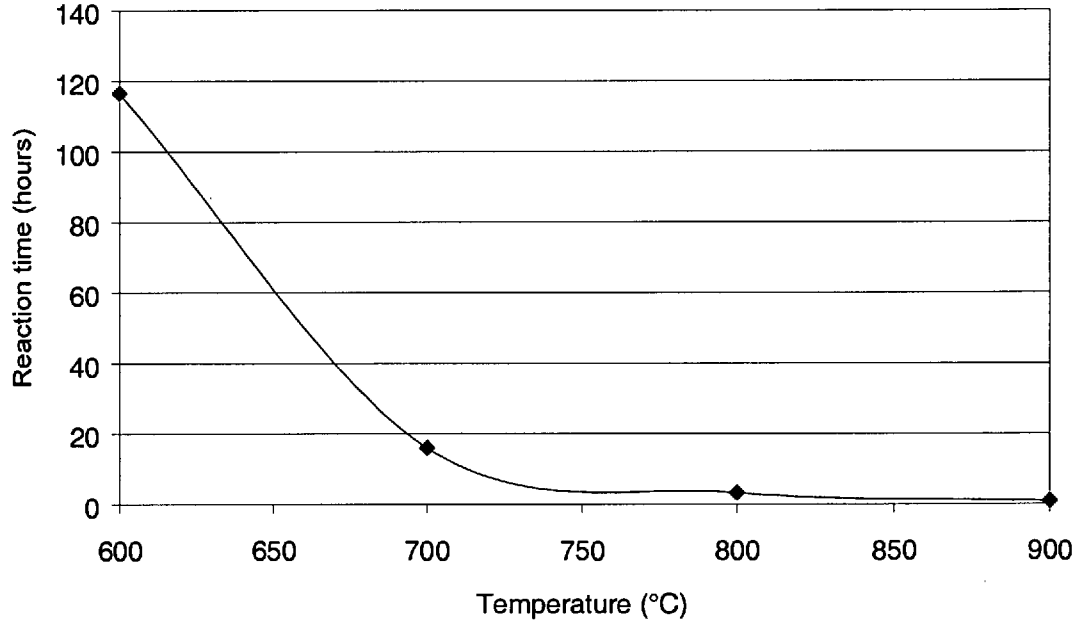


Figure 9-20 The time for a 1 μm boron particle to react fully to form TiB. Data calculated using data from Reeves (1992) detailed in §8.2.2.1

10 HOT TENSILE PROPERTIES OF MECHANICAL MILLED Ti-6Al-4V AND Ti-6Al-4V+0.5B BILLETS IN COMPARISON WITH CONVENTIONAL Ti-6Al-4V.

10.1 Results

The superplastic properties of the conventional Ti-6Al-4V were assessed for comparison with the powder metallurgy samples. Superplastic forming of the conventional Ti-6Al-4V shows the highest elongation to failure and lowest flow stresses when the material was tested at 900°C and a strain rate of 6×10^{-4} s^{-1} (Figure 10-1 a and b). Trials were undertaken to assess the effect of gas atomisation, milling and a fine dispersion of TiB on the superplastic properties of Ti-6Al-4V. These trials were only undertaken on the Ti-6Al-4V+0.5B that had been milled for 60T seconds, where a fine distribution of TiB was achieved in Ti-6Al-4V and few unprocessed areas were observed.

Superplastic forming of the Ti-6Al-4V gas atomised powder resulted in lower tensile elongations to failure ~~compared to~~ than the conventional Ti-6Al-4V (Figure 10-2). The flow stress of the gas atomised powders was similar to conventional Ti-6Al-4V when testing at 900°C at a strain rate of $6x10^{-4}s^{-1}$, however it was much higher when testing at 800°C (Figure 10-3). The cross section of the gas atomised tested samples showed an equiaxed α microstructure and cavitation (Figure 10-4).

The mechanical milled Ti-6Al-4V had a lower elongation to failure than both the conventional and gas atomised Ti-6Al-4V (Figure 10-2). The general observations when testing Ti-6Al-4V that had been milled for 60 T seconds and consolidated were as follows:

1. The optimum HIPing temperature for the milled Ti-6Al-4V for superplastic forming was found to be 750°C and the optimum superplastic forming conditions was found to be at 900°C and a strain rate of $6 \times 10^{-4}s^{-1}$ (Figure 10-5a).
2. Increasing the HIP temperature increased the flow stress when testing at 900°C and a strain rate of $6x10^{-4}s^{-1}$(Figure 10-5b).
3. Reducing the test temperature from 900°C reduced the total elongation to failure (Figure 10-6) and increased the flow stress of the material (Figure 10-3).
4. Increasing the strain rate at which milled Ti-6Al-4V was deformed reduced the

tensile elongation and increased the flow stress (Figure 10-7)

There were few exceptions to these general observations, however when milled Ti-6Al-4V was HIPed at 700°C (the lowest temperature tested) it had a high flow stress, similar to the sample HIPed at 900°C, whereas the general trend shows reducing flow stress with reducing HIP temperature. Reasons for this observation are discussed in § 10.2.5.

All the milled Ti-6Al-4V samples showed evidence of cavitation in the gauge length after hot tensile testing (Figure 10-8). However, cavitation was not observed in the head of the test pieces (Figure 10-8b). Assessment of the cavitation found it to be located primarily at the grain boundary areas (Figure 10-8c). In addition to the fine porosity observed in all the hot tensile samples produced by powder processing, gross cavitation was observed in samples HIPed at 700°C (Figure 10-8d).

The effect of HIP temperature on the hot tensile properties of Ti-6Al-4V+0.5B was similar to those when testing the milled Ti-6Al-4V. The general observations that were specific to the Ti-6Al-4V+0.5B are as follows:

1. The elongation to failure of Ti-6Al-4V+0.5B HIPed at 800°C and tested at 900°C and $6x10^{-4}s^{-1}$ was not as high as the milled Ti-6Al-4V (~560% compared with 800% for Ti-6Al-4V+0.5B and Ti-6Al-4V respectively, see Figure 10-9a)
2. In spite of the lower elongation to failure observed in Ti-6Al-4V+0.5B compared with Ti-6Al-4V, lower flow stresses were observed in the boron containing samples (Figure 10-9).
3. At high strain rates of ~ $0.01s^{-1}$ and higher, the Ti-6Al-4V+0.5B HIPed at either 700°C or 800°C out performed the milled Ti-6Al-4V and conventional Ti-6Al-4V in terms of elongation to failure (Figure 10-10).

Figure 10-11 shows the microstructure of the milled Ti-6Al-4V + 0.5B that was HIPed and tested at 900°C at a strain rate of 6 x $10^{-4}s^{-1}$. The TiB particles are aligned generally in the tensile direction. Areas can be seen that contain large α grains, which are free from TiB (Figure 10-11 a), and these regions extend parallel to the tensile direction. Cavitation was observed and appeared to be concentrated in the fine grained reinforced areas, however, the cavitation did not appear to relate to the TiB particles. Although the TiB needles were mostly aligned in the tensile direction (Figure 10-11 a), some of the TiB needles appeared to bend as they passed from one grain to another and this is

indicated by 'i'. A TiB needle can also be seen in Figure 10-11 normal to the tensile direction and is indicated by 'ii'. In some grains shear along a TiB needle was observed and this is indicated by 'iii' on Figure 10-11.

10.2 Discussion

Despite an apparently ideal starting microstructure for superplastic deformation all of the milled Ti-6Al-4V based materials exhibited relatively low elongations to failure (maximum ~ 1250 %) compared with conventional sheet Ti-6Al-4V (1800%) after testing under identical conditions (Figure 10-1 and Figure 10-5). The HIPed gas atomised Ti-6Al-4V, which had a lamellar microstructure, also exhibited higher elongations to failure at 800 and 900°C than the milled Ti-6Al-4V. In industry the maximum elongation used during superplastic component manufacture is approximately 300%. However, extensive cavitation was observed in all of the material produced by powder metallurgy, and qualitatively this appeared to be most pronounced in the milled material. This is a potential reason for the low elongations observed. This cavitation was also observed after relatively low strains of ~200%. Cavitation is seldom observed in Ti-6Al-4V because of the excellent accommodation behaviour of the high diffusivity β phase during grain boundary sliding based deformation (Hamilton (1984)). The reasons for cavitation in the powder metallurgy samples and the low elongations observed are complex and probably interrelated. However, a number of distinctive factors can affect superplastic performance of Ti-6Al-4V are: grain size, grain size distribution, β phase volume fraction at the deformation temperature, microporosity and argon entrapment. These are discussed in turn with particular reference to cavitation. In addition, the effect of TiB on hot tensile properties and as an internal marker is discussed.

10.2.1 Microstructural morphology

Unexpectedly, given the lamellar microstructure, the gas atomised Ti-6Al-4V, HIPed and tensile tested at the same temperatures as the milled Ti-6Al-4V (Figure 10-2), exhibited higher elongations to failure than the milled Ti-6Al-4V. The lower tensile elongation in the milled Ti-6Al-4V is suprising since an equiaxed α microstructure is preferable for superplastic flow and is consistent with the lower flow stress reported compared with the gas atomised Ti-6Al-4V (Figure 10-3). It is thought that with increasing superplastic strain the lamellae present in the gas atomised Ti-6Al-4V were sheared to produce an equiaxed structure and this accounted for the high initial flow stresses observed. The resulting equiaxed structure, which was more suitable for

superplastic deformation, was observed in the sectioned test piece (Figure 10-4). This is consistent with other observations of deformation in lamellar microstructures (Wisbey (1995), Ito and Hasegawa (1980)) and is also reflected in the high initial flow stresses recorded (Ito and Hasegawa (1980)).

The low tensile elongation in the milled Ti-6Al-4V compared with the gas atomised Ti-6Al-4V cannot be accounted for by the morphology of the α phase. Argon entrapment may offer an explanation for the differences in superplastic extension observed between the gas atomised and milled Ti-6Al-4V and this is discussed in § 10.2.5.

10.2.2 Grain size

The milled Ti-6Al-4V HIPed and tensile tested at 700, 800 and 900°C had a much lower elongation to failure (160, 360 and 540 % respectively) than the conventional sheet Ti-6Al-4V (460, 1060 1200 % respectively) tested at the same temperatures. The mean grain sizes for the sheet Ti-6Al-4V, and the milled Ti-6Al-4V HIPed at 900°C and 800°C are 5 μm, 8 μm and 3 μm respectively. Since the grain size of the milled Ti-6Al-4V HIPed at 800°C is smaller than the sheet Ti-6Al-4V the difference in grain size alone cannot fully account for the low elongations of the milled Ti-6Al-4V compared with the conventional Ti-6Al-4V. However the effect of finer grain sizes was observed when the milled Ti-6Al-4V was HIPed at lower temperatures and tensile tested at 900°C. The highest elongation was observed after HIPing at 750°C resulting in 1250 % tensile elongation compared with 530 % after HIPing at 900°C (where both samples were tested at 900°C at $6x10^{-4}s^{-1}$ (Figure 10-5). Therefore the grain size had a significant effect on the elongation measured. Indeed higher elongations may be possible by testing at an optimum strain rate.

Paton and Hamilton (1979) record that changes in grain size are reflected in the flow stress measured. This is consistent with the higher flow stress seen in the milled Ti-6Al-4V which was HIPed and tested at 900°C compared with the conventional rolled Ti-6Al-4V and the milled Ti-6Al-4V HIPed at 750, 800°C and 850°C and were then tested at 900°C (Figure 10-3b). However, a lower flow stress would have been expected from the milled Ti-6Al-4V HIPed and tested at 700°C, compared to the conventional Ti-6Al-4V, because of the finer grain size (Figure 10-5a) but this was not the case and reasons for this are discussed in §10.2.5. Although the grain size plays a major ~~roll~~ role in

the maximum elongation achieved, the grain size alone was not thought to be responsible for the low extensions observed.

10.2.3 Grain size distribution

The grain size distribution of the milled Ti-6Al-4V when HIPed at 800 and 900°C can be seen in Figure 8-14 to Figure 8-17 and were found to vary widely; between 2-10 μm and 4-22 μm when HIPed at 800°C and 900°C respectively and heat treated. This grain size distribution was found to increase during heat treatment (§8.2.3.2). These larger grains can account for a large proportion of the sample by volume. This grain size distribution, along with the larger average grain size, can also contribute to the low tensile elongation. Studies have suggested that increasing grain size variation can lead to reduced strain rate sensitivity (Paton and Hamilton (1979)) and high flow stresses (Paton and Hamilton (1979), Ghosh and Raj (1981)). A higher flow stress was observed in the milled Ti-6Al-4V HIPed and tested at 900°C when compared with conventional rolled Ti-6Al-4V. However, the milled Ti-6Al-4V HIPed and tested at 800°C also had a higher flow stress even though in the as HIPed condition the variation in grain size was small. Therefore grain size distribution may be a factor in the high flow stresses but the volume fraction of β phase (§8.2.1) is thought to dominate.

Paton and Hamilton (1979) have also discussed how a wide distribution of grain sizes might cause cavitation and this is clearly of relevance to the milled Ti-6Al-4V material. It was proposed that the presence of large grains may impede grain switching events during deformation (Paton and Hamilton (1979)) and accommodating the geometric mismatch of large grains during grain boundary sliding may also increase the probability of cavitation. Ito and Hasegawa (1980) have shown increased cavitation with increasing grain size (not distribution) when testing at relatively low temperatures. However, it should be noted that Paton and Hamilton (1979) did not report cavitation even when some grains were as large as 20 μm. The cavities observed in this study were not found to relate to large grained regions. In fact, large grained areas were not easily observed on the sectioned test piece and of the milled Ti-6Al-4V samples. Thus the grain size distribution observed in the milled Ti-6Al-4V was unlikely to have resulted in the gross cavitation observed.

10.2.4 Volume fraction of β

It is generally recognised that the presence of approximately 40-50 % β phase is required to give optimum superplastic behaviour in Ti-6Al-4V (Hamilton (1984)). However, it was noted that the initial microstructure of the milled Ti-6Al-4V at 900°C (i.e. at the start of high temperature testing) contained only 29 % volume fraction β phase. Potential reasons for the development of this microstructure have been discussed (§8.2.1). The low β volume fraction may be another contribution to the cavitation and the low elongations to failure measured in the milled Ti-6Al-4V samples. The flow stress measured for the milled Ti-6Al-4V is significantly higher than those measured for conventional Ti-6Al-4V: 30 % higher at 900°C and 50 % higher at 800°C. This may be a result of the low β phase volume fraction (Hamilton (1984)), which would be expected to increase the flow stress for the samples tested at both 800 and 900°C. A homogenising heat treatment at 800°C for 100 hours of the milled Ti-6Al-4V HIPed at 800°C resulted in the expected proportions of α and β phases. Superplastic forming of this material gave similar tensile results to that of the milled Ti-6Al-4V HIPed at 900°C, therefore the metastable structure of the as HIPed alloy was not directly responsible for the cavitation and low elongations observed (Figure 10-6).

10.2.5 Argon entrapment and consolidation defects

A potential factor in the development of extensive cavitation during superplastic testing could be fine residual porosity from the hot isostatic pressing or entrapment of argon during the gas atomisation and the milling process. The argon entrapment in the milled Ti-6Al-4V is thought to be associated with, firstly, the argon gas atomisation where gas pores are observed at the centre of the powder particles and secondly, the milling process may trap pockets of argon between welded powder particles. The argon levels seen in this study (0.45 ppm for gas atomised Ti-6Al-4V and 1.54 ppm for milled Ti-6Al-4V) agree well with data published for gas atomised TiAl (Gerling *et al.* (1998)). The entrapped argon in the gas atomised Ti-6Al-4V is a third of that measured for the milled Ti-6Al-4V and this qualitatively corresponds to the lower levels of cavitation observed in the superplastically deformed gas atomised Ti-6Al-4V compared with the milled Ti-6Al-4V (compare Figure 10-4 and Figure 10-8). However, upon static annealing at 900°C in air, no porosity was observed in the milled Ti-6Al-4V unlike γ–TiAl where porosity was observed after heat treating at 1066°C (Choi *et al.* (1990)). Although a direct comparison cannot be made with the work of Choi *et al.*

(1990), they show that argon entrapment can lead to porosity on subsequent heat treatment. In this case porosity was observed after the application of temperature and strain, because porosity was observed in the gauge length but not in the head of the test specimen (Figure 10-8 b and c). This is consistent with Dowson *et al.* (1998) who have reported on the formation of pores during superplastic testing of low pressure spray formed and hot rolled Ti-6Al-4V and speculated that these pores were related to argon entrapment.

Since cavitation is likely to initiate fracture, the lower cavitation levels in the gas atomised Ti-6Al-4V may be a major contributor to the higher elongations observed compared with the equivalent milled Ti-6Al-4V. This unfortunately poses problems for the use of gas atomisation as a source for powder that may be subject to subsequent hot forming operations. It may be possible that by using TiH_2 or hydrogen atmospheres the greater amount of fracturing during milling would inhibit the incorporation of argon gas in sealed pockets. This would also have the added advantage of ensuring that the fine powders are retained after milling making them more amenable to packing and consolidation process.

A related potential cause of cavitation is residual porosity from HIPing. Figure 10-8 is a section of the milled Ti-6Al-4V, which was HIPed at 700°C and tested at 900°C at a strain rate of 6×10^{-4} s^{-1}. A large band of porosity can be seen along the tensile direction and is greater than 250 μm in length. This banding might result from the incomplete bonding of powder allowing delamination at the powder particle boundaries and enabling enhanced cavitation. No evidence of powder delamination was observed in milled Ti-6Al-4V after HIPing at 900°C. Work by Smarsly *et al.* (1985) on Ti-6Al-4V produced by powder spraying under a vacuum has shown that even after HIPing at 950°C and 245 MPa porosity was observed with sizes of 100 nm. In the milling Ti-6Al-4V samples no evidence for such pores were observed, but pores of this size are difficult to detect.

10.2.6 The effect of TiB on the superplastic properties

The aim of the current study was to produce a fine stable grain size in Ti-6Al-4V by mechanical milling to give a material that was suitable for high strain rate superplasticity or superplasticity at lower temperatures. In general, the material produced by mechanical milling with boron addition had a finer grain size than either

conventional Ti-6Al-4V or milled Ti-6Al-4V and this resulted in better superplastic properties at strain rates of 6 x $10^{-2}s^{-1}$ (compare Figure 10-7 and Figure 10-10). However, the performance of the material over a range of superplastic conditions was complicated by cavitation. The effects of the finer grain size and TiB are discussed in more detail below.

10.2.7 The effect of TiB as a grain pinner on the superplastic properties

Predictive models (Arieli and Mukherjee (1980), Gifkin (1976), Gittus (1977)) show the dependence of strain rate and flow stress on the grain size. These models suggest a reduction in grain size from 10 μm to 1 μm would enable an increase in the forming rate of 100 times. In keeping with these models, a reduction in grain size from 10 μm in conventional Ti-6Al-4V to less than 2 μm for the milled Ti-6Al-4V+0.5B resulted in a significant improvement in the elongation to failure at 6 x $10^{-2}s^{-1}$ (Figure 10-10). It is likely that the increase in grain boundary area enhances grain boundary sliding and diffusion related accommodation mechanisms.

To enable grain sizes finer than 1 μm to be retained powder samples were HIPed at a range of temperatures to limit the thermal exposure and hence the grain size. The effect on grain size of reducing the HIP from 900°C to 800°C can be seen in Figure 8-13. Further reductions in the HIP temperature were found to result in a finer grain size, for example 500 nm in milled Ti-6Al-4V and 100 nm in milled Ti-6Al-4V+0.5B when HIPed at 600°C (Brown *et al.* (1999a)). However, as discussed previously in §9.4.4 at lower HIPing temperatures (600-700°C) incomplete bonding between the powders was found (Figure 9-7). The HIPing temperature is a limiting factor when producing titanium via a powder metallurgy process. Further improvements may be possible in producing this material with the nanoscale grain size by extending the HIPing time to allow further diffusion and bonding to occur, or to use a combination of HIPing and mechanical work to break up the particle boundaries and encourage bonding.

The tensile elongations of the milled Ti-6Al-4V+0.5B were, however, much lower than those of the milled Ti-6Al-4V processed under similar conditions, e.g. 540% and 940% respectively for samples HIPed at 800°C and tested at 900°C using a strain rate of $6x10^{-4}s^{-1}$ (compare Figure 10-7 with Figure 10-10), even though the grain size of the milled Ti-6Al-4V+0.5B was apparently lower (Figure 8-13). However, there was no evidence to suggest that the TiB caused cavitation during superplastic forming because

the porosity was rarely located at TiB particles and more often found within the α grains, on α/α boundaries and α/β boundaries. This is supported by Kobayashi *et al.* (1994) and Korzh *et al.* (1997), where neither author reported cavitation when hot forming Ti-6Al-4V with TiN and TiB particles. In this study, qualitatively, more cavitation was observed in the fine grain areas which contain TiB than the larger grain TiB free areas (Figure 10-11).

If TiB were to be detrimental to the superplastic flow of this material, by inhibiting grain boundary sliding, the flow stress should have higher than that observed for Ti-6Al-4V. However Figure 10-3b and Figure 10-9b show similar or lower flow stresses in milled Ti-6Al-4V+0.5B compared to conventional Ti-6Al-4V. Additionally the flow stress of the milled Ti-6Al-4V+0.5B is lower than milled Ti-6Al-4V processed and tested under identical conditions, e.g. peak flow stress when testing at 900°C at a strain rate of $6 \times 10^{-4}s^{-1}$ is 15 MPa for milled Ti-6Al-4V+0.5B HIPed at 800°C, 23 MPa milled Ti-6Al-4V HIPed at 800°C and 30 MPa for conventional Ti-6Al-4V. This is in agreement with work by Agrawal *et al.* (1980) who observed reduced flow stresses in Ti-6Al-4V with additions of yttria particles.

It is suggested that the reason for the lower elongation to failure at low strain rates ($< 6x10^{-3}s^{-1}$) in the milled Ti-6Al-4V+0.5B is not related to the TiB needles, but is related to preferential flow in the fine grained areas that contain TiB. Hence the large grained, TiB free, areas see little strain and consequently no strain assisted argon cavitation can be seen. In the fine grained areas, which contain the TiB needles, preferential flow occurs and strain assisted argon cavitation nucleates and grows rapidly and hence early failure occurs. Work by Paton and Hamilton (1979) shows agreement with this study where, in spite of a small number of coarse grains, low flow stresses and high strain rate sensitivity values were retained although the tensile elongation was low.

At higher strain rates ($>6x10^{-3}s^{-1}$) the converse was true, i.e. a higher elongation to failure was observed in the Ti-6Al-4V+0.5B compared with the milled Ti-6Al-4V powders (compare Figure 10-7 and Figure 10-10). In this instance it is suggested that the finer grain size of the Ti-6Al-4V+0.5B dominated and hence better tensile elongations were observed. The effect of the preferential flow and subsequent strain assisted argon cavitation in the fine grained TiB pinned areas was limited by the short time available for nucleation and growth of these cavities.

10.2.8 Effect of fine grain size on forming temperature.

It is difficult to comment on the effect of finer grain sizes on the superplastic forming temperature because the strain assisted argon cavitation combined with the large grained areas are thought to have masked the superplastic performance of the milled Ti-6Al-4V+0.5B. This work does show however higher elongation to failure at 900°C than 800°C. Paton and Hamilton (1979) suggest that significant differences in the volume fraction of the α and β phases would affect the deformation mechanisms since the diffusion kinetics of differ by two orders of magnitude. The conventional Ti-6Al-4V has a high tensile elongation at both 800 and 900°C where the β volume fraction may vary from between 30% and 50% over this range. For commercial superplastic forming operations flow stress is an important consideration and at 800°C the peak flow stress is 65 MPa, which is more than double the value at 900°C. A reduction in the grain size has been shown to produce material with lower peak flow stresses at both 800°C and 900°C compared to conventional Ti-6Al-4V tested at the same temperatures (Figure 10-3b and Figure 10-9b). However, the peak flow stress of the milled Ti-6Al-4V+0.5B at 800°C is still twice that compared with conventional Ti-6Al-4V tested at 900°C at 60 MPa and 30 MPa respectively. Work by Korzh *et al.* (1997) has reported 450-600% elongation to failure at 600°C at a strain rate of $1.7 \times 10^{-3}s^{-1}$ with a flow stress of 20-50 MPa and an initial grain size in the region of 270-600 nm in Ti-6Al-4V with approximately 0.25 wt.%ZrB_2. Salishchev *et al.* (1993) have similarly shown work on the Russia alloy VT8 (Ti-6Al-3.2Mo) with an initial grain size of 60 nm. At 600°C and a strain rate of $6 \times 10^{-4}s^{-1}$ an elongation of 600% was achieved with a flow stress of 150 MPa. The effect of temperature on the superplastic properties of milled Ti-6Al-4V+0.5B has been marred by the strain induced argon cavitation and the low β volume fractions observed in the powder metallurgy material. However, other work suggests that by significantly refining the grain size it may be possible to superplastically form titanium at lower temperatures. It is important however, for superplastic forming using argon gas pressure to blow the sheet material into a die, that flow stress at these temperatures remain low.

10.2.9 TiB as an internal marker for superplastic flow in Ti-6Al-4V

Many theories debate the mechanism by which the large strains that are observed during superplastic flow are accommodated. Generally it is accepted that superplastic flow occurs by grain boundary sliding and this is accommodated by a variety of processes

including: diffusion, dislocation climb, recrystallisation, grain boundary migration and slip (Arieli and Mukherjee (1980), Gifkin (1976), Gittus (1977)). Blackwell and Bate (1999) have proposed that intragranular slip is the dominant mechanism and grain boundary sliding and other processes are the accommodation mechanism. Metallography of the pre- and post- superplastic deformation microstructures of the milled Ti-6Al-4V may contribute to the current debate over the nature of superplastic deformation mechanisms.

The superplastic deformation of the Ti-6Al-4V + 0.5B results in the initial random orientation of the TiB needles aligning in the general direction of the tensile axis (compare Figure 8-12 and Figure 10-11). Some of the TiB needles appear to pass from one α grain to another, along the α/β boundaries and other needles can be seen within α grains (Figure 10-11). TiB needle alignment has been noted after mechanical work such as extrusion (Yolton and Moll (1995), Soboyejo *et al.* (1994)) and rolling (Brown *et al.* (1961)). However more subtle features can be observed in Figure 10-11b 'i', where a TiB needle within an α grain can be seen perpendicular to the tensile axis and could be interpreted as an example of grain rotation. Figure 10-11a 'i' indicates one of many examples showing a wavy or bent TiB needle which passes from one α grain to the boundary between two α grains and could be the result of grain boundary sliding. ~~Evidence of~~ Bent or wavy TiB needles, which pass from one α grain to another, can also be seen and suggest grain boundary sliding. Equally, evidence of intragranular slip along a TiB needle boundary can be seen in Figure 10-11b 'ii'. These micrographs are taken from one sample, which has been tested at one strain rate and one temperature to failure, and therefore no definitive conclusions can be drawn from this work. Work that has explored the mechanisms by which large superplastic strains are accommodated used both internal and surface markers. The use of surface markers has been questioned as a method for determining the characteristic in the bulk of the sample because of the extra degree of freedom at the surface (Blackwell and Bate (1999)). Surface techniques and internal markers can be criticised because only small strains, of the order of 60%, can be used and this is not representative of superplastic flow which is normally considered to enable elongation's of at least 400% and often greater than 1000%. It is therefore suggested that the TiB needles within Ti-6Al-4V suggest agreement with grain boundary sliding, grain rotation and intragranular slip as mechanisms that enable superplastic flow to occur. It is additionally suggested that further investigation of

Ti-6Al-4V with TiB as an internal marker may offer further evidence on the mechanisms of superplastic flow over a wider range of strains at different strain rates and possibly different temperatures.

10.3 SUMMARY

- The mechanically milled powders had an apparently ideal equiaxed fine grained microstructure for superplastic forming. In spite of this, low tensile elongations were achieved. Extensive cavitation of the powder metallurgy samples tested was responsible for the low tensile elongations observed. The likely cause of the cavitation was a result of argon entrapment during the gas atomisation and mechanical milling. Cavitation is produced by the application of temperature and strain.
- The TiB did not appear to have any detrimental effect on the superplastic properties of the Ti-6Al-4V and improved superplastic properties were observed in the Ti-6Al-4V+0.5B at strain rates higher than those usual for the superplastic forming of Ti-6Al-4V.
- TiB may also be useful in future studies as an internal marker might offer a tool for investigating superplastic deformation.

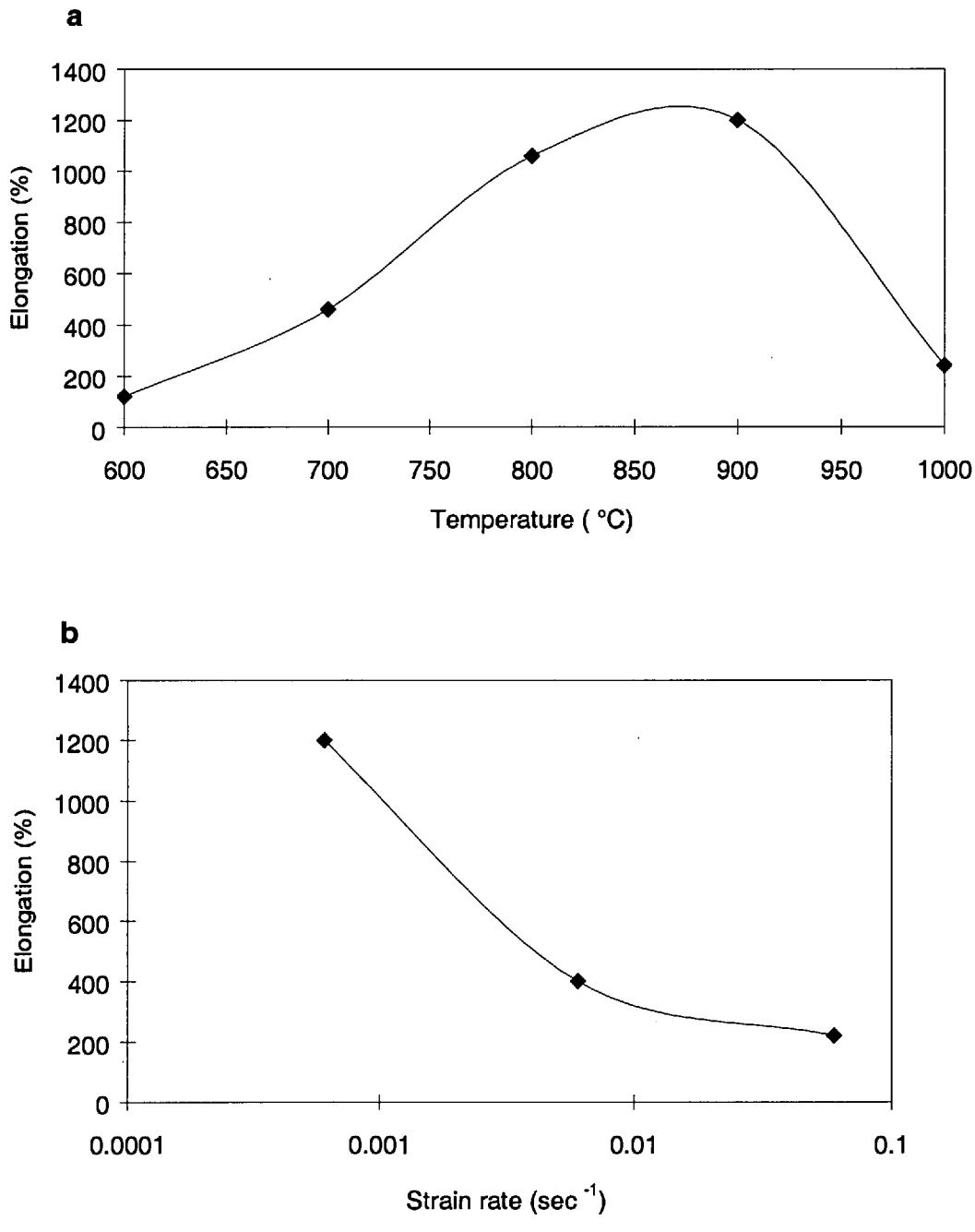


Figure 10-1 Graphs showing the superplastic properties of conventional Ti-6Al-4V shows the effect of (a) temperature at a strain rate of $6x10^{-4}s^{-1}$ and (b) strain rate on the elongation to failure of conventional Ti-6Al-4V

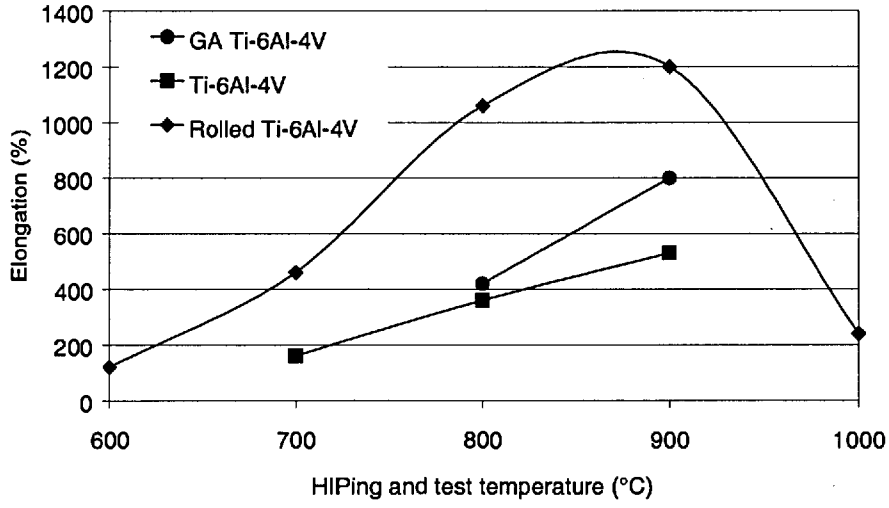
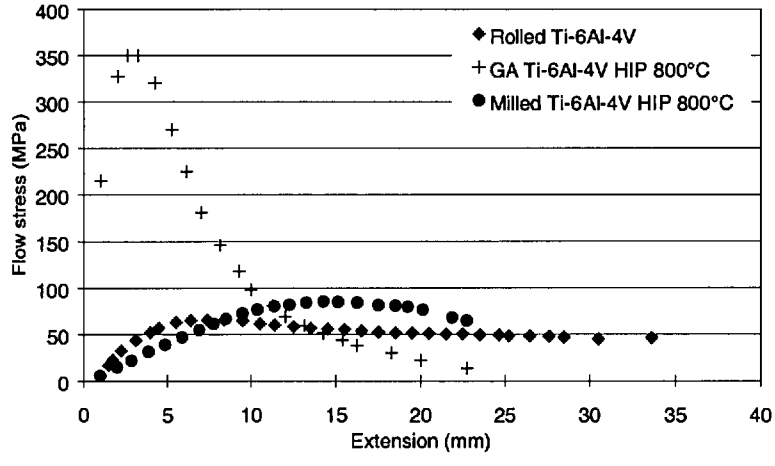


Figure 10-2 Graphs showing the superplastic properties of gas atomised Ti-6Al-4V and milled Ti-6Al-4V tested at their HIPing temperatures at a strain rate of $6x10^{-4}s^{-1}$ and compared with conventional Ti-6Al-4V tested at a range of temperatures.

a



b

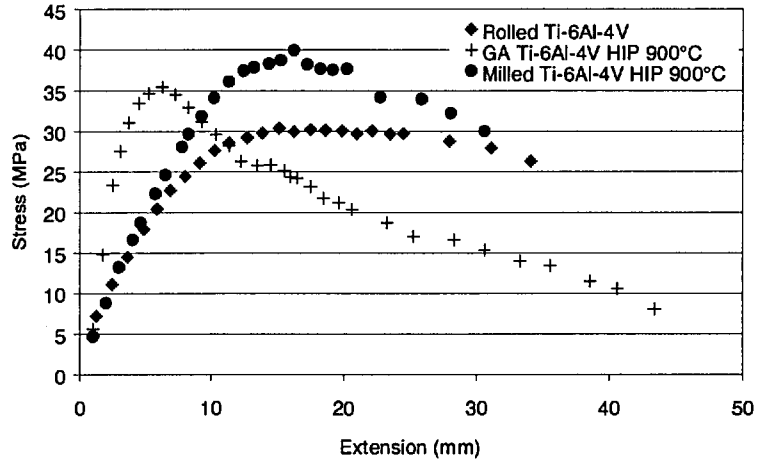


Figure 10-3 Graphs showing the flow stress of gas atomised Ti-6Al-4V compared with conventional Ti-6Al-4V tested at a strain rate of $6x10^{-4}s^{-1}$ at (a) 800°C and (b) 900°C.

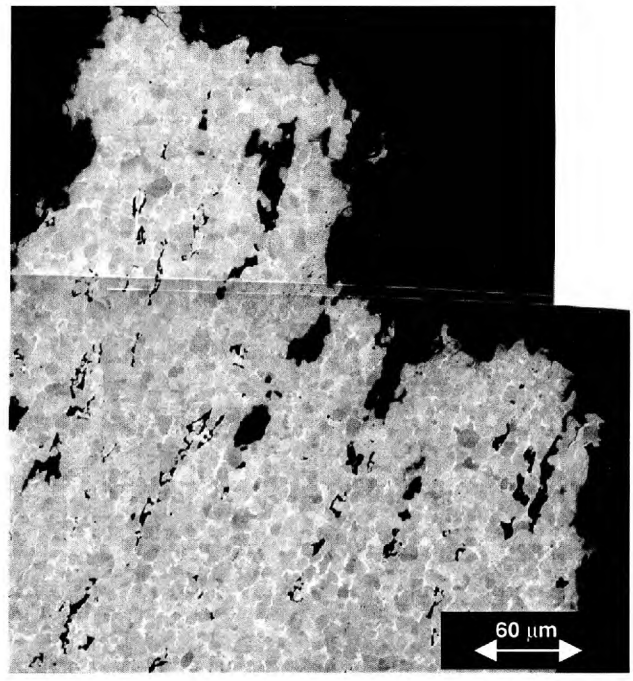


Figure 10-4 A SEM micrograph showing a cross section of the gas atomised sample HIPed 900°C and tested at 900°C at a strain rate of $6x10^{-4}s^{-1}$. Cavitation can be seen in the cross section.

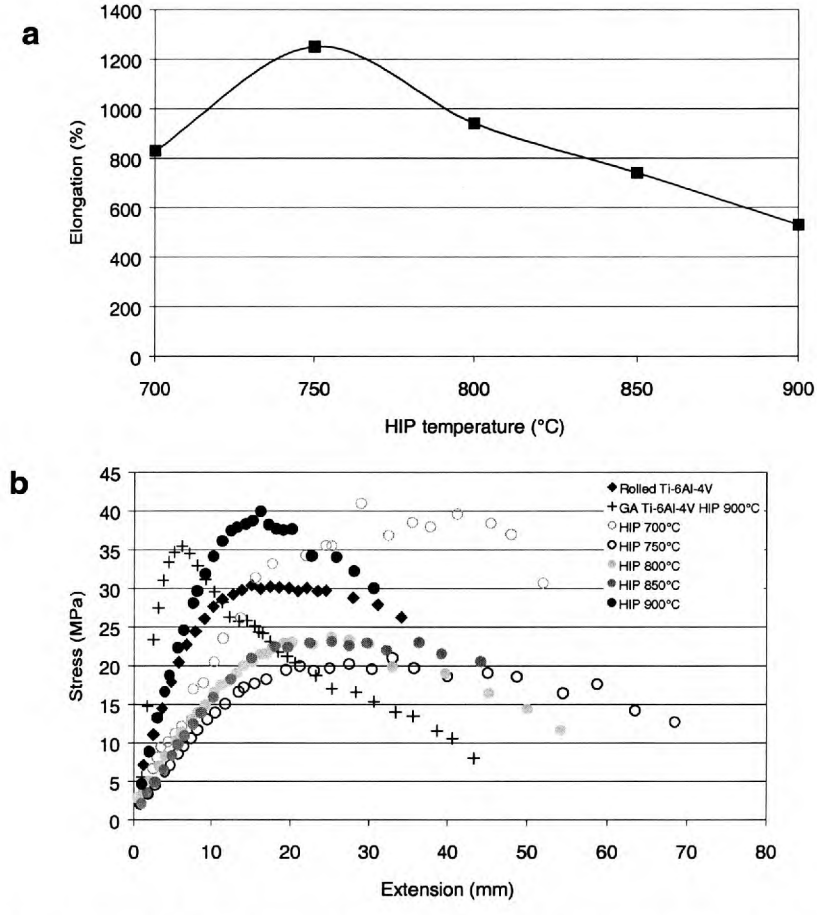


Figure 10-5 Graphs showing the superplastic properties of milled Ti-6Al-4V HIPed at a range of temperatures and tested at 900°C and tested at a strain rate of $6x10^{-4}s^{-1}$, where (a) shows the tensile elongation and (b) shows the flow stress.

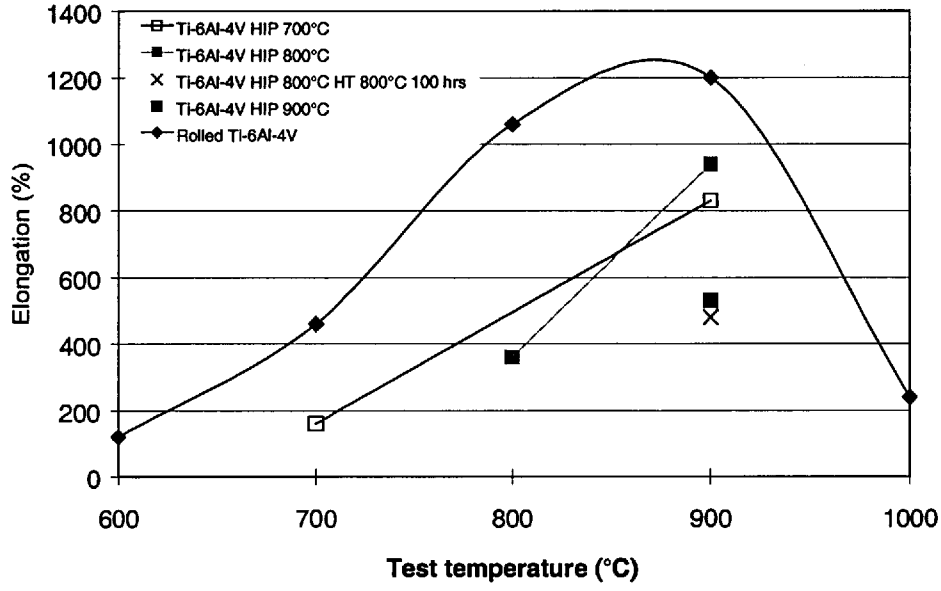
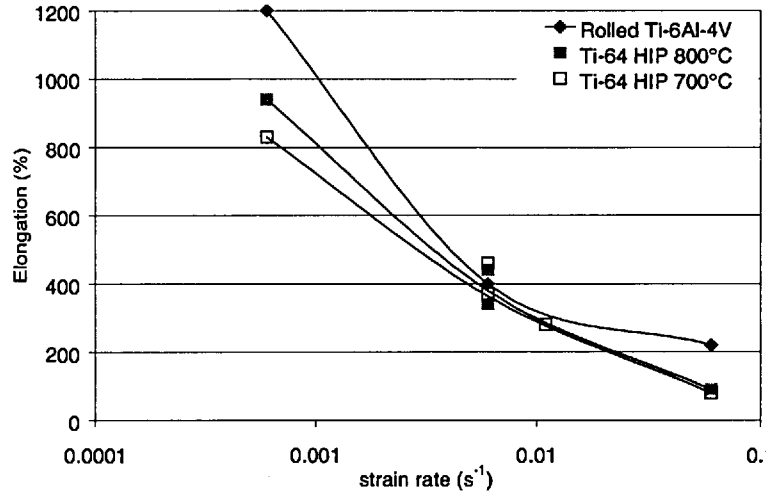


Figure 10-6 A graph showing the tensile elongation of milled Ti-6Al-4V HIPed at a range of temperatures and tested at their HIPing temperatures at a strain rate of $6x10^{-4}s^{-1}$.

a



b

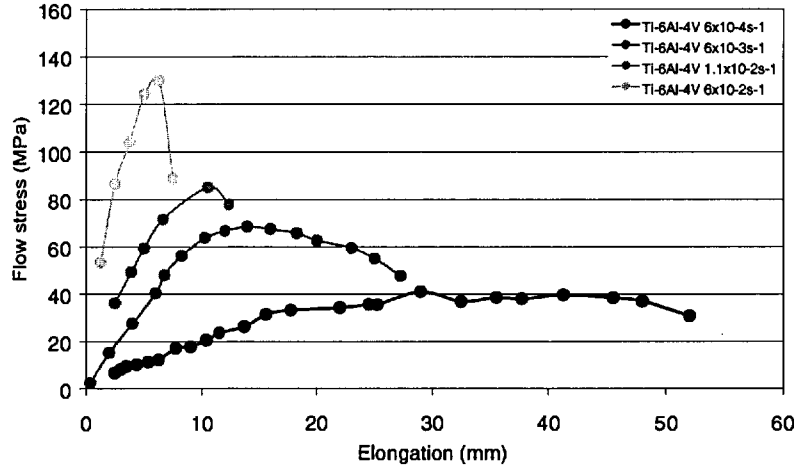


Figure 10-7 Graphs showing the superplastic properties of milled Ti-6Al-4V HIPed at various temperatures and tested at 900°C at different strain rates, where (a) shows the elongation and (b) the flow stress in comparison with conventional Ti-6Al-4V.

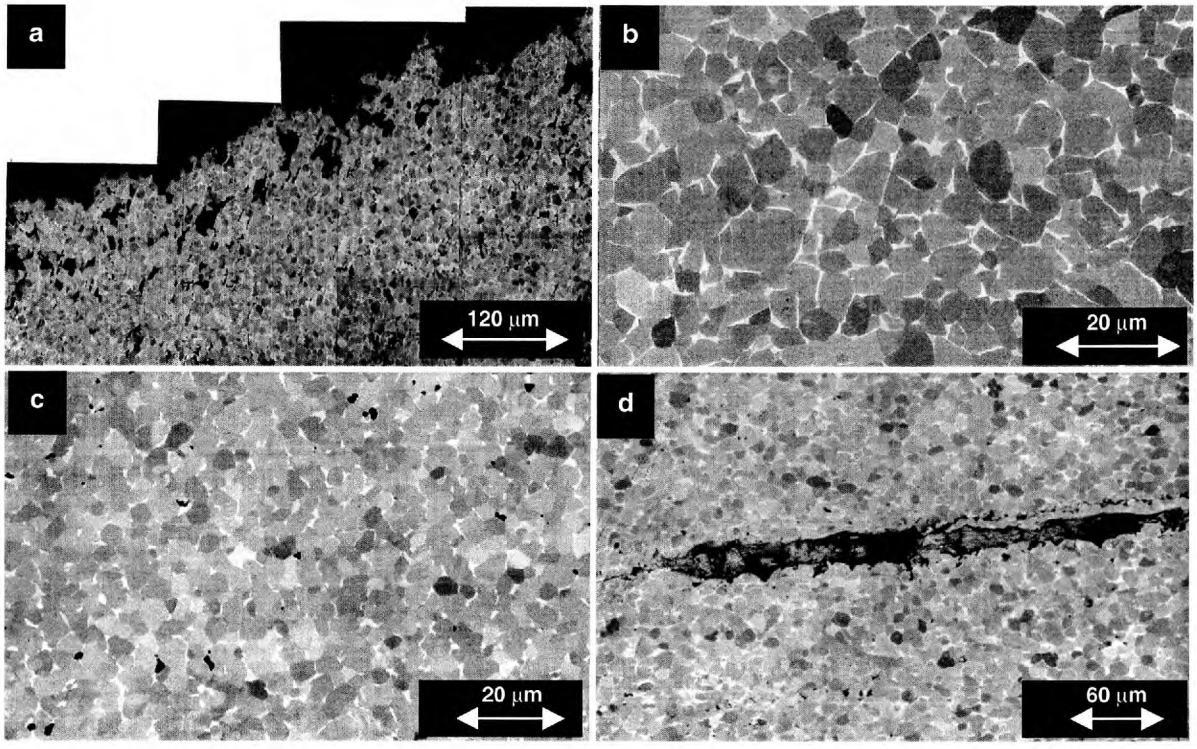


Figure 10-8 Micrographs of superplastic formed milled Ti-6Al-4V are shown where, (a) shows cavitation in gauge length of the HIPed and formed at 900°C at a strain rate of $6x10^{-4}s^{-1}$, (b) shows no cavitation in the head of the sample HIPed and formed at 900°C at a strain rate of $6x10^{-4}s^{-1}$, (c) shows cavitation in the gauge length of sample HIPed at 800°C, tested at 900°C at a stain rate of $6x10^{-4}s^{-1}$ and (d) shows grows cavitation in the sample HIPed at 700°C, tested at 900°C at a strain rate of $6x10^{-4}s^{-1}$.

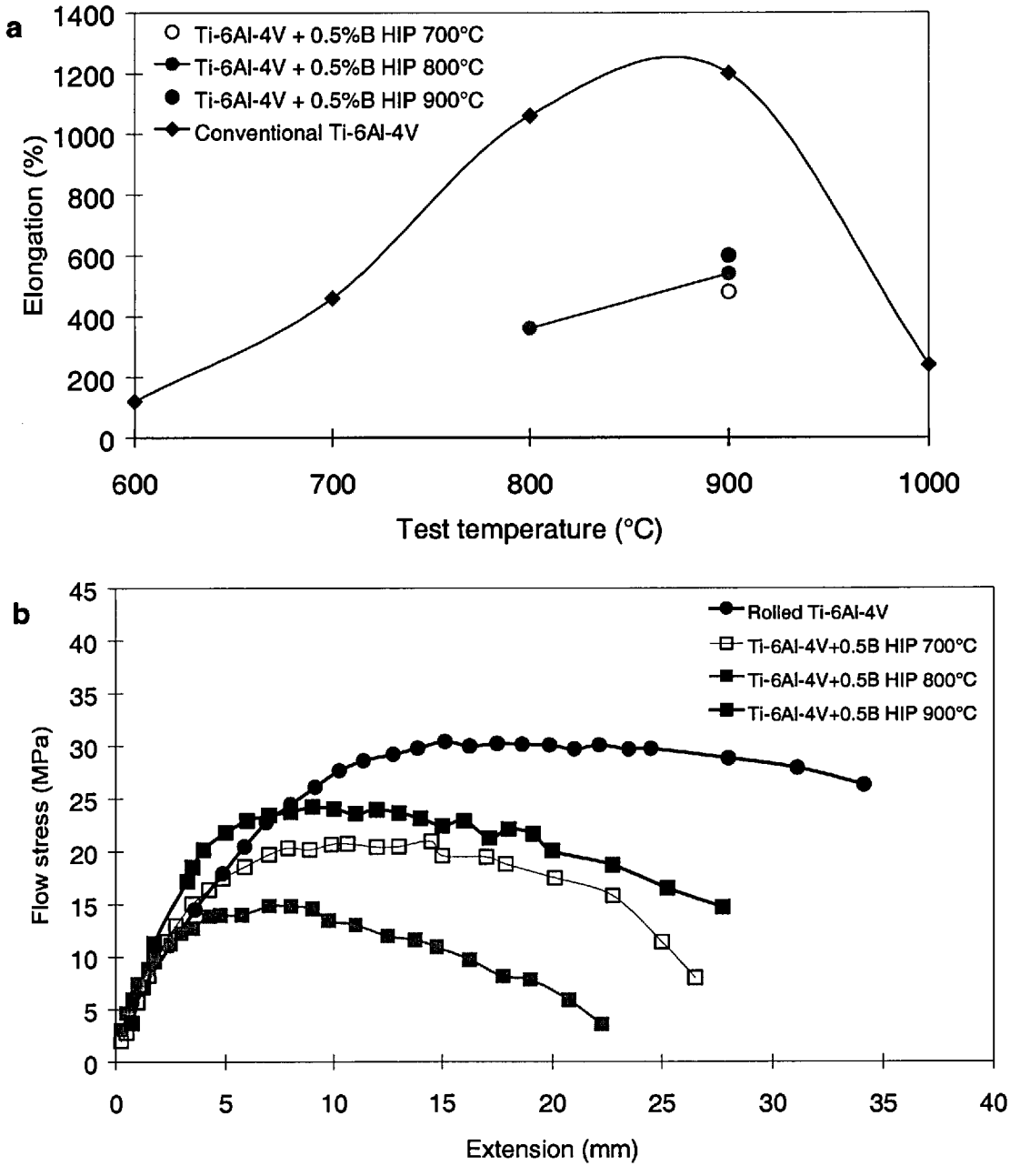


Figure 10-9 Graphs shows the superplastic properties of Ti-6Al-4V+0.5B milled showing (a) the tensile elongation of samples tested at their HIPing temperature at a strain rate of $6x10^{-4}s^{-1}$ and (b) the flow stresses.

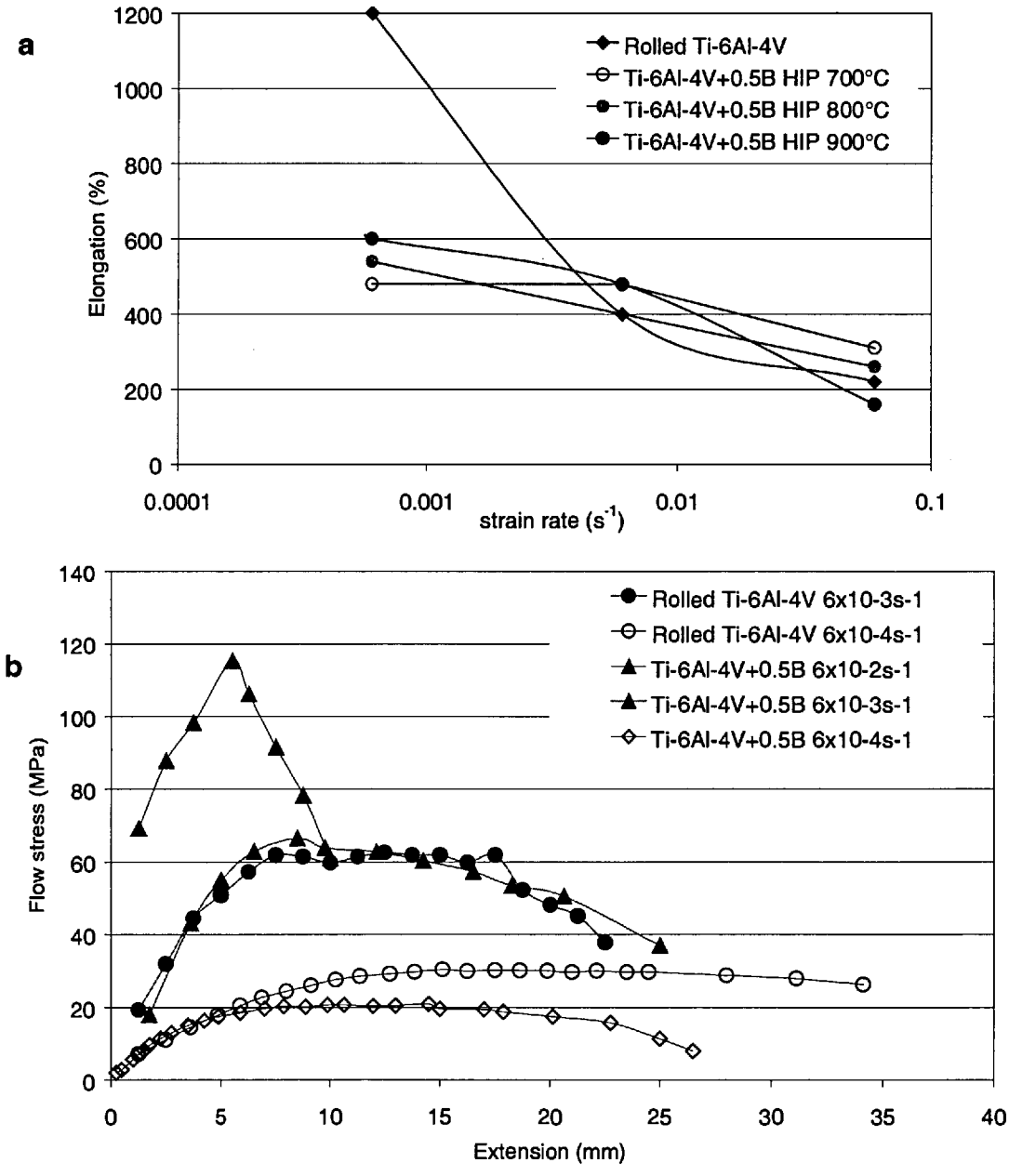


Figure 10-10 Graphs show the superplastic properties of Ti-6Al-4V+0.5B milled and HIPed at various temperatures showing the (a) tensile elongation with increasing strain rate and (b) the flow stresses. after testing at 900°C

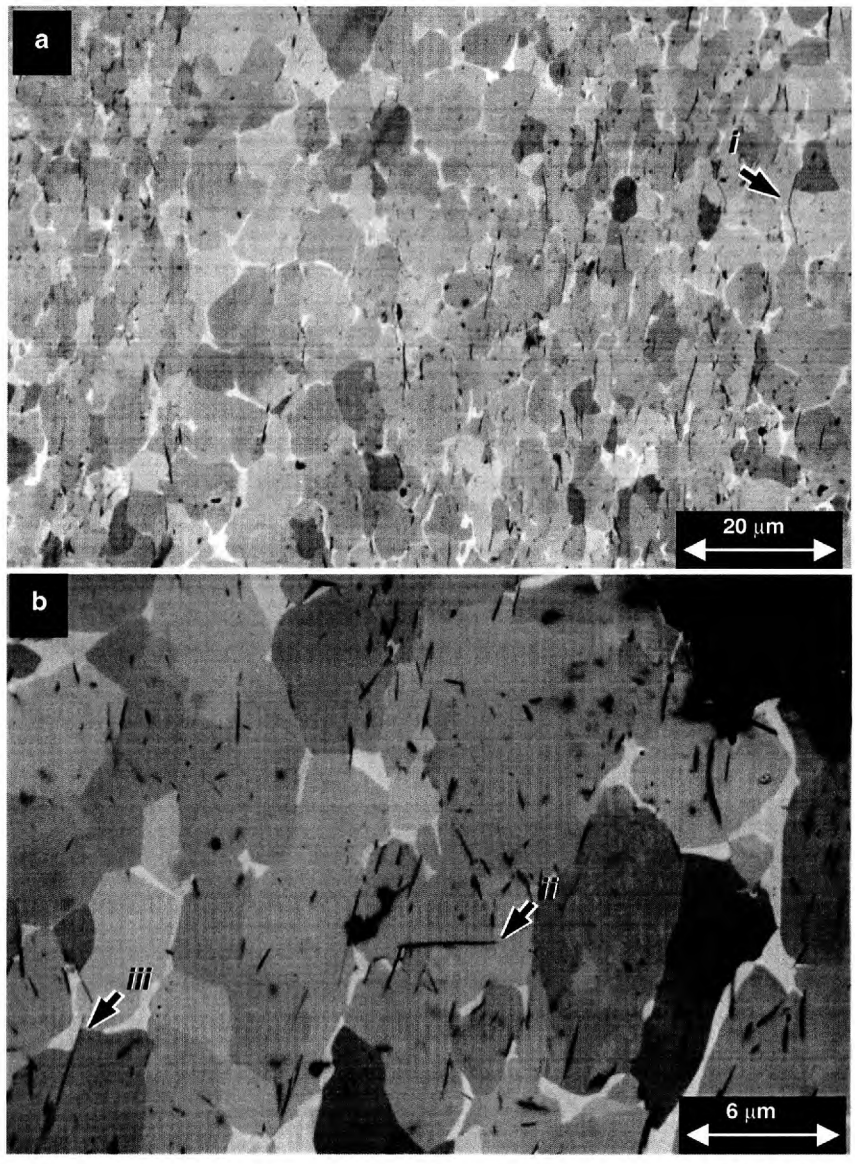


Figure 10-11 SEM images showing the Ti-6Al-4V+0.5B HIPed at 900°C and tested at 900°C at a strain rate of $6x10^{-4}s^{-1}$ where (a) shows the TiB particles aligned in the tensile direction and (b) shows the 'i' particles which bend around α grains, 'ii' particles that normal to the tensile direction and 'iii' shows a grain which has been sheared along a TiB needle.

11. CONCLUSIONS

- Interstitial contamination is critical to the successful mechanical milling of titanium and its alloys. Unfortunately, when interstitial contamination during milling is minimised there is a detrimental effect in terms of the ability to process the titanium powders. Welding was found to dominate during milling and this was prevalent when milling titanium alone.
- Boron or TiB_2 can be blended or milled with titanium (alloy) powders and HIPed to give consolidated billets. When HIPing the boron or TiB_2 precursor reacts with the titanium to produce TiB in the form of needles. Full reaction of the precursors to form TiB occurs after heat treatment at 1300°C for 8 hours.
- Mechanical milling improves the distribution of the TiB with the titanium (alloy) matrix. A combination of finer powder size, an open powder structure and milling with hydrogen further improved the distribution of TiB. Using fine powders, powders with an open structure, milling with hydrogen and using TiB_2 as a precursor to TiB offer the best potential to produce a successful titanium particulate MMC. Heat treatment also offers the potential to further improve microstructure and subsequent mechanical properties.
- Mechanical milling of Ti-6Al-4V produces a metastable microstructure, which was thought to have been produced by pipe diffusion of vanadium in the heavily dislocated powders. During HIPing dislocation free grains are achieved as a result of either recovery or recrystallisation and resulted in equiaxed α grains with a β phase at the grain boundaries, which is heavily enriched with vanadium. Long term high temperature heat treatments are required to achieve the equilibrium proportions through lattice diffusion. This metastable microstructure, resulting in low initial volume fractions of β phase, may have had a detrimental effect on the superplastic properties of titanium.
- Mechanical milling does not have a detrimental effect on the properties of Ti-6Al-4V. The addition of boron or TiB_2 improves the stiffness of titanium and its alloys. The distribution of the TiB clearly affected the tensile strength and ductility

of the titanium alloys. The best distributions of TiB gave the greatest improvements in tensile strength and the highest ductility of the titanium MMCs.

- Gas atomisation and mechanical milling resulted in entrapped argon within the Ti-6Al-4V powders. The argon resulted in strain induced cavitation during high temperature tensile deformation.
- TiB had a grain pinning effect when distributed within the milled Ti-6Al-4V. TiB was not detrimental to the superplastic properties of Ti-6Al-4V and the finer grain size achieved as a result of the TiB resulted in improved superplastic properties compared with conventional Ti-6Al-4V particularly at higher strain rates.

12. FUTURE WORK

This program of work has demonstrated the difficulties in mechanical milling titanium and its alloys. A key factor in achieving good mechanical properties for Ti MMCs is obtaining a good distribution of TiB within the titanium matrix. The use of hydrogen and titanium hydride in controlling the powder particle size and encouraging fracture has been demonstrated and it is hoped this will enable better distributions of TiB to be achieved. It is suggested that future work should be undertaken on mechanical milling titanium MMCs using hydrogen to optimise the distribution of the TiB precursor.

Once homogeneous distributions have been achieved further optimisation of the mechanical properties may be possible through heat treatment. A heat treatment study assessing the effect of TiB needle size on the room temperature properties should be undertaken.

Materials for engineering application need to be formed into component shapes. The ability to forge, extrude and roll titanium MMCs should be assessed. An improvement of the mechanical properties may be achieved by using these forming processes.

Ti-6Al-4V and Ti matrices were chosen to produce titanium MMCs however, other alloys may be preferable. Beta titanium alloys may be a suitable matrix and have the advantage of being heat treatable to enable the mechanical properties to be tailored.

The full range of mechanical properties needs to be considered including creep, hot tensile, fatigue, fracture toughness and wear resistance. Wear resistance may be a valuable property for the application of Ti MMCs. One failing of titanium is its poor wear resistance and the use of Ti MMC components or titanium components with a functionally graded layer may enhance the range of applications for titanium. The development of laser fabrication may offer the potential for commercial exploitation of functionally graded materials.

To produce a material for high strain rate superplasticity a fine stable grain size is required. TiB did not retain its fine size at the processing temperature. A different particulate that remains fine should be selected. One such particulate may be yittria. Mechanical milling with such a fine particle, possibly in the presence of hydrogen to inhibit argon entrapment may result in a HIPed billet where the grain size is retained at

the nanometer scale. High strain rate or lower temperature superplasticity may be possible in the absence of cavitation caused by entrapped argon.

β titanium alloys have two orders of magnitude faster diffusivity than the α phase, however, grain growth at superplastic forming temperatures limits their application. By incorporating a fine stable particle, such as yttria, with fine grains produced by mechanical milling it may be possible to retain fine grain sizes at the superplastic forming temperatures. It is suggested that a β alloy is selected and milled using hydrogen (to enhance fracturing during milling) and with yttria which has a fine particles size, such as 40 nm. It is hoped that milling with hydrogen will enhanced fracture of the titanium powders and inhibit argon being incorporated during milling. The powders should then be consolidated at a range of temperatures and deformed at a range of temperatures and strain rates to characterise the superplastic performance of the material.

13. REFERENCES

Abe and Johnson 1992 — Y. R. Abe, W. L. Johnson, Stability of nanocrystalline structures in the Ti-Cu system, Materials Science Forum **88-90**, 513-520 (1992).

Agrawal *et al.* 1980 — S. P. Agrawal, R. R. Boyer, E. D. Weisert, Effect of small amounts of yttria on the superplastic behaviour of Ti-6Al-4V, H. Kimura, O. Izumi, Eds., Proceeding of the fourth international conference on Titanium, Japan (AIME, 1980).

Arieli and Mukherjee 1980 — A. Arieli, A. K. Mukherjee, A model for the rate-controlling mechanism in superplasticity, Material Science and Engineering **45**, 61-70 (1980)

Askill 1970 — J. Askill, Tracer diffusion data for metals, alloys and simple oxides (Plenum, 1970).

Bania et al. 1980 — P.J. Bania, G.A. Lenning, J.A. Hall, Development of properties of Ti-15-3-3-3, R.R Boyer, H.W Rosenburg, Eds., Beta Titanium Alloys in the 1980's, Atlanta, USA (AIME, 1980).

Benjamin 1970 — J. S. Benjamin, Metall. Trans **1**, 2943-2951 (1970)

Blackwell and Bate 1999 — P. L. Blackwell, P. S. Bate, Superplastic deformation without relative grain translation?, JIMIS-9 Conference "Towards innovation in superplasticity II", Kobe, Japan **304-6**, 189-194 (Materials Science Forum, 1999).

Bormann 1993 — R. Bormann, Mechanical alloying: fundamental mechanisms and applications, F. Aldinger, Ed., Materials by powder technology, PTM '93, 247-258 (DGM Informationsgesellschaft, Oberursel, 1993).

Boyer 1994 — R. Boyer, Materials Properties Handbook, Titanium alloys. W. Scott, Ed. (ASM International, Ohio, 1994).

Brandstotter and Lengauer 1997 — J. Brandstotter, W. Lengauer, Multiphase reaction diffusion in transition metal-boron systems, Journal of alloys and compounds **262-263**, 390-396 (1997).

Brown *et al.* 1999a — A. Brown, R. Brydson, C. Hammond, A. Wisbey, T. M. T. Godfrey, The role of boron in the mechanical milling of Ti-6%Al-4%V powders, Nanocomposite and Nanocomposites III, **581**, 265-270 Boston, USA (MRS, 1999).

Brown *et al.* 1999b — A. Brown, R. Brydson, C. Hammond, A. Wisbey, T. M. T. Godfrey, The microstructure and superplastic properties of clean mechanically alloyed titanium - titanium boride alloys, superplasticity – current status and future potential, Boston, USA **601**, 229-234 (MRS, 1999).

Brown *et al.* 1961 — A. R. G. Brown, H. Brooks, K. S. Jepson, G. I. Lewis, "High modulus titanium alloys based on the titanium boron system" MET/PHYS. 343 (RAE, 1961)

BSI2TA10 1974 — BSI2TA10, Specification for sheet of titanium-aluminium-vanadium alloy. British standard: Aerospace series. (1974).

Choi *et al.* 1990 — B. W. Choi, Y. G. Deng, C. McCullough, B. Paden, R. Mehrabian, Densification of rapidly solidified titanium aluminide powders 1. Comparison of experiments to HIPing models, Acta Metallurgica et Materialia **38**, 2225-2243 (1990).

Clyne and Withers 1993 — T. W. Clyne, P. J. Withers, An introduction to metal matrix composites (Cambridge University Press, 1993).

Donachie 1988 — M. J. Donachie, Titanium, A technical guide. M. J. Donachie, Ed. (ASM International, Ohio, 1988).

Dowson *et al.* 1998 — A. L. Dowson, P. Blackwell, M. Jones, J. M. Young, M. A. Duggan, Hot rolling and superplastic forming response of net shape processed Ti-6Al-4V produced by centrifugal spray deposition, Materials Science and Technology **14A**, 640-650 (1998).

Dubey *et al.* 1997 — S. Dubey, R. J. Lederich, W. O. Soboyejo, Fatigue and fracture of damage tolerant in-situ titanium matrix composites, Metallurgical and materials transactions A **28A**, 1997-2037 (1997).

El-Nasr *et al.* 1996 — A. A. El-Nasr, F. A. Mohamed, J. C. Earthman, High temperature rupture of an SiC particulate reinforced Al composite under multiaxial stress states, Materials science and engineering **A214**, 33-41 (1996).

Fan 1993 — Z. Fan, Microstructure and mechanical properties of multiphase materials, Phd., The University of Surrey (1993)

Fan and Miodownik 1995 — Z. Fan, A. Miodownik, Microstructural evolution in rapidly solidified Ti-7.5Mn-0.5B alloy, Acta Materialia **44**, 93-110 (1995).

Fan *et al.* 1995 — Z. Fan, L. Chandrasekaran, C. M. Ward-Close, A. Miodownik, The effect of pre-consolidation heat treatment on TiB morphology and mechanical properties of rapidly solidified Ti-6Al-4V –XB alloys. Scripta Metallurgica et Materialia **6**, 833-838 (1995).

Fan *et al.* 1997 — Z. Fan, H. J. Niu, A. P. Miodownik, T. Saito, B. Cantor, Microstructure and mechanical properties of insitu Ti/TiB MMCs produced by a blended elemental powder metallurgy method. Key engineering materials. 413-430 (1997).

Fecht *et al.* 1989 — H. J. Fecht, E. Hellstern, Z. Fu, W. L. Johnson, Nanocrystalline metals and compounds prepared by high energy ball milling, T. G. Gasbarre, W. F. Jandeska, Eds. **2**, 111 (MPIF Princeton, 1989).

Frommeyer and Von Czarnowski 1990 — G. Frommeyer, P. Von Czarnowski, High strain rate superplasticity and strength properties of two-phase a titanium- intermetallic Ti-12Co-5Al and Ti12Ni-5Al alloys, Zeitschrift fur Metallkunde **10**, 756-760 (1990).

Fujii *et al.* 1995 — H. Fujii, S. Soeda, M. Hanaki, H. Okano, Development of high performance, low alloy Ti-Fe-O-N series, P. A. Blenkinsop, W. J. Evans, H. M. Flower, Eds., Titanium '95 Science and technology, Birmingham, UK **3**, 2309-2316 (IOM, 1995).

Furuta *et al.* 1999 — T. Furuta, T. Yamaguchi, Y. Shibata, T. Saito, P/M titanium metal matrix composite for exhaust valve, 9th World Conference on Titanium, St. Petersburg, Russia (to be published ,1999).

Gardiner *et al.* 1996 — R. W. Gardiner, P. S. Goodwin, S. B. Dodd, B. W. Viney, Non-equilibrium synthesis of new materials, Advanced performance materials **3**, 343-364 (1996).

Gerling *et al.* 1998 — R. Gerling, R. Leitgeb, F. P. Schimansky, Porosity and argon concentration in gas atomised gamma TiAl powder and hot isostatically pressed compacts, Materials Science and Engineering **A252**, 239-247 (1998).

Ghosh and Hamilton 1979 — A. K. Ghosh, C. H. Hamilton, Mechanical behaviour and hardening characteristics of a superplastic Ti-6Al-4V alloy, Metallurgical Transactions **10A**, 699-706 (1979).

Ghosh and Raj 1981 — A. K. Ghosh, R. Raj, Grain size distribution effect in superplasticity, Acta Metallurgica **29**, 607-616 (1981).

Gifkin 1976 — R. C. Gifkin, Grain boundary sliding and its accommodation during creep and superplasticity, Metallurgical Transactions **7A**, 1225-1232 (1976).

Gittus 1997 — J. H. Gittus, Theory of superplastic flow in two-phase materials: roles of interphases-boundary dislocations, ledges and diffusion., Journal of Engineering Materials and Technology **99**, 244-251 (1977).

Godfrey 1996 — T. M. T. Godfrey, Mechanical alloying of PREP commercial purity titanium powder. (un published work, 1996).

Godfrey *et al.* 1999 — T. M. T. Godfrey, A. Wisbey, P. S. Goodwin, C. M. Ward-Close, "The production of Ti-6Al-4V sheet and its superplastic properties" DERA/MSS/TR990302 (DERA, 1999)

Godfrey *et al.* 2000 — T. M. T. Godfrey, A. Wisbey, P. S. Goodwin, K. Bagnall, C. M. Ward-Close, Microstucture and tensile properties of mechanically alloyed Ti-6Al-4V with boron additions, Material Science and Engineering A, **282 (1-2)**, 240-250 (2000).

Goodwin 1995 — P. S. Goodwin, Control of contamination during mechanical alloying of titanium based materials, W.J. Evans, H.M. Flower, P.A. Blenkinsop, Ed., Titanium 1995, Birmingham, UK, **3**, 2626 (IOM, 1995).

Goodwin and Ward-Close 1993 — P. S. Goodwin, C. M. Ward-Close, Process control in the mechanical alloying of TiAlNb alloys, J. J. deBarbadillo, F. H. Froes, R. Schwarz, Eds., 2nd International Conference on Structural Applications of Mechanical Alloying, Vancouver, Canada. 139-148 (ASM International, 1993).

Goodwin *et al.* 1995 — P.S. Goodwin, A. Wisbey, H.S.Ubhi, Z.D.A Kulikowski, P. Gasson, C.M. Ward-Close, Synthesis of particulate reinforced titanium MMC by mechanical alloying, P. A. Blenkinsop, W. J. Evans, H. M. Flower, Eds., Titanium 95, Birmingham, UK, **3** 2874-2881 (IOM, 1995).

Goodwin *et al.* 1997 — P. S. Goodwin, T. M. T. Hinder, A. Wisbey, C. M. Ward-Close, Recent progress in the clean mechanical alloying of advanced materials, M. D. Baro, S. Surinach, Eds., Mechanically alloyed and nanocrystalline materials, Barcelona, Spain, 953-962 (Trans Tech Publications, 1997)

Hagashi and Mabuchi 1997 — K. Higashi, M. Mabuchi, Critical aspects of high strain rate superplasticity, A.H Chokshi, Ed., Superplasticity in Advanced Materials, Bangalore, India **243-249**, 267-276 (Trans Tech Publications, 1997).

Hamilton 1984 — C. H. Hamilton, Superplasticity in titanium alloys, S. P. Agrawal, Ed., Superplastic forming, Los Angeles, USA 13-22 (ASM, 1984).

Harris *et al.* 1993 — A. M. Harris, G. B. Schaffer, N. W. Page, The evolution of microstructure and particle morphology during mechanical alloying of ductile metals, J. J. deBarbadillo, F. H. Froes, R. Schwarz, Eds., Proc. Of the 2nd International conference on structural applications of mechanical alloying, Vancouver, British Columbia, Canada, 15 (ASM International, 1993).

Hinder 1995 — T. M. T. Hinder, A microstructural comparison of gas atomised and ball milled gamma TiAl powders, Master of Engineering, The University of Birmingham (1995).

Hinder 1997 — T.M.T. Hinder, A. Wisbey, P.S.Goodwin, C.M. Ward-Close, "The production and evaluation of particulate reinforced MMC steel" DRA/SMC/CR972068 (1997).

Hu and Loretto 1994a — D. Hu, M. H. Loretto, Coarsening of TiC particles in rapidly solidified Ti-6Al-4V – TiC composite, Journal of alloys and compounds **209**, 167-173 (1994).

Hu and Loretto 1994b — D. Hu, M. H. Loretto, Microstructural characterisation of a gas atomised Ti-6Al-4V-TiC composite, Scripta Metallurgica et Materialia **31**, 543-548 (1994).

Hu *et al.* 1995a — D. Hu, T. P. Johnson, M. H. Loretto, Tensile properties of gas atomised Ti-6Al-4V-TiC composite, P. A. Blenkinsop, W. J. Evans, H. M. Flower, Eds. Titanium 95, Eighth world conference on titanium, International Convention Centre; Birmingham, UK. 22-26 Oct 95, **3**, 2867 (IOM, 1995).

Hu *et al.* 1995b — D. Hu, T. P. Johnson, M. H. Loretto, Ti-6Al-4V-TiB composite produced via gas atomization, Advances in powder metallurgy and particulate materials, Seattle, USA, **3**, 109-116 (MPIF, 1995b).

Inagaki 1995 — H. Inagaki, Enhanced superplasticity in high strength Ti alloys, Zeitschrift fur Metallkunde **86**, 643-650 (1995).

Ito and Hasegawa 1980 — Y. Ito, A. Hasegawa, Deformation behaviour of Ti-6Al-4V alloy under superplastic deformation, H. Kimura, O. Izumi, Eds., Titanium '80 Science and Technology, Kyoto, Japan, **2**, 983-992 (AIME, 1980).

Johnson *et al.* 1998 — C. H. Johnson, S. K. Richter, C. H. Hamilton, J. J. Hoyt, Static grain growth in a microduplex Ti-6Al-4V alloy, Acta Materiallia **47**, 23-29 (1998).

Jones 1972 — R. L. Jones, The effects of grain size refinement on the mechanical properties of unalloyed titanium, R. I. Jaffee, H. M. Burke, Eds., Titanium science and technology (2), Massachusetts (1972).

Jong *et al.* 1992 — E. N. T. Jong, H. M. Flower, D. R. F. West, Interfacial reaction kinetics in a- and b- titanium based metal matrix composites, F. H. Froes, I.L. Caplan ., Ed., Titanium '92 Science and Technology, San Diego **3**, 2561-2568 (Minerals, Metals and Materials Society, 1992).

Kaibyshev *et al.* 1981 — O. A. Kaibyshev, I. V. Kazachkov, R. M. Galeev, J. Mat. Sci **16**, 2501 (1981).

Kazakov and Kvasnitsky 1985 — N. F. Kazakov, V. F. Kvasnitsky, in Diffusion bonding of materials, N. F. Kazakov, Ed. (Pergamon Press Ltd, Oxford, 1985) pp. 170-185.

Kobayashi *et al.* 1994 — M. Kobayashi, S. Ochiai, K. Funami, C. Ouchi, S. Suzuki, Superplasticity of fine TiC and TiN dispersed Ti-6Al-4V alloy composites, T. Langdon, Ed., Superplasticity in advanced materials ICSAM-94, Moscow, Russia. 549-554 (Trans Tech Publications, 1994).

Korzh *et al.* 1997 — A. V. Korzh, A. F. Belyavin, D. B. Snow, Low temperature superplasticity in EB PVD titanium alloys, A. H. Chokshi, Ed., Superplasticity in Advanced Materials ICSAM -97, Bangalore, India **243-245**, 603-608 (Trans Tech Publications, 1997).

Lauer *et al.* 1997 — S. Lauer, Z. Guan, H. Wolf, T. Wichert, The phase formation at mechanically alloyed Ti-Al compounds, M. D. Baro, Surinach, Eds., Mechanically alloyed, metastable and nanocrystalline materials, Barcelona, Spain, **2**, 485-490 (Trans Tech Publications, 1997).

Lederich *et al.* 1984 — R. J. Lederich, S. M. l. Sastry, J. E. O'Neal, Microstructural refinements for superplastic forming optimization in titanium alloys, G. Lutjering, U. Zwicker, W. Bunk, Eds., Fifth international conference on titanium, Munich, Germany, **2** 695-702 (DGM, 1984).

Lewandowski *et al.* 1989 — J. J. Lewandowski, C. Lui, W. H. Hunt, Effects of matrix microstructure and particle distribution on fracture of an Al MMC, Material Science and Engineering **A107**, 241-255 (1989).

Liu *et al.* 1995 — Q. Liu, W. Yang, G. Ghen, Superplasticity of two phase alpha-titanium-intermetallics Ti-(Co,Ni)-Al alloys, Acta Metallurgica et Materialia **43**, 3571-3582 (1995).

Liu *et al.* 1998 — X. D. Liu, M. Nagumo, M. Umemoto, Mechanical milling of pure Ti and pure Zr, Materials Transactions, JIM **39**, 463-468 (1998).

Lu and Lai 1998 — L. Lu, M. O. Lai, Mechanical alloying (Kluwer Academic Publishers, ed. 1st, 1998).

Mahoney 1994 — M. W. Mahoney, in ASM handbook of titanium alloys. (ASM International, Ohio, 1994).

Massalski *et al.* 1986 — T. B. Massalski, J. L. Murray, L. H. Bennett, H. Baker, Eds., Binary alloy phase diagrams, vol. 1-2 (American Society for Metals, 1986).

McDarmaid *et al.* 1985 — D. S. McDarmaid, A. W. Bowen, P. G. Partridge, Superplastic anisotropy in Ti-6Al-4V alloy, F.H. Froes, IL. Caplan, Ed., Titanium Science and Technology, San Diego **2**, 689-694 (DGM, 1985).

McQuillan and McQuillan 1956 — A.D McQuillan, M.K. McQuillan, Titanium. (Butterworths Scientific Publications, 1956).

Mishin and Herzig 1999 — Y. Mishin, C. Herzig, Grain boundary diffusion: recent progress and future research, Materials Science and Engineering **260**, 55-71 (1999).

Murphy *et al.* 1997 — A.M. Murphy, S.J. Howard, T.W. Clyne, The effect of particle clustering on the deformation and failure of Al-Si reinforced with SiC particles: A quantitative study, Key Engineering Materials. **127-131**, 919-928 (Trans Tech publications, 1997).

Murray 1987 — L. J. Murray, Phase diagrams of binary titanium alloys (ASM International, 1987).

Nieh *et al.* 1997 — T. G. Nieh, J. Wadsworth, O. D. Sherby, Superplasticity in metals and ceramics. S. Suresh. D.R Clarke, I.M. Ward, Eds., Cambridge Solid State Science Series (University Press, Cambridge, Cambridge, 1997).

Oehring and Bormann 1991 — M. Oehring, R. Bormann, Nanocrystalline alloys prepared by mechanical alloying and ball milling, Material science and engineering **A134**, 1330-1333 (1991).

Oehring *et al.* 1995 — M. Oehring, F. Appel, T. Pfullmann, R. Bormann, Preparation and mechanical properties of TiAl alloys with submicron grain size, Materials Science Forum **197-181**, 435-442 (1995).

Ohering and Bormann 1993 — M. Ohering, R. Bormann, The formation of metastable Ti-Al solid solutions by mechanical alloying and ball milling. Journal of Materials Research **8**, 2819-2829 (1993).

Paton and Hamilton 1979 — N. E. Paton, C. H. Hamilton, Microstructural influences on superplasticity in Ti-6Al-4V, Metallurgical Transactions **10A**, 241-250 (1979).

Pearce 1987 — R. Pearce, Superplasticity - an Overview, Superplasticity. AGARD Lecture Series No. 168, Neuilly-sur-Seine (AGARD, NATO, 1987).

Peters *et al.* 1983 — M. Peters, G. Lutjuering, G. Ziegler, Control of microstructures of (a + b) - titanium alloys, Zeitschrift fur Metallkunde, **74**, 274 – 282 (1983).

Philliber *et al.* 1995 — J. A. Philliber, F. C. Dary, F. W. Zok, C. G. Levi, Flow and creep behaviour of Ti/TiB In-situ composites, P.A Blenkinsop, W.J. Evans, H.M. Flower, Eds., Titanium 95, Eighth world conference on titanium, International Convention Centre, Birmingham, UK. **3**, 2714 (IOM, 1995).

Porter and Easterling 1981 — D.A. Porter, K.E. Easterling, Phase transformations in metals and alloys, (Padstow, 1981)

Price and Kohler 1984 — P. Price, S. Kohler, in Metals Handbook. E. Klar, Ed. (ASM, Ohio, 1984), **7**, 419-443.

Ranganath and Mishira 1996 — S. Ranganath, R.S. Mishira, Steady state creep behaviour of particulate reinforced titanium matrix composites, Acta materialia. **44**, 927-935 (1996).

Reeves 1992 — A. J. Reeves, The effect of interfacial reactions on the properties of titanium-matrix composites reinforced with SiC and TiB_2 particulate, DPhil, Cambridge (1992).

Saito 1995 — T. Saito. A cost effective P/M Titanium matrix composite for automobile use. Advanced performance materials **2**, 121-144 (1995).

Saito *et al.* 1995b — T. Saito, F. Furuta, Y. Yamaguchi, Development of low cost titanium matrix composite, F.H Froes, J. Storer, Eds., Recent advances in titanium metal matrix composites. 33-44 (The Minerals, Metals and Materials Society, 1995).

Saito *et al.* 1995 — T. Saito, H. Takamiya, F. Furuta, Hot workability and mechanical properties of a TiB particle reinforced PM beta-titanium matrix composite, P. A. Blenkinsop, W. J. Evans, H. M. Flower, Eds., Titanium 95, Eighth world conference on titanium, International Convention Centre, Birmingham, UK **3**, 2859-2866 (IOM, 1995).

Saito *et al.* 1995 — T. Saito, T. Furuta, H. Takamiya, Sintering behaviour and thermal stability of a TiB Particle reinforced PM Beta-Titanium Matrix composite, P. A. Blenkinsop, W. J. Evans, H. M. Flower, Eds., Titanium '95, Eighth world conference on titanium, International Convention Centre, Birmingham, UK. **3**, 2763-2770 (IOM, 1995).

Salishchev *et al.* 1993 — G. A. Salishchev, O. R. Valiakhmetov, R. M. Galeyev, Formation of submicrocrystalline structure in the titanium alloy VT8 and its influence on mechanical properties, Journal of materials science **28**, 2898-2902 (1993).

Sastry *et al.* 1980 — S. M. L. Sastry, P. S. Pao, K. K. Sankaran, High temperature deformation of Ti-6Al-4V, H. Kimura, O. Izumi, Eds., Titanium '80 Science and Technology, Kyoto, Japan. **2**, 873-886 (AIME, 1980).

Sastry *et al.* 1984 — S. M. L. Sastry, T. C. Peng, J. E. O'Neal, Design and development of advanced titanium alloys by rapid solidification technology, G. Lutjering, U. Zwicker, W. Bunk, Eds., 5th international conference on titanium, Munich, Germany. **1**, 397 (Deutche gesellscaft fur metallkunde e.v, 1984).

Shultz 1988 — L. Shultz, Glass formation by mechanical alloying. Journal of less common metals **145**, 233-249 (1988).

Simmons *et al.* 1997 — J. W. Simmons, D. E. Alman, J. A. Hawk, Abrasive wear behaviour of P/M titanium matrix composites, The International Journal of Powder Metallurgy **33**, 9-11 (1997).

Small *et al.* 1999 — D. A. Small, G. R. MacKay, R. A. Dunlap, Hydriding reactions in ball-milled titanium, Journal of alloys and compounds **284**, 312-315 (1999).

Smarsley et al 1985 — W. Smarsly, Y. T. Lee, G. Welsch, Microporosity in hot isostatically pressed Ti-6Al-4V powder compacts, Metallurgical transactions **16A**, 1831-1834 (1985).

Smith 1993 — W. Smith, Structure and properties of engineering alloys. M. Clark, Ed. (McGraw-Hill Inc, ed. 2, 1993).

Smithells 1983 — C.J. Smithells, Smithells Metals Reference Book. E. A. Brandes, Ed. (Butterworths, ed. 6, 1983).

Soboyejo *et al.* 1994 — W. O. Soboyejo, R. J. Lederich, S. M. L. Sastry, Mechanical behaviour of damage tolerant TiB whisker reinforced in situ titanium matrix composites. Acta Metallurgica et Materialia. **42**, 2579-2591 (1994).

Srivatsan *et al.* 1995 — T. S. Srivatsan, W. O. Soboyejo, R. J. Lederich, Cyclic plastic strain response and fracture behaviour of a TiB whisker reinforced titanium alloy metal matrix composite, F. H. Froes, J. Storer, Eds., Recent Advances In Titanium Metal Matrix Composites, Ohio, USA. 225-244 (TMS, 1995).

Suryanarayana *et al.* 1990 — C. Suryanarayana, R. Sundaresan, F. H. Froes, Mechanical alloying of titanium alloys, F. H. Froes, J. J. deBarbadillo, Eds., Structural applications of mechanical alloying, Myrtle Beach, South Carolina, USA. 193-201 (ASM International, 1990).

Sysoeva *et al.* 1996 — N. V. Sysoeva, I. G. Polyakova, I. G. Karpova, Structure and microhardness of granules of VT22 alloy additionally alloyed with carbon and boron, Metal Science and Heat treatment **38**, 527-530 (1996).

Tarrant 1998 — A. Tarrant, Personal Communication, (1998).

Taya and Arsenault 1989 — M. Taya, R. Arsenault, Metal matrix composites, thermomechanical behaviour (Pergamon Press plc, Oxford, ed. 1, 1989).

Tong *et al.* 1995 — W. Tong, G. Ravichandran, T. Christman, T. Vreeland, Processing SiC particulate reinforced titanium based metal matrix composites by shock wave consolidation, Acta Metallurgica et Materialia **43**, 235-250 (1995).

Tsang et al. 1997 — H. T. Tsang, C. G. Chao, C. Y. Ma, Effects of volume fraction of reinforcement on tensile and creep properties of in-situ TiB/Ti MMC. Scripta Materialia **37**, 1359-1365 (1997).

Upadhyaya *et al.* 1994 — D. Upadhyaya, R. Brydson, P. Tsakiropoulos, C. M. Ward-Close, F. H. Froes, A comparison of SCS6/Ti-6Al-4V and Sigma SM1240/Ti-6Al-4V composite systems: A microstructural characterisation, F. H. Froes, J. Storer, Eds., Recent advances in titanium metal matrix composites, Rosemont, Illinois, USA. 139-145 (TMS, 1994).

Wang *et al.* 1993 — K. Y. Wang, T. D. Shen, M. X. Quan, W. D. Wei, Hall-Petch relationship in nanocrystalline titanium produced by ball-milling, Journal of Materials Science Letters **12**, 1818-1820 (1993).

Ward-Close *et al.* 1995 — C. M. Ward-Close, D.M.J Wilkes, P. S. Goodwin, P. G. Partridge, K. E. Bagnall, Microstructural study of titanium-magnesium alloys, W.J. Evans, H.M. Flower, P.A. Blenkinsop, Ed., Titanium 95, Birmingham, UK, **2**, 2673 (IOM, 1995).

Warren *et al.* 1995 — J. Warren, L. M. Hsiung, H. N. G. Wadley, High temperature deformation behaviour of physical vapor deposited Ti-6Al-4V, Acta Metallurgica et Materialia **43**, 2773-2787 (1995).

Wisbey 1995 — A. Wisbey, Superplastic flow of cast lamellar microstructures in Ti-6Al-4V. (1995).

Yolton and Moll 1995 — C. F. Yolton, J. H. Moll, Evaluation of a discontinuously reinforced Ti-6Al-4V composite, P.A. Blenkinsop, W.J. Evans, H.M. Flower, Eds., Titanium 95, Eighth world conference on titanium, International Convention Centre, Birmingham, UK. **3**, 2755 (IOM, 1995).

Appendix A - Powder details

Gas atomised powders

Ti-6Al-4V (wt %) and Ti powder was purchased from Crucible Research, USA. The tables below list the manufacturers release specification for these powders.

Chemical Analysis (weight %)

Material	Al	V	Fe	C	O	N	H	Ti
Ti-6Al-4V	6.18	3.93	0.045	0.059	0.105	0.012	--	Balance
Ti	--	--	0.047	0.065	0.113	0.012	--	Balance

Size Distributions (% under)

Material	250μm	177μm	149μm	105μm	74μm	63μm	53μm	44μm
Ti-6Al-4V	100	77.3	65.1	40.1	21.6	14.2	10.3	7.1
Ti	97.4	75.0	62.8	38.8	20.5	13.5	9.5	6.4

Material	Tap density g/cc (ASTM B527)	Flow rate Seconds (ASTM B213)
Ti-6Al-4V	2.79	28
Ti	2.92	24

Sponge fines titanium

The titanium sponge fines (Ti_{sf}), with an average particle size of 100 μm came from old stock which was produced by Deeside Titanium UK using the Kroll process.

Titanium hydride powder

The TiH_2 powder came from two sources: Timet UK and Chemetall. This powder had a fine particle size of approximately 45 μm.

Hydride dehydride powder

The hydride de-hydride (HDH) Ti-15V-3Cr-3Al-3Sn (wt %) powder with a particle size of less than 45 μm in size and was supplied by Teledyne-Wah Chang, USA.

Boron

Amorphous boron powder with a nominal particle size of 1 μm was purchased from H.C. Stark, Germany.

Typical chemical analysis (ppm)

Al	Ba	Bi	Ca	Cd	Cu	Fe	Mg	Mn	N	Na	Ni	O	Si	B
100	50	50	400	50	50	2000	35000	800	1000	400	100	33000	400	Balance

Titanium diboride

TiB_2 with a mean particle size of 7 μm was purchased from H. C. Stark, Germany.

Typical chemical analysis (ppm) unless otherwise stated

B (wt%)	C	O	N	Fe	Ti
30.2	1100	4900	1800	540	Balance

Appendix B – The effect of dislocation density, grain size and temperature on the diffusion mechanism in α titanium.

A version of Ficks first law of diffusion is:

$$\delta = \sqrt{Dt}$$

where δ is the diffusion distance, D is the diffusivity at a given temperature, t is the reaction time.

$$D = D_0 \exp\left(\frac{-Q}{RT}\right)$$

where D_0 is the diffusion coefficient, Q is the activation energy, R is the gas constant and T is the temperature.

Grain boundary diffusion (D_b) can be described by:

$$D_b = \left(\frac{\partial}{d}\right) D_{b0} \exp\left(\frac{-Q_b}{RT}\right)$$

where D_{b0} is the grain boundary diffusion coefficient, Q_b is the activation energy for grain boundary diffusion, ∂ is the grain boundary thickness and d is the grain size.

Pipe diffusion (D_p) can be described by:

$$D_p = g.D_{p0} \exp\left(\frac{-Q_p}{RT}\right)$$

where D_{p0} is the pipe diffusion coefficient, Q_p is the activation energy for pipe diffusion and g is the cross sectional area of pipe per unit area.

DATA

$D_0 = 6.4 \times 10^{-8}$
$Q = 123$ kJmol^{-1}

Source data (Askill (1970))

$$\frac{D_p}{D_b} = 3200$$

given a grain size of 2-10 μm and a grain boundary thickness of 1 nm, a dislocation density of 10^5 and pipe thickness of 1 nm

therefore $D_p = 64\ D_b$

Source data (Johnson *et al.* (1998))

$Q_b = Q/2$

Source data (Mishin and Herzig (1999))

Given this data the diffusivity for lattice, grain boundary diffusion and pipe diffusion were calculated.

ASSUMPTIONS

$D_o = D_b$

The grain boundary thickness is 1 nm
The grain size increased with temperature as shown in Figure B-1.
The number atoms the matrix was 10^{13}. The dislocation density reduced from 10^{12} to 10^5 (typical for annealed materials) at 600°C as shown in Figure B-2.

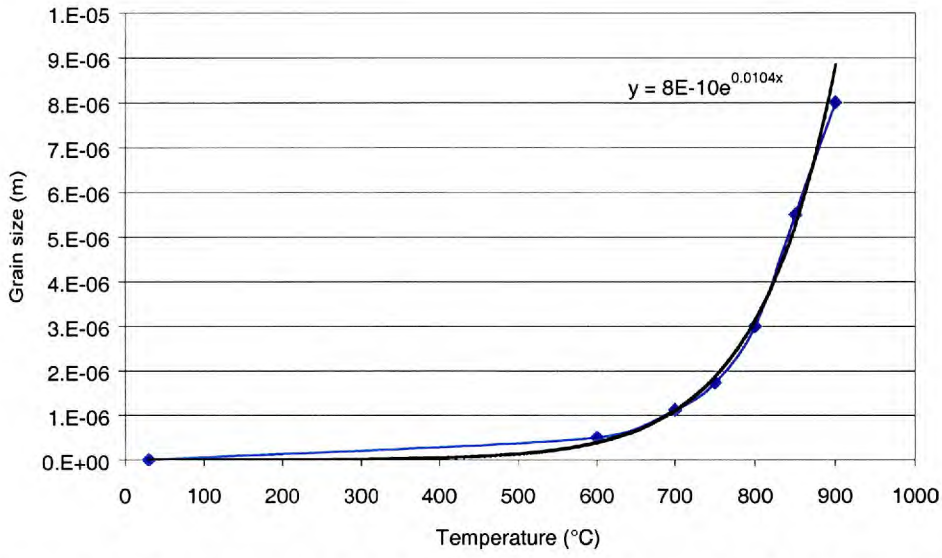


Figure B-1. Grain growth of Ti-6Al-4V produced by mechanical milling for 60T seconds and hot isostatic pressing for 2 hours at 150 MPa.

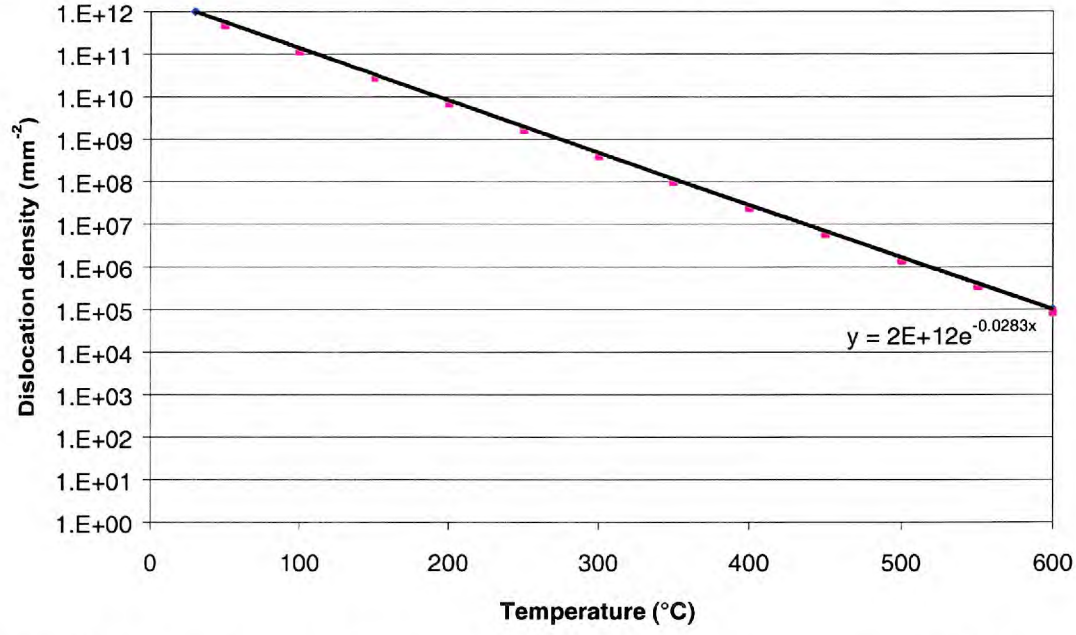


Figure B-2 The reduction in dislocation density with increasing temperature. Given a dislocation density of 10^{12} (mm^{-2}) at room temperature in mechanically alloy powders and an annealed structure (with a dislocation density of 10^5 mm^{-2}) at 600°C.